REPUBLIQUE DU CAMEROUN
Paix-Travail-Patrie

UNIVERSITE DE YAOUNDE I

CENTRE DE RECHERCHE ET DE FORMATION DOCTORALE EN SCIENCES, TECHNOLOGIES ET GEOSCIENCES
UNITE DE RECHERCHE ET DE FORMATION DOCTORALE PHYSIQUE ET APPLICATIONS

FACULTE DES SCIENCES

B.P 812 Yaoundé
Email: crftstg@uyi.uninet.cm

REPUBLIC OF CAMEROON
Peace-Work-Fatherland

THE UNIVERSITY OF YAOUNDE I

POSTGRADUATES SCHOOL OF SCIENCE, TECHNOLOGY AND GEOSCIENCES
RESEARCH AND POSTGRADUATE TRAINING UNIT FOR PHYSICS AND APPLICATIONS

FACULTY OF SCIENCE

P.O.BOX 812 Yaoundé
Email: crftstg@uyi.uninet.cm

DEPARTMENT OF PHYSICS
LABORATORY OF NUCLEAR, ATOMIC, MOLECULAR PHYSICS AND BIOPHYSICS
OPTION: ATOMIC, MOLECULAR PHYSICS AND BIOPHYSICS

COUPLED NONLINEAR WAVES IN NEURONAL MICROTUBULES

Thesis

Submitted and defended in fulfillment of the requirements for the Degree of **Doctorat/Ph.D in Physics**

By

TANKOU Eric

Master of Science in Physics
Registration number: 08W0595

Under the supervision of

MOHAMADOU Alidou

Professor,
University of Maroua,
Cameroon

ACADEMIC YEAR: 2024 - 2025

UNIVERSITÉ DE YAOUNDÉ I
THE UNIVERSITY OF YAOUNDE I

FACULTÉ DES SCIENCES
FACULTY OF SCIENCES

DÉPARTEMENT DE PHYSIQUE
DEPARTMENT OF PHYSICS

ATTESTATION DE CORRECTION DE THÈSE DE DOCTORAT/Ph.D

Nous soussignés, Professeur **NDJAKA Jean-Marie** et Professeur **BEN-BOLIE Germain Hubert**, respectivement Président et Membre du jury de Thèse de Doctorat/Ph.D. de Monsieur **TANKOU Eric**, Matricule **08W0595**, préparée sous la direction du Professeur **MOHAMADOU Alidou,** à l'Université de Yaoundé I, intitulée : **« COUPLED NONLINEAR WAVES IN NEURONAL MICROTUBULES »**, soutenue le **Vendredi, 09 Mai 2025**, en vue de l'obtention du grade de Docteur/Ph.D. en Physique, Spécialité **Physique des Rayonnements et Biophysique,** option **Physique Atomique, Moléculaire et Biophysique,** attestons que toutes les corrections conformément aux remarques et suggestions des membres du jury de soutenance ont été effectuées.

En foi de quoi, la présente attestation lui est délivrée pour servir et valoir ce que de droit.

Fait à Yaoundé, le 10 JUIN 2025

Membre

Pr. BEN-BOLIE Germain Hubert

Président du jury

Pr. NDJAKA Jean-Marie

Chef de Département de Physique

UNIVERSITÉ DE YAOUNDÉ I * FACULTÉ DES SCIENCES * Le Chef de Département DÉPARTEMENT DE PHYSIQUE

Pr. NDJAKA Jean-Marie

UNIVERSITÉ DE YAOUNDÉ I **Faculté des Sciences** Division de la Programmation et du Suivi des Activités Académiques		THE UNIVERSITY OF YAOUNDE I **Faculty of Science** Division of Programming and Follow-up of Academic Affaires
LISTE DES ENSEIGNANTS PERMANENTS		**LIST OF PERMANENT TEACHING STAFF**

ANNÉE ACADEMIQUE 2024/2025
(Par Département et par Grade)
DATE D'ACTUALISATION 30 septembre 2024

ADMINISTRATION

1. **DOYEN :** OWONO OWONO Luc Calvin, *Professeur*
2. **VICE-DOYEN / DPSAA:** NDJIGUI Paul-Désiré, *Professeur*
3. **VICE-DOYEN / DSSE :** NYEGUE Maximilienne Ascension, *Professeur*
4. **VICE-DOYEN / DRC :** NOUNDJEU Pierre, *Maître de Conférences*
5. **Chef Division Administrative et Financière :** NDOYE FOE Florentine Marie Chantal, *Maître de Conférences*
6. **Chef Division des Affaires Académiques, de la Recherche et de la Scolarité DAARS :** AJEAGAH Gideon AGHAINDUM, *Professeur*

1- DÉPARTEMENT DE BIOCHIMIE (BC) (44)

N°	NOMS ET PRÉNOMS	GRADE	OBSERVATIONS
1.	BIGOGA DAIGA Jude	Professeur	En poste
2.	FEKAM BOYOM Fabrice	Professeur	En poste
3.	KANSCI Germain	Professeur	En poste
4.	MBACHAM FON Wilfred	Professeur	En poste
5.	MOUNDIPA FEWOU Paul	Professeur	*Chef de Département*
6.	NGUEFACK Julienne	Professeur	En poste
7.	NJAYOU Frédéric Nico	Professeur	En poste
8.	OBEN Julius ENYONG	Professeur	En poste
9.	ACHU Merci BIH	Maître de Conférences	En poste
10.	AKINDEH MBUH NJI	Maître de Conférences	En poste
11.	ATOGHO Barbara MMA	Maître de Conférences	En poste
12.	AZANTSA KINGUE GABIN BORIS	Maître de Conférences	En poste
13.	BELINGA née NDOYE FOE F. M. C.	Maître de Conférences	*Chef DAF / FS*
14.	DAKOLE DABOY Charles	Maître de Conférences	En poste
15.	DONGMO LEKAGNE Joseph Blaise	Maître de Conférences	En poste
16.	DJUIDJE NGOUNOUE Marceline	Maître de Conférences	En poste
17.	DJUIKWO NKONGA Ruth Viviane	Maître de Conférences	En poste
18.	EFFA ONOMO Pierre	Maître de Conférences	*VD/FS/Univ Ebwa*
19.	EWANE Cécile Annie	Maître de Conférences	En poste
20.	KENGNE NOUEMSI Anne Pascale	Maître de Conférences	En poste
21.	KOTUE TAPTUE Charles	Maître de Conférences	En poste
22.	LUNGA Paul KEILAH	Maître de Conférences	En poste
23.	MANANGA Marlyse Joséphine	Maître de Conférences	En poste
24.	MBONG ANGIE M. Mary Anne	Maître de Conférences	En poste
25.	MOFOR née TEUGWA Clotilde	Maître de Conférences	*Doyen FS / UDs*
26.	NANA Louise épouse WAKAM	Maître de Conférences	En poste
27.	NGONDI Judith Laure	Maître de Conférences	En poste
28.	Palmer MASUMBE NETONGO	Maître de Conférences	En poste
29.	PECHANGOU NSANGOU Sylvain	Maître de Conférences	En poste
30.	TCHANA KOUATCHOUA Angèle	Maître de Conférences	En poste
31.	BEBEE Fadimatou	Chargée de Cours	En poste
32.	BEBOY EDJENGUELE Sara N.	Chargé de Cours	En poste
33.	FONKOUA Martin	Chargé de Cours	En poste
34.	FOUPOUAPOUOGNIGNI Yacouba	Chargé de Cours	En poste
35.	KOUOH ELOMBO Ferdinand	Chargé de Cours	En poste
36.	MBOUCHE FANMOE Marceline J.	Chargé de Cours	En poste
37.	OWONA AYISSI Vincent Brice	Chargé de Cours	En poste
38.	WILFRED ANGIE ABIA	Chargé de Cours	En poste
39.	BAKWO BASSOGOG Christian Bernard	Assistant	En Poste
40.	ELLA Fils Armand	Assistant	En Poste
41.	EYENGA Eliane Flore	Assistant	En Poste

42.	MADIESSE KEMGNE Eugenie Aimée	Assistant	En Poste
43.	MANJIA NJIKAM Jacqueline	Assistant	En Poste
44.	WOGUIA Alice Louise	Assistant	En Poste

2- DÉPARTEMENT DE BIOLOGIE ET PHYSIOLOGIE ANIMALES (BPA) (50)

1.	AJEAGAH Gideon AGHAINDUM	Professeur	*DAARS/FS*
2.	DIMO Théophile	Professeur	En Poste
3.	DJIETO LORDON Champlain	Professeur	En Poste
4.	DZEUFIET DJOMENI Paul Désiré	Professeur	En Poste
5.	ESSOMBA née NTSAMA MBALA	Professeur	*CD et Vice Doyen/FMSB/UYI*
6.	KEKEUNOU Sévilor	Professeur	*Chef de Département*
7.	NJAMEN Dieudonné	Professeur	En poste
8.	NOLA Moïse	Professeur	En poste
9.	TAN Paul VERNYUY	Professeur	En poste
10.	TCHUEM TCHUENTE Louis Albert	Professeur	*Inspecteur de service / Coord.Progr./MINSANTE*
11.	ZEBAZE TOGOUET Serge Hubert	Professeur	En poste

12.	ALENE Désirée Chantal	Maître de Conférences	*Vice Doyen/ Uté Ebwa*
13.	ATSAMO Albert Donatien	Maître de Conférences	En poste
14.	BILANDA Danielle Claude	Maître de Conférences	En poste
15.	DJIOGUE Séfirin	Maître de Conférences	En poste
16.	GOUNOUE KAMKUMO Raceline épse FOTSING	Maître de Conférences	En poste
17.	JATSA BOUKENG Hermine épse MEGAPTCHE	Maître de Conférences	En Poste
18.	KANDEDA KAVAYE Antoine	Maître de Conférences	En poste
19.	LEKEUFACK FOLEFACK Guy B.	Maître de Conférences	En poste
20.	MAHOB Raymond Joseph	Maître de Conférences	En poste
21.	MBENOUN MASSE Paul Serge	Maître de Conférences	En poste
22.	MEGNEKOU Rosette	Maître de Conférences	En poste
23.	MOUNGANG Luciane Marlyse	Maître de Conférences	En poste
24.	NOAH EWOTI Olive Vivien	Maître de Conférences	En poste
25.	MONY Ruth épse NTONE	Maître de Conférences	En Poste
26.	MVEYO NDANKEU Yves Patrick	Maître de Conférences	En poste
27.	NGUEGUIM TSOFACK Florence	Maître de Conférences	En poste
28.	NGUEMBOCK	Maître de Conférences	En poste
29.	TAMSA ARFAO Antoine	Maître de Conférences	En poste
30.	TOMBI Jeannette	Maître de Conférences	En poste

31.	AMBADA NDZENGUE GEORGIA ELNA	Chargé de Cours	En poste
32.	BASSOCK BAYIHA Etienne Didier	Chargé de Cours	En poste
33.	ETEME ENAMA Serge	Chargé de Cours	En poste
34.	FEUGANG YOUMSSI François	Chargé de Cours	En poste
35.	FOKAM Alvine Christelle Epse KENGNE	Chargé de Cours	En poste
36.	FOSSI TANKOUA Olivia Epse DJEUTCHOUANG SAYANG	Chargé de Cours	En poste (transfert Uté de Dla)
37.	GONWOUO NONO Legrand	Chargé de Cours	En poste
38.	KOGA MANG DOBARA	Chargé de Cours	En poste
39.	LEME BANOCK Lucie	Chargé de Cours	En poste

40.	MAPON NSANGOU Indou	Chargé de Cours	En poste
41.	METCHI DONFACK MIREILLE FLAURE EPSE GHOUMO	Chargé de Cours	En poste
42.	NGOUATEU KENFACK Omer Bébé	Chargé de Cours	En poste
43.	NJUA Clarisse YAFI	Chargée de Cours	*Chef Div. Uté Bamenda*
44.	NWANE Philippe Bienvenu	Chargé de Cours	En poste
45.	TADU Zephyrin	Chargé de Cours	En poste
46.	YEDE	Chargé de Cours	En poste
47.	YOUNOUSSA LAME	Chargé de Cours	En poste

48.	KODJOM WANCHE Jacguy Joyce	Assistante	En poste
49.	NDENGUE Jean De Matha	Assistant	En poste
50.	ZEMO GAMO Franklin	Assistant	En poste

3- DÉPARTEMENT DE BIOLOGIE ET PHYSIOLOGIE VÉGÉTALES (BPV) (32)

1.	AMBANG Zachée	Professeur	*Chef de Département*
2.	DJOCGOUE Pierre François	Professeur	En poste
3.	MBOLO Marie	Professeur	En poste
4.	MOSSEBO Dominique Claude	Professeur	En poste
5.	NDONGO BEKOLO	Professeur	En poste
6.	ZAPFACK Louis	Professeur	En poste
7.	ANGONI Hyacinthe	Maître de Conférences	En poste
8.	BIYE Elvire Hortense	Maître de Conférences	En poste
9.	MAHBOU SOMO TOUKAM. Gabriel	Maître de Conférences	En poste
10.	MALA Armand William	Maître de Conférences	En poste
11.	MBARGA BINDZI Marie Alain	Maître de Conférences	*DAAC /UDla*
12.	NGALLE Hermine BILLE	Maître de Conférences	En poste
13.	NGONKEU MAGAPTCHE Eddy L.	Maître de Conférences	*CT / MINRESI*
14.	TONFACK Libert Brice	Maître de Conférences	En poste
15.	TSOATA Esaïe	Maître de Conférences	En poste
16.	ONANA JEAN MICHEL	Maître de Conférences	En poste
17.	DJEUANI Astride Carole	Chargé de Cours	En poste
18.	GONMADGE CHRISTELLE	Chargé de Cours	En poste
19.	MAFFO MAFFO Nicole Liliane	Chargé de Cours	En poste
20.	MANGA NDJAGA JUDE	Chargé de Cours	En poste
21.	NNANGA MEBENGA Ruth Laure	Chargé de Cours	En poste
22.	NOUKEU KOUAKAM Armelle	Chargé de Cours	En poste
23.	NSOM ZAMBO EPSE PIAL ANNIE CLAUDE	Chargé de Cours	*En détachement/UNESCO MALI*
24.	GODSWILL NTSOMBOH NTSEFONG	Chargé de Cours	En poste
25.	KABELONG BANAHO Louis-Paul-Roger	Chargé de Cours	En poste
26.	KONO Léon Dieudonné	Chargé de Cours	En poste
27.	LIBALAH Moses BAKONCK	Chargé de Cours	En poste
28.	LIKENG-LI-NGUE Benoit C	Chargé de Cours	En poste
29.	TAEDOUNG Evariste Hermann	Chargé de Cours	En poste
30.	TEMEGNE NONO Carine	Chargé de Cours	En poste
31.	DIDA LONTSI Sylvere Landry	Assistant	En poste
32.	METSEBING Blondo-Pascal	Assistant	En poste

4- DÉPARTEMENT DE CHIMIE INORGANIQUE (CI) (27)

1.	GHOGOMU Paul MINGO	Professeur	*Ministre Chargé de Mission PR*
2.	NANSEU NJIKI Charles Péguy	Professeur	En poste
3.	NDIFON Peter TEKE	Professeur	*CT MINRESI*
4.	NENWA Justin	Professeur	En poste
5.	NGOMO Horace MANGA	Professeur	*Vice Chancelor/UB*
6.	NJIOMOU C. épse DJANGANG	Professeur	En poste
7.	NJOYA Dayirou	Professeur	En poste
8.	ACAYANKA Elie	Maître de Conférences	En poste
9.	EMADAK Alphonse	Maître de Conférences	En poste
10.	KAMGANG YOUBI Georges	Maître de Conférences	En poste
11.	KEMMEGNE MBOUGUEM Jean C.	Maître de Conférences	En poste
12.	KENNE DEDZO GUSTAVE	Maître de Conférences	En poste
13.	MBEY Jean Aime	Maître de Conférences	En poste
14.	NDI NSAMI Julius	Maître de Conférences	*Chef de Département*
15.	NEBAH Née NDOSIRI Bridget NDOYE	Maître de Conférences	*Sénatrice/SENAT*
16.	NYAMEN Linda Dyorisse	Maître de Conférences	En poste
17.	PABOUDAM GBAMBIE AWAWOU	Maître de Conférences	En poste
18.	TCHAKOUTE KOUAMO Hervé	Maître de Conférences	En poste
19.	BELIBI BELIBI Placide Désiré	Maître de Conférences	*Chef Service/ ENS Bertoua*
20.	CHEUMANI YONA Arnaud M.	Maître de Conférences	En poste
21.	KOUOTOU DAOUDA	Maître de Conférences	En poste
22.	MAKON Thomas Beauregard	Chargé de Cours	En poste
23.	NCHIMI NONO KATIA	Chargée de Cours	En poste
24.	NJANKWA NJABONG N. Eric	Chargé de Cours	En poste
25.	PATOUOSSA ISSOFA	Chargé de Cours	En poste
26.	SIEWE Jean Mermoz	Chargé de Cours	En Poste
27.	BOYOM TATCHEMO Franck W.	Assistant	En Poste

5- DÉPARTEMENT DE CHIMIE ORGANIQUE (CO) (33)			
1.	Alex de Théodore ATCHADE	Professeur	*DEPE/Univ. Bertoua*
2.	DONGO Etienne	Professeur	*Vice-Doyen/FSE/UYI*
3.	NGOUELA Silvère Augustin	Professeur	*Chef de Département UDS*
4.	PEGNYEMB Dieudonné Emmanuel	Professeur	*Recteur UBertoua/ Chef de Département*
5.	MBAZOA née DJAMA Céline	Professeur	En poste
6.	MKOUNGA Pierre	Professeur	En poste
7.	AMBASSA Pantaléon	Maître de Conférences	En poste
8.	EYONG Kenneth OBEN	Maître de Conférences	En poste
9.	FOTSO WABO Ghislain	Maître de Conférences	En poste
10.	KAMTO Eutrophe Le Doux	Maître de Conférences	En poste
11.	KENMOGNE Marguerite	Maître de Conférences	En poste
12.	MVOT AKAK CARINE	Maître de Conférences	En poste
13.	NGO MBING Joséphine	Maître de Conférences	*Chef de Cellule MINRESI*
14.	NGONO BIKOBO Dominique Serge	Maître de Conférences	*C.E.A/ MINESUP*
15.	NOTE LOUGBOT Olivier Placide	Maître de Conférences	*Dir ENS/Uté Bertoua*
16.	NOUNGOUE TCHAMO Diderot	Maître de Conférences	En poste
17.	TABOPDA KUATE Turibio	Maître de Conférences	En poste
18.	TAGATSING FOTSING Maurice	Maître de Conférences	En poste
19.	OUAHOUO WACHE Blandine M.	Maître de Conférences	En poste
20.	ZONDEGOUMBA Ernestine	Maître de Conférences	En poste
21.	MESSI Angélique Nicolas	Chargé de Cours	En poste
22.	MUNVERA MFIFEN Aristide	Chargé de Cours	En poste
23.	NGNINTEDO Dominique	Chargé de Cours	En poste
24.	NGOMO Orléans	Chargée de Cours	En poste
25.	NONO NONO Éric Carly	Chargé de Cours	En poste
26.	OUETE NANTCHOUANG Judith Laure	Chargée de Cours	En poste
27.	SIELINOU TEDJON Valérie	Chargé de Cours	En poste
28.	TCHAMGOUE Joseph	Chargé de Cours	En poste
29.	TSAFFACK Maurice	Chargé de Cours	En poste
30.	TSAMO TONTSA Armelle	Chargé de Cours	En poste
31.	TSEMEUGNE Joseph	Chargé de Cours	En poste
32.	NDOGO ETEME Olivier	Assistant	En poste
33.	NGUEMDJO CHIMEZE Valery Wilfried	Assistant	En poste

6- DEPARTEMENT DES ENERGIES RENOUVELABLES (ER) (1)			
1.	BODO Bertrand	Professeur	*Chef de Département*

7- DÉPARTEMENT D'INFORMATIQUE (IN) (22)

1.	ATSA ETOUNDI Roger	Professeur	*Chef de Division des SI/ MINESUP*
2.	FOUDA NDJODO Marcel Laurent	Professeur	*Inspecteur Général Académique/ MINESUP*

3.	NDOUNDAM Réné	Maître de Conférences	En poste
4.	TSOPZE Norbert	Maître de Conférences	En poste

5.	ABESSOLO ALO'O Gislain	Chargé de Cours	*Chef de Cellule MINFOPRA*
6.	AMINOU HALIDOU	Chargé de Cours	*Chef de Département*
7.	DJAM Xaviera YOUH - KIMBI	Chargé de Cours	En Poste
8.	DOMGA KOMGUEM Rodrigue	Chargé de Cours	En poste
9.	EBELE Serge Alain	Chargé de Cours	En poste
10.	EKODECK Stéphane Gaël Raymond	Chargé de Cours	En poste
11.	HAMZA Adamou	Chargé de Cours	En poste
12.	JIOMEKONG AZANZI Fidel	Chargé de Cours	En poste
13.	KOUOKAM KOUOKAM E. A.	Chargé de Cours	En poste
14.	MELATAGIA YONTA Paulin	Chargé de Cours	En poste
15.	MESSI NGUELE Thomas	Chargé de Cours	En poste
16.	MONTHE DJIADEU Valery M.	Chargé de Cours	En poste
17.	NZEKON NZEKO'O ARMEL JACQUES	Chargé de Cours	En poste
18.	OLLE OLLE Daniel Claude Georges Delort	Chargé de Cours	*Directeur Adjoint ENSET Ebolowa*
19.	TAPAMO Hyppolite	Chargé de Cours	En poste

20.	BAYEM Jacques Narcisse	Assistant	En poste
21.	MAKEMBE. S . Oswald	Assistant	*Directeur CUTI*
22.	NKONDOCK. MI. BAHANACK.N.	Assistant	En poste

8- DÉPARTEMENT DE MATHÉMATIQUES (MA) (34)			
1.	AYISSI Raoult Domingo	Professeur	*Chef de Département*
2.	KIANPI Maurice	Maître de Conférences	En poste
3.	MBANG Joseph	Maître de Conférences	En poste
4.	MBEHOU Mohamed	Maître de Conférences	*Chef de Division/ENSPY*
5.	MBELE BIDIMA Martin Ledoux	Maître de Conférences	*Chef de Département de modélisation et applications industrielles/ENSPY*
6.	NOUNDJEU Pierre	Maître de Conférences	*VDRC/FS/UYI*
7.	TAKAM SOH Patrice	Maître de Conférences	En poste
8.	TCHAPNDA NJABO Sophonie B.	Maître de Conférences	*Directeur/AIMS Rwanda*
9.	TCHOUNDJA Edgar Landry	Maître de Conférences	En poste
10.	AGHOUKENG JIOFACK Jean Gérard	Chargé de Cours	*Chef Cellule MINEPAT*
11.	BOGSO ANTOINE Marie	Chargé de Cours	En poste
12.	BITYE MVONDO Esther	Chargé de Cours	En poste
13.	CHENDJOU Gilbert	Chargé de Cours	En poste
14.	DJIADEU NGAHA Michel	Chargé de Cours	En poste
15.	DOUANLA YONTA Herman	Chargé de Cours	En poste
16.	KIKI Maxime Armand	Chargé de Cours	En poste
17.	KOKOMO AYISSI Eric Brice	Chargé de Cours	En poste(transfert de l'université de Douala)
18.	LOUMNGAM KAMGA Victor	Chargé de Cours	En poste
19.	MBAKOP Guy Merlin	Chargé de Cours	En poste
20.	MBATAKOU Salomon Joseph	Chargé de Cours	En poste
21.	MENGUE MENGUE David Joël	Chargé de Cours	*Chef Dpt /ENS Université d'Ebolowa*
22.	MBIAKOP Hilaire George	Chargé de Cours	En poste
23.	NGUEFACK Bernard	Chargé de Cours	En poste
24.	NIMPA PEFOUKEU Romain	Chargée de Cours	En poste
25.	OGADOA AMASSAYOGA	Chargée de Cours	En poste
26.	POLA DOUNDOU Emmanuel	Chargé de Cours	*En stage*
27.	TENKEU JEUFACK Yannick Léa	Chargé de Cours	En poste
28.	TCHEUTIA Daniel Duviol	Chargé de Cours	En poste
29.	TETSADJIO TCHILEPECK M. Eric.	Chargé de Cours	En poste
30.	FOKAM Jean Marcel	Assistant	En poste
31.	GUIDZAVAI KOUCHERE Albert	Assistant	En poste
32.	MANN MANYOMBE Martin Luther	Assistant	En poste
33.	MEFENZA NOUNTU Thiery	Assistant	En poste
34.	NYOUMBI DLEUNA Christelle	Assistant	En poste

9- DÉPARTEMENT DE MICROBIOLOGIE (MIB) (24)

1.	ESSIA NGANG Jean Justin	Professeur	*Chef de Département*
2.	NYEGUE Maximilienne Ascension	Professeur	*Vice-Doyen / DSSE*
3.	SADO KAMDEM Sylvain Leroy	Professeur	En poste
4.	ASSAM ASSAM Jean Paul	Maître de Conférences	En poste
5.	BOUGNOM Blaise Pascal	Maître de Conférences	En poste
6.	KOUITCHEU MABEKU Epse KOUAM Laure Brigitte	Maître de Conférences	En poste
7.	MUNE MUNE Martin Alain	Maître de Conférences	En poste
8.	RIWOM Sara Honorine	Maître de Conférences	En poste
9.	NJIKI BIKOÏ Jacky	Maître de Conférences	En poste
10.	TCHIKOUA Roger	Maître de Conférences	*Chef de Service de la Scolarité*
11.	ESSONO Damien Marie	Chargé de Cours	En poste
12.	LAMYE Glory MOH	Chargé de Cours	En poste
13.	MEYIN A EBONG Solange	Chargé de Cours	En poste
14.	MONI NDEDI Esther Del Florence	Chargé de Cours	En poste
15.	NKOUDOU ZE Nardis	Chargé de Cours	En poste
16.	NKOUE TONG Abraham	Chargé de Cours	En poste
17.	TAMATCHO KWEYANG Blandine Pulchérie	Chargé de Cours	En poste
18.	SAKE NGANE Carole Stéphanie	Chargé de Cours	En poste
19.	TOBOLBAÏ Richard	Chargé de Cours	En poste
20.	EZO'O MENGO Fabrice Télésfor	Assistant	En poste
21.	EHETH Jean Samuel	Assistant	En poste
22.	MAYI Marie Paule Audrey	Assistant	En poste
23.	NGOUENAM Romial Joël	Assistant	En poste
24.	NJAPNDOUNKE Bilkissou	Assistant	En poste

10. DEPARTEMENT DE PHYSIQUE (PHY) (42)			
1.	BEN- BOLIE Germain Hubert	Professeur	En poste
2.	BIYA MOTTO Frédéric	Professeur	*DG/HYDRO Mekin*
3.	DJUIDJE KENMOE épouse ALOYEM	Professeur	En poste
4.	EKOBENA FOUDA Henri Paul	Professeur	*Vice-Recteur. Uté Ngaoundéré*
5.	ESSIMBI ZOBO Bernard	Professeur	En poste
6.	EYEBE FOUDA Jean sire	Professeur	En poste
7.	HONA Jacques	Professeur	En poste
8.	NANA ENGO Serge Guy	Professeur	En poste
9.	NANA NBENDJO Blaise	Professeur	En poste
10.	NDJAKA Jean Marie Bienvenu	Professeur	*Chef de Département*
11.	NJANDJOCK NOUCK Philippe	Professeur	En poste
12.	SAIDOU	Professeur	*Chef de centre/IRGM/MINRESI*
13.	SIMO Elie	Professeur	En poste
14.	TABOD Charles TABOD	Professeur	*Doyen FSUniv/Bda*
15.	TCHAWOUA Clément	Professeur	En poste
16.	WOAFO Paul	Professeur	En poste
17.	ZEKENG Serge Sylvain	Professeur	En poste
18.	ENYEGUE A NYAM épse BELINGA	Maître de Conférences	*Chef de Division de la formation continue et à distance/ENSPY*
19.	FEWO Serge Ibraïd	Maître de Conférences	En poste
20.	FOUEJIO David	Maître de Conférences	*Chef Cell/ MINADER*
21.	MBINACK Clément	Maître de Conférences	En poste
22.	MBONO SAMBA Yves Christian U.	Maître de Conférences	En poste
23.	MELI'I Joelle Larissa	Maître de Conférences	En poste
24.	MVOGO ALAIN	Maître de Conférences	En poste
25.	NDOP Joseph	Maître de Conférences	En poste
26.	SIEWE SIEWE Martin	Maître de Conférences	En poste
27.	VONDOU Derbetini Appolinaire	Maître de Conférences	En poste
28.	WAKATA née BEYA Annie Sylvie	Maître de Conférences	*Directeur/ENS/UYI*
29.	WOULACHE Rosalie Laure	Maître de Conférences	*En stage depuis février 2023*
30.	ABDOURAHIMI	Chargé de Cours	En poste
31.	AYISSI EYEBE Guy François Valérie	Chargé de Cours	En poste
32.	CHAMANI Roméo	Chargé de Cours	En poste
33.	DJIOTANG TCHOTCHOU Lucie Angennes	Chargée de Cours	En poste
34.	EDONGUE HERVAIS	Chargé de Cours	En poste
35.	KAMENI NEMATCHOUA Modeste	Chargé de Cours	En poste
36.	LAMARA Maurice	Chargé de Cours	En poste
37.	NGA ONGODO Dieudonné	Chargé de Cours	En poste
38.	OTTOU ABE Martin Thierry	Chargé de Cours	*Directeur Unité de production des réactifs/IMPM*

39.	TEYOU NGOUPO Ariel	Chargé de Cours	En poste
40.	TOGUEU MOTCHEYO Alain Bertrand	Chargé de Cours	En poste
41.	WANDJI NYAMSI William	Chargé de Cours	En poste
42.	SOUFFO TAGUEU Merimé	Assistant	En poste

11- DÉPARTEMENT DE SCIENCES DE LA TERRE (ST) (34)			
1.	EKOMANE Emile	Professeur	*Chef Div./Uté Ebolowa*
2.	GANNO Sylvestre	Professeur	En poste
3.	NDJIGUI Paul-Désiré	Professeur	*Vice-Doyen /DPSAA*
4.	NGOS III Simon	Professeur	En poste
5.	NKOUMBOU Charles	Professeur	En poste
6.	ONANA Vincent Laurent	Professeur	*Chef de Département/Uté. Eb.*
7.	YENE ATANGANA Joseph Q.	Professeur	*Chef Div. /MINTP*
8.	BISSO Dieudonné	Maître de Conférences	*Chef de Département*
9.	Elisé SABABA	Maitre de Conférences	En poste
10.	EYONG John TAKEM	Maître de Conférences	En poste
11.	FUH Calistus Gentry	Maître de Conférences	*Sec. D'Etat/MINMIDT(ai)*
12.	MBIDA YEM	Maitre de Conférences	En poste
13.	MBESSE Cécile Olive	Maitre de Conférences	En poste
14.	METANG Victor	Maître de Conférences	En poste
15.	NGO BIDJECK Louise Marie	Maître de Conférences	En poste
16.	NGUEUTCHOUA Gabriel	Maître de Conférences	*CEA/MINRESI*
17.	NJILAH Isaac KONFOR	Maître de Conférences	En poste
18.	TCHAKOUNTE Jacqueline épse NUMBEM	Maître de Conférences	*Chef. Cell /MINRESI*
19.	TCHOUANKOUE Jean-Pierre	Maître de Conférences	En poste
20.	TEMGA Jean Pierre	Maître de Conférences	En poste
21.	ZO'O ZAME Philémon	Maître de Conférences	*DG/ART*
22.	ANABA ONANA Achille Basile	Chargé de Cours	En poste
23.	BEKOA Etienne	Chargé de Cours	En poste
24.	MAMDEM TAMTO Lionelle Estelle, épouse BITOM	Chargée de Cours	En poste
25.	NGO BELNOUN Rose Noël	Chargée de Cours	En poste
26.	NGO'O ZE ARNAUD	Chargé de Cours	En poste
27.	NOMO NEGUE Emmanuel	Chargé de Cours	En poste
28.	NTSAMA ATANGANA Jacqueline	Chargée de Cours	En poste
29.	TCHAPTCHET TCHATO De P.	Chargé de Cours	En poste
30.	TEHNA Nathanaël	Chargé de Cours	En poste
31.	FEUMBA Roger	Chargé de Cours	En poste
32.	MBANGA NYOBE Jules	Chargé de Cours	En poste
33.	KOAH NA LEBOGO Serge P.	Assistant	En poste
34.	TENE DJOUKAM Joëlle Flore, épouse KOUANKAP NONO	Assistante	En poste

Répartition chiffrée des Enseignants de la Faculté des Sciences de l'Université de Yaoundé I

NOMBRE D'ENSEIGNANTS					
DÉPARTEMENT	**Professeurs**	**Maîtres de Conférences**	**Chargés de Cours**	**Assistants**	**Total**
BCH	08 (01)	22 (13)	08 (03)	06 (04)	**44 (20)**
BPA	11 (01)	19 (09)	16 (05)	03 (01)	**49 (16)**
BPV	06 (01)	10 (02)	14 (07)	02 (00)	**32 (10)**
CI	07 (01)	14 (03)	05 (01)	01 (00)	**27 (05)**
CO	06 (01)	14 (05)	11 (03)	02 (00)	**33 (09)**
ER	01 (00)		/	/	**01 (0)**
IN	02 (00)	02 (00)	15 (01)	03 (00)	**22 (01)**
MAT	01 (00)	08 (00)	20 (01)	05 (01)	**34 (02)**
MIB	03 (01)	07 (03)	09 (05)	05 (02)	**24 (11)**
PHY	17 (01)	12 (04)	12 (01)	01 (00)	**42 (06)**
ST	07 (00)	14 (03)	11 (03)	02 (01)	**34 (07)**
Total	**69 (07)**	**122 (42)**	**121 (30)**	**30 (09)**	**342 (88)**

Soit un total de **342 (88)** dont :

- Professeurs **69 (07)**
- Maîtres de Conférences **123 (41)**
- Chargés de Cours **120 (30)**
- Assistants **30 (09)**

( ) = Nombre de Femmes **88**

ENSEIGNANTS SOUS CONTRAT DE COLLABORATION

1.	BELL JOSEPH MARTIN	547019U	17/06/1957	Sakbayeme	M	10/11/1986	RETRAITE - CONTRAT DE COLLABORATION	PR
2.	DJOUFAC WOUMFO EMMANUEL	547069Z	09/01/1957	Ngaoundéré	M	04/05/1990	RETRAITE - CONTRAT DE COLLABORATION	PR
3.	ELIMBI ANOINE.	546958X	30/11/1955		M		RETRAITE - CONTRAT DE COLLABORATION	PR
4.	FOMENA ABRAHAM	546778X	10/11/1958	Batcham	M	01/12/1986	RETRAITE - CONTRAT DE COLLABORATION	PR
5.	GHOGOMU TIH RAPH	547004-K	23/12/1956	BAMBALANG	M	13/10/1982	RETRAITE - CONTRAT DE COLLABORATION	PR
6.	KAMTCHOUING PIERRES	143299X	13/09/1955	Nkongsamba	M	01/10/1988	RETRAITE - CONTRAT DE COLLABORATION	PR
7.	LAMINSI SAMUEL	143149J	301/12/1953		M		RETRAITE - CONTRAT DE COLLABORATION	PR
8.	NGADJUI TCHALEU BONAVENTURE	546959-G	15/09/1953	FONTSIGA	M	12/08/1982	RETRAITE - CONTRAT DE COLLABORATION	PR
9.	NGO BILONG ANASTASIE épse TIH	546164-I	27/12/1955	MBANGA	F	28/07/2000	RETRAITE - CONTRAT DE COLLABORATION	MC
10.	NKENGFAC K EPHRAIM AUGUSTIN	546948-F	17/06/1955	YAOUNDE	M	01/09/1983	RETRAITE - CONTRAT DE COLLABORATION	PR
11.	NDIKONTAR MAURICE KOR	169784G	09/05/1958	Mbaa	M	10/01/1991	RETRAITE - CONTRAT DE COLLABORATION-EN COURS DE SIGNATURE	PR
12.	NJIOKOU FLOBERT	547321H	11/06/1958	Nkongsamba	M	03/05/1993	RETRAITE - CONTRAT DE COLLABORATION-EN COURS DE SIGNATURE	PR
13.	BENG NEE NINTCHOM PENLAP VERONIQUE	546643B	07/01/1957	Melong I	F	02/10/1992	RETRAITE-CONTRAT DE COLLABORATION	PR
14.	FOKOU ELIE	546725J	08/06/1957	Fiéla-Bamendjinda	M	01/04/1988	RETRAITE-CONTRAT DE COLLABORATION EN COURS DE FINALISATION	PR
15.	TCHOUANKEU JEAN CLAUDE	547295-E	06/01/1959	Douala	M	01/12/1989	RETRAITE-CONTRAT DE COLLABORATION EN COURS DE FINALISATION	PR
16.	BOYOMO ONANA						CONTRATS TRAITES LORS DU CONSEIL D'UNIVERSITE DU 12 JUILLET 2024	MC
17.	WANDJI JEAN	162242M	09/06/1958	Bangou	M			UYI
18.	YOUMBI EMMANUEL	547332Z	12/02/1959	Bangou	M	Bangou		PR
19.	NGODO MELINGUI JEAN	500475X	05/09/1958	Endoum		20/10/2005		MC
20.	KOFANE TIMOLEON CREPIN							PR
21.	NGAMENI EMMANUEL	547277-C	24/04/1959	Mbanga	M			PR
22.	BITOM DIEUDONNE	547050X	23/11/1958	Ambam	M			PR

DEDICATION

To my Father Mr NGAKOU François,

Who left us twelve years ago.

ACKNOWLEDGMENTS

At the end of this doctoral thesis, I am deeply grateful for having had the opportunity to learn from and work with so many brilliant teachers, collaborators and students. I am happy to express my sincere gratitude to all those who, from near or far, have accompanied me during these years of doctoral work and have contributed directly or indirectly to the realization of this document, because a work like this needs a lot of help. Nevertheless, I will do my best to condense my thoughts on the subject.

I would like to thank the Rector of the University of Yaounde I, the persons responsible of the Faculty of Science and, the Research and Postgraduate Training Unit in Physics and Applications for giving and confirming permission for me to pursue my thesis.

I would like to express my deep gratitude to my director, **Professor Alidou MOHAMADOU**, for his valuable time and cognitive resources in making this work a success. He agreed to guide this thesis despite the multiple academic, administrative and family tasks that fall to him. The completion of this work would not have been possible without his meticulous vision of nonlinear physics. Excellently **Professor MOHAMADOU** has well coordinated the follow-up of all the work on this thesis, providing very pertinent orientations and assessments. His humility, simplicity, teaching, advice and scientific logic have been and will remain a scientific mirror for me.

In particular also, I would like to express my warmest thanks to **Professor TABI Conrad Bertrand**, who not only enabled me to discover but also to enter this rich and fascinating field of biophysics, namely the science of the cellular microtubule network system. His precious time, his advice and his mastery of this complex domain were of capital aid to me in the accomplishment of this work. Also, his passion for research, his love of a job well done, his assiduity in completing a project, his zeal and perseverance in the search for original and aesthetic results, his particular interest in the transfer of skills and autonomy are just some of the virtues that I have received from this great hero of biophysics.

Afterwards, I would like to express my sincere gratitude to **Professor KOFANE Timoléon Crépin**, who made a major contribution to the completion of this scientific work. I appreciate his exceptional personality, his sense of humor and his passion for everything that can be integrated, as well as his scientific and human qualities. The opportunity to discuss with him the theory of solitons in biological systems, his pedagogical attitude and his constant need for understanding remain for me a model of identification.

I would like to extend my warmest thanks to the honorable members of the Jury, who agreed to set aside their many occupations to assess this work. I express to them all my greatest respect.

My deepest thanks also go to **Professor OWONO OWONO Luc Calvin**, Dean of the Faculty of Science and Head of the Physics Department at the higher teacher training college of the University of

Yaoundé I. I thank him infinitely for his qualities as a man, his rigor and the quality of his teaching.

I would like to thank **Professor NDJAKA Jean Marie Bienvenu**, Head of the Department of Physics, Faculty of Science of the University of Yaoundé I. I am very grateful for his administrative contribution and his encouragements.

I am very grateful to **Professor EKOBENA FOUDA Henri Paul**, Head of the Atomic, Molecular and Biophysical Physics Option, for his advices and constructive discussions. In recent years, this laboratory has not only welcomed and trained many students, but has also enhanced the image of our institution through remarkable scientific contributions.

I am very grateful to **Professor BEN-BOLIE Germain Hurbert**, Head of the Nuclear, Atomic, Molecular Physics and Biophysical Laboratory, for his encouragement and the quality of his teaching.

Also I would like to thank **Professor WOAFO Paul**, Chairman of the Cameroon Physical Society for his teaching specially in numerical methods.

Likewise, I would like to thank **Professor MVOGO Alain**, Teacher of Biophysical Laboratory for his valuable advices and encouragements.

I am very grateful to my teachers of the Department of Physics in general and of the laboratory of Biophysics in particular, for their effort and determination to carry out competitive students with good background. I have named: **Professor TCHAWOUA Clément, Professor ESSIMBI ZOBO, Professor PEMHA Elkana, Professor ZEKENG Serge, Professor KENFACK JIOTSA Aurelien, Professor BOUETOU BOUETOU Thomas, Professor DJUIDJE Germaine, Professor SIEWE SIEWE Martin, Professor NANA ENGO, Professor NANA NBENDJO, Professor FOTSA Fernande, Professor BODO Bertrand, Professor MBINACK Clément, Professor FEWO Serge, Professor SAIDOU, Professor HONA Jacques, Professor VONDOU Derbetini.**

I also take this opportunity to thank all my academic elders: **Dr BANSI KAMDEM Delphin, Dr ADAMOU Dang KOKO, Dr BELOBO BELOBO Didier, Dr ETEME Armand Sylvin, Dr MGOUBI, Dr MAÏNA Ibrahim, Dr TEUMA Michel** for their multitude exchanges and helps.

Special thanks to my class mates **Dr KUIPOU William** and **Dr KENNE Thierry** for their multitude exchanges, contributions and encouragements.

Additionally, I am grateful to **Dr NGNINZALONG Carlos, Dr NDJAWA Pavel, Dr KEPNANG PEUBEU Maxime, Dr NDIOKO Jean Paul, Dr ZANGA Dieudonné, Dr FOGNO Roméo, Dr KAMGA Samuel, Dr TALLA Calvin, Dr NZOTCHA Urbain, Dr TENKEU Janvier, Dr FEUDJIO Florent, Dr DONKENG Hatou, Dr TAKOUTSING Cédric, Dr FOUEDJI Chenceline, Dr TABAPSI Rostand, Mr TABI DZOU and Mr SIGNE Eric** for their kindness, availabilities and their encouragements and for many fruitful discussions.

I would not forget to thank:

✓ My mothers **Mrs MATCHOUP Pauline, MAGNE Christine** and **MAZOKOU Christine** for their permanent valuable advices, encouragements and her support.

✓ My brothers and sisters: **TAKOUKAM David, Mrs CHENDJOU Jannette, TCHINDA Felix, SADEU Michel, TAKAM Prosper, FOTSING Felix, NZOKOU Andre** and **SOKAMTE Junior** for their

valuable advices and encouragements. All the members of my family, in particular for all their encouragements.

✓ My friends like **FOTSING Maximin, KAMGANG Raphael, KANKEU Romuald, CHEN-DJOU Martial, CHEUDJOU Chistian, SOH Rostan, TAKAM Victor, SOH Michel, KEPSIEU Blondel, MABOU Michael, CHOULA Pascal**, for their moral support and encouragements.

✓ My loving companion **Erine F. MAGNE**. I would like to express my deep gratitude and admiration to her for all the sacrifices she has made.

I say thank you to all those that I certainly forget to mention the names here.

Contents

List of Figures

LIST OF ABBREVIATIONS

ATP : Adenosine Triphosphate

CCGL : Coupled Complex Ginzburg-Landau

CCNLS : Coupled Complex Nonlinear Schrödinger

CGL : Complex Ginzburg-Landau

CNLS : Coupled Nonlinear Schrödinger

DNA : Deoxyribonucleic Acid

GDP : Guanosine Diphosphate

GL : Ginzburg-Landau

GTP : Guanosine Triphosphate

IF : Intermediate Filament

JEF : Jacobian Elliptic Function

kDa : kiloDalton

MAP : Microtubule Associated Protein

MCAK : Mitotic Centromere-Associated Kinesin

MF : Microfilament

MI : Modulational Instability

MT : Microtubule

MTOC : Microtubule Organizing Center

NLDEs : Nonlinear Differential Equations

NLS : Nonlinear Schrödinger

ODE : Ordinary Differential Equation

PDEs : Partial Differential Equations

PF : Protofilament

RK4 : Fourth-order Runge-Kutta

RLC : Resistor, Inductor and Capacitor

RNA : Ribonucleic Acid

α, β, γ : alpha, beta and gamma

γ-TuRC : gamma-Tubuline Ring Complex

ABSTRACT

Many of the activities of biological cells are carried out via microtubules (MTs). The exploration of nonlinear waves in biological structures is of ever-increasing interest and today covers a multitude of systems, including muscular tissues, the heart, neuronal networks and many others. The work of this thesis focuses on understanding the processes of generation and propagation of coupled nonlinear excitations associated with the collection and transport of energy in the MTs of eukaryotic cells in general and neuronal in particular. To this end, two developed mathematical models of MTs are used for the investigations. These are Zdravkovic's radial angular model, which describes the structural motion of tubulin dimers, and Tuszynski's electrical transmission line model, explaining the conduction of ionic flux through the microtubular cylinder. Thanks to the semi-discrete approximation method close to the continuum limit including multiple scales, we obtain from the generic models, three systems of nonlinear equations of coupled amplitude including, two of Schrödinger, simple and complex and, one of complex Ginzburg-Landau. Their analysis in the modulational instability leads to the derivation of the modulational instability gain. The necessary parametric regions capable of informing on the existence of single and multimode soliton trains with relevant and biophysically acceptable results in this cytoplasmic medium are obtained. The fourth-order Runge-Kutta numerical analysis leads to the verification of the validity of the analytical results.

One of the coupled modes introduces a robust soliton-kink envelope solution, of which the characteristics are discussed in relation to the intrinsic dipolar energy. This is important for energy transport in the polymerization / depolymerization mechanism of MTs. Another set of results suggests that the competing effects of transport memory and nonlinearity affect energy processing in cytoplasmic MTs both in the formation of localized soliton-breather excitations and in the emergence of impulses recognized for efficient neuronal communication. Moreover, we show that the dissipation phenomenon contributes to the control and processing of ionic pulse transfer involving neuronal MTs with the emergence of coupled ionic soliton trains.

Thus the influence of the large amount of information relayed through MTs networks comes with interesting biological implications in neurons and many other eukaryotic cell types.

Keywords: Microtubules; Neuronal Networks; Energy Transport; Coupled Amplitude Equations; Transport Memory; Dipolar Energy; Dissipation.

RÉSUMÉ

De nombreuses activités des cellules biologiques sont réalisées par l'intermédiaire des microtubules (MTs). L'exploration des ondes non linéaires dans les structures biologiques connait un intérêt sans cesse croissant et couvre aujourd'hui une multitude de systèmes notamment, les tissus musculaires, le cœur, les réseaux neuronaux et bien d'autres. L'étude faite dans cette thèse porte sur la compréhension des processus de génération et de propagation des excitations couplées non linéaires associées à la collecte et au transport d'énergie dans les MTs des cellules eucaryotes en général et neuronaux en particulier. A cette fin, deux modèles mathématiques développés de MTs sont utilisés pour les investigations. Il s'agit du modèle angulaire radial de Zdravković, qui décrit le mouvement structural des dimères de tubuline et du modèle des lignes électriques de transmission de Tuszyński, expliquant la conduction du flux ionique à travers le cylindre microtubulaire. Grâce à la méthode d'approximation semi-discrète proche de la limite du continuum incluant des échelles multiples, nous obtenons à partir des modèles génériques, trois systèmes d'équations non linéaires d'amplitude couplée dont, deux de Schrödinger, simple et complexe et, un de Ginzburg-Landau complexe. Leur analyse dans l'instabilité modulationnelle conduit à la dérivation du gain d'instabilité modulationnelle. Les régions paramétriques nécessaires et capables d'informer sur l'existence des trains de soliton simples et multimodes avec des résultats pertinents et biophysiquement acceptables dans ce milieu cytoplasmique sont obtenues. L'analyse numérique de Runge-Kutta d'ordre quatre mène à la vérification de la validité des résultats analytiques.

L'un des modes couplés introduit une solution robuste d'enveloppe de soliton-kink, dont les caractéristiques sont discutées par rapport à l'énergie dipolaire intrinsèque. Ce qui est important pour le transport d'énergie dans le mécanisme de polymérisation / dépolymérisation des MTs. Un autre pan de résultats suggère que les effets compétitifs de la mémoire de transport et de la non linéarité affectent le traitement de l'énergie dans les MTs cytoplasmiques tant sur la formation des excitations localisées de type soliton-breather que sur l'émergence des impulsions reconnues pour une communication neuronale efficiente. Plus encore, nous montrons que le phénomène de dissipation contribue au contrôle et traitement du transfert de l'impulsion ionique impliquant les MTs neuronaux avec l'apparition des trains de soliton ionique couplé.

Ainsi l'influence de la grande quantité d'informations relayées à travers les réseaux de MTs s'accompagne des implications biologiques intéressantes dans les neurones et dans bien d'autres types de cellules eucaryotes.

Mots clés : Microtubules; Réseaux Neuronaux; Transport d'Énergie; Equations d'Amplitude Couplée; Mémoire de Transport; Energie Dipolaire; Dissipation.

GENERAL INTRODUCTION

Today, biological systems are central to the development of nonlinear science because of the exceptional complexity of their interpretation and understanding. They generally emerge as a large collective of interconnected biochemical units called cells. Thus, from a structural point of view, the basic architectural unit of any biological system is the cell. The cell contains mainly a part called the cytoplasm, with around eighty per cent water molecules in its composition. In addition to water molecules, eukaryotic cells have a cytoskeleton in their cytoplasm made up of three different types of filamentous structures: actin-based microfilaments (MFs), intermediate filaments (IFs) (e.g. neurofilaments, keratin, etc.) and tubulin-based microtubules [1]. These cytoskeletal networks are mainly involved in a multitude of roles in the cell, with different types of directed movement [2,3]. MTs are the major cytoskeletal component, highly dynamic with a well-known structure [4]. In vivo and In vitro, observations show that MTs are quite voluminous with a high degree of physiological dynamism [5]. Since then, interest in this molecule has grown steadily, particularly when its physiological properties make it possible to study it using mathematical modelling.

0.1 Context and motivation for the thesis

The Biophysics Laboratory was created some fifteen years ago in the Physics Department of the University of Yaoundé I. It was set up to contribute to the development of research in fundamental physics applied to biology in the Central African Sub-Region and in Cameroon in particular. Since then, a number of research areas have been explored. These include the protein field, molecular swimmers, neuroscience and the dynamics of the deoxyribonucleic acid (DNA) present in all cells. Recently, in 2014, the laboratory decided to broaden its field of research and is now interested in MTs. This is how my introduction to research at Master's degree level came to be focused on MTs. As the first student to work in this new direction in the laboratory, the results obtained in the master's thesis are satisfactory. We found that the microtubular network contained in the intracellular space of eukaryotic cells assumes essential vital functions linked to their dynamics and variable spatial configurations during the cell cycle. It also integrates the flow of information reaching the cell into a particular structural organization. It was shown that this flow of information could be explained by the generation and propagation of nonlinear waves along microtubules, although this was still in its infancy. It is with the intention of continuing with this work begun in the Master's cycle that this thesis is being written. It should be noted that we are not the first in the world to have an interest in MTs. A lot of work has already been done at other universities. In anatomical and physiological research, for example, enormous progress

has been made in explaining the complex dynamics of these biological molecules in their environment [6–10]. In other directions and based on experimental observations, biophysicists have proposed mathematical models describing the behaviour of MTs in the cytosol with significant physical parameters. These include structural models linked to the movement of microtubule components [11–16] and the electrical transmission line model explaining microtubule ionic conduction [17]. In these models, the authors explain the movements linked to MTs using nonlinear waves with single frequency modes. We were inspired by the idea of coupling frequency modes, mainly in the DNA research carried out in our laboratory. In their studies, Tabi et al [18] showed that different classes of waves could coexist and carry a large amount of energy, making it possible to explain specific biological processes such as the initiation of transcription and the open states observed during the reading of the genetic code by Ribonucleic Acid (RNA)messenger. Our main motivation came from the fact that MTs evolve in the same cellular environment as DNA. Given that MTs are active in many biological processes, we also thought we would contribute to understanding their dynamic behaviour via multi-mode waves propagation. In reality, there are several other micro-particles or parameters in the cytoplasmic environment that could strongly influence the movement of MTs.

0.2 Problematic and objectives of the thesis

Biomolecular dynamics is a fascinating subject linked to the fundamental phenomena of life. It is therefore described by nonlinear mechanisms. The major concerns of this thesis are to:

- Show that two waves of different frequencies can coexist in microtubules;

- Find the parametric conditions favorable to optimal generation and propagation of multi-mode signals through MTs within the cytoplasm.

We know that the processing of information related to complex biological systems by manipulating the equations of mathematical models is a great asset for physicists. It is for this reason that the answer to our concerns must involve the harmonious development of a combination of some analytical and numerical methods. These methods are crucial to the study of the stable propagation of excitations, with the major aim of contributing to an optimum understanding of the complex phenomena linked to the essential roles of MT networks.

0.3 Outline of the thesis

We have divided this thesis into three chapters:

Chapter 1 will deal, on the one hand, with the biological generality of MTs and, on the other hand, with a review of the literature focusing on their biophysical behaviour. More specifically, in this section we will first present the biological structure and essential functions of the microtubule molecule. Secondly, some interesting mathematical models of nonlinear dynamics imitating the behaviour of MTs in their biotope and implemented by some authors will be introduced.

Chapter 2 will concentrate, on the one hand, on an in-depth description of the models chosen for our task in this thesis, with details of the ideal case without perturbation and the case influenced by some parameters and behaviour of the cytoplasmic environment. On the other hand, the analytical and numerical methods used for the investigation will be highlighted. These are the multiple-scale expansion method, the modulational instability analysis, the JEF method, the semi-discrete approximation method, the modified Hirota's Bilinear method and the Runge-Kutta fourth-order numerical simulation scheme. Three systems of equations with amplitudes coupled by two frequency modes will be derived:

- a system of coupled nonlinear Schrödinger equations (CNLS) ;

- a system of complex coupled nonlinear Schrödinger equations (CCNLS) with its coefficients taking into account the transport memory constant, and

- a system of complex coupled Ginzburg-Landau equations (CCGL).

Chapter 3 is dedicated to the presentation and discussion of the obtained results. The parametric zones of our biophysical system likely to some solitonic and localized structures will be produced and discussed through the growth rate of MI. By means of analytical methods, the construction of solitonic solutions of kink / breather and pulse at a single frequency mode; then multi-modes will be proposed. These solitonic solutions present relevant new characteristics. Using direct numerical simulations, we show that their propagation will be manifested by the appearance of trains of modulated solitons. We will discuss the behaviour of these results with respect to the impact of parameters such as the dipole energy, the dissipation coefficient and the transport memory constant.

This thesis will end with a general conclusion and a few future directions that could be investigated.

CHAPTER I

LITERATURE REVIEW ON MICROTUBULES

I.1 Introduction

Research to date shows that the interpretation and understanding of biological phenomena in general, and of MTs in particular, remains fairly complex. This is because of the diversity and very small size of the micro particles interacting in the biological environment. For example, the polymerization or depolymerization of MTs in the cell, the transcription and replication of DNA, the intracellular transport of organelles and vesicles, cell communication, ionic conduction and the dynamics of neuronal cells are just some of the phenomena that are not easy to understand. This has prompted researchers to take a closer look, and fundamental processes based on physico-chemical and biological mechanisms have been established. These shape and theoretically describe the complex biological phenomena in an acceptable way. In this chapter, we will first give a background of biological generalities on MTs. Secondly, some existing physico-mathematical models related to the complex understanding of MTs are reviewed.

I.2 Biological background on microtubules

I.2.1 Definition and structure of microtubules

MTs are a major component of the protein filaments in the cytoplasm of all eukaryotic cells, playing a multitude of biological roles. Morphologically, they are hollow cylinders formed from protofilaments, which in turn are composed of a series of proteins called tubulin dimers [19, 20]. Since MTs are an element responsible for intracellular movements and therefore necessary for the survival of the cell, it is important to know its architectural composition. Thus, by transmission electron microscopy, tubulins are seen as slightly acidic globular proteins, with an apparent molecular weight of 50kDa (1Da being the atomic unit of mass), present in the cell as α-tubulin, β-tubulin and γ-tubulin [20]. The α,β-tubulin are capable of fusing to form dimers (see Figure 1). The longitudinal assembly of dimers or heterodimers together allows the formation of protofilaments (PFs) and the lateral assembly of these protofilaments forms the microtubule, as upon the Figure 1. Microtubules have a three left-handed helix structure (corresponding to the stacking of three left-handed helices on top of each other) with a pitch of 12 nm. In vitro, from purified tubulin, it is possible to reconstitute microtubules with between 12 and 17 protofilaments, the distribution of the latter being a Gaussian centered on 14 [21]. In vivo, on the other hand, almost all microtubules have 13 protofilaments and are referred to as 13-symmetric [22–24]. Microtubules with 13 protofilaments form hollow tubes of 25nm outer diameter

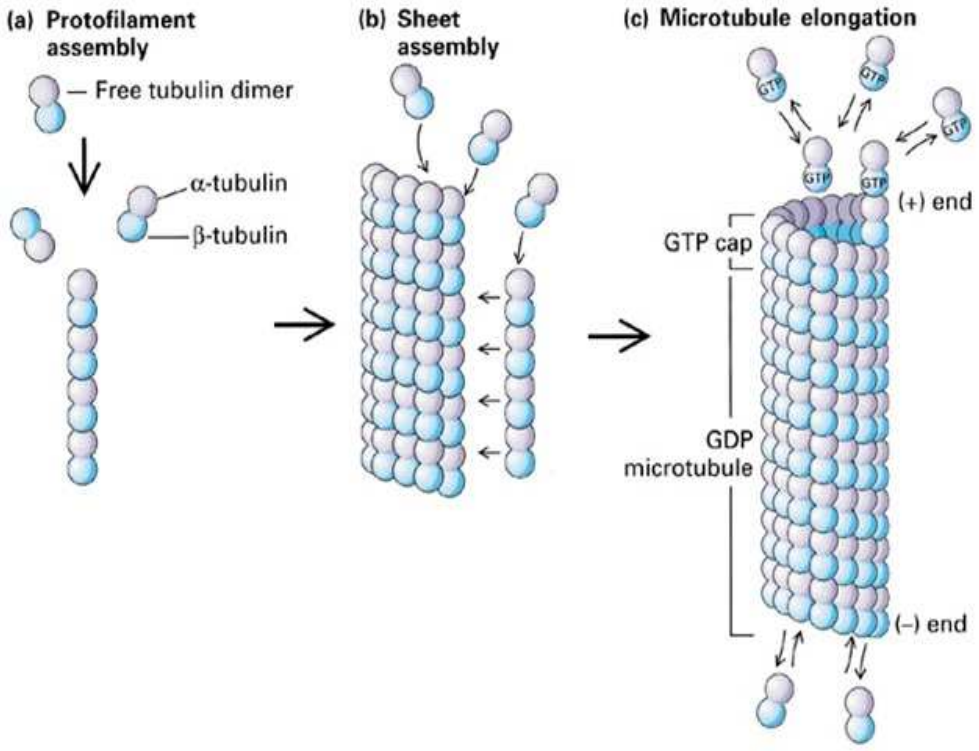

Figure 1: Microtubule structure: a) assembly of α and β-tubulin-tubulin dimers in protofilaments(PF), b) sheet assembly of 13 linear PFs and c) MT elongation, tubulin heterodimers are the building blocks of MTs. The β subunit binds Guanosine Triphosphate (GTP) and eventually hydrolyze it to Guanosine Diphosphate(GDP) [20].

and 15nm inner diameter (see Figure 1). MTs can reach a length of 50 μm with an average length of 25 μm. Only with 13-symmetry does each protofilament remain straight along the microtubule (with other symmetry, the protofilaments curl along the microtubule) [21]. In this configuration, the α-tubulins of one protofilament interact laterally with the α-tubulins of another protofilament, as do the β-tubulins. However, there is an area called the groove where the α-tubulins of one protofilament interact laterally with the β-tubulins of another protofilament [21] (see Figure 1). Due to the head-to-tail assembly of tubulin heterodimers, microtubules are polarized. The two ends are referred to as negative (-) and positive (+) ends [23]. Within each heterodimer, α-tubulin is on the negative end of the microtubule while β-tubulin is on the positive end. The elongation of microtubules takes place from nuclei, the gamma-Tubuline Ring Complex (γ-TuRCs) located at the Microtubules Organizing Center (MTOCs) [24]. These nuclei, visible in electron microscopy, are ring-shaped structures with a diameter similar to that of microtubules. Also these nuclei contain a particular tubulin, γ-tubulin, on which microtubule nucleation depends [25].

I.2.2 Dynamical behavior of microtubules

Microtubules are highly dynamic structures [26]. In vitro, there is an addition of tubulin at both ends but the addition of tubulin at the positive end is much faster than at the negative end. In vivo, the negative end is stabilized.There is a flow phenomenon towards the negative end, with microtubules tending to lose tubulin dimers at the negative end while gaining them at the positive end [27]. This resulting in

a flow of tubulin from the plus end of the microtubules towards the minus end. Thus, the microtubule maintains a relatively constant position and size [27]. The equilibrium between the addition and loss of tubulin at both ends of the microtubules has for consequence the alternation between polymerization and depolymerization phases. This process, known as dynamic instability, is an intrinsic property of microtubules. It is characterized by four parameters whose two velocities and two frequencies notably, the speed and the frequency of polymerization and, the speed and the frequency of depolymerization [28]. The necessary energy for this dynamic instability comes from the hydrolysis of Guanosine Triphosphate(GTP) on tubulin during microtubule assembly. This hydrolysis is not essential for polymerization, but it is necessary for destabilization [28]. The transition from a polymerization phase to a depolymerization phase is called a catastrophe, while the transition from a depolymerization phase to a polymerization phase is called rescue [28]. In vivo and In vitro observations are complementary. There are also so-called pause phases during which neither polymerization nor depolymerization of the microtubule occurs [29, 30] (see Figure 2). Each tubulin has a GTP binding site, these sites are called N

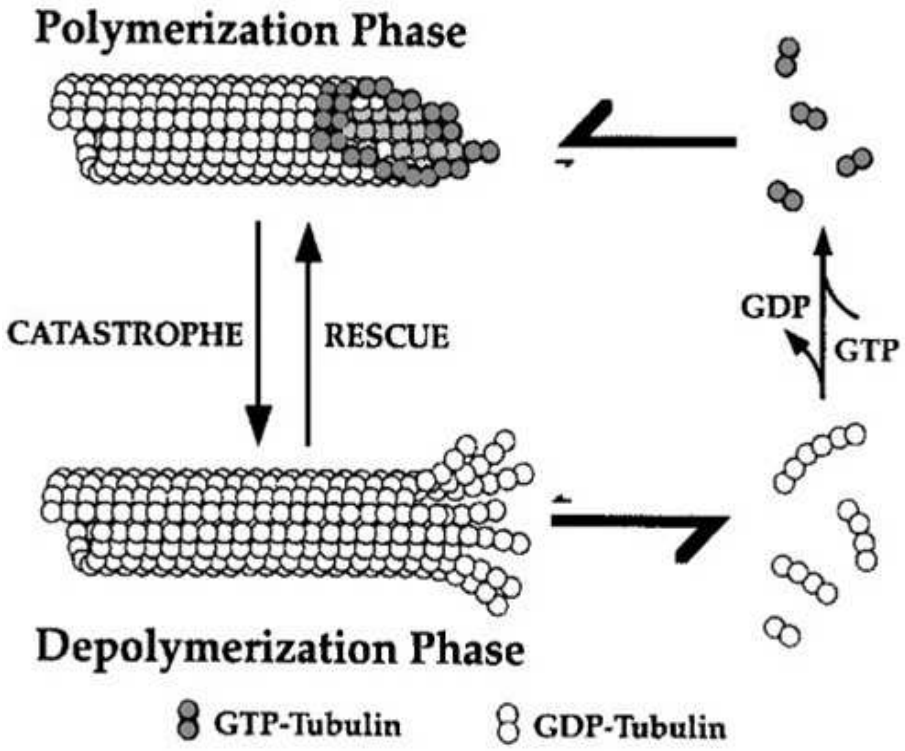

Figure 2: Dynamic properties of MTs: dynamic instability is characterized by the coexistence of polymerizing and depolymerizing MTs [28].

and E for α-tubulin and β-tubulin, respectively. The N site of α-tubulin is buried at the interaction zone between the two subunits of the heterodimer making the GTP bound to this site non-exchangeable and non-hydrolysable [31]. In contrast, the E site of β-tubulin is exposed when there is no interaction with α-tubulin of another heterodimer, so its GTP is exchangeable but only dimers with β-tubulin bound to GTP are competent for polymerization [32, 33]. Upon interaction with another heterodimer, the GTP of the E-site is hydrolyzed to Guanosine Diphosphate(GDP) [34]. Microtubule growth and GTP hydrolysis are thus coupled. Following the hydrolysis of GTP to GDP, a rearrangement of the tubulin

structure takes place, which generates constraints in the dimer. These constraints are released during depolymerization, causing the passage from a straight to a curved structure of the heterodimer [28,35]. The body of microtubules is mainly composed of GDP-bound tubulin but the presence of a GTP coif at the (+) end forces the maintenance of the straight structure of heterodimers. Loss of this GTP coif leads to catastrophe events during which the profilaments adopt a curved structure and thus detach from the microtubules and depolymerize [36].

I.2.3 Microtubule Associated Proteins

The Microtubules dynamics In vivo have higher polymerization rates than those observed In vitro. This implies more frequent alternations between growth and decreasing at the ends [36]. These differences are due to the presence in the cell, the proteins (i.e. the Microtubules Associated Protein) regulating nucleation as well as internal and external signals, which modify both the dynamics and organization of the microtubule cytoskeleton.

I.2.3.1 Regulatory proteins

The proteins that act on microtubule dynamics are regulated via their availability during the cycle, their localization, and for some their phosphorylation state [37]. These Microtubules Associated Protein (MAPs) are found along the microtubules as well as at their extremities where they play a role that can be stabilizing or destabilizing. Among the non-motor MAPs, we can mention: Mitotic Centromere-Associated Kinesin (MCAK), which stabilizes the curved shape of dimers and thus facilitates the disassembly of microtubules by hydrolyzing Adenosine Triphosphate (ATP) [38]; MAP1, MAP2, MAP3 proteins that bind laterally to microtubules and stabilize them; and Tau protein, which stabilizes the microtubules in axons. In addition to GTP hydrolysis and association with other proteins, a large number of post-translational modifications (acetylation, tyrosinylation/detyrosinylation, polyglutamylation, polyglycylation,) influence microtubule dynamics. These modifications are often found in cilia and flagella and in some cases in axons and are generally associated with stable microtubules [39].

I.2.3.2 Motor proteins

Motor proteins play a cargo role in the cell [40]. They are essential for intracellular trafficking, the best example of this function being the transport of neurotransmitters along the axon of neurons. Motor proteins are also involved in the positioning of organelles and the positioning of mitotic chromosomes. Microtubules are a kind of highway of the cell on which motor proteins can move in an organized manner (see Figure 3). Depending on their direction of movement, motor proteins can be classified into two main categories: kinesins, which mostly move towards the (+) end of microtubules, and dyneins, which move towards the (-) end of microtubules [41]. The energy for the movement of motor proteins along the microtubules is provided by the hydrolysis of ATP [42]. The movement of motor proteins along mi-

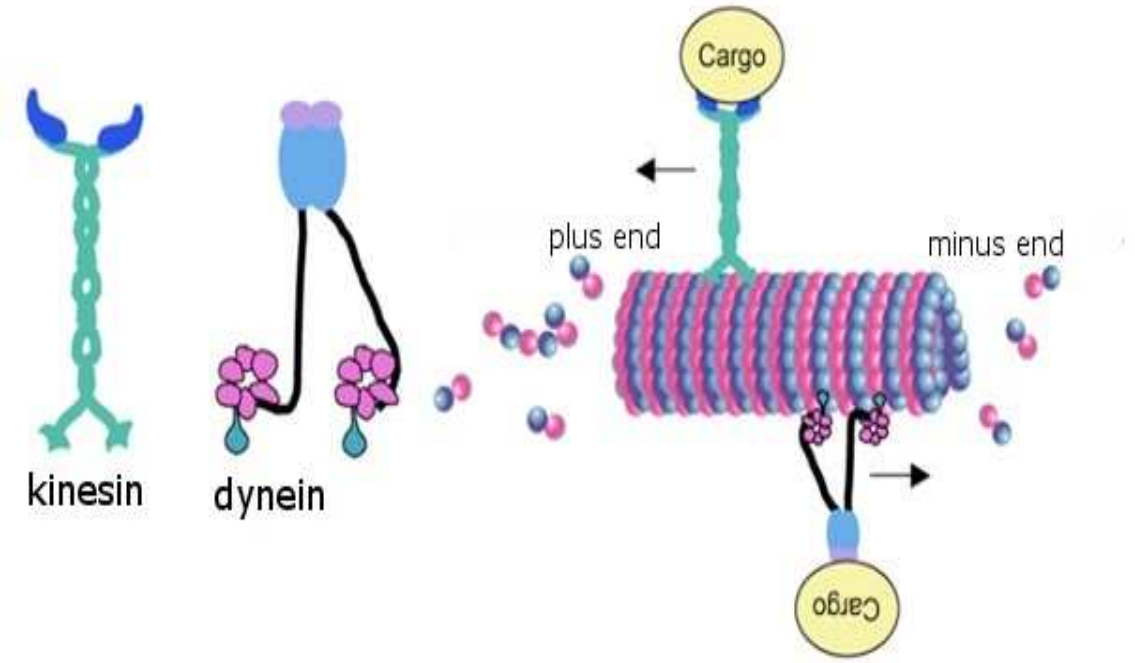

Figure 3: Typical kinesin and dynein bounds to a microtubule: Movement anterograde mediated by kinesin, motor activated by ATP, on guides microtubular and movement retrograde by dynein [40].

crotubules is largely favored by 13-symmetry, which allows for straight protofilaments, so that a motor protein always remains on the same side of the microtubule during its movement. The transport performed by kinesin is anterograde while that of dynein is retrograde (see Figure 3). Motor proteins also play a role in the formation and stability of the mitotic spindle. They exert forces on the microtubules, allowing them to slide relative to each other, and to form and maintain a bipolar spindle. Dyneins are also essential for the movement of cilia and flagella. Their action will cause the microtubules to slide locally relative to each other, resulting in the bending of the cilium or flagellum [43].

I.2.4 Functions and neuronal microtubules

I.2.4.1 Neuron

Neurons are the basic cells of the nervous system. These nerve cells are responsible for the reception and transmission of nerve impulses and form long, interconnected fibres [44]. They are composed of a cell body or soma which contains a nucleus, an axon and one or more dendrites(see Figure 4) [45]. Depending on the information or messages the neurons receive, they are able to emit electrical signals, propagate them along the axons and transmit them to other cells. Neurons have the property of being excitable and if stimulations are of adequate intensity, the cell responds by developing a bioelectric signal called an action potential [46]. The neuron is able to propagate this and conduct it along the axon to the end of its extensions. This excitation is transmitted to the post-synaptic cell elements, which gives neurons the property of conductivity [47]. In most non-neuronal cells, MTs are nucleated from an organizing centre called the centrosome. Their negative ends are anchored at the centrosome while their positive ends radiate throughout the cytoplasm (see Figure 4). The same is true in undifferentiated

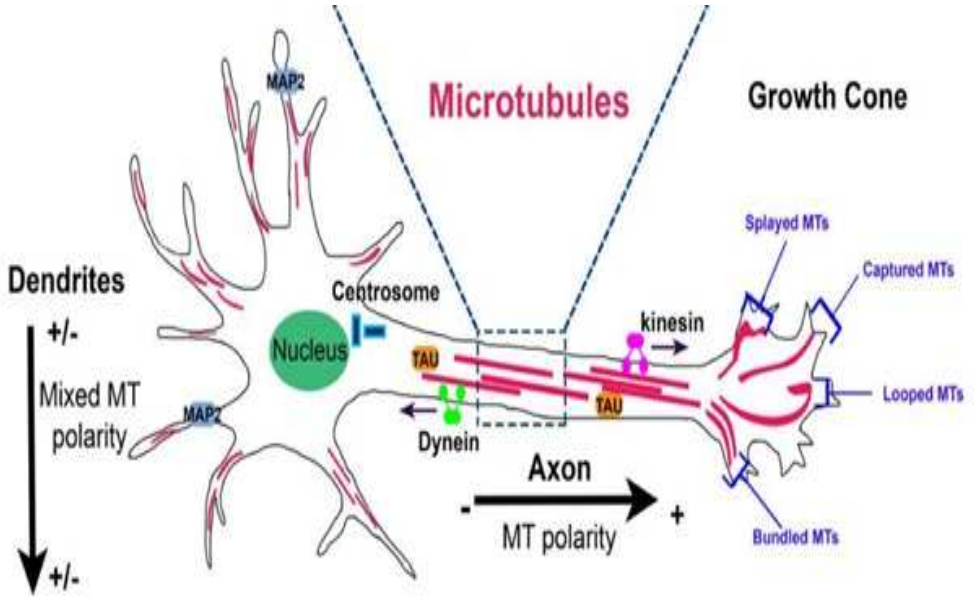

Figure 4: Microtubule organization in neurons. MT organization is tightly regulated in the different neuronal compartments. In axon, MTs form stable, polarized bundles with uniform polarity orientation, exposing their plus minus ends away from the cell body. In proximal dendrites, MTs are organized in antiparallel bundles oriented with their plus ends pointing away or toward the soma. In the growth cone, MTs adopt four characteristic distributions: splayed, captured at the cortical matrix, looped, and bundled. At the top, MT structure (slide view and end view) is shown [45].

neuronal cells. In differentiated neuronal cells, MTs are no longer anchored at the centrosome [48, 49]. They are nucleated at the centrosome but are then transported into the neuritic extensions. Neuritic MTs are indeed highly organized: in axons, their negative end is located at the cell body and their positive end points to the axon terminal. But in dendrites, MTs are oriented in both directions [50]. It has been shown that the positive end of some axonal MTs can serve as a relay nucleation centre [51]; MTs cannot be continuous throughout the axon. The MAP2 and tau proteins are found exclusively in neuronal cells and participate, among other things, in the determination of dendritic and axonal structures respectively during development(see Figure 4). Both proteins stabilize microtubules, which promotes the addition of tubulin polymers, thus accelerating microtubule growth [52].

I.2.4.2 Essential functions of microtubules

Thanks to their dynamic assembly-disassembly properties and their ability to interact with many cellular factors, microtubules participate in essential eukaryotic functions such as motility, intracellular trafficking and cell division [53]. Microtubules also play an important role in neuronal functions, including consciousness and memory mechanisms. Several research studies in biology and even biophysics show that MTs are responsible for the maintenance and morphological variation of the cell. They are involved in intracellular trafficking by forming real rails along which motor proteins move and transport various organelles and vesicles. They are also essential for cell division, during which they form a complex and dynamic bipolar structure (the mitotic spindle) necessary for the correct segregation of chromosomes during mitosis [54]. This mitotic spindle consists of two symmetrical and

antiparallel arrays of microtubules, one end of which interacts with the chromosomes and the other is anchored at both poles. After breaking the nuclear envelope, the chromosomes are captured by the microtubules and oscillate between the two poles, before positioning themselves on the equatorial plate in metaphase [55].

MTs also have very important neuronal roles. The mechanisms of consciousness and memory involve nerve cells. MTs play a major role in the growth of neurons and the maintenance of their asymmetric morphology, but also have key structural and motile roles in transport within the cytoplasm of these nerve cells and in the development of their extensions [56]. This multitude of functions is explained by the dynamic and structural properties of microtubular networks. Neuronal growth is highly dependent on the behaviour and dynamics of MTs, because are found in axons and dendrites. During neuronal development, the neuron becomes polarized when one of its extensions accelerates its growth to become an axon. This axon and the others (dendrites) have a growth cone at the end. The polarity of the neuron is an important feature in establishing the morphological and functional difference between the two types of neuronal extension [57]. In axons, MTs are all oriented parallel with their positive end towards the growth cone, whereas in dendrites they are randomly oriented in both directions [58].

In axons, MTs are all oriented parallel with their positive end towards the growth cone, whereas in dendrites they are oriented in both directions, in a random fashion [58]. In the neuron, the microtubular network serves as the rails on which the molecular motors (dynein and kinesins) will specifically associate to allow the transport of cargo vesicles from the cell body to the axon tip or vice versa. MTs are also important for the transport of vesicles between the endoplasmic reticulum and the Golgi apparatus [59]. they also play a role in maintaining the organization of organelles such as the Golgi apparatus.

I.2.5 Pathologies linked to the dysfunction of neuronal microtubules

The nervous system performs multiple functions during its dynamics and which have repercussions throughout the body. The latter can fail in many conditions. An alteration of the nervous system can lead to quite serious complications. Because the nervous system remains essential to the proper functioning of the body of a living being. Neuronal degeneration includes several pathologies such as Alzheimer's, Parkinson's disease, multiple sclerosis, etc [60]. These diseases are becoming increasingly common in our environment and are generally age-related [61]. Indeed, as we age, we expect a decline in intellectual faculties and memory, but in neurodegenerative diseases, this decline is much more rapid than normal. Among the causes of these diseases, a malfunction of the MTs could be cited. Since the MAP proteins (MAP2 and Tau) are effectors that stabilize MTs and thus promote normal neuron development, a link has been shown to the function of the tau protein in Alzheimer's disease [62]. In the nervous tissue of Alzheimer's patients, tau forms abnormal aggregates, characterized in most cases by hyper-phosphorylation of the protein [62] (see Fig. 5)). Their massive detachment from microtubules greatly reduces the stability of the latter along the axon. This observable aspect, characterized by microtubule instability, is thought to be one of the main causes of the disease symptoms [63].

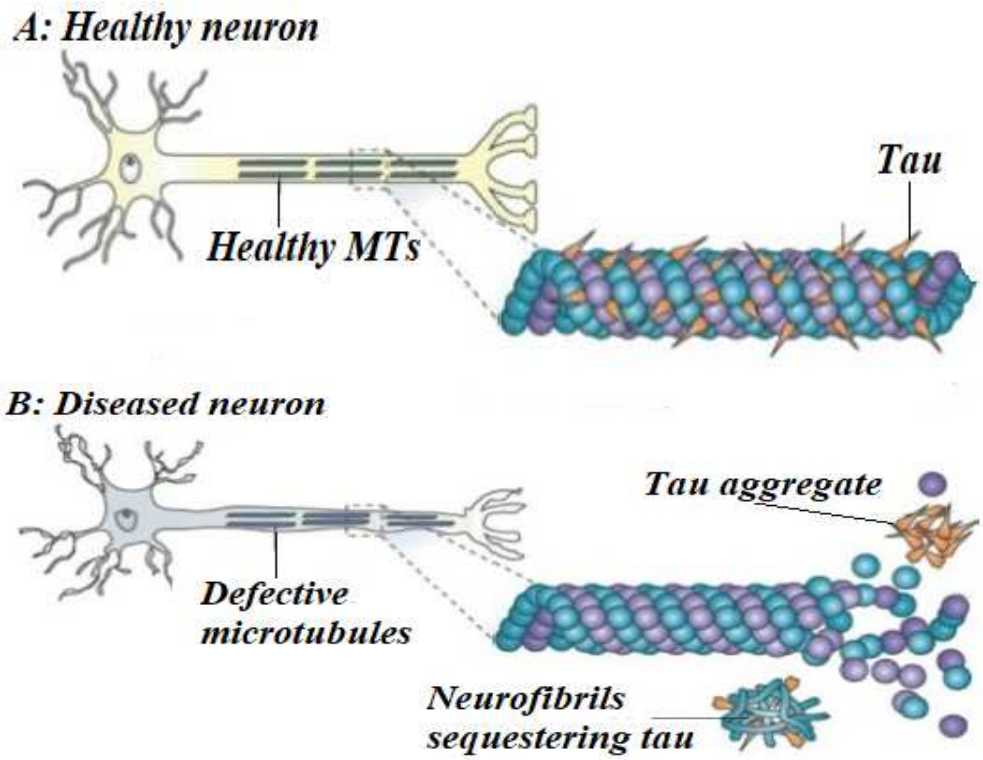

Figure 5: Morphology of healthy microtubules compared with that of microtubules in Alzheimer's disease. (A) Tau facilitates microtubule stabilisation and is abundant in the neuron axon. (B) Tau function compromised by neurofibrils and Tau detachment from microtubules by destabilising them [62].

It is important to mention here that biologists, and mainly physiologists, have done enormous research to explain the dynamics, interactions and functions related to MTs in eukaryotic cells of living beings. In the same way, the mathematical physics models will emerge for further explanation.

I.3 Mathematical models of microtubules

New tools for understanding the nonlinear movements of MTs, just as interesting and linked to the performance of their multiple tasks, were developed by biophysicists from 1993 onwards. These are mathematical models with parameters that are physically manipulable and biologically significant.

I.3.1 Original model of microtubules

This model was established about 30 years ago by Satarić and his collaborators [11]. It represents the basic structural model. It has been improved over time and several others have followed with the common aim of exploring in depth the nonlinear dynamics of MTs. Biological systems in general, and MTs in particular, have a high number of degrees of freedom. To reduce this number of degrees of freedom and be able to better manipulate the model equations, the idea came from the work of Frôhlich [64], in which he studied regular oscillators of coupled dipoles interacting through resonant (i.e. frequency-specific) forces. The basic argument presented in starting Satarić's model is that the MT system has a strong uniaxial dielectric anisotropy. This can allow the MTs dipolar oscillator network to be effectively described by reducing the number of degrees of freedom [11]. Thus this Satarić source model assumes

only one degree of freedom per movement of the dipolar dimer in the PF. A generalized coordinate u_n used is the projection of the top of the dimer likely to rotate with respect to the direction of the PF (the axis of the MT cylinder) at a position n. Since the longitudinal projection of the dimer displacement interacts with the rest of the lattice by a mean-field force due to an anharmonic crystal field potential, the introduction of the double-well potential model is valid [65]. The total action of the surrounding dimers on the dipole at a position n is qualitatively described by a double-well potential [11] as

$$V_d(u_n) = -\frac{1}{2}Au_n^2 + \frac{1}{4}Bu_n^4, \tag{1}$$

where u_n is the longitudinal displacement of the nth dimer, A and B are model parameters such that $B > 0$ and independent of temperature, while A is typically a linear function of temperature that can change sign at an instability temperature T_c, i.e. $A = a(T - T_c)$ and $a > 0$. Being an electric dipole, the dimer in the almost uniform intrinsic electric field parallel to the microtubule axis acquires the additional potential energy associated with this dipole, given by [11]:

$$V_{el}(u_n) = -Cu_n \quad ; \quad C = qE, \tag{2}$$

where q denotes the effective mobile charge of a single dimer and E is the amplitude of the intrinsic electric field. Thus the two potentials combined lead to the general potential:

$$V(u_n) = V_d\left(u_n\right) + V_{el}\left(u_n\right), \tag{3}$$

The Hamiltonian model of a PF can be given as follows:

$$H = \sum_n \left[\frac{m}{2}\dot{u}_n^2 + \frac{k}{2}(u_{n+1} - u_n)^2 + V(u_n)\right], \tag{4}$$

where the point $(\cdot)$ means the first derivative with respect to time, m is the mass of the dimer and k is the parameter of the inter-dimer interaction in the same PF. The first term of this expression Hamiltonian represents the kinetic energy of the dimer and the second is the potential energy of the chemical interaction between neighbouring dimers belonging to the same PF. By introducing the viscosity force $F_v = -\gamma\,\dot{u}_n$ (γ, viscosity coefficient) contributed by the solvent in the medium, the dynamic equation of motion obtained with the application of Hamiltonian formalism is written [11]:

$$m\ddot{u}_n = k(u_{n+1} + u_{n-1} - 2u_n) + Au_n - B{u_n}^3 + qE - \gamma\,\dot{u}_n. \tag{5}$$

For a less complex solution of equation (5), the continuum approximation $u_n(t) \rightarrow u(x,t)$ and the series expansion of $u_{n\pm1}$ are applied. After this step, a change of variable $\xi = \kappa x - \omega\, t$, with k and ω as constants, followed. Finally the use of the dimensionless function $u = \sqrt{\frac{A}{B}}\,\psi$ and some considerations between the parameters allowed the authors to obtain the final nonlinear ordinary differential equation

in the form:

$$-\psi'' - \rho\psi' - \psi + \psi^3 - \sigma = 0, \tag{6}$$

where $\sigma = \frac{qE}{A\sqrt{\frac{A}{B}}}$, $\psi' = \frac{d\psi}{d\xi}$ and $\rho = \frac{\gamma\omega}{A}$, with $\omega^2 = \frac{k\ell^2\kappa - A}{m}$. Solving equation (6) led to a kink-type solution shown in Fig. 6. The required parameters of this first model were estimated using available experimental data [66]. The main result obtained, which is a kink-type excitation that can propagate with a single velocity within the given range of parameters, is proportional to the modulus of the electric field E [67]. Satarić et $a\ell$ predicted that these excitations could be observed experimen-

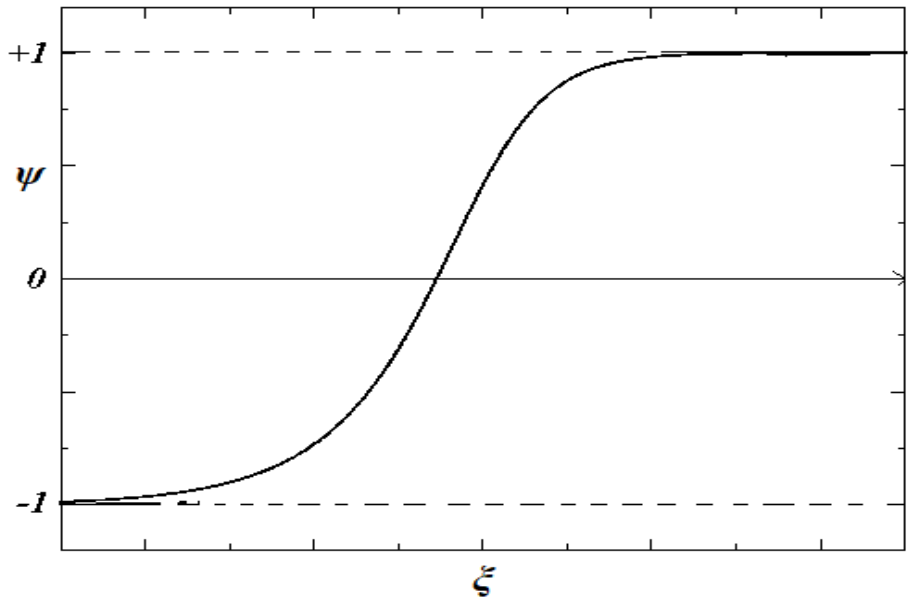

Figure 6: The kinklike excitation : A solution of Eq.(6) [11].

tally, for example, by neutron scattering and polarization experiments [68, 69]. The authors say that kink solitons are not easily formed, but they are solutions of the equation describing motion with a fairly considerable amount of energy. So, in the immediate vicinity of the critical temperature T_c, these excitations can easily take shape [70]. However, because of their topological stability, they are not easily destroyed once they are formed either. The creation of kinks could also be stimulated by the release of a good amount of energy produced, for example, during the hydrolysis of guanosine triphosphate. Thus at normal concentrations of existing GTP molecules, kink excitations are expected to be generated, as a consequence of the conformational change of these molecules. It is also mentioned that the kink propagation obtained would distribute the energy of hydrolysis to the preferential end of an MT and that this energy would be used to detach the dimers. This is a picture in line with a hypothesis put forward in a paper by Krischner and Mitchison [71], stating that the rate of polymerization is limited in principle only by the rate of diffusion of the monomer subunits in the MT polymer (i.e. by the concentration of the constituent monomers in solution). As a result, and with the elongation of MTs, the propagation of kinks becomes an important new factor and introduces disassembly at the negative end, the speed of which will be proportional to the rate of excitations arriving per unit time at the negative end. It

has also been shown that kinks can be totally reflected by an attractive impurity (MAP binding point) from the lattice in the MT structure if their velocities are within specific resonance velocity ranges [72]. Consequently, if the velocity of the excitations is within such a range, the rate of arrival of excitations at the negative end will decrease or even stop as the number of MAPs increases. This can lead to a significant reduction in the rate of MT disassembly. This is a mechanism that could offer a number of interesting possibilities for the transmission and storage of information.

This was a first step towards quantitative modelling of the behaviour of microtubule structure. Subsequently, other more improved models were developed.

I.3.2 U-model of microtubules

As mentioned above, this model [12] improves on the source model with the presence of an important parameter. It also assumes only one degree of freedom per tubulin dimer. This refers to the longitudinal displacement of a dimer occupying a position n along the PF and also referred to as a U_n [12]. For more precision, the U-model is based on an angular degree of freedom, but the U_n-coordinate is a

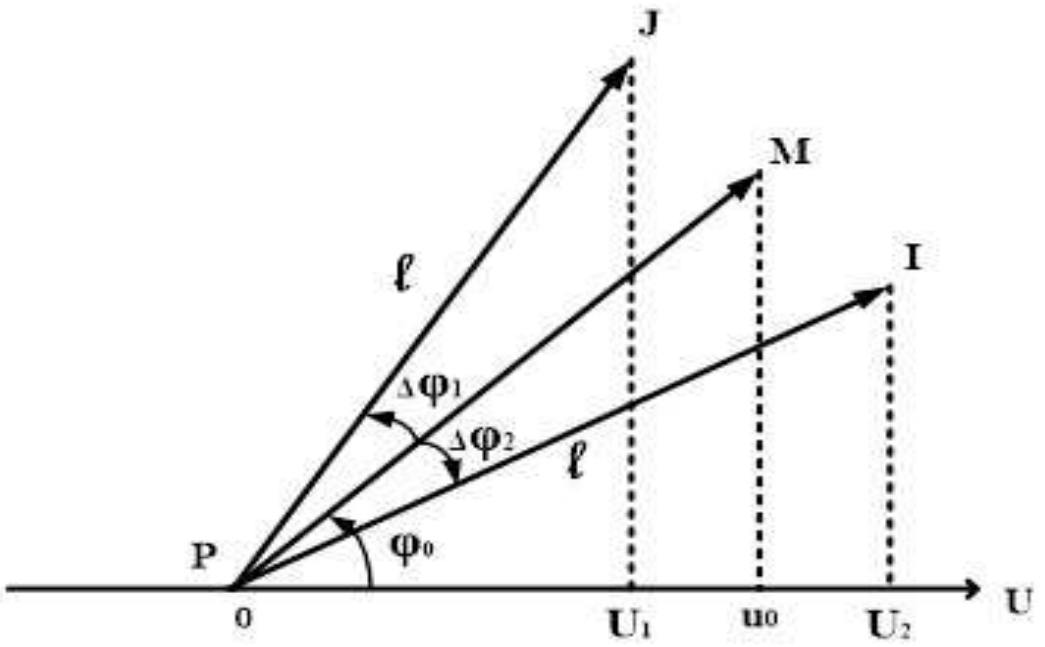

Figure 7: Scheme of demonstration of the U-model of MT [13].

projection of the top of the dimer onto the PF direction (see Fig. 7). On this figure, we can see that a *U*-coordinate belongs to the PF direction. An angle between the PF direction and a ground reference state of the PM dimer is φ_0(see Fig. 7). The tubulin dimer performs angular oscillations from the PI to PJ direction and the projection of its tip belongs to the interval $U_1 < U < U_2$ [13]. The same explanations as for the original Satarić model, lead to the following identical Hamiltonian:

$$H = \sum_n \left[\frac{m}{2}\dot{u}_n^2 + \frac{k}{2}(u_{n+1} - u_n)^2 - \frac{1}{2}Au_n^2 + \frac{1}{4}Bu_n^4 - Cu_n \right], \tag{7}$$

Identical transformations and calculations already introduced in the previous sub-section are also applied here and easily lead to the following ordinary nonlinear differential equation:

$$\alpha\psi'' - \rho\psi' - \psi + \psi^3 - \sigma = 0, \tag{8}$$

where $\sigma = \frac{qE}{A\sqrt{\frac{A}{B}}}$, $\rho = \frac{\gamma\omega}{A}$ and $\alpha = \frac{m\omega^2 - kl^2\kappa^2}{A}$ It is clear from the comparison of equations (6) and (8) that for $\alpha = -1$, both are equal. It is therefore clear that this approach is improved and is more general. In this model, the interesting fact is the calculation of the value of the parameter α. This parameter is very useful because it allows to understand the physics behind Eq.(8) and its solutions [12].

The parameters ρ and σ were treated as an input in order to determine the values of the dynamic parameters of the system, including α. Using the Modified extended tanh-function method [13], the

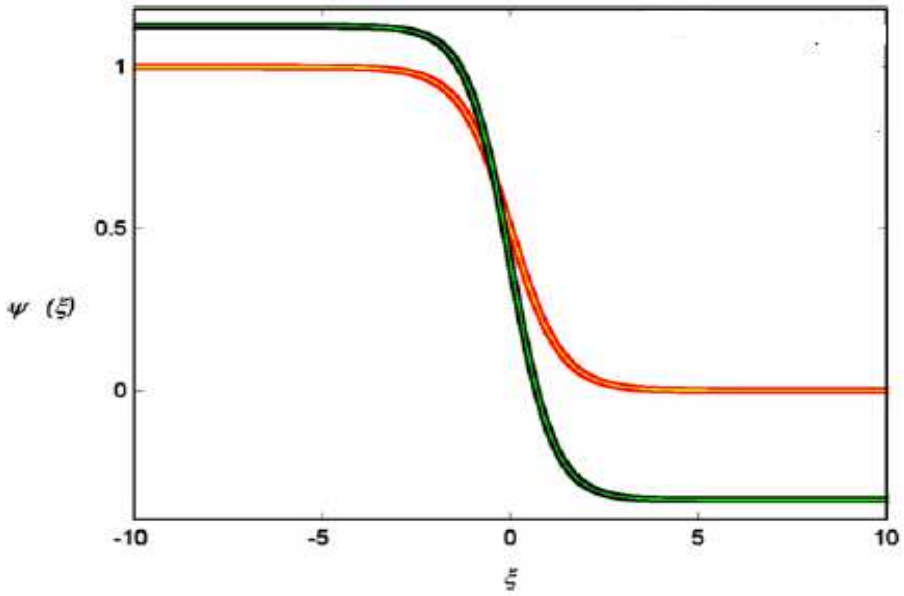

Figure 8: Analytical antikink soliton solutions with $\rho = 1$ for respectively, $\sigma = 0$ (red line) and $\sigma = 0.3$ (green line) [12].

authors found that the final analytical result obtained from equation (8) for the motion of the tubulin dimer depended only on the parameters that determine the values of ρ and σ. This analytical result is shown in Fig. 8, for two values of the σ parameter and for $\rho = 1$ [13]. This is clearly an antikink soliton whose width is plausibly proportional to the viscosity. It was pointed out that α should be negative, indicating strong chemical bonding between neighbouring dimers in PFs [11]. Numerical experiments were also carried out and one of the best results is given in Fig. 9, for the α parameters for which the analytical procedure did not give solutions [12]. Thus, the authors established that, as the α parameter multiplies only one derivative in equation (8), it does not influence the asymptotic solutions determined by σ. Secondly, for small absolute values of α, the antikink soliton is narrow and has a shape similar to the tanh function. This would mean that the transition between the initial position and the final position of the tubulin dimer is rapid and regular. On the other hand, for a large absolute value of α, the dimer undergoes oscillations before stabilizing at the final value. We also noticed that

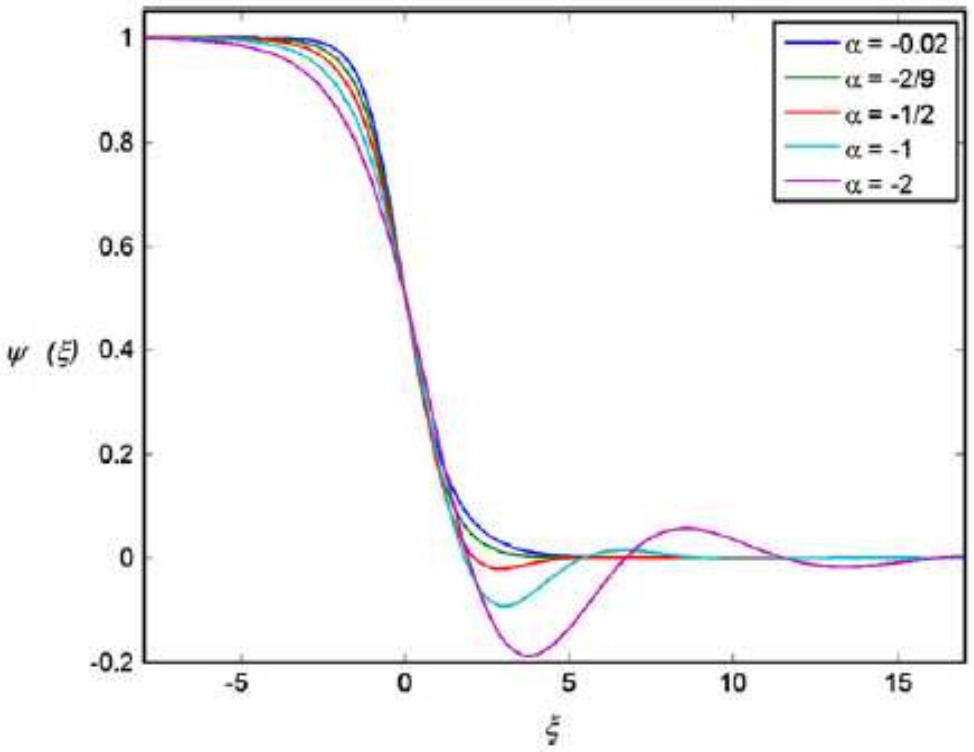

Figure 9: Numerical antikink soliton solutions with $\rho = 1$, $\sigma = 0$ for different values of α. [12].

the period and amplitude of the oscillations increased with absolute value of α. These results indicate that there is an optimal parameter α for a given process to occur and, in this case, the dynamics of the MT is described when the system is at the minimum of the potential well. It has been suggested that the antikink soliton acts on the actual direction and sense of transport of cellular cargoes via motor proteins [73]. In other words, the cell compartment requiring a specific cargo would initiate the antikink excitation obtained, sending it as a signal along the nearest MT, which would activate the appropriate transport motor [74, 75] and the delivery would be made to the intended destination. Depending on the chosen coordinates describing the dimer oscillations, another basic model has been introduced. The radial model [14] and called φ-model which we will define in the next subsection.

I.3.3 φ-model of microtubules

The previous model describes the longitudinal dynamics of a single PF due to the fact of that, the interactions between dimers of the same PFs are stronger than those between dimers of different PFs. And thus, a dependence on the electric field strength E would completely disappear. But in reality, these interactions between dimers of different PFs must be taken into account with great precision. For a better understanding of the matter, the expression of the potential energy $-Cu_n$ in the U-model [12] did not take into account the distance d (see Fig. 10) between the centres of the positive and negative charges inside the dipole. To solve this problem, a new model is introduced. This model is called φ-model [14], in which the degree of freedom is still angular, but the φ-angle coordinate is an angular displacement in the radial direction of the considered dimer with respect to the direction of the electric field $\vec{E} = \vec{E}_1 + \vec{E}_2$ [14]. This means that the influence of dimers of different neighbouring PFs is taken

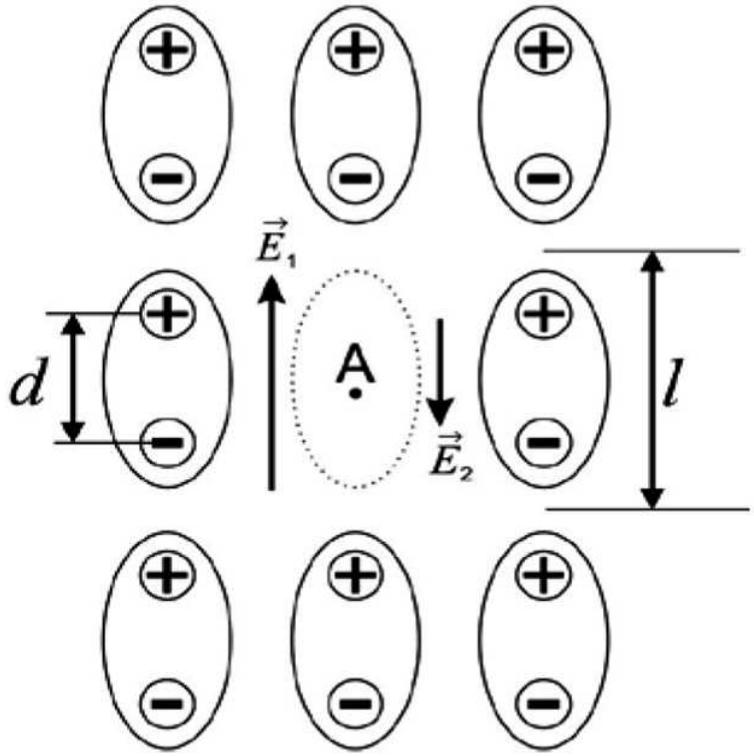

Figure 10: A segment of three protofilaments (PF1, PF2 and PF3, from left to right) with the fields $\vec{E_1}$ and $\vec{E_2}$ in the point A, arising from the same protofilament PF2 and from the neighbouring PFs, respectively. The dipole moment p of the tubulin dimer has the displacement of the opposite charges depicted with d [14].

into account through the $\vec{E_2}$ field as it comes from these neighbouring PFs. This is very significant in this model because the $\vec{E_1}$ field acquires a large value due to those of the electric dipole moment $\vec{p}$ and the dimension ℓ (see Fig. 10). As a logical consequence, the $\vec{E_2}$ field, being in the opposite direction to $\vec{E_1}$, decreases the value of the $\vec{E}$ field. The dipole potential energy of a dimer in this case is given by the relation:

$$U = -\vec{p} \cdot \vec{E}. \tag{9}$$

The expression of the Hamiltonian of a single PF will be:

$$H = \sum_n \left[\frac{I}{2}\dot{\varphi}_n^2 + \frac{k}{2}(\varphi_{n+1} - \varphi_n)^2 - pE + pE\left(\frac{{\varphi_n}^2}{2} - \frac{{\varphi_n}^4}{24}\right)\right], \tag{10}$$

where, as in subsection above, the first two terms represent the kinetic energy and the potential energy of chemical interaction between dimers belonging to the same PF respectively. With I the moment of inertia of the dimer, k the inter-dimer interaction constant in the same PF [76]. Considering the viscosity force by a moment $M_\varphi = -\Gamma\dot{\varphi}$, with Γ the viscosity coefficient, we obtain the following dynamic equation of motion:

$$\alpha_\varphi \psi'' - \rho_\varphi \psi' + \psi - \psi^3 = 0, \tag{11}$$

where $\varphi = \psi\sqrt{6}$, $\alpha_\varphi = \frac{I\omega^2 - k_\varphi l^2 \kappa^2}{pE}$ and $\rho_\varphi = \frac{\omega\Gamma}{pE}$.

The α_φ parameter measures the predominance between the rotational kinetic energy of the tubulin dimer and its potential energy of interaction with other adjacent chemically bound dimers. These quantities are further balanced by the modulus of the intrinsic electric field E effective [14]. The flexi-

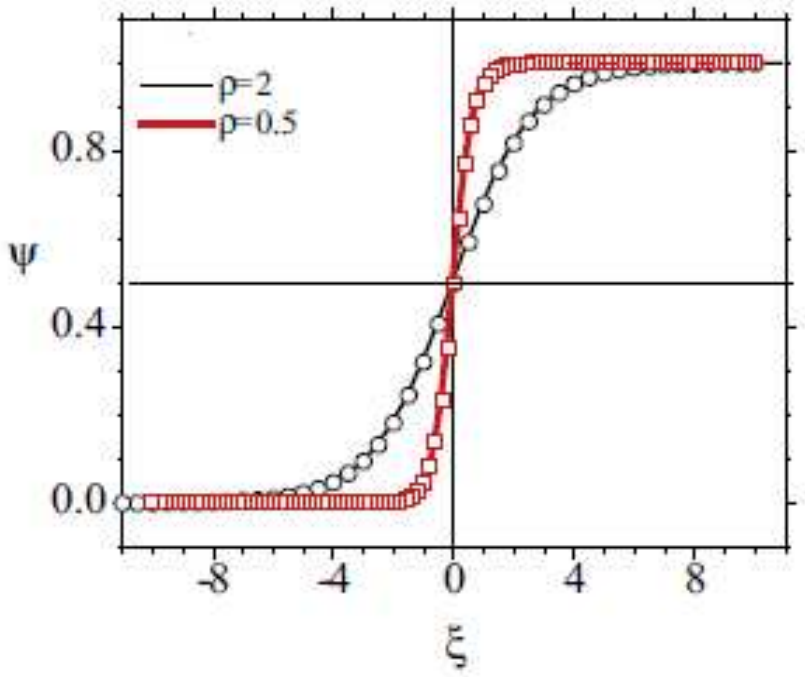

Figure 11: The analytical (solid lines) and numerical (dots) kink-solutions of Eq.(11) for $\rho_\varphi = 0.5$ and $\rho_\varphi = 2$ [14].

bility of the chemical bonds and the strong increase in the kinetic energy of the dimer [77], caused by a release of energy produced by the hydrolysis of GTP, leads to a positive value of the α_φ parameter [78]. This means that kinetic energy should predominate, but the presence of an additional dipolar potential would be sufficient to prevent PF degradation when such excitation is away from the ends of the MT. This fact indicates that dipolar potential energy would play a crucial role in stabilizing PFs and thus sustaining polymerization. Determination of the values of the ρ_φ and α_φ parameters led to very interesting results [14]. Zdravković and co-workers use two methods [79,80] to obtain the results shown in Figs. 11 an 12. These two figures show that the very complex dynamics of MTs can be explained by the existence of soliton kinks (Fig. 11) and breathers (Fig. 12) and, which would play different roles. The agreement between the analytical (solid lines) and numerical (dotted lines) solutions is observed. It is also shown that these solitonic solutions are affected by the viscosity of the physiological environment and the maximum dipole energy pE. It was suggested that the conformational angle φ would take values from zero to $\sqrt{6}$ radians. Initially, in the stable MT, all the dimers are in the right-hand configuration along the corresponding PFs. When GTP hydrolysis energy is released, torsional excitations should be created [77]. This means that the dimers rotate through the angle φ from the major axes in the radial direction. Of course, the excited dimers will soon spontaneously return to the initial stable configuration. The viscosity effects behaved exactly as expected, as even low viscosity significantly affects either

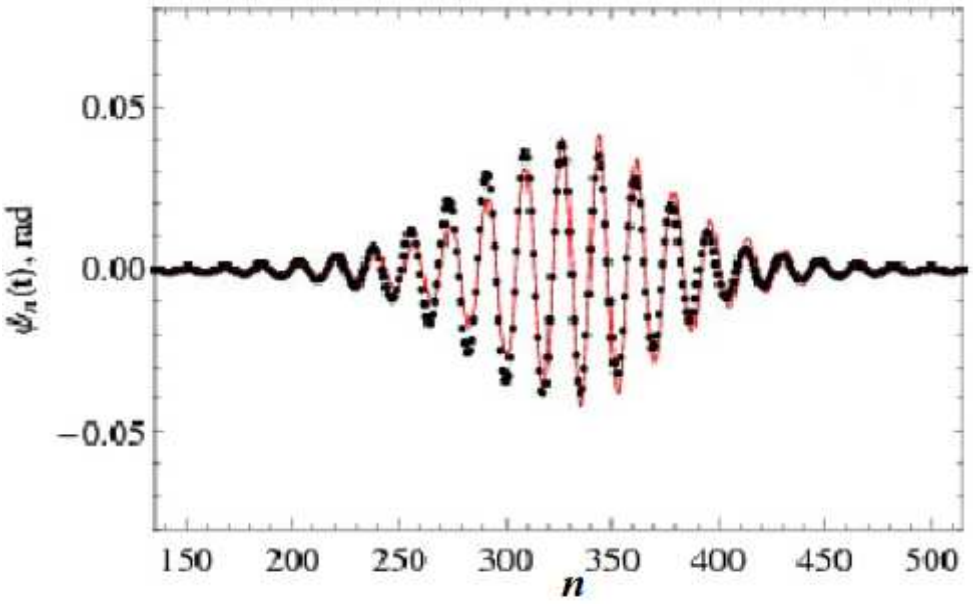

Figure 12: The analytical (thin solid line) and numerical (dots) Low-amplitude breather solutions with parameters: $\eta = 0.49$ and $\beta_\varphi = 0$ [81].

the breather amplitude or the slope of the kink soliton. The authors stated in their work that the kinks explained the collapse of the MTs [70]. As for breathers, they could be responsible for triggering the motor proteins to start moving [13]. This latter perception was supported in the context of the electrical regulation of the nervous system. This is because the speed of propagation of the breather is comparable to that of neuronal impulses in axons [82]. As the longest MTs (several mm) are located inside the axons of nerve cells, the correlation mentioned may indicate an important role for breathers and other non-linear excitations in the regulation of neuronal activity [83].

In other work, researchers have pointed out that the motion of dimers is not only angular, but also translational. This translational movement has also made a decisive contribution to the study of microtubule dynamics.

I.3.4 Z-model of microtubules

This model was introduced in the interest of studying the true translational motion of a tubulin dimer [15]. In the previous models, the dimer has one angular degree of freedom. The longitudinal projection one (U-model) and the angle φ for the φ-model, but since it can be implied that a dimer has the shape of an ellipsoid with a width of about 4 nm [84], the approach of the study should take into account more than one degree of freedom. Normally, a dimer has six degrees of freedom, three of which are angular and three translational. The real and most general study would have been to introduce a six degree of freedom model. It is clear that this would produce an extremely complicated model. For this reason, researchers have tried to understand the dynamics of MTs via only one degree of freedom per dimer. For this model, called the Z-model [15], only one degree of freedom per dimer is also assumed. In Figure 13, it can be seen that there is a longitudinal shift of $8\ell/13$ between the two neighbouring PFs [4,85]. The Z_n coordinate is nothing more than the value of this shift of the dimer at position n. It

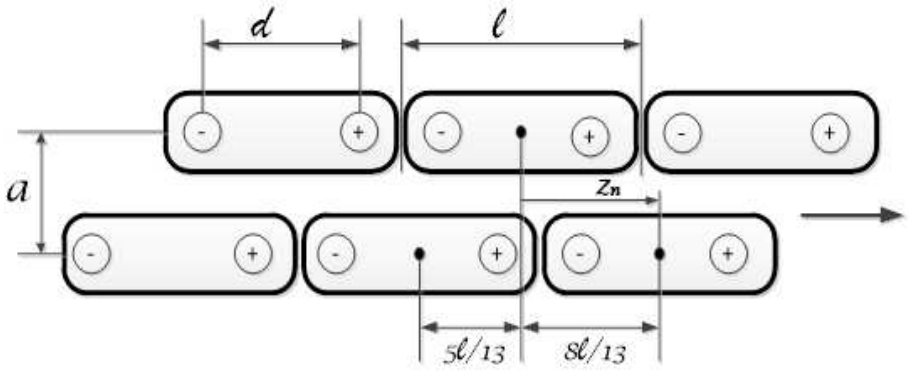

Figure 13: A segment of two longitudinally offset neighbouring protofilaments [15].

should be noted here that the fact that the bonds between dimers along the same PF are stronger than those between dimers of neighbouring PFs [34, 86] is at the origin of this study. Therefore, longitudinal displacements of dimers of the same PF would be interesting to study the nonlinear dynamics of the MT. The average influence of weak bonds with collateral PFs is described by the nonlinear double-well potential. The appropriate Hamiltonian model for a PF is [15]:

$$H = \sum_n \left[\frac{m}{2} \dot{z}_n^2 + \frac{k}{2}(z_{n+1} - z_n)^2 + V(z_n) \right], \tag{12}$$

where

$$V(z_n) = -Cz_n - \frac{1}{2}Az_n^2 + \frac{1}{4}Bz_n^4 \qquad ; \qquad C = qE. \tag{13}$$

We can see that all the terms and parameters in relation (12) where $V(z_n)$ given by Eq.(13), are exactly the same as those in relation (7) of the U-model, with the only difference that the z_n coordinate replaces u_n [13]. Except that here z_n refers to a real longitudinal coordinate along the PF-axis whereas u_n was the projection of the dimer top onto the PF direction [15]. An important advantage of the Z-model is that it allows the estimation of the electrical field strength and the total energy of the MT. The numerical and analytical treatment of the equation of motion arising from the Hamiltonian (12) allowed the authors to represent the results in Fig. 14. These particular solutions, which are also antikink solitons as in the U-model above, have asymptotic behaviour and are centred at $\xi = 0$. They were obtained for certain values of the σ parameter that affect the width and slope of the soliton. Although the working procedure remains the same as for the U-model [12], these parameter values allowed the authors to achieve other equally interesting objectives on some useful estimates in the MTs environment. According to this model, the antikink soliton would also be responsible for energy transfer along the MT. The model made it possible to estimate some very useful and important physical quantities. These are, in particular, the velocity and width of the soliton, the intrinsic effective electric field of a PF and the total energy of the MT [4, 87].

In addition to these structural atomic models, which we have presented, an equally interesting as-

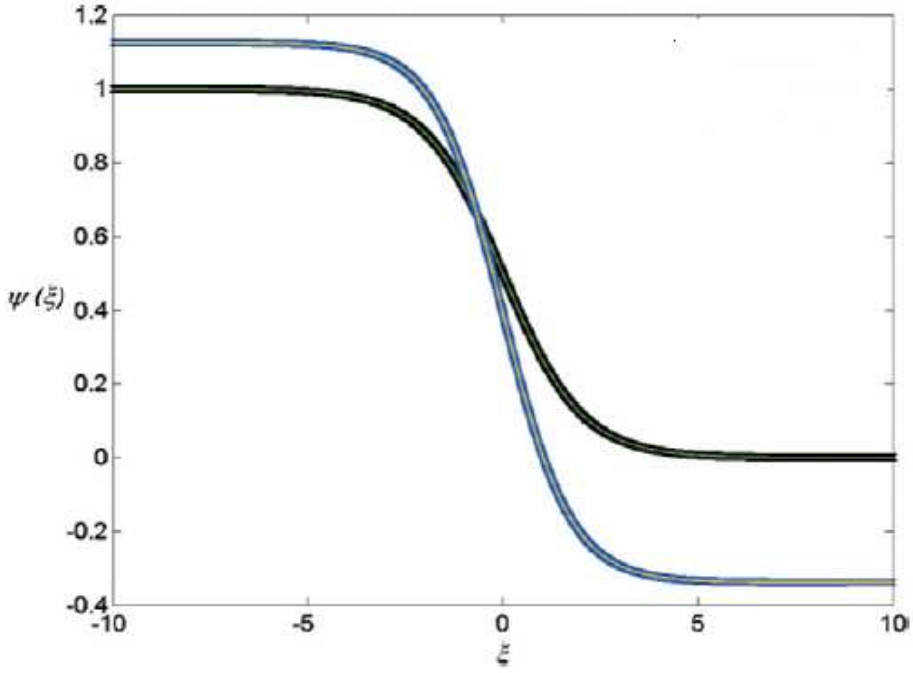

Figure 14: Antikink soliton solutions of derived equation from relation (12) with $\rho = 1.5$ for respectively, $\sigma = 0$ (black line) and $\sigma = 0.3$ (blue line) [15].

pect of the study of MTs was explored through a other model called the nonlinear electrical transmission line model.

I.3.5 The nonlinear electrical transmission line model of microtubules

Experimental observations indicate that, in addition to their well-documented structural role, MTs may play an important functional role in signalling at the subcellular level [88]. This functional role could potentially be essential for ionic conduction. The idea of examining MTs in the physiological context of polyelectrolyte characteristics was inspired by experimental and theoretical results obtained instead on actin filaments [17, 89], having almost the same behavior as MTs. The conditions enabling MTs to act as electrical transmission lines due to the ionic flow along their length have therefore been established. In view of the many observations made, a model was developed in which each basic element of the MTs is considered to be an electrical portion with capacitive, inductive and resistive characteristics presented by Fig. 15, has emerged. On the basis of Kirchhoff's laws, a discrete nonlinear partial differential equation of an elementary MT ring is established and analyzed [88]:

$$\begin{aligned} \mathrm{L}\frac{d^2}{dt^2}\left[C_0\left(V_n - bV_n^2\right)\right] &= V_{n+1} + V_{n-1} - 2V_n - r_1 C_0 \frac{d}{dt}\left(V_n - bV_n^2\right) \\ -r_2 C_0 \left[2\frac{d}{dt}\left(V_n - bV_n^2\right) - \frac{d}{dt}\left(V_{n+1} - bV_{n+1}^2\right) - \frac{d}{dt}\left(V_{n-1} - bV_{n-1}^2\right)\right], \end{aligned} \tag{14}$$

In this mathematical model (14), the variable capacitor has a charge $Q_n = C_0(V_n - bV_n^2)$ [88], with C_0, the constant elementary capacitance and b the nonlinearity parameter. The constant L represents the effective inductance of the nth ring chosen, r_1 and r_2 the respective longitudinal and transverse

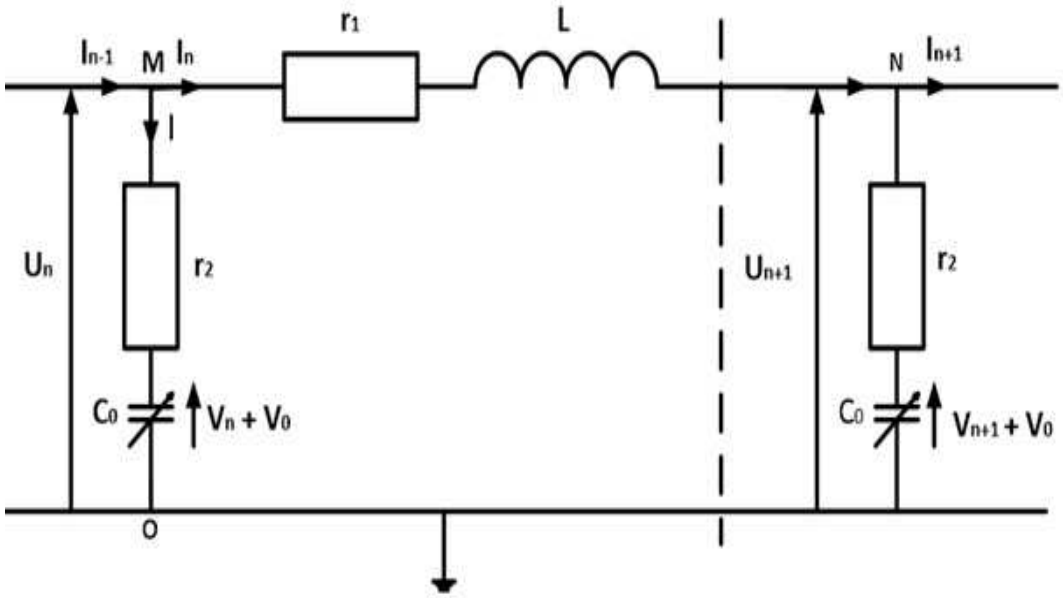

Figure 15: Schematic representation of the dissipative nonlinear electrical transmission line describing the electronic analog of the microtubule model [88].

components of the medium resistance. The potential across the capacitor of the nth elementary ring is

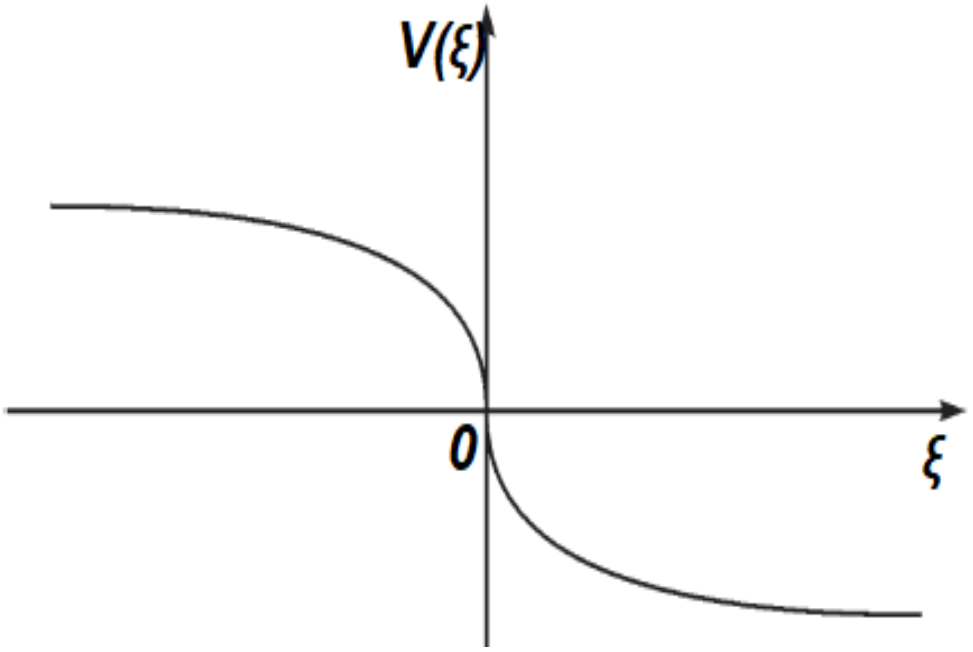

Figure 16: The antikink profile of ionic potential propagating with small velocity along MT [88].

V_n and, for the capacitors of the rings preceding and following this nth ring, the potentials are denoted V_{n-1} and V_{n+1} respectively. The charge on this elementary capacitor varies non-linearly with voltage due to the increasing concentration of counterions in the cytosol [90]. The very small positive parameter b therefore takes account of the nonlinearity in this charge. It is clearly shown that the important feature of the MT capacitance non-linearity arises naturally from the beta-tubulin tail structure [91] and the values of the r_1, r_2, C_0 and L elements have been estimated using the available experimental data and

the known MT geometry [92,93]. The second order nonlinear differential equation (14) for the electrical potential propagating along the MT was evaluated and a soliton solution, with a localized antikink front profile, is shown in Fig. 16. This profile would propagate at a speed reasonably close to the experimental results, as for example for the Ca^{2+} ion waves caused by the reticulum compartments of the endosome [94,95]. It has been shown that its antikink solitons resist well in the face of certain rates of disturbance in the biological environment [96]. At the same time, the possible impact of endogenous (intrinsic) electric fields inside the cell on the dynamics of ionic antikinks was confirmed and could modify their amplitude, frequency and phase [97].

I.4 Scope and specific problematic of the thesis

Without being exhaustive, the above microtubular models each present important points. Some of them have biophysically significant and measurable parameters (U, φ-radial and electrical transmission line models). The others, having been modeled under some parametric considerations and neglected physiological aspects, present the most fundamental properties of MTs. These include the original semi-angular and longitudinal-Z models. Among all these mathematical models, the angular-φ and transmission line models have attracted our attention, not only because their parameters are biophysically significant and experimentally measurable, but also because they have been the most widely explored in recent years. Fundamentally, they simulate the real biological behaviour of MTs in eukaryotic cells in general, including neurons. All these models give rise to nonlinear differential equations (NLDEs). In addition to the single-frequency mode nonlinear waves found as solutions of NLDEs, we also propose to look at understanding microtubule dynamics through multi-frequency mode excitations. With the very tiny size of various interacting substances in the biological environment and once the systems of coupled amplitude equations have been derived by two frequency modes, the specific concerns that arise are:

- What are the appropriate solutions of the derived systems of coupled amplitude equations?

- Assuming that the effects of viscosity (friction) are minimized, what is the impact of the intrinsic electrical field (dipole energy) of the MTs on signal propagation?

- Taking into account the intense friction, how does the transport memory constant affect the coupled excitation along the MTs?

- As the biological medium is naturally dissipative, what influence does the dissipation coefficient have on the propagation of the coupled ionic wave through the MTs?

- What are the most favorable parameter ranges for stable propagation of the constructed excitations?

I.5 Specific objectives

To answer the specific questions of our research, the analytical and numerical analysis of the mathematical models of the circumscribed physical systems is essential. So specifically, our aims are:

- To show how to arrive at the equations for amplitudes coupled by two frequency modes (CNLS, CCNLS and CCGL);

- To carry out a parametric analysis of the modulational instability of the derived coupled systems;

- To construct analytically and numerically the appropriate solutions for describing the dynamics of the MTs;

- To study the impact and behaviour of some specific coefficients on the propagation of signals in the MTs;

- And to propose biophysical and biological interpretations of the obtained results.

I.6 Conclusion

This first chapter has enabled us to understand the anatomy and physiology of MTs, with the key point being their role in the activity of cells in general and neurons in particular. Thus microtubules are important and responsible for the maintenance and morphological variation of the cell. They are essential for the transport of vesicles and organelles serving as communication between cells. These filaments are also significantly involved in neuronal functions where they ensure neuritic growth and therefore allow better transmission of nerve impulses. We then reviewed the mathematical models already introduced that attempt to explain the dynamics of MTs in their environment. Primarily the structural and electrical transmission line models. It is interesting to note that Satarić's original atomic model has been improved several times, ranging from the semi angular U-model to the longitudinal Z-model via the radial φ-model. All these atomic models present differential equations of almost the same form (the original-, U-, φ- and Z- models) but with biophysically different considerations and parameters. The electrical transmission line model, on the other hand, is better suited to the functional study of ionic conduction in the MT environment and signalling at the subcellular level. All of these models each produced biophysically acceptable results. Thanks to the geometry close to the real facts of biological environments, the ionic model and the radial φ-model particularly caught our attention. In the remainder of the work, we propose to use these two selected models to contribute not only to the description of the nonlinear dynamics of MTs in single oscillation modes, but also to add multi-mode vibrations.

CHAPTER II

MODELS AND METHODOLOGY

II.1 Introduction

In order to achieve our goal in this thesis, analytical and numerical methods for solving the equations of motion are of paramount importance. In this chapter, we present the methods used to explore the microtubule environment. Before applying some of these methods to the derivation of the coupled amplitude equations, we will first give some details of the selected models.

II.2 Developed radial and electrical line models of microtubules

This subsection is devoted to an in-depth description of the two models used in the work.

II.2.1 Precision on the developed Hamiltonian of the φ-model

In their explanation on this radial model (see Fig. 10), Zdravković et $a\ell$ [14] consider the dimer in the middle, belonging to PF2. It perceives too electric fields of the neighbouring dimers. The field $\vec{E}_1$ comes from the dimers belonging to the same PF2, while $\vec{E}_2$ is the longitudinal component of the field which originates from the dimers belonging to the neighbouring PFs (i.e. PF1 and PF3). Details about the calculations of the fields above are published in [15]. It might be noticed that PF1 and PF3, in Fig. 10, should be respectively displaced up and down in order to match the real MT structure, i.e. its intrinsic helicity. These displacements lead to a component of $\vec{E}_{2P}$ in perpendicular direction to $\vec{E}_1$. However, the component $\vec{E}_{2P}$ is not taken into account in the present model as being irrelevant for the considered degree of freedom. The tubulin dimers within PFs can perform conformational changes that may propagate along either individual PFs or small groups of PFs. The bending of PFs during disassembly of MT is the consequence of such cooperative conformations [98]. It was shown that the relative displacement of two neighboring dimers can reach 32° prior disrupting PF. In addition, the angular displacements of the monomers within a single dimer can be up to 13° [99]. These facts motivated Zdravković and co-workers to restrict his new modeling to the angular conformations of dimers φ in radial directions from the line of the dipolar electric field $\vec{E} = \vec{E}_1 + \vec{E}_2$. Therefore, the authors assume that the whole dimer rotates and the corresponding angular displacement is φ. As a whole, the different interactions taking place in the microtubule are listed as follows:

- A dimer's kinetic energy is represented by the term:

$$T(\dot{\varphi_n}) = \frac{I}{2}\dot{\varphi_n^2}, \tag{15}$$

where the dot means a first derivative with respect to time and I is a moment of inertia of the single dimer.

- The potential energy of the chemical interaction between adjacent dimers belonging to the same PF is represented by the term:

$$V = \frac{k}{2}(\varphi_{n+1} - \varphi_n)^2, \tag{16}$$

with k stands for inter-dimer bonding interaction within the same PF, which is provided by the link between the corresponding protruding loops [76].

- A dipolar potential energy of a single dimer is simply expressed as a scalar product

$$U(\varphi) = -\vec{p}.\vec{E} = -pE\cos\varphi_n, \tag{17}$$

where p is an electric dipole moment and given relation $p = q_0 d$ with q_0 represents the excess charge of the monomer within the dipole and E is the intrinsic electric field strength.. It is assumed that the inequalities $p > 0$ and $E > 0$ hold.

- The chemical interaction between the neighbouring dimers belonging to different PFs are introduced through an electric field.

Since interactions between dimers from the same PFs are stronger than the ones between dimers form different PFs, in the nearest neighbour approximation, the expression for the resulting Hamiltonian of one PF in a discrete version is:

$$H = \sum_n [\frac{I}{2}\dot{\varphi_n^2} + \frac{k}{2}(\varphi_{n+1} + \varphi_n)^2 - pEcos\varphi_n]. \tag{18}$$

Here the integer n determines the position of the dimer in the PF. The values of the parameters are: $I = \frac{5}{16}m\ell^2$ with $m = 1.8 \times 10^{-22}kg$ [100] the mass of the single dimer, $k = 0.1eV$ [81] and the electric dipole moment is $p = 1.13 \times 10^{-27}C.m$ [87]. From the Hamiltonian above (Eq.18), it is possible to obtain the following crucial semi-discrete equation describing the ideal motion of a tubulin dimer:

$$I\ddot{\varphi_n} - k(\varphi_{n+1} + \varphi_{n-1} - 2\varphi_n) + pEsin\varphi_n = 0, \tag{19}$$

where $\ddot{\varphi_n} = \frac{d^2\varphi_n}{dt^2}$. For this model, we have studied two cases: the case without taking into account the effects of the slowing down forces and the case with consideration of the impact of the interactions of the MTs evolutionary environment.

II.2.1.1 Case with minimized cytoplasmic viscosity effect

We first assume that the impact of the viscosity of the cell medium is not taken into account. Thus, after a limited third-order series expansion of the sine function in the previous relation (19), the approx-

imate equation of the nth dimer can take the following form:

$$\ddot{\varphi_n} - C(\varphi_{n+1} + \varphi_{n-1} - 2\varphi_n) + \omega_0^2(\varphi_n - \alpha\varphi_n^3) = 0, \tag{20}$$

where $C = \frac{k}{I}$, $\omega_0^2 = \frac{pE}{I}$ and $\alpha = -\frac{1}{6}$. This equation contains nonlinear terms and is a crucial equation whose solutions explains nonlinear dynamics of MTs. It is interesting to relate this analysis to nonlinear excitations. In the linear approximation, the dispersion relation for the linear vibrations of PFs can be found by considering only linear terms in Eq.(20). This is given by:

$$\omega^2 = \omega_0^2 + 4C\sin^2\left(\frac{q\ell}{2}\right), \tag{21}$$

with q being the wavelength and $\ell = 8nm$ the tubulin dimers spacing. $\omega_{min} = \omega_0$ is the lower cut-off frequency, while $\omega_{max} = \sqrt{\omega_g^2 + 4C}$ is the upper cut-off frequency. The corresponding dispersion curve is depicted in Fig. 17 , where ω_0 and ω_{max} are clearly indicated. However, ω is found to be very

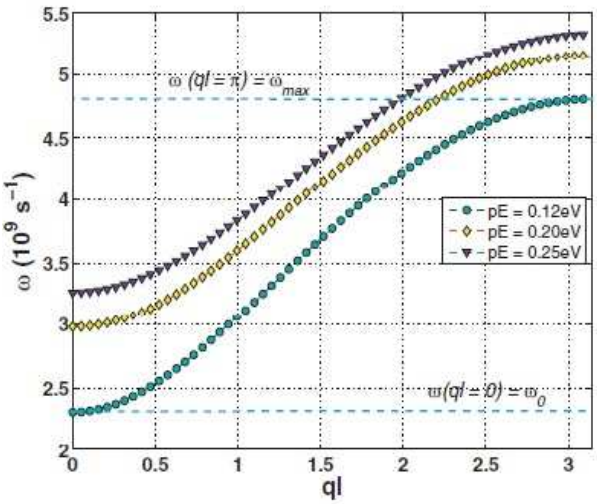

Figure 17: The panel shows the dispersion relation (21) under the influence of the dipolar energy pE .While the upper and lower cutoff frequencies are indicated, they also increase with pE.

sensitive to the variations of pE. It is in fact evident that ω_0 and ω_{max} are increasing functions of pE , which shows the importance of the dipolar potential in the dynamics of MTs. We then assume $\omega_0^2 \gg 4C$ because of the discreteness of the PF lattice. Furthermore, it has been argued that the viscous damping brought by the cytoplasm viscosity is minimized by the ion density around the MT [101], that is the reason why damping effects will not be considered in this sub-part.

II.2.1.2 Case with intense cytoplasmic dampening and transport memory effect

The semi-discrete equation (19) describes the ideal dynamics of the dimer at position n in the cytoplasmic medium without the presence of the damping brought by the MT surroundings and the effect of certain biological micro-entities on the movement of the dimers. Taking into account such effects may result in the single damping term $M_\Gamma = -\Gamma\frac{d\varphi_n}{dt}$, where Γ represents the damping coefficient or

viscosity [102]. The dynamics of the dimers at the $n-$th site in the cell, approaching reality then takes the form:

$$I\frac{d^2\varphi_n}{dt^2} - k\left(\varphi_{n+1} + \varphi_{n-1} - 2\varphi_n\right) + pE\left(\varphi_n - \frac{\varphi_n^3}{6}\right) = -\Gamma\frac{d\varphi_n}{dt}. \tag{22}$$

From the fact that tubulin dimers are very dense along microtubular PFs and have an inter-dimer distance of the order of nanometers, it is possible to switch to the continuum limit approximation [88] of the model equation. In doing so, we assume that $n\ell \to x$ and $\varphi_n(t) \to \varphi(x,t)$, with $\ell = 8$nm (the interval between two dimers of the same protofilament). The use of the generalized coordinate $\varphi\left(x,t\right) = \varphi$ and the Taylor's expansion of the discrete terms φ_{n+1} and φ_{n-1}, i.e.($\varphi_{n\pm1} \to \varphi \pm \ell\frac{\partial\varphi}{\partial x} + \frac{\ell^2}{2}\frac{\partial^2\varphi}{\partial x^2} \pm \frac{\ell^3}{3!}\frac{\partial^3\varphi}{\partial x^3} + \ldots$), in equation (22) lead to the continuous second order partial differential equation :

$$I\frac{\partial^2\varphi}{\partial t^2} - k\ell^2\frac{\partial^2\varphi}{\partial x^2} + pE\left(\varphi - \frac{\varphi^3}{6}\right) = -\Gamma\frac{\partial\varphi}{\partial t}. \tag{23}$$

Generally in biological media, solvent molecules (e.g. water) cause a low damping rate (i.e. low viscosity) in contrast to some other micro-entities, which have rather a high damping rate. These small biological particles would therefore cause a strong damping on the movement of the MTs. It is important to mention that the viscosity coefficient Γ is a parameter that allows us to quantify and control the degree of damping in the system. It should also be noted that the motion of highly damped systems, according to several investigations [103, 104], may induce the memory effects. To describe mathematically the supposedly highly damped movement of the MTs, equation (23) undergoes a series of transformations with the involvement of rescaled time and space variables. Thus, we have from Eq.(23) the following relationship:

$$\frac{\partial^2\varphi}{\partial t^2} + \frac{\Gamma}{I}\frac{\partial\varphi}{\partial t} = r_1\frac{\partial^2 v}{\partial x^2} - \omega_0^2\left(\varphi - \frac{1}{6}\varphi^3\right), \tag{24}$$

with $r_1 = \frac{k\ell^2}{I}$ and $\omega_0^2 = \frac{pE}{I}$. From the rescaled variables $t \to \frac{\omega_0^2 I}{\Gamma}\cdot t$ and $x \to \left(\frac{\omega_0^2}{r_1}\right)^{\frac{1}{2}}x$, Eq.(24) can be rewritten as :

$$e\frac{\partial^2\varphi}{\partial t^2} + \frac{\partial\varphi}{\partial t} = \frac{\partial^2\varphi}{\partial x^2} - \varphi + \frac{1}{6}\varphi^3, \quad \text{where} \quad e = \frac{\omega_0^2 I^2}{\Gamma^2}. \tag{25}$$

The expression relating the parameter e to the others of the model shows that, as the viscosity coefficient increases, the value of e decreases. Therefore, for the strongly damped limit ($\Gamma \to \infty$), e must tend to zero. So, under such considerations, the relation (25) is reduced to :

$$\frac{\partial\varphi}{\partial t} = \frac{\partial^2\varphi}{\partial x^2} - \varphi + \frac{1}{6}\varphi^3, \tag{26}$$

which represents the continuous equation for the dynamics of a dimer in a highly damped environment without transport memory effects. In this work, we consider the effect due to the high viscosity of the

cell cytoplasm in which the frictional forces interact with other forces when moving the MT protein PFs [105]. Among the frictional forces mentioned, those describing strong interactions between particles in the medium will induce memory effects on the behaviour of the MTs system under study [106]. In the context of DNA dynamics, memory effects have been considered to model the vibrational behavior of the DNA molecule in its biological environment [104]. The memory effects have been explained with advanced mathematical and computational techniques [107]. As the fractional parameter gets closer to 1, the behavior of a biological system at a particular point becomes less dependent on its previous point. However, for a small order (close to 0), the memory phenomenon becomes more noticeable and pronounced [108]. On the other hand, these memory effects were exclusively used in the Newtonian equations of motion of a strongly damped particle [109]. More recently, Guimfack et al. [110] investigated the stochastic response of fractional-order generalized biorhythmic Van der Pol oscillator subjected to delayed feedback displacement and Gaussian white noise excitation. This allowed them to bring more insights into understanding memory effects in biological systems, which is intrinsically related to introducing fractional-order derivatives, along with some inherent fluctuations that can be materialized by considering noise effects. In their work, Okaly et al. [111] also introduced memory effects directly into the Peyrard-Bishop-Dauxois model describing the propagation of nonlinear waves in DNA dynamics. They showed that transport memory effects on the dynamics of base pairs could allow physiological control of the amount of energy required to break the hydrogen bonds between the bases that make up the molecule. From by the above, the application of modern computational techniques will lead to improved model of description of our studied biophysical phenomenon. Following a similar procedure [111], we introduce transport memory by reformulating Eq.(26) in the following non-local form:

$$\frac{\partial \varphi}{\partial t} = \int_0^t f(t-\tau)\frac{\partial^2 \varphi}{\partial x^2} d\tau - \eta\left(\varphi - \frac{1}{6}\varphi^3\right), \tag{27}$$

where η is a constant known as the quadratic growth rate. It accounts for the degree of nonlinearity of the system. $f\,(t) = \gamma e^{-\gamma t}$ is the transport memory function, which describes the finite nature of the diffusion or inverse diffusion time [112, 113]. The diffusion time is the ratio $\frac{1}{\gamma}$, while for inverse diffusion it is simply γ. As the system is not purely diffusive, the function defining the transport memory is decreasing in finite time. This respects the rule that most biological systems have a finite diffusion time. Thus the decay in time indicates the time between different diffusion events [114]. The propagation equation for the rational and modulated excitations of a constant velocity particle in a medium is related to its diffusive incoherent motion by the intermediate Eq.(27). A decay characterizes the diffusion equation in the extreme limits of the parameter γ, with on one side γ tending towards zero and to infinity on the other. Note here that as a function of the diffusion time and with the constant γ taken arbitrarily, Eq.(27) describes an oscillatory motion for very small times and when the time becomes large the motion is decreasing [114, 115]. The continuous integral symbol present in this intermediate

equation (27) makes it difficult to use. Thus the general mathematical rule of calculation given by [116]:

$$\begin{aligned} l\frac{\partial}{\partial t}\left[\int_{b_1(t)}^{b_2(t)} f\left(t,\tau\right)\cdot h(x,\tau)d\tau\right] &= \frac{\partial b_2\left(t\right)}{\partial t}\left[f\left(t,b_2(t)\right)\cdot h(x,(b_2(t))\right] \\ -\frac{\partial b_1\left(t\right)}{\partial t}\left[f\left(t,b_1(t)\right)\cdot h(x,(b_1(t))\right] &+ \int_{b_1(t)}^{b_2(t)}\frac{\partial f\left(t\right)}{\partial t}h(x,\tau)d\tau, \end{aligned} \tag{28}$$

is used in differentiation to obtain the equation of the motion for the tubulin dimers in their environment with memory effect and is easily solvable. By differentiating equation (27) in time, we first obtain the following result:

$$\frac{\partial^2\varphi}{\partial t^2} = \frac{\partial}{\partial t}\left[\int_0^t f\left(t-\tau\right)\cdot\frac{\partial^2\varphi}{\partial x^2}d\tau\right] + \eta\left(1-\frac{\varphi^2}{2}\right)\frac{\partial\varphi}{\partial t}, \tag{29}$$

which, from Eq.(28) we can consider:

$$\frac{\partial}{\partial t}\left[\int_0^t f\left(t-\tau\right)\cdot\frac{\partial^2\varphi}{\partial x^2}d\tau\right] = \frac{\partial}{\partial t}\left[\int_{b_1(t)}^{b_2(t)} f\left(t,\tau\right)\cdot h(x,\tau)d\tau\right], \tag{30}$$

where, by identification, we find the expressions of some inherent functions as follows:

$$\begin{aligned} &b_1\left(t\right)=0 \quad , \quad b_2\left(t\right)=t \quad , \quad h(x,\tau)=\frac{\partial^2\varphi}{\partial x^2} \quad \text{and} \\ &f\left(t,\tau\right)=f\left(t-\tau\right)=\gamma e^{-\gamma(t-\tau)}. \end{aligned} \tag{31}$$

Using the previous functions in Eqs.(30) and (31) with the application of Eq.(28) into the differentiation of Eq.(29) leads to the crucial equation of motion:

$$\frac{\partial^2\varphi}{\partial t^2} + \left(\gamma+\eta-\frac{\eta}{2}\varphi^2\right)\frac{\partial\varphi}{\partial t} = \gamma\frac{\partial^2\varphi}{\partial x^2} - \eta\gamma\left(\varphi-\frac{\varphi^3}{6}\right), \tag{32}$$

which represents the second order differential equation whose solutions explain the movement of microtubules in the cytoplasm of eukaryotic cells with transport memory effects. In equation (32), the term $\left(\gamma+\eta-\frac{\eta}{2}\varphi^2\right)\frac{\partial\varphi}{\partial t}$ accounts for the damping of tubulin dimers as they move through the cell environment. And consequently, it depends on the transport memory under consideration. Neglecting the coefficient η which gives information on the degree of nonlinearity of the system, we find from relation (32) the classical linear form of one-dimensional D'Alembert wave equations propagating in a damped medium. In most of the nonlinear phenomena that describe the human environment, the concerns arise when solving the model equation. Obviously, obtaining the solutions of Eq.(32) seems very complex. However, some techniques for obtaining exact solutions of the soliton type can be used [117, 118]. Among these methods, those allowing the use of a special ansatz [119] and the multiple-sale [120] are of interest to us in the solutions of Eq.(32).

II.2.2 Derivation of spatio-temporal equation of an electrical circuit model

Although the atomic model so far is the subject of much investigation and understanding of the dynamics of MTs, microscopic and experimental observations of the cytoplasmic medium reveal the existence of a coordinated set of ionic motion around and even through these MTs. The properties of the ionic waves that move along these polymer tubes in the cytosol are modeled in this subsection. MTs are linked to the regulation of a number of ion channels and thus contribute to the electrical activity of excitable cells [121]. Particularly, as the brain is a medium of information transfer by electrical signals, it has been shown that neurons could use MTs in cognitive processing via some associated proteins [19, 122]. It is worth mentioning that the way in which MTs function and process electrical information is still largely unknown. Here, therefore, due to the ionic flow surrounding the length of MTs, a physical model in which studies of the conditions allowing them to act as non-linear electrical transmission lines is proposed. In this model, each tubulin dimer is taken as an electrical circuit element with resistive, capacitive and inductive behaviour. These dimer characteristics are derived from the polyelectrolyte nature of MTs. This nature allows us to keep in mind that MTs are mainly negatively charged on their outer surface. This results in the non-uniformity of the charge distribution along the polymer. This also plays a crucial role in the modeling of MTs as an electrical cable with 13 parallel currents composed of ion flows. It is worth recalling that the polyelectrolyte nature of MTs comes from the fact that tubulin is formed from many amino acids that physiologically have many negatively charged residues [88]. Accordingly, Manning's theory [123] would determine the conditions under which each MT should attract counterions (positive) from the solution to its surface, while other ions (negative) from the same cytosol solution will be repelled so that a cylindrical ion-depleted zone is created around the MT. This depleted layer has a thickness ℓ_B, the so-called Bjerrum length, which is defined as the distance from the surface of the MT at which the coulombic energy of the surface charges balances the thermal agitation of the solution: $e_0^2/(4\pi\varepsilon_0\varepsilon\ell_B) = k_BT$, where e_0 is the charge of an electron, ε_0 is the permittivity of vacuum, ε is the relative permittivity of the cytosol, k_B is Boltzmann's constant and T is a given temperature of the medium. Based on the fact that the depleted layer would act as a dielectric medium located between the MT surface and the cytosol solution, it could also provide both a capacitive and resistive component for the electrical characteristics of the FPs. For the sake of accuracy, the depleted zone is therefore considered as a dielectric between two charged cylindrical plates around the MTs. The capacitive component represents the parallel linear condensed layer and the non-linear layer of the tubulin tails perpendicular to the surface of the MT. The resistive component comes from two contributions: one whose conductivity/resistivity of the ion flow is parallel to the MT axis and the other whose resistivity of the ion cloud flows between the two cylindrical plates is perpendicular to the polymer surface. The inductive component of the circuit that is added to the previous two is due to the actual helical structure of the MT, which like a solenoid should induce a helical ionic flow in the medium.

In order to derive the model equation, we consider a discrete nonlinear mono-inductance transmis-

sion line of microtubule whose unit is shown in Fig. 15. The studied discrete model of MTs is made of a succession of such N adjacent unit cells,which individually contain a linear inductance L in series with a linear resistance r_1, a cylindrical capacitor C_0 connected in series with a transversal resistivity r_2. The capacitor is biased by a constant voltage V_0 and depends on the voltage V_n, for low voltage, at the nth section so that:

$$Q_n = C_0 \left(V_n - \alpha_1 V_n^2 - \alpha_2 V_n^3 \right), \tag{33}$$

where C_0 is the capacitance in the linear regime, with α_1 and α_2 being positive parameters that account for nonlinearities in the charge. We introduce the discrete potential in one unit section of the MT, where Kirchhoff's laws for the currents and voltages are applied. The idea is to develop a spatiotemporal equation for the potential over the capacitance as a function of the model's parameters. For the calculations of this work, the parameter values [88] used are: $L = 0.8 \times 10^{-15} H$, $r_1 = 10^9 \Omega$, $r_2 = 7 \times 10^6 \Omega$, $C_0 = 0.13 \times 10^{-14} F$, $\alpha_1 = 0.03 \quad Volts^{-1}$, $\alpha_2 = 0.0019 \quad Volts^{-2}$. From these Kirchhoff's laws based on Fig. 15, we get the following from segment MN:

$$u_n - u_{n+1} = r_1 I_n + L \frac{dI_n}{dt}. \tag{34}$$

The relation between the current entering segment MO and the current across the capacitance is given by:

$$I_{n-1} - I_n = \frac{dQ_n}{dt}. \tag{35}$$

The voltage across the input to the elementary section, u_n, may be written in the following form:

$$u_n = r_2 \left(I_{n-1} - I_n \right) + \left(V_n + V_0 \right), \tag{36}$$

where V_n is the potential over the capacitance and V_0, the bias voltage of the capacitor. Combining the previous relations (33), (34), (35) and (36), it is easy to show that the spatiotemporal evolution of the waves voltage $V_n(t)$ within the microtubule network is governed by the following improved equation:

$$\begin{aligned} &\frac{d^2 V_n}{dt^2} - \omega_0^2 \left(V_{n+1} + V_{n-1} - 2V_n \right) + \beta_0 \frac{dV_n}{dt} - \beta_1 \frac{d}{dt} \left(V_{n+1} + V_{n-1} - 2V_n \right) - \beta_0 \frac{d}{dt} \left(\alpha_1 V_n^2 + \alpha_2 V_n^3 \right) \\ &- \frac{d^2}{dt^2} \left(\alpha_1 V_n^2 + \alpha_2 V_n^3 \right) + \beta_2 \frac{d}{dt} \left(V_{n+1}^2 + V_{n-1}^2 - 2V_n^2 \right) + \beta_3 \frac{d}{dt} \left(V_{n+1}^3 + V_{n-1}^3 - 2V_n^3 \right) = 0, \end{aligned} \tag{37}$$

where $\omega_0^2 = \frac{1}{LC_0}$, $\beta_0 = \frac{r_1}{L}$, $\beta_1 = \frac{r_2}{L}$, $\beta_2 = \alpha_1 \beta_0$, $\beta_3 = \alpha_2 \beta_1$ and $n = 1, 2, ..., N$ (N being the number of cells considered).

By considering the dissipative coefficients β_0 and β_1 in the order of ε^3, the dispersion relation for

the linear vibrations of PFs can be found by taking only linear terms in Eq.(37). This is given by:

$$\omega^2 - 4\omega_0^2 \sin^2\left(\frac{k}{2}\right) = 0, \tag{38}$$

where ω_0 is the characteristic frequency of the elementary cell, k being the wavelength. Under these conditions, the propagation without absorption of a wave for real k is only possible if $\omega \leq 2\omega_0$. The system therefore exhibits a low-pass type behavior. At the wave number $k = 0$, the eigenfrequency spectrum has a lower cutoff $\omega_{\min} = 0$, corresponding to direct current part, while for $k = \pi$, $\omega_{\max} = 2\omega_0$, the alternating current part is the upper cut-off frequency. It is therefore sufficient to restrict the study of the $\omega(k)$ function to the $[0, \pi]$ interval of the values of k in order to fully describe the dynamic behavior of the tubulin dimer chain in MTs. The linear spectrum then has a gap $[0, 2\omega_0]$ due to the discrete effects of the network. From the previous relation (38), we deduce the group speed

$$V_g = \frac{\partial \omega}{\partial k} = \frac{\omega_0^2 \sin(k)}{\omega}. \tag{39}$$

We see that this group speed is not constant, but depends on frequency $\omega(k)$, which obviously implies a dispersive behavior of the system. It is good to know that the group velocity V_g is a physical speed, it corresponds to the speed of energy propagation and therefore, to the speed of information transport, and therefore cannot exceed the speed light. We see that this group speed is not constant, but depends of the frequency $\omega(k)$, which obviously implies a dispersive behavior of the system. It is good to know that the group velocity V_g is a physical speed; it corresponds to the speed of energy propagation and to the rate of information transport, and therefore cannot exceed the speed of light. The shapes of curves

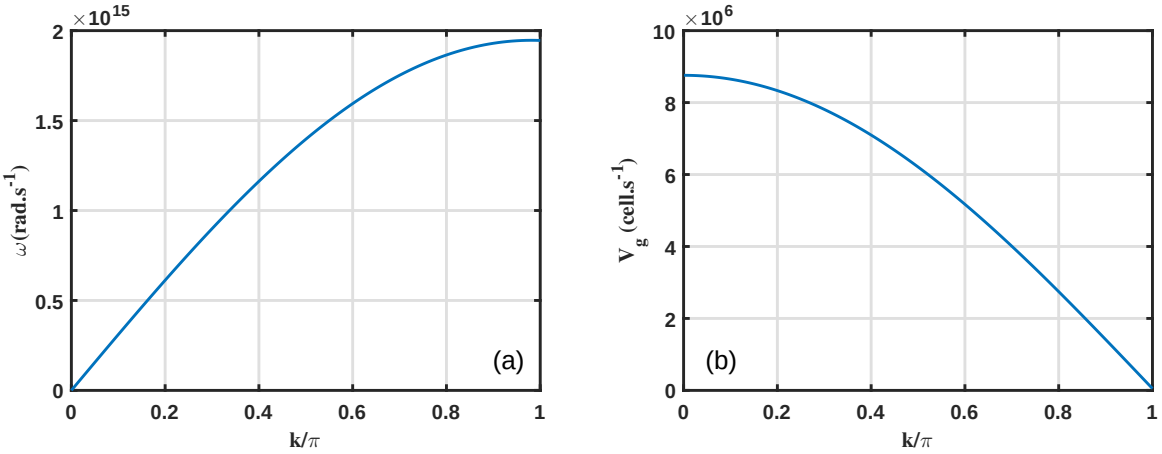

Figure 18: Panels shows the dispersion relation (a) and the group velocity (b), both versus the wavenumber k of the plane wave signal along the protofilaments, with $0 \leq k \leq \pi$.

of the dispersion relation (38) and the group velocity (39) are plotted in Fig. 18, where they clearly show the interval in which the values of the wavenumbers k are restricted. The coming part here will be used in the search of the coupled cubic CGL equations from the equation (37) whose solutions are generally of soliton type.

II.3 Analytical methods and coupled amplitude equations

II.3.1 The multiple scale expansion method

This technique called the multiple scale analysis follows the concept of expanding the solution into a perturbation series and including multiple temporal and spatial scales. The multiple-scale expansion method, which consists of expanding the field quantities into asymptotic series of the smallness parameter and solving the resulting differential equation of various orders of the same parameter. One obtain the NLS equations or nonlinear GL equations. The main objective in this subsection is to show that the amplitude equation for the radial angular φ-model of Zdravković can be splinted into a set of CNLS equations. For this purpose, starting from the complex character for microtubules lattices, the asymptotic expansion is used to investigate the effects of nonlinearity and discreteness in the system. It implies a trial solution of the form [124, 125]:

$$\varphi_n = \epsilon\varphi_{n,n}^{(1)} + \epsilon^2\varphi_{n,n}^{(2)} + \epsilon^3\varphi_{n,n}^{(3)} + \cdots = \sum_{j=1}^{\infty} \epsilon^j \varphi_{n,n}^{(j)}, \tag{40}$$

with $\varphi_{n,m}^{(j)} = \varphi^{(j)}(\xi_n, T, \theta_{0,m}(t), \theta_{max,m}(t))$, where ϵ is a small parameter denoting the relative amplitude of the excitation; $\xi_n = \epsilon(nl - \mu t)$ and $T = \epsilon^2 t$ are the multiple scale slow variables. The subscripts n and m represent ξ_n and $\theta_{0,m}(t)$ (or $\theta_{max,m}(t)$), respectively. μ is a small variable that will be determined by a solvability condition. The fast variables $\theta_{0,m}(t)$ and $\theta_{max,m}(t)$ represent the phases of two carrier waves. This implies the use of the derivative:

$$\frac{d}{dt} = \frac{\partial}{\partial t} - \epsilon\mu\frac{\partial}{\partial \xi_n} + \epsilon^2\frac{\partial}{\partial T}. \tag{41}$$

For the discreteness term, we can be used the expansion [18, 124]:

$$\begin{aligned}\varphi_{n\pm1} =& \epsilon\varphi_{n,n\pm1}^{(1)} + \epsilon^2\left(\varphi_{n,n\pm1}^{(2)} \pm \ell\frac{\partial\varphi_{n,n\pm1}^{(1)}}{\partial\xi_n}\right) + \epsilon^3\left(\varphi_{n,n\pm1}^{(3)} \pm \ell\frac{\partial\varphi_{n,n\pm1}^{(2)}}{\partial\xi_n}\right.\\ &\left. + \frac{\ell^2}{2}\frac{\partial^2\varphi_{n,n\pm1}^{(1)}}{\partial\xi_n^2}\right) + \cdots .\end{aligned} \tag{42}$$

Substituting Eqs.(40), (41) and (42) into Eq.(20) and comparing the power of ϵ , we obtain a hierarchy of equations about $\varphi_{n,n}^{j}$ $(j = 1, 2, 3, \ldots)$. The whole problem, through this procedure, reduces to the set of following equations:

$$(\frac{\partial^2}{\partial t^2} + \omega_1^2)\varphi_{n,n}^{(j)} - C(\varphi_{n,n+1}^{(j)} - \varphi_{n,n-1}^{(j)}) = M_{n,n}^{(j)}, \quad j = 1, 2, 3, \ldots, \tag{43}$$

where $\omega_1^2 = \omega_g^2 + 2C$ and $M_{n,n}^{(j)}$ being given by:

$$\begin{aligned}
M_{n,n}^{(1)} =& 0, \\
M_{n,n}^{(2)} =& 2\mu \frac{\partial^2 \varphi_{n,n}^{(1)}}{\partial t \partial \xi_n} + Cl \frac{\partial}{\partial \xi_n}(\varphi_{n,n+1}^{(1)} - \varphi_{n,n-1}^{(1)}), \\
M_{n,n}^{(3)} =& 2\mu \frac{\partial^2 \varphi_{n,n}^{(2)}}{\partial t \partial \xi_n} - \mu^2 \frac{\partial^2 \varphi_{n,n}^{(1)}}{\partial \xi_n^2} - 2\frac{\partial^2 \varphi_{n,n}^{(1)}}{\partial t \partial T} + Cl \frac{\partial}{\partial \xi_n}(\varphi_{n,n+1}^{(2)} - \varphi_{n,n-1}^{(2)}) \\
&+ \frac{Cl^2}{2} \frac{\partial^2}{\partial \xi_n^2}(\varphi_{n,n+1}^{(1)} + \varphi_{n,n-1}^{(1)}) - \omega_g^2 \alpha (\varphi_{n,n}^{(1)})^3, \\
&\dots,
\end{aligned} \tag{44}$$

which can be solved order by order. In order to describe the possibility of wave mixing during the radial dislocations in MTs, the equation (44) is solved step by step at different orders, where for $j = 1$, we assume the solution of the system to be of the form:

$$\varphi_{n,n}^{(1)} = Q_1(T, \xi_n) e^{i\theta_{0,n}(t)} + Q_2(T, \xi_n) e^{i\theta_{max,n}(t)} + c.c., \tag{45}$$

where c.c. stands for complex conjugates. Q_1 and Q_2 are two undetermined envelope functions. For both cut-off modes, we have $\theta_{0,n}(t) = \omega(q = 0)t = -\omega_g t$ and $\theta_{max,n}(t) = \pi n - \omega(q = \frac{\pi}{l})t = \pi n - \omega_{max} t$, and $\varphi_{n,n}^{(1)}$ becomes

$$\varphi_{n,n}^{(1)} = Q_1(T, \xi_n) e^{-i\omega_g t} + (-1)^n Q_2(T, \xi_n) e^{-i\omega_{max} t} + c.c. \tag{46}$$

By letting $j = 2$, the solvability condition imposes $\mu = 0$ and $\xi_n = \epsilon n l$, and we have the second-order approximation equation:

$$(\frac{\partial^2}{\partial t^2} + \omega_1^2)\varphi_{n,n}^{(2)} - C(\varphi_{n+1}^{(2)} - \varphi_{n-1}^{(2)}) = 0, \tag{47}$$

which admits plane wave solutions that can be written in the general form

$$\varphi_{n,n}^{(2)} = B_1(T, \xi_n) e^{-i\omega_g t} + (-1)^n B_2(T, \xi_n) e^{-i\omega_{max} t} + c.c., \tag{48}$$

with B_1 and B_2 being two constant amplitudes. Besides, we can assume $B_1 = B_2 = 0$, which leads to

$$\varphi_{n,n}^{(2)} = 0, \tag{49}$$

a solution with no impact on the nonlinear and dispersive behaviors of the model under study.

When $j = 3$, the solvability conditions leads to the following set of equations in Q_1 and Q_2 :

$$i\frac{\partial Q_1}{\partial T} + H_1\frac{\partial^2 Q_1}{\partial \xi_n^2} + (\zeta_{11}|Q_1|^2 + \zeta_{12}|Q_2|^2)Q_1 = 0 \tag{50}$$

$$i\frac{\partial Q_2}{\partial T} - H_2\frac{\partial^2 Q_2}{\partial \xi_n^2} + (\zeta_{21}|Q_1|^2 + \zeta_{22}|Q_2|^2)Q_2 = 0. \tag{51}$$

where $H_1 = \frac{C\ell^2}{2\omega_0}$, $H_2 = \frac{C\ell^2}{2\omega_{max}}$, $\zeta_{11} = -\frac{3\alpha\omega_0}{2}$, $\zeta_{12} = -\alpha\omega_0$, $\zeta_{21} = -\frac{\alpha\omega_0^2}{\omega_{max}}$, $\zeta_{22} = -\frac{3\alpha\omega_0^2}{2\omega_{max}}$.

In equations (50) and (51), there exist cross-phase modulation terms denoted by $|Q_\nu|^2 Q_{3-\nu}(\nu = 1, 2)$, which will drastically change the property of the nonlinear localized excitations. In comparison with the case of a single lower or upper cutoff mode being excited separately [126, 127].

The above set of equations can be rewritten using the original variables by letting $(\psi_1, \psi_2) = \epsilon(Q_1, Q_1)$, along with the change of variables $\xi_n = \epsilon n\ell$ and $T = \epsilon^2 t$ with $x = n\ell$, so that

$$i\frac{\partial \psi_1}{\partial t} + H_1\frac{\partial^2 \psi_1}{\partial x^2} + (\zeta_{11}|\psi_1|^2 + \zeta_{12}|\psi_2|^2)\psi_1 = 0 \tag{52}$$

$$i\frac{\partial \psi_2}{\partial t} - H_2\frac{\partial^2 \psi_2}{\partial x^2} + (\zeta_{21}|\psi_1|^2 + \zeta_{22}|\psi_2|^2)\psi_2 = 0. \tag{53}$$

Details of computations of these coupled amplitude equations (52) and (53) are given in appendix part A3.(165)-(169)

The above set of CNLS equations is coupled nonlinearly through the coefficients ζ_{12} and ζ_{21} . When these coefficients are equal and $H_2 = -H_1$, the Manakov's system is recovered [128]. Otherwise, these equations will be decoupled if $\zeta_{21} = \zeta_{12} = 0$, leading to individual NLS equations. The solutions for Eqs.(52) and (53) depend on the sign of their coefficients, plotted in Fig. 19. Obviously, H_1 and H_2 are

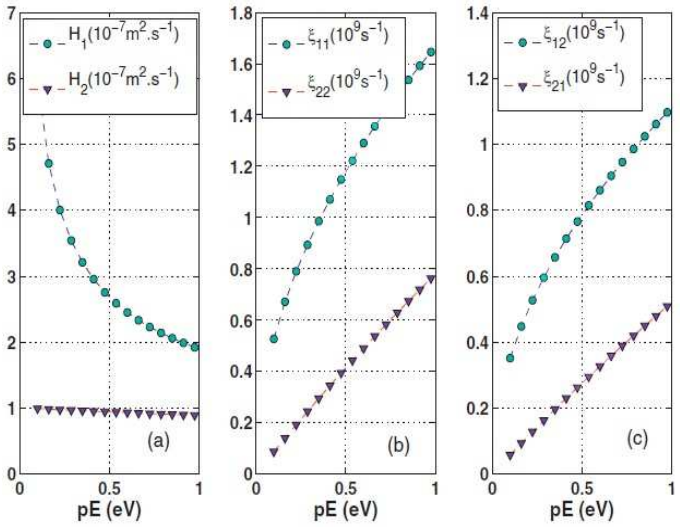

Figure 19: The panels show the parameters for the set of coupled NLS equations versus pE . Panel (a) clearly shows how H_1 and H_2 are decreasing functions of pE , while panels (b) and (c) show that ζ_{jj} and ζ_{ij} are increasing functions of pE ..

positive dispersion terms with respect to pE (Fig. 19(a)). The same is observed for ζ_{11} and ζ_{22} (Fig. 19(b)) and for ζ_{12} and ζ_{21} (Fig. 19(c)). However, H_1 and H_2 decrease with increasing pE , while ζ_{ii} and ζ_{ij} (

$j \neq i$) are increasing functions of the dipolar energy pE.

II.3.2 The semi-discrete approximation method

The perturbation method called the semi-discrete approximation is a technique in which the continuum approximation is introduced for the wave envelope while the phase of the carrier wave is kept discrete completely. From this method used in Refs. [129, 130] the short wavelength envelope solitons was obtained. The application of this method allows one to investigate how the plane wave is modulated by nonlinear effects.

In general that leads either the NLS type or the CGL whose solutions are generally of soliton type. For more explanation, we use the following nonlinear discrete differential equation of model [129]:

$$G\left(\ddot{u}_n(t), \dot{u}_n(t), u_n(t), u_{n+1}(t), u_{n-1}(t), u_n^2(t), u_n^3(t), ..., u_n^\nu(t)\right), \tag{54}$$

where $\nu = 4, 5, 6, \cdots$. And one assume also that its solution $u_n(t)$, with the independent multiple scale variables $T_i = \epsilon^i t$ and $X_i = \epsilon^i x$ $(i = 1, 2, ...)$ where $\epsilon \ll 1$, can take the following form [130]:

$$\begin{aligned} u_n(t) =& \epsilon u_1\left(X_1, X_2, ..., T_1, T_2...,\right) e^{i\theta} + \epsilon^2 \left[u_{20}\left(X_1, X_2, ..., T_1, T_2...,\right)\right. \\ &\left. + u_2\left(X_1, X_2, ..., T_1, T_2...,\right) e^{2i\theta}\right] + c.c \end{aligned} \tag{55}$$

with $\theta = kx - \omega t$ where $x = n\ell$. n represent the unit cell number, ℓ is the length of this unit cell. Parameters k and ω respectively stand for the wavenumber, and angular frequency.

After inserting of the solution (55) into the nonlinear discrete differential equation of model (54) and by using the continuum approximation:

$$u_{j,n\pm1} = u_j \pm \epsilon\ell\left(\frac{\partial u_j}{\partial X_1}\right) \pm \varepsilon^2\ell^2\left(\frac{\partial u_j}{\partial X_2}\right) + \epsilon^2\frac{\ell^2}{2!}\left(\frac{\partial^2 u_j}{\partial X_1^2}\right) \pm \epsilon^3\frac{\ell^3}{3!}\left(\frac{\partial^3 u_j}{\partial X_1^3}\right) + \cdots, \quad j = 1, 2, \tag{56}$$

and the temporal derivative operators:

$$\begin{aligned} \frac{\partial}{\partial t} &= \frac{\partial T_1}{\partial t}\frac{\partial}{\partial T_1} + \frac{\partial T_2}{\partial t}\frac{\partial}{\partial T_2} + \cdots, \\ \frac{\partial^2}{\partial t^2} &= \left(\frac{\partial}{\partial t}\right)^2 = \epsilon^2\frac{\partial^2}{\partial T_1^2} + 2\epsilon^3\frac{\partial^2}{\partial T_1 \partial T_2} + \epsilon^4\frac{\partial^2}{\partial T_2^2} + 0\left(\epsilon^5\right), \end{aligned} \tag{57}$$

yields a series of inhomogeneous system for u_1, u_{20} and u_2 polynomial in $e^{i\Lambda\theta}$, $\Lambda = 0, 1, 2...$ that will be solve later at different orders of perturbation parameter ϵ.

II.3.2.1 Obtaining the system of the Coupled Complex Ginzburg-Landau Equations from an nonlinear electrical transmission line model of microtubules

Solving the discrete Eq.(37) is not an easy task. Moreover, the work's main purpose is to study solitons made up of carrier waves modulated by an envelope signal, also called envelope solitons; it

is suitable to apply the semi-discrete approximation. To proceed,we consider β_0 and β_1 are perturbed parameters of order ϵ^3. Through this process, the nonlinear Eq.(37) is transformed into two coupled CGL equations that describe the amplitudes of the oscillations of nonlinear coupled impulses along microtubules. In the interval of frequencies $[0, 2\omega_0]$, we choose to couple any two packets of waves centered (k_1, ω_1) and (k_2, ω_2) with $k_2 = \alpha k_1$ ($\alpha \in [0, 1]$)for our study, and we assume the following solution for Eq.(37):

$$V_n(t) = \epsilon\left(B_1 e^{i\theta_1} + B_2 e^{i\theta_2}\right) + \epsilon^2\left(B_{30} + B_3 e^{2i\theta_1} + B_{40} + B_4 e^{2i\theta_2}\right) + C.C., \tag{58}$$

where $\theta_1 = k_1 n - \omega_1 t, \theta_2 = k_2 n - \omega_2 t$, with k_1 and k_2 being the normal mode wavenumbers and ω_1 and ω_2 their associated frequencies. In the semi-discrete approximation, the undetermined envelope functions $B_q (q = 1, 2, 3, 4)$ are supposed to be independent from the fast variables t and n. This otherwise implies that they are functions of the slow variables $X_j = \epsilon^j x$ and $T_j = \epsilon^j t$, with $j \geq 1$. This implicitly means that a continuum limit approximation is made with the wave amplitudes, while the discrete nature of the phase is preserved. Moreover, into account the asymmetry of the charge-voltage relation given by Eq.(33), The direct terms $B_{30}(X_1, T_1, T_2)$, $B_{40}(X_1, T_1, T_2)$ and the second harmonic terms $B_3(X_1, T_1, T_2)$, $B_4(X_1, T_1, T_2)$ are added to the fundamental ones $B_1(X_1, T_1, T_2)$ and $B_2(X_1, T_1, T_2)$ respectively. Inserting Eq.(58) in Eq.(37) and using a following Taylor's expansion

$$B_{j,n\pm1} = B_j \pm \varepsilon h\left(\frac{\partial B_j}{\partial X_1}\right) + \varepsilon^2\frac{h^2}{2!}\left(\frac{\partial^2 B_j}{\partial X_1^2}\right) \pm \varepsilon^3\frac{h^3}{3!}\left(\frac{\partial^3 B_j}{\partial X_1^3}\right) + \cdots, \quad j = 1, 2, 3, 4, \tag{59}$$

yields, after some standard calculations, a series of inhomogeneous equations at different orders of perturbation parameter ε.

The first orders of perturbation $\left(\varepsilon, e^{i\theta_1}\right)$ and $\left(\varepsilon, e^{i\theta_2}\right)$ lead to the dispersion relations of linear waves for the two wave packets (k_1, ω_1) and (k_2, ω_2) taken into the interval of frequencies $[0, 2\omega_0]$:

$$\begin{aligned} \omega_1^2 - 4\omega_0^2 \sin^2\left(\frac{k_1}{2}\right) &= 0 \\ \omega_2^2 - 4\omega_0^2 \sin^2\left(\frac{k_2}{2}\right) &= 0, \end{aligned} \tag{60}$$

They are identical to the expression given by Eq.(38). The second orders of perturbation $\left(\varepsilon^2, e^{i\theta_1}\right)$ and $\left(\varepsilon^2, e^{i\theta_2}\right)$, lead to the following results, including the group speeds V_{g1} and V_{g2} :

$$\begin{aligned} \frac{\partial B_1}{\partial T_1} &= -V_{g1}\frac{\partial B_1}{\partial X_1} \quad \text{with} \quad V_{g1} = \frac{\partial \omega_1}{\partial k_1} = \frac{\omega_0^2 \sin(k_1)}{\omega_1}, \\ \frac{\partial B_2}{\partial T_1} &= -V_{g2}\frac{\partial B_2}{\partial X_1} \quad \text{with} \quad V_{g2} = \frac{\partial \omega_2}{\partial k_2} = \frac{\omega_0^2 \sin(k_2)}{\omega_2}. \end{aligned} \tag{61}$$

From Eq.(61), the non-zero solutions B_1 and B_2 can be written in the forms $B_1 = B_1(\xi, T_2)$ and $B_2 = B_2(\xi', T_2)$, where $\xi = X_1 - V_{g1}T_1$ and $\xi' = X_2 - V_{g2}T_2$.

Always with the second orders of perturbation, but for which we have rather the exponential term

$e^{2i\theta}$, that is to say with the orders $\left(\varepsilon^2, e^{2i\theta_1}\right)$ and $\left(\varepsilon^2, e^{2i\theta_2}\right)$, the relations between the second harmonics B_3 and B_4 and the fundamental terms B_1 and B_2 give respectively

$$\begin{aligned} B_{30} &= B_{40} = 0 \\ B_3 &= \frac{\alpha_1\omega_1^2 + \frac{1}{2}i\omega_1\left(\beta_0\alpha_1 + 4\beta_2\sin^2(k_1h)\right)}{\omega_1^2 - \omega_0^2\sin^2(k_1h)}B_1^2 \\ B_4 &= \frac{\alpha_1\omega_2^2 + \frac{1}{2}i\omega_2\left(\beta_0\alpha_1 + 4\beta_2\sin^2(k_2h)\right)}{\omega_2^2 - \omega_0^2\sin^2(k_2h)}B_2^2. \end{aligned} \tag{62}$$

Finally, at the third orders $\left(\varepsilon^3, e^{i\theta_1}\right)$ and $\left(\varepsilon^3, e^{i\theta_2}\right)$, using the expressions of the relation (62), we recover the group velocities (61), while the slow envelope evolution of the solitonic ionic waves in microtubules are described by the coupled equations

$$\begin{aligned} i\frac{\partial B_1}{\partial T_2} - S_1\frac{\partial^2 B_1}{\partial \xi^2} - \sigma_1|B_1|^2B_1 - \rho_1|B_2|^2B_1 &= iA_1B_1 \\ i\frac{\partial B_2}{\partial T_2} - S_2\frac{\partial^2 B_2}{\partial \xi'^2} - \sigma_2|B_2|^2B_2 - \rho_2|B_1|^2B_2 &= iA_2B_2, \end{aligned} \tag{63}$$

Further introducing the change of variables $\xi' = X_1 - V_{g2}T_1 = \xi + (V_{g1} - V_{g2})\,T_2$, Eqs. (63) becomes

$$\begin{aligned} i\frac{\partial B_1}{\partial T_2} - S_1\frac{\partial^2 B_1}{\partial \xi^2} - \sigma_1|B_1|^2B_1 - \rho_1|B_2|^2B_1 &= iA_1B_1 \\ i\frac{\partial B_2}{\partial T_2} + \left(\frac{V_{g2} - V_{g1}}{\epsilon}\right)\frac{\partial B_2}{\partial \xi} - S_2\frac{\partial^2 B_2}{\partial \xi^2} - \sigma_2|B_2|^2B_2 - \rho_2|B_1|^2B_2 &= iA_2B_2. \end{aligned} \tag{64}$$

By using the dependent variable transformation [131] $B_2 \to B_2\exp\left\{-i\left(\frac{\Delta V_g}{2S_2}\xi + \frac{\Delta V_g^2}{4S_2}T_2\right)\right\}$, with $\Delta V_g = \frac{V_{g1} - V_{g2}}{\epsilon}$, the above Eqs.(64) becomes

$$\begin{aligned} i\frac{\partial B_1}{\partial T_2} - S_1\frac{\partial^2 B_1}{\partial \xi^2} - \sigma_1|B_1|^2B_1 - \rho_1|B_2|^2B_1 &= iA_1B_1 \\ i\frac{\partial B_2}{\partial T_2} - S_2\frac{\partial^2 B_2}{\partial \xi^2} - \sigma_2|B_2|^2B_2 - \rho_2|B_1|^2B_2 &= iA_2B_2, \end{aligned} \tag{65}$$

whose coefficients S_1, S_2, A_1, A_2, ρ_1, ρ_2, σ_1 and σ_2 are given by:

$$S_1 = \frac{V_{g1}^2 - h^2\omega_0^2\cos(k_1h)}{2\omega_1},\ S_2 = \frac{V_{g1}^2 - h^2\omega_0^2\cos(k_2h)}{2\omega_2},\ A_1 = -\frac{1}{2}\left(\beta_0 + 4\beta_3\sin^2\left(\frac{k_1h}{2}\right)\right),$$
$$A_2 = -\frac{1}{2}\left(\beta_0 + 4\beta_3\sin^2\left(\frac{k_2h}{2}\right)\right),\ \sigma_1 = \sigma_{1r} + i\sigma_{1i},\ \sigma_2 = \sigma_{2r} + i\sigma_{2i},\ \rho_1 = \rho_{1r} + i\rho_{1i} \quad and$$
$$\rho_2 = \rho_{2r} + i\rho_{2i}$$

with the parameters $\sigma_{1r}, \sigma_{2r}, \sigma_{1i}, \sigma_{2i}, \rho_{1r}, \rho_{2r}, \rho_{1i}$ and ρ_{2i} given in appendix A1 in Eq.(163). The derived equations given by the relation (65) are indeed coupled at the level of the fourth term each of the left part of the equality and are known as the system of coupled complex equations of Ginzburg-Landau. They describe the evolution of ionic waves in this studied electrical circuit model of the microtubules in living cells.

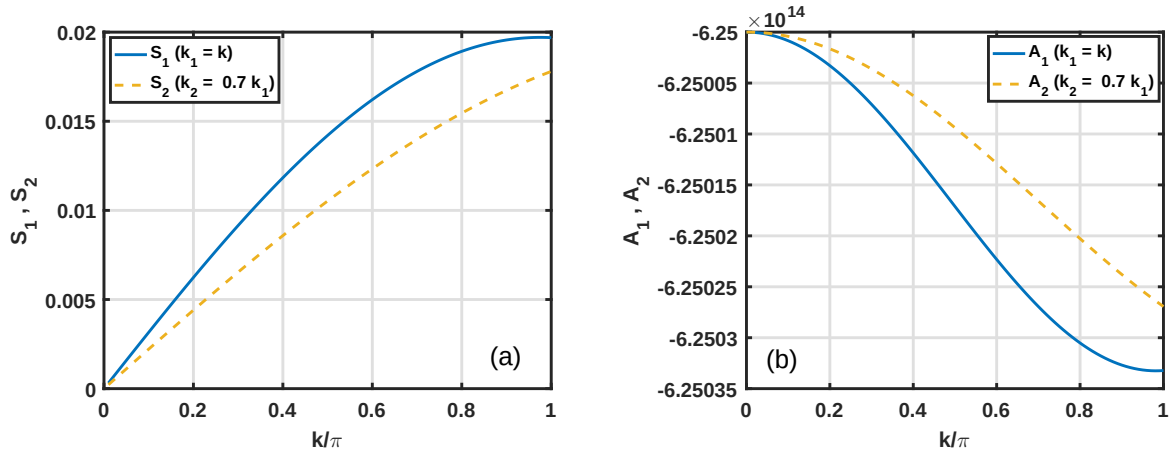

Figure 20: (a) shows the dispersion coefficients S_1 and S_2 of Eqs.(65), while (b) displays their dissipative coefficients A_1 and A_2 of versus the wavenumber k, with $k = k_1$ and $k_2 = \alpha k_1$, so that $\alpha = 0.7$ (yellow dashed line) corresponds to S_2 and A_2, functions of k_2.

According to the plots of Fig. 20(a), the dispersion coefficients S_1 and S_2 are all positively increasing with respect to k, while Fig. 20(b) shows the dissipative coefficients A_1 and A_2 that are negatively decreasing functions of the wavenumber $k = k_1$, with $k_2 = \alpha k_1$. Along the same line, the complex self-phase modulation nonlinear coefficients σ_1 and σ_2, and the coupling coefficients ρ_1 and ρ_2 parameters, responsible for cross-phase modulation are complex parameters and the variations of their real and imaginary parts are summarized in Fig. 21 versus the wavenumber k. We should, however, stress that if the ρ_1 and ρ_2 are set to null, we obtain two decoupled CGL equations. The CGL equations finds applications in many context and has actually been useful in physical systems related to biophysics [132,133], plasma physics [134], electrical lattices [135–137], Bose-Einstein condensation [138,139], nonlinear optics, lasers and meta-materials [140–145], to cite a few. Most of the studied systems probe the efficiency of the CGL equation in signal processing with good example being ionic waves transmission and amplification in neuronal microtubule networks [146, 147], neural networks [148, 149], along with pattern formation in many other physical systems. Interestingly, one of the techniques that have been widely used in characterizing pattern formation in the CGL equation is the MI mechanism, a consequence of the competition between nonlinearity and dispersion [140, 143–145, 150]. In relation to MI phenomenon, spatiotemporal chaos has been identified in the CGL equation [151,152]. Weber et al [153] also reported transition to spatiotemporal turbulence from traveling waves resulting from instabilities, while solutions such as spiral waves were found [154].

II.3.2.2 Obtaining the system of the Coupled Complex Nonlinear Schrödinger Equations with memory effect for radial angular model of microtubule

As the size of the MTs in the cell is minimal, we have considered that the movement performed by them is of small amplitudes. To derive the coupled amplitude equations for the protein protofilament network and to appreciate the interaction of the solitary solutions, we introduce a change of the

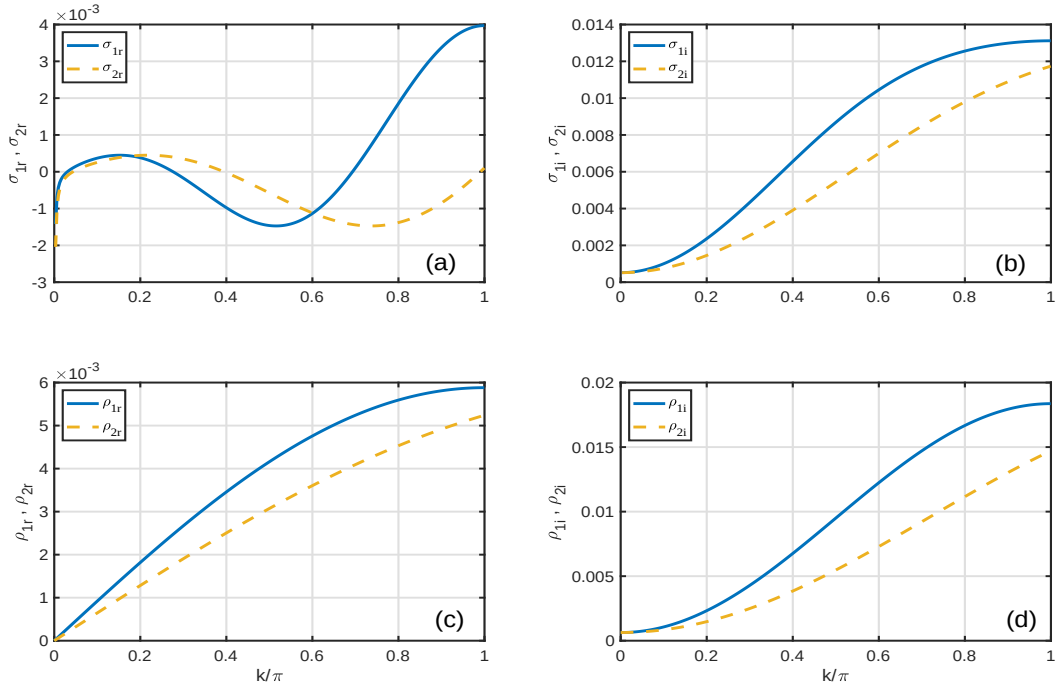

Figure 21: Panels (a) and (b) show, respectively the real and imaginary part of the coefficients $\sigma_1 = \sigma_{1r} + i\sigma_{1i}$ and $\sigma_2 = \sigma_{2r} + i\sigma_{2i}$ of Eqs.(65) versus the wavenumber k. Panels (c) and (d) display plots of the coefficients $\rho_1 = \rho_{1r} + i\rho_{1i}$ and $\rho_2 = \rho_{2r} + i\rho_{2i}$ versus the wavenumber k, with $k = k_1$ and $k_2 = \alpha k_1$ ($\alpha = 0.7$).

dependent variable around its equilibrium point as follows:

$$\varphi(x,t) = \varepsilon\phi(x,t), \tag{66}$$

where ε is a very small parameter in front of the number 1, which accounts for the order of the excitation and ϕ, a new physical dependent variable. Applying the change of variable from eq.(66) into eq.(32), the problem to be solved becomes :

$$\frac{\partial^2\phi}{\partial t^2} + \left(\eta_0 - \varepsilon^2\eta_1\phi^2\right)\frac{\partial\phi}{\partial t} = \gamma\frac{\partial^2\phi}{\partial x^2} - \omega_0^2\left(\phi - \varepsilon^2\eta_2\phi^3\right), \tag{67}$$

where $\eta_0 = \gamma + \eta$; $\eta_1 = \frac{\eta}{2}$; $\eta_2 = \frac{1}{6}$ and $\omega_0^2 = \eta\gamma$. To obtain the CCNLS equations whose modulated soliton solutions can explain the transport of energy and information along microtubules, we consider the following the ansatz that includes two oscillation modes [155]:

$$\phi(x,t) = V_1 e^{i\theta_1} + V_2 e^{i\theta_2} + C.C + \varepsilon\left(V_{01} + V_{02} + V_{11}e^{2i\theta_1} + V_{22}e^{2i\theta_2} + C.C\right), \tag{68}$$

where $V_j = V_j(X_1, X_2, T_1, T_2)$; $V_{0j} = V_{0j}(X_1, X_2, T_1, T_2)$ and $V_{jj} = V_{jj}(X_1, X_2, T_1, T_2)$ with $j = 1, 2$ are complex amplitudes to be determined. The $\theta_j = q_j x - \omega_j t$ ($j = 1, 2$) are carrier phases, depending on the fast variables t and x, with q_j and ω_j respectively, the wave numbers and angular frequencies of two wave packets, and C.C. denoting the complex conjugate. The terms V_{0j} and V_{jj} of first and second

harmonics added to the fundamental terms V_j are taken as disturbance terms because of the nonlinear character of Eq. (67). The functions V_j, V_{0j} and V_{jj} depend on the slow variables of multiple scales $T_j{=}\varepsilon^j t$ and $X_j = \varepsilon^j x$ with $j = 1, 2$. Introducing Eq.(68) into Eq.(67), and then setting the quantities proportional to the different orders $\left(\varepsilon^j, e^{i\theta_n}\right)$ and $\left(\varepsilon^j, e^{i2\theta_n}\right)$ to zero with $j = 0, 1, 2$ and $n = 1, 2$, the following results are obtained:

• For $j = 0$ and $n = 1, 2$ at the orders $\left(\varepsilon^0, e^{i\theta_1}\right)$ and $\left(\varepsilon^0, e^{i\theta_2}\right)$, we find respectively, the complex equations of unknowns ω_1 and ω_2,

$$\begin{aligned} \omega_1^2 + i\eta_0\omega_1 - \omega_0^2 - \gamma q_1^2 = 0 \\ \omega_2^2 + i\eta_0\omega_2 - \omega_0^2 - \gamma q_2^2 = 0, \end{aligned} \tag{69}$$

leading to linear complex angular frequencies:

$$\omega_1 = \omega_{1r} + i\omega_{1i} \quad ; \quad \omega_2 = \omega_{2r} + i\omega_{2i}, \tag{70}$$

where

$$\begin{aligned} \omega_{1r}^2 {=}\gamma_1^2 \left[1 - \left(\frac{\eta_0}{2\gamma_1}\right)^2\right], \qquad \omega_{2r}^2 = \gamma_2^2 \left[1 - \left(\frac{\eta_0}{2\gamma_2}\right)^2\right] \\ \text{and} \quad \omega_{1i} = \omega_{2i} = -\frac{\eta_0}{2}, \end{aligned} \tag{71}$$

with $\gamma_1 = \sqrt{\omega_0^2 + \gamma q_1^2}$ and $\gamma_2 = \sqrt{\omega_0^2 + \gamma q_2^2}$.

While the imaginary parts $\omega_{1i} = \omega_{2i}$ of the angular frequencies are constant, we have limited ourselves to plotting the real parts $(\omega_{1r}, \omega_{2r})$ as a function of the wave numbers q_1 and q_2 belonging to the interval $[q_s; \pi]$ for three values of the transport memory constant γ in Figs. 22(a) and 22(b). In the first panel of fig. 22, the influence of the memory effect on the propagation of the excitation along the cellular microtubules is clearly perceptible because the growth of the parameter γ implies that of the real angular frequencies ω_{1r} and ω_{2r}. At the same time, we also see that the shapes of these decreasing curves are similar, but with an increase in the threshold value of the wave number q_s, which moves further away from zero, thus decreasing the range of choice of wave numbers q_1 and q_2 of the wave packets, characterized by the pairs of values (ω_{1r}, q_1) and (ω_{2r}, q_2) used in this work.

These first results show that for $\eta_0 = 0$, the angular frequencies of both vibration modes become real. Therefore, the damping forces acting on the motion of the MTs cancel out, while the dependence of the memory effect created by these forces remains (see Eq.(67)) and is controlled by η, the nonlinearity degree of the system. It also follows from the expressions in Eq.(71) that the complex angular pulsations (see Eq.(70)) only exist from the threshold value q_s of the wave number $q \geq q_s$ given by $q_s = \sqrt{\frac{1}{\gamma_{1,2}}\left(\frac{\eta_0^2}{4} - \omega_0^2\right)}$.

• For $j = 1$ and $n = 1, 2$, at the $\left(\varepsilon^1, e^{i\theta_1}\right)$, $\left(\varepsilon^1, e^{i\theta_2}\right)$, we obtain respectively, the differential

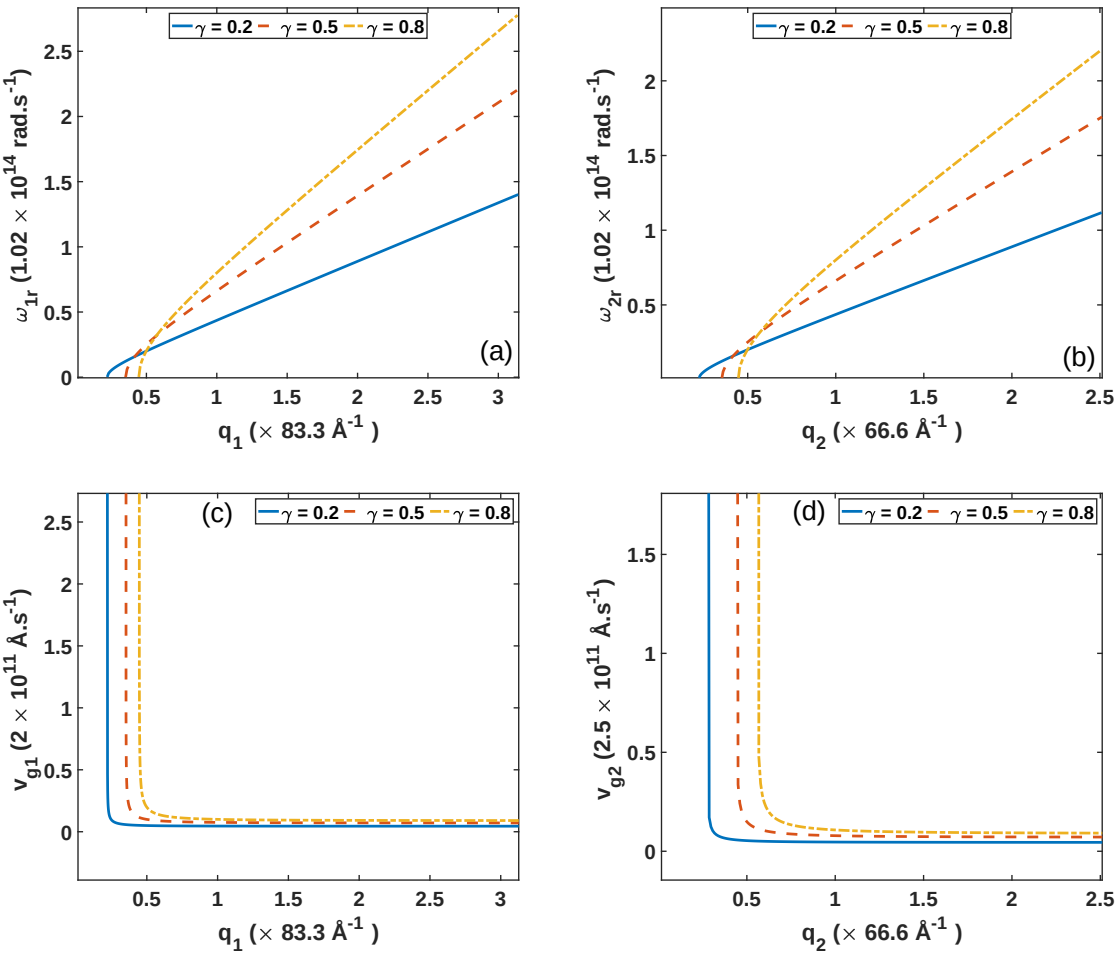

Figure 22: Representative curves of the real part of the angular pulsation and group velocity of the wave as a function of the wavenumbers q(q_1 and q_2) for $q_2 = 0.8q_1$ and $\eta = 0.002$. Panels (a), (b), (c) and (d) show the influence of the memory constant γ on these quantities.

equations :

$$\begin{aligned}(\eta_0 - 2i\omega_1)\,\frac{\partial V_1}{\partial T_1} &= 2i\gamma q_1 \frac{\partial V_1}{\partial X_1} \quad , \\ (\eta_0 - 2i\omega_2)\,\frac{\partial V_2}{\partial T_1} &= 2i\gamma q_2 \frac{\partial V_2}{\partial X_1},\end{aligned} \tag{72}$$

which lead to the determination of the physical velocities of propagation of information along the protofilaments, also known as group velocities, given by:

$$V_{g1} = \frac{\gamma q_1}{\omega_{1r}} \quad ; \quad V_{g2} = \frac{\gamma q_2}{\omega_{2r}}. \tag{73}$$

Note that unlike the angular frequencies (Eq.(70)) which have real and imaginary parts, the group velocities are real quantities. Figs. 22(c) and 22(d) also shows the influence of the memory effect on group speeds V_{g1} and V_{g2}, plotted as a function of the wave numbers q_1 and q_2. We observe that for a given value of the constant γ taken between 0 and 0.9, the curves of group velocities decrease as a function of q_1 and q_2 respectively. But in both cases the limit minimum value of the group velocity increases slightly with the growth of γ. These curves keeping the same gaits would mean that the

interaction between tubulin dimers could manifest as waves of the same nature in close spatial period intervals. Moreover, the effect of transport memory could also contribute to limit the decrease of the propagation or transport speed of information through the cellular MTs channel.

• For $j = 1$ and $n = 1, 2$, at the $\left(\varepsilon^1, e^{0\times\theta_1}\right)$, $\left(\varepsilon^1, e^{0\times\theta_2}\right)$ and $\left(\varepsilon^1, e^{i2\theta_1}\right)$, $\left(\varepsilon^1, e^{i2\theta_2}\right)$, the first and second harmonics, respectively, lead to:

$$V_{01} = V_{02} = 0 \quad ; \quad V_{11} = V_{22} = 0. \tag{74}$$

• Finally, for $j = 2$ and $n = 1, 2$, at the $\left(\varepsilon^2, e^{i\theta_1}\right)$, $\left(\varepsilon^2, e^{i\theta_2}\right)$, the complex amplitudes V_1 and V_2 verify the equations:

$$\begin{aligned}
&(\eta_0 - 2i\omega_1)\frac{\partial V_1}{\partial T_2} - 2i\gamma q_1\frac{\partial V_1}{\partial X_2} + \frac{\partial^2 V_1}{\partial T_1^2} - \gamma\frac{\partial^2 V_1}{\partial X_1^2} \\
&- \left(3\omega_0^2\eta_2 - i\eta_1\omega_1\right)|V_1|^2 V_1 - \left(6\omega_0^2\eta_2 - 2i\eta_1\omega_1\right)|V_2|^2 V_1 = 0 \\
&(\eta_0 - 2i\omega_2)\frac{\partial V_2}{\partial T_2} - 2i\gamma q_2\frac{\partial V_2}{\partial X_2} + \frac{\partial^2 V_2}{\partial T_1^2} - \gamma\frac{\partial^2 V_2}{\partial X_1^2} \\
&- \left(3\omega_0^2\eta_2 - i\eta_1\omega_2\right)|V_2|^2 V_2 - \left(6\omega_0^2\eta_2 - 2i\eta_1\omega_2\right)|V_1|^2 V_2 = 0
\end{aligned} \tag{75}$$

Using the shifted variables $\xi_m = X_m - V_{g1}T_m$, $\xi'_m = X_m - V_{g2}T_m$ and $\tau_m = T_m$ with $m = 1, 2$, Eqs.(72) and (73) are transformed and introduced into the system of equations (75) with the simple combination $\xi'_1 = \xi_1 + (V_{g1} - V_{g2})\,T_1$ $(m = 1)$, to give :

$$\begin{aligned}
&i\frac{\partial V_1}{\partial \tau_2} + P_1\frac{\partial^2 V_1}{\partial \xi_1^2} + Q_1|V_1|^2 V_1 - R_1|V_2|^2 V_1 = 0, \\
&i\frac{\partial V_2}{\partial \tau_2} + P_2\frac{\partial^2 V_2}{\partial \xi_1^2} + i\left(\frac{V_{g2} - V_{g1}}{\varepsilon}\right)\frac{\partial V_2}{\partial \xi_1} + Q_2|V_2|^2 V_2 - R_2|V_1|^2 V_2 = 0
\end{aligned} \tag{76}$$

To make the second equation of the system (76) easy to handle, we cancel the term in $\frac{\partial V_2}{\partial \xi_1}$ via the gauge transformation [131] $V_2 = V_2\exp[-i(\frac{D}{2P_2\varepsilon}\xi_1 + \frac{D^2}{4P_2}\tau_2)]$, with $D = V_{g1} - V_{g2}$. By setting $\tau = \tau_2 = \varepsilon^2 t$ and $\xi = \xi_1 = \varepsilon t$, the system of equations (76) reduces to :

$$\begin{aligned}
&i\frac{\partial V_1}{\partial \tau} + P_1\frac{\partial^2 V_1}{\partial \xi^2} + Q_1|V_1|^2 V_1 - R_1|V_2|^2 V_1 = 0 \\
&i\frac{\partial V_2}{\partial \tau} + P_2\frac{\partial^2 V_2}{\partial \xi^2} + Q_2|V_2|^2 V_2 - R_2|V_1|^2 V_2 = 0,
\end{aligned} \tag{77}$$

where

$$\begin{aligned}
&P_1 = \frac{\gamma - V_{g1}^2}{2\omega_{1r}}, \quad P_2 = \frac{\gamma - V_{g2}^2}{2\omega_{2r}}, \quad Q_1 = Q_{1r} + iQ_{1i}, \\
&Q_2 = Q_{2r} + iQ_{2i}, \quad R_1 = R_{1r} + iR_{1i}, \quad R_2 = R_{2r} + iR_{2i},
\end{aligned} \tag{78}$$

with the expressions for Q_{1r}, Q_{2r}, Q_{1i}, Q_{2i}, R_{1r}, R_{2r}, R_{1i} and R_{2i}, given in appendix A2 in Eq.(164).

The system of equations (77) with some of its complex coefficients is indeed the expected one, i.e.

it has two complex coupled Schrodinger-type equations. The dispersive coefficients P_1 and P_2 are real, while Q_1, Q_2 (the cubic nonlinearity coefficients) and R_1, R_2 (coupling coefficients), respectively, are complex. By another name, the set of Eqs. (77) can also, but abusively, be called the complex Ginzburg-Landau (CGL) equations due to the complex form of some coefficients. However, compared to the standard CGL equation, an explicit linear dissipative term is absent [138,156–158]. Examples of similar form of nonlinear complex coupled GL equations with dissipative terms different from zero allowed Tankou et al [155] to study the dynamics of ionic waves in a dissipative network of MTs mimicking their electrophysiological behaviour, while Bansi and collaborators [159] used in to study the wave propagation in a viscoelastic tube filled with viscous fluid.

Note that in addition to the nonexistent dissipative terms, if the imaginary parts of the coupling and nonlinearity coefficients are assumed to be zero i.e. $R_{1i} = R_{2i} = Q_{1i} = Q_{2i} = 0$, then the system of Eqs.(77) reduces rather to a system of two Coupled Nonlinear Schrodinger equations similar to others in the literature already obtained by some authors in the same field and others as well [18,160,161].

Looking closely at our obtained Eqs.(77) system, it has the particularity of having all its six coefficients depending on the memory constant γ and the degree of nonlinearity η. At the same time, its decoupling leads directly to two uncoupled complex GL equations of the same form, as obtained in Ref. [111] in the context of study the transport memory effects on nonlinear wave propagation in a damped DNA model. It is important to mention that obtaining the analytical solutions of the system of equations (77) is essential for further progress in understanding the propagation of coupled signals in a damped MT network in the living cell.

II.3.3 The Modulational instability method

Modulational instability is a universal process that is inherent to most nonlinear wave systems in nature. Many theoretical and experimental works have revealed that MI is the direct way through which localized patterns emerge in many nonlinear systems. This phenomenon was predicted by Benjamin and Feir [162] for waves on deep water and by Bespalov and Talanov [163] for electromagnetic waves in nonlinear media with cubic nonlinearity. It is a result of the interplay between nonlinearity and dispersion and arises inhomogeneous nonlinear media. Nonlinear discrete and continues systems are the examples of these inhomogeneous media. This process of MI has been observed in many branch of physics such as plasma physics [164], nonlinear optics [165], nonlinear electrical transmission lines [166] and biological systems [167–170]. The increasing interest in the way energy spread in protein molecules in general and in DNA and microtubules in particular is a consequence of its importance in biology. MI consists in the input of plane wave which propagates through the system, which can become unstable for a small perturbation under specific conditions. Long time evolution leads to the growth of side bands near the fundamental wave and a mutual exchange of energy.

In what follows, we explain the procedure of MI through the model equation of a given biological system. The analysis on the stability previous system starts by assuming that the plane wave solution

of a given equation with a cubic/quintic nonlinearity is in the form:

$$u(x,t) = U_0 e^{i(kx-\omega t)}, \tag{79}$$

where ω and k are respectively, the angular frequency and the wavenumber of the carrier wave. Substituting the previous expression (79) into the amplitude equation describing the model, leads to the relationships between the constant amplitude U_0, k and ω known as the nonlinear dispersion relation. The linear stability of the wave plane solution can be investigated by looking a solution in the form:

$$u(x,t) = U_0 \left[1 + \theta(x,t)\right] e^{i(kx-\omega t)}, \tag{80}$$

where the modulated amplitude of perturbation $\theta(x,t)$ is assumed to be small in comparison with the corresponding parameters of the carrier wave. Inserting this perturbation wave plane into the equation of model and neglecting the higher nonlinear terms, we obtain the linear equation which describes the evolution for the perturbation. After, we assume the perturbation $\theta(x,t)$ in the form:

$$\theta(x,t) = \theta_1 e^{i(qx-\Omega t)} + c.c, \tag{81}$$

where q and Ω represent respectively, the wave number and the perturbation frequency of the modulation, which are much smaller than those of the carrier wave, θ_1 is the constant amplitudes and $c.c$ denotes complex conjugation. By substituting the expression (81) into the previous linear equation for the perturbation and after linearization, we obtain an homogeneous system for constant amplitude, which leads to the problem of solving the nonlinear dispersion relation in Ω.

As Ω is a function of q and k (ie $\Omega = \Omega(q,k)$), the following growth rate of instability

$$K = \left|\mathrm{Im}(\Omega(q,k))\right|, \tag{82}$$

is determined and allow us to have the parametric regions of the system where the plane wave is instable or stable.

In our frame work, so we applied this technique to shown that the MI is precursor of solitons and localized structures formation in cellular microtubules, with the presence and the effect of the electrical field on the one hand, and the dissipation on the other hand in the medium. Then, for the analysis, the CNLS equations (see the system of Eqs.(52),(53)) and the CCGL equations (see system of Eq.(65)) are used for our application.

Another major difficulty in the search for an understanding of biophysical phenomena is to construct the adequate solutions of the mathematical amplitude equations of the proposed physical model for their description. Several methods have been proposed to solve differential-difference equations and to obtain exact solutions to nonlinear partial differential equations. One can think of the inverse scattering method [171], the tanh method [172], the JEF method [160, 173], F-expansion

method [174, 175], Bäcklund transformation method [125], Hirota's modified method [99], Hirota's direct method [176] and homogeneous balance method [177] and so on. In the following part, we present the methods for the resolution of the obtained nonlinear differential equations (CNLS and CCGL equations). Among these above methods, we used those of Jacobian and Hirota's modified for this purpose.

II.3.4 The Jacobian Elliptic Function Method

As advertise above, the essential purpose of this subsection is to study whether and how Jacobian elliptic functions can be used to understand our biophysical phenomena. In particular, we present the usefulness of these functions in solving the set of CNLS equations (52) and (53)). we firstly recall some general following properties of Jacobian elliptic functions $sn(x)$, $cn(x)$ and $dn(x)$ [178, 179]:

$$\frac{d[dn(x)]}{dx} = -m^2 sn(x)cn(x), \tag{83}$$

$$\frac{d[cn(x)]}{dx} = -sn(x)dn(x), \tag{84}$$

$$\frac{d[sn(x)]}{dx} = cn(x)dn(x), \tag{85}$$

$$dn^2(x) = 1 - m^2 sn^2(x), \tag{86}$$

$$cn^2(x) + sn^2(x) = 1. \tag{87}$$

where m (with $0 < m < 1$) is a modulus of jacobian elliptic functions.

When $m \longrightarrow 1$, the JEFs degenerate into hyperbolic functions, that is,

$$sn(x) \to \tanh(x), \tag{88}$$

$$cn(x) \to \sec h(x), \tag{89}$$

$$dn(x) \to \sec h(x). \tag{90}$$

Also, for $m \longrightarrow 0$, these functions degenerate into trigonometric functions, that is

$$sn(x) \to \sin(x), \tag{91}$$

$$cn(x) \to \cos(x), \tag{92}$$

$$dn(x) \to 1. \tag{93}$$

Secondly, the application of this Jacobian method mentioned above on a nonlinear differential equation is taken as an example: let the following NLS equation [180]

$$i\frac{\partial F}{\partial \tau} + P\frac{\partial^2 F}{\partial \zeta^2} + Q|F|^2 F = 0, \tag{94}$$

where P and Q are the dispersion and the nonlinearity parameters, the Coordinates ζ and τ are the

following rescaled time and space variables:

$$\tau = \epsilon^2 t \quad \text{and} \quad \zeta = \epsilon\left(n\ell - \mu t\right), \tag{95}$$

with μ, the group velocity [80] or a small variable that will be determined by a solvability condition [160]. The types of solutions to this equation (94) strongly depend on the sign of its coefficients P and Q. And thus, its solution begins with a type of the following transformation:

$$F\left(\zeta,\tau\right) = g\left(\xi\right) e^{i(K_1\zeta - k_2\tau)}, \quad \text{with} \quad \xi = K\zeta - \alpha\tau, \tag{96}$$

which by substituting into Eq.(94), changes it in:

$$(k_2 - PK_1^2)g + PK^2\frac{\partial^2 g}{\partial\xi^2} + Qg^3 = 0, \tag{97}$$

with $\alpha = 2PKK_1$. We look for the solution of Eq.(97) in the form [180]:

$$g(\xi) = \beta_0 + \beta_1 f(\xi), \tag{98}$$

where $f(\xi)$ = [$sn(\xi)$, $cn(\xi)$, $dn(\xi)$] and β_0, β_1 are to be determined. Hence, using some basic formulae concerning JEFs given by relations from Eq.(83) to Eq.(87), we will study the possible solution expressed through $dn(\xi)$ only and we find for $\beta_0 = 0$,

$$\beta_1^2 = \frac{2PK^2}{Q}, \qquad k_2 = P(K_1^2 + K^2m^2 - 2K^2). \tag{99}$$

Such solution deeply depend also on the signs of the parameter P/Q (see Eq.(83)). As the interval for the modulus is $0 < m < 1$, the solution exists only if $P > 0$, $Q > 0$ or $P < 0$, $Q < 0$.

Therefore, by Eqs. (95), (96), (98) and (99), the evolution of the exact analytical solution of the NLS equation (94) is found for $PQ > 0$ and to a limit $m \to 1$.

Finally in step three, by knowing the function F and from some reduction expressions that we will evoke in Chapter 3, we can easily construct the solutions of the stating mathematical equation describing the studied physical model. In this work, we have for example the discrete spatio-temporal equation (19) of which the solutions sufficiently explain the nonlinear dynamic of MTs.

II.3.5 The Hirota's Modified Bilinear Method

Hirota's Method has been one of the most successful direct techniques for constructing exact solutions to various nonlinear PDEs from mathematical physics and soliton theory. Hirota [181] developed a method for solving nonlinear equations without requiring the complex technique of inverse scattering method, too used generally in many non-equilibrium physical systems. In concrete terms, the principle of the Hirota's bilinear method lies on the implementation of the Hirota's bilinear operator, which trans-

forms the nonlinear evolution equations into several coupled bilinear equations. This act decomposes the original complicated equation into a series of relatively simple equations [182, 183]. Depending on the nature of the physical problem, several modifications and improvements are made to obtain an even larger class of nonlinear waves, hence the name of modified Hirota method. As an example of the path, we assume the generalized CGL equation and describing the propagation of waves [184]:

$$i\frac{\partial\chi(x,t)}{\partial t}+p\frac{\partial^2\chi(x,t)}{\partial x^2}+q|\chi(x,t)|^2\chi=i\gamma\chi(x,t), \tag{100}$$

where $p=p_r+ip_i$, $q=q_r+iq_i$ and $\gamma=\gamma_r+i\gamma_i$ respectively, represent the dispersion, the nonlinearity, and the dissipation coefficients. To solve the nonlinearly CGL Eq.(100) by Hirota's modified method, one can take its solutions in the form:

$$\chi(t,x)=\frac{Ge^{i(Kx-\Omega t)}}{F^{(1+i\alpha)}}, \tag{101}$$

where α, K, Ω, G and F are assumed to be real. Note that in the starting method of Hirota, he took this solution only as $\chi(t,x)=\frac{G}{F}$, while the one below is improved by the presence of the complex terms $e^{i(Kx-\Omega t)}$ and $1+i\alpha$ more.

Here, in general the modified Hirota bilinear operator to use is define by:

$$\begin{aligned}D^m_{\alpha,x}D^n_{\alpha,t}\left(G\cdot F\right)=&\left[\frac{\partial}{\partial x}-\left(1+i\alpha\right)\frac{\partial}{\partial x'}\right]^m\times\left[\frac{\partial}{\partial t}-\left(1+i\alpha\right)\frac{\partial}{\partial t'}\right]^n\\&\times G\left(x\right)\cdot F\left(x'\right)\big|_{x=x',t=t'}\end{aligned} \tag{102}$$

$$\hat{\alpha}=\left(1+i\alpha\right)\left(2+i\alpha\right), \tag{103}$$

for non-negative integers m and n. To obtain some exact soliton solutions of the CGL equation above, one substitute Eq.(101) into Eq.(100) and apply the modified Hirota operators Eqs.(102) and (103) to have the following system of two coupled bilinear equations:

$$\left[\Omega-pK^2-\gamma+iD_{t,x}+2ipKD_{\alpha,x}+pD^2_{\alpha,x}\right]\left(G\cdot F\right)=0 \tag{104}$$

$$\left[p\hat{\alpha}D^2_{0,x}+i\gamma-\lambda\right]\left(F\cdot F\right)-q|G|^2=0, \tag{105}$$

with λ is the free complex constant to be determined and the positive integers m and n are taken to 1 and 0 respectively. This system of bilinear Eqs. (104) and (104) can make it possible to have a variety soliton solutions under very specific conditions of parameters. Among these mentioned soliton solutions, we can cite among others darks, breathers, kinks, anti-kinks, pulses and shocks. In this thesis, we chose to obtain the pulse-typed soliton solutions because of the electrical activity of neuronal microtubules in the transport of cellular information. Thus, the solutions of the system of two CCGL equations (see Eq.(65)) that we have derived are proposed from this modified Hirota bilinear method.

II.4 The Fourth order Runge-Kutta numerical method

It is known that nonlinear differential equations are not easy to solve analytically. The analytical methods, under condition to a certain number of approximation, make it possible to obtain approximate solutions. So in order to confirm these results, it is imperative to use other more precise methods: numerical simulation methods. From these last methods, we then verify the stability of our analytical approaches obtained. To carry out this work, the nonlinear differential of order greater than one are firt transformed into a system of several nonlinear ODEs. Many different numerical methods have been proposed and used in an attempt to solve accurately various types of ordinary differential equations [185]. However there are a handful of methods known and used universally [186] such that the Runge-Kutta method, the pseudo-spectral method, Newton-Raphson method, Euleur method, the Adams-Bashforth and Backward Differentiation Formula methods. All these methods discretize the differential system to produce a discrete system of equation or map [187]. In this work, we use the fourth order Runge-Kutta method to solve the discrete nonlinear differential equations which describe Mts dynamic. The forth-order Runge-Kutta method is a technique for approximating solutions to ordinary differential equations [186, 188]. It was first developed by the German mathematician C. Runge in 1894 and subsequently improved by M.W. Kutta in 1901. This method is based on the numerical techniques of integration of the trapezoids and Simpson [189]. It is very stable and to set up. For the procedure, let us therefore consider the following system of three first-order ODEs :

$$\frac{dx}{dt} = f_1(t, x, y, z), \qquad x(t_0) = x_0 \tag{106}$$

$$\frac{dy}{dt} = f_2(t, x, y, z), \qquad y(t_0) = y_0 \tag{107}$$

$$\frac{dz}{dt} = f_3(t, x, y, z), \qquad z(t_0) = z_0 \tag{108}$$

where at the initial time t_0 the corresponding values of x, y and z are x_0, y_0 and z_0 respectively. The function f_j with $j = 1, 2, 3$ and the initial data t_0, x_0, y_0 and z_0 are given. The application of the RK4 makes it possible to find the values of the variables x, y and z at successive time intervals $\Delta t = h$. The iterative numerical scheme of this method is given by the three expressions:

$$\begin{aligned} x_{i+1} &= x_i + \frac{L_1 + 2L_2 + 2L_3 + L_4}{6}, \\ y_{i+1} &= y_i + \frac{K_1 + 2K_2 + 2K_3 + K_4}{6}, \\ z_{i+1} &= z_i + \frac{Q_1 + 2Q_2 + 2Q_3 + Q_4}{6}. \end{aligned} \tag{109}$$

with $i = 0,\ 1, 3,\ 4, ...$ stands for the iteration number, $h > 0$ represents the step-size and

$$
\begin{aligned}
&L_1 = hf_1\left(t_i, x_i, y_i, z_i\right); \qquad L_2 = hf_1\left(t_i + \frac{h}{2}, x_i + \frac{L_1}{2}, y_i + \frac{K_1}{2}, z_i + \frac{Q_1}{2}\right),\\
&K_1 = hf_2\left(t_i, x_i, y_i, z_i\right); \qquad K_2 = hf_2\left(t_i + \frac{h}{2}, x_i + \frac{L_1}{2}, y_i + \frac{K_1}{2}, z_i + \frac{Q_1}{2}\right),\\
&Q_1 = hf_3\left(t_i, x_i, y_i, z_i\right); \qquad Q_2 = hf_3\left(t_i + \frac{h}{2}, x_i + \frac{L_1}{2}, y_i + \frac{K_1}{2}, z_i + \frac{Q_1}{2}\right),\\
&L_3 = hf_1\left(t_i + \frac{h}{2}, x_i + \frac{L_2}{2}, y_i + \frac{K_2}{2}, z_i + \frac{Q_2}{2}\right); \quad L_4 = hf_1\left(t_i + h, x_i + L_3, y_i + K_3, z_i + Q_3\right),\\
&K_3 = hf_2\left(t_i + \frac{h}{2}, x_i + \frac{L_2}{2}, y_i + \frac{K_2}{2}, z_i + \frac{Q_2}{2}\right); \quad K_4 = hf_2\left(t_i + h, x_i + L_3, y_i + K_3, z_i + Q_3\right),\\
&Q_3 = hf_3\left(t_i + \frac{h}{2}, x_i + \frac{L_2}{2}, y_i + \frac{K_2}{2}, z_i + \frac{Q_2}{2}\right); \quad Q_4 = hf_3\left(t_i + h, x_i + L_3, y_i + K_3, z_i + Q_3\right).
\end{aligned}
$$

Here x_{i+1}, y_{i+1} and z_{i+1} are the RK4 approximations of $x(t_{i+1})$, $y(t_{i+1})$ and $z(t_{i+1})$, respectively and the next value x_{i+1} or y_{i+1} or z_{i+1} is determined by the present value (x_i) or (y_i) or (z_i) plus the weighted average of four increments, where each increment is the product of the size of the interval, h, and an estimated slope specified by function f_j on the right-hand side of the ODEs. Note that the above results are necessary and sufficient to find the numerical solutions of Eqs.(106)-(108) as long as it remains continuous. But in a discrete model, one needs moreover the boundary conditions whose choice depends on the studied problem. During our investigations, we have employed periodic boundary conditions since the different models explored are assumed to be cyclic. For example, a lattice of tubulin dimers with nearest neighbors interactions obeys the following boundary conditions

$$
Y_{1-j} = Y_{M-j+1} \quad ; \quad Y_{M+j} = Y_j \quad , \quad j = 1, 2, 3, ... \tag{110}
$$

The RK4 method is a fourth-order method, meaning that the local truncation error is on the order of $O(h^5)$, while the total accumulated error is on the order of $O(h^4)$.

II.5 Conclusion

This second chapter was devoted to the methodical approaches used in this thesis. Firstly, we made a thorough development of the observations from the Zdravković radial angular model (see Fig. 10), with as main interpretations the formulation of the different types of energies acting on the MT network and whose resultant led to the discrete Hamiltonian of a PF. This Hamiltonian was then used to obtain the discrete nonlinear differential equation for the motion of the MTs in the eukaryotic cell, neglecting all friction (see Eq.(20)) on the one hand and considering it to be very intense on the other (see Eq.(22)).

In the same way as above, but with the MT behaving more like an electrical transmission line (see Fig. 15), we also used Kirchhoff's laws to arrive at the discrete spatio-temporal differential equation (37) for the evolution of ionic waves governed by electrical voltage. Subsequently, the multiple scale expansion and semi-discrete approximation methods were presented and applied in turn to the differ-

ential equations of the two models studied. This allowed us to derive three systems of two equations with coupled amplitudes: the first, CNLS; the second, CCNLS incorporating the effects of transport memory; and the third, CCGL. We should point out however that, these coupled Schrödinger and GL equations appear for the first time in the study of MT dynamics, as far as the two models mentioned here are concerned.

We have also presented general MI theories and, methods for analytically solving of Jacobian Elliptic Functions and the Modified Bilinear Hirota. The application of these techniques to the above coupled amplitude equation systems will be carried out in the next chapter, for the search and parametric determination of the instability regions where soliton structures are located. Finally, the numerical analysis method (i.e. RK4) was presented and will be used again in Chapter 3 to verify the stability of the predicted analytical solutions.

CHAPTER III

RESULTS AND DISCUSSION

III.1 Introduction

Many explorations of researchers in the field of biophysics in general are focused on various phenomena, including the propagation of nonlinear waves (pulse solitons, kinks/anti-kinks, breathers, dark ...) with energy transport, the formation of localized structures and the environmental impact on information transfer in biological media, to name a few. Especially in the living cell and more precisely on MT's filaments, these nonlinear excitations have received increasing attention in recent years and are widely considered to be responsible for several phenomena, such as the polymerization/depolymerization process, ionic conductivity in the cell, trafficking of materials by motor proteins, signalling processes and information transport in neurons.

In the previous chapters, we have discussed generalities about microtubules with a particular emphasis on their crucial roles in differentiated and non-differentiated cells of the nervous system, Zdravković's radial and Tuszińsky's electrical transmission lines mathematical models. The mathematical methods used to achieve our goals have been indicated. In this third chapter, we started with the application of MI analysis on the systems of CNLS equations (52) and (53) and CCGL equations (65) to show that there would exist the formation of solitonic or localized structures in our biophysical systems. Subsequently, the JEF and Modified Hirota methods are used to construct the analytical solutions of the coupled Schrödinger and GL systems of equations. Finally, to confirm that the analytical methods employed are sound, we perform a numerical analysis of the starting problem situations via the RK4 algorithm and plot the different result curves obtained. With supporting discussions, we also study the influence of the electrical field and some specific parameters of the cytoplasmic environment on the nonlinear dynamics of the MTs.

III.2 Modulational instability of coupled waves in microtubules

This part tells us about the type of excitations that can support our two studied models through MI.

III.2.1 MI of coupled waves in MTs networks of φ-model

As mentioned above in chapter 2, one of the direct mechanisms solitonic structures emerge in nonlinear systems is through MI. We are interested here in the coupled nonlinear Schrodinger system of equation. In order to investigate the possibility of wave mixing in the set of Eqs.(52) and (53), we assume the plane waves $\psi = \psi_{j0}e^{i\omega_j t}$ as solutions, where the real constants $\omega_j (j = 1, 2)$, and the complex

constants amplitudes ψ_{j0} are characterized by the dispersion relations

$$\omega_j = \zeta_{jj}|\psi_{j0}|^2 + \zeta_{jk}|\psi_{k0}|^2, \quad j,k = 1,2 \quad \text{with} \quad k \neq j. \tag{111}$$

The stability of these plane wave solutions can be investigated by slightly perturbing their amplitudes as $\psi = (\psi_{j0} + \epsilon\psi_j)e^{i\omega_j t}$ [190]. After some linearization around the unperturbed solutions and using condition Eqs.(111) , we write $\psi_j = u_j + iv_j$ and $\psi_{j0} = a_j + ib_j$, which leads to the following real and imaginary parts for Eqs.(52) and (53):

$$H_1\frac{\partial^2 u_1}{\partial x^2} - \frac{\partial v_1}{\partial t} + \zeta_{11}\left(2a_1^2u_1 + 2a_1b_1v_1\right) + \zeta_{12}\left(2a_1a_2u_2 + 2a_1b_2v_2\right) = 0 \tag{112}$$

$$H_1\frac{\partial^2 v_1}{\partial x^2} + \frac{\partial u_1}{\partial t} + \zeta_{11}\left(2a_1b_1u_1 + 2b_1^2v_1\right) + \zeta_{12}\left(2a_2b_1u_2 + 2b_1b_2v_2\right) = 0 \tag{113}$$

$$H_2\frac{\partial^2 u_2}{\partial x^2} - \frac{\partial v_2}{\partial t} + \zeta_{21}\left(2a_1a_2u_1 + 2a_2b_1v_1\right) + \zeta_{22}\left(2a_2^2u_2 + 2a_2b_2v_2\right) = 0 \tag{114}$$

$$H_2\frac{\partial^2 v_2}{\partial x^2} + \frac{\partial u_2}{\partial t} + \zeta_{21}\left(2b_1b_2v_1 + 2a_1b_2u_1\right) + \zeta_{22}\left(2a_2b_2u_2 + 2b_2^2v_2\right) = 0. \tag{115}$$

Furthermore, from the previous assumption, inserting $u_j = u_{j0}e^{i(\lambda x - \Omega t)} + c.c.$ and $v_j = v_{j0}e^{i(\lambda x - \Omega t)} + c.c.$ ($j = 1.2$) into Eqs.(112)-(115), where λ and Ω are the perturbation wavenumber and the frequency, respectively, which are much smaller than those of the carrier wave, and $c.c.$ stands for the complex conjugate, we therefore obtain an homogeneous system for u_{j0} and v_{j0} as follows

$$\begin{pmatrix} -i\Omega + 2\zeta_{11}a_1b_1 & -H_1\lambda^2 + 2\zeta_{11}b_1^2 & 2\zeta_{12}a_2b_1 & 2\zeta_{12}b_1b_2 \\ -H_1\lambda^2 + 2\zeta_{11}a_1^2 & i\Omega + 2\zeta_{11}a_1b_1 & 2\zeta_{12}a_1a_2 & 2\zeta_{12}a_1b_2 \\ 2\zeta_{21}a_1b_2 & 2\zeta_{21}b_2b_1 & -i\Omega + 2\zeta_{22}a_2b_2 & -H_2\lambda^2 + 2\zeta_{22}b_2^2 \\ 2\zeta_{21}a_1a_2 & 2\zeta_{21}b_1a_2 & -H_2\lambda^2 + 2\zeta_{22}a_2^2 & i\Omega + 2\zeta_{22}a_2b_2 \end{pmatrix} \begin{pmatrix} u_{10} \\ v_{10} \\ u_{20} \\ v_{20} \end{pmatrix} = \begin{pmatrix} 0 \\ 0 \\ 0 \\ 0 \end{pmatrix}. \tag{116}$$

The condition for the above system to have nontrivial solutions is obtained by setting its determinant to zero, which leads to the following quartic polynomial nonlinear dispersion relation:

$$\Omega^4 - R\Omega^2 + S = 0, \tag{117}$$

whose solutions are either real or complex, with

$$R = \left(H_1^2 + H_2^2\right)\lambda^4 - 2\left(H_1\zeta_{11}\left|\psi_{10}\right|^2 + H_2\zeta_{22}\left|\psi_{20}\right|^2\right)\lambda^2,$$
$$S = H_1^2H_2^2\lambda^8 - 2H_1H_2\left(H_2\zeta_{11}\left|\psi_{10}\right|^2 + H_1\zeta_{22}\left|\psi_{20}\right|^2\right)\lambda^6 + 4H_1H_2\left|\psi_{10}\right|^2\left|\psi_{20}\right|^2\left(\zeta_{11}\zeta_{22} - \zeta_{12}\zeta_{21}\right)\lambda^4$$

- For the system to be stable under modulation, the conditions $R > 0$, $S > 0$ and $\Delta = R^2 - 4S > 0$

should be fulfilled. Eq. (117) admits two solutions as:

$$\Omega_+^2 = \frac{1}{2}\left[R + \sqrt{R^2 - 4S}\right], \quad \Omega_-^2 = \frac{1}{2}\left[R - \sqrt{R^2 - 4S}\right]. \tag{118}$$

In this framework, the instability is a purely growing mode and we have the growth rate instability $\Gamma = \sqrt{-\Omega_-^2}$.

• On the other hand, if $\Delta = R^2 - 4S < 0$, there exists a domain of the wavenumber λ of the perturbation for which Ω^2 is negative. In this range, the solution of Eq. (117) are complex and so that Ω^2 has a nonvanishing imaginary part. The plane wave will be unstable if this imaginary part of Ω

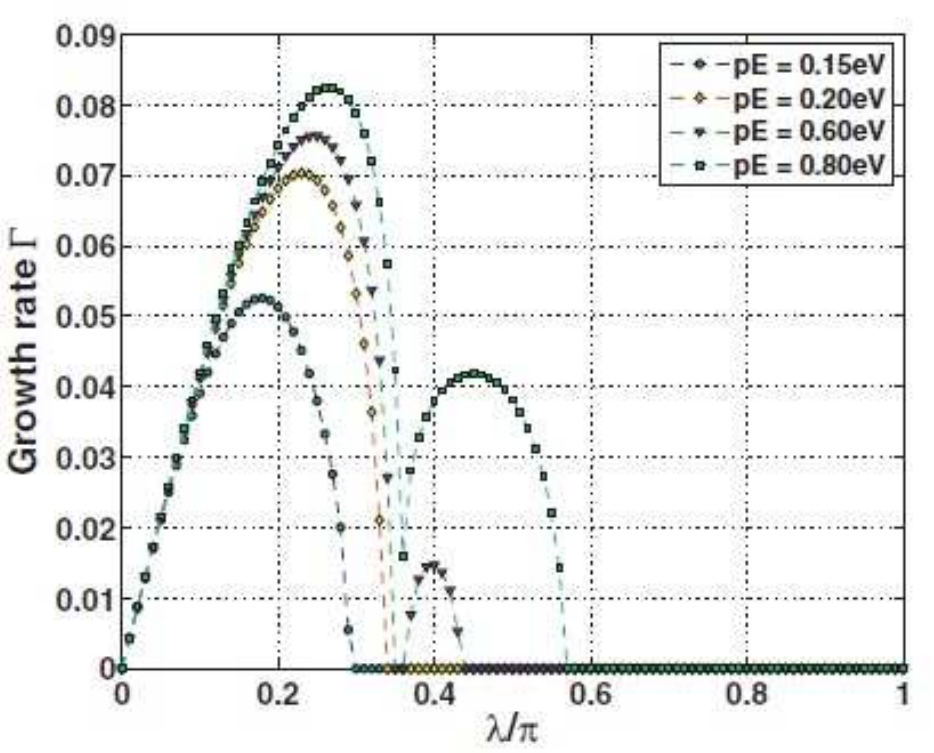

Figure 23: The growth rate of MI is plotted for the coupled mode versus the perturbation wavenumber λ. It is obvious that increasing the dipolar energy contributes to expand the instability region. There also appears another region of instability, where nonlinear waves in protofilaments.

is positive, leading the perturbation to grow exponentially. Consequently, the plane wave tends to self-modulate with a wavenumber λ corresponding to the growth rate:

$$\Gamma = Im(\Omega_\pm^2) = \pm\frac{1}{2}\sqrt{4S - R^2}. \tag{119}$$

The corresponding growth rate of instability is plotted versus the wavenumbers of perturbation, λ, in Fig. 23. The above growth rate of instability implies that the condition $\sqrt{4S - R^2} > 0$ should be satisfied for wave instability to take place. On studying the influence of the dipolar energy on the behavior of the of the growth rate of instability, one sees that for $pE = 0.15$ eV, there is only one region of instability, where modulated waves are expected. That region is situated in the interval $0 < \lambda < 0.30\pi$, and gets expanded for $pE = 0.20$ eV. Wave instability now spans in the interval $0 < \lambda < 0.55\pi$. However,

beyond that value of the dipolar energy, there emerges another region of instability $0.35\pi < \lambda < 0.45\pi$ for $pE = 0.60$ eV. Further increasing the later also expands the two regions of parameter for MI to develop gets large as well. Regions of instability are those where the dimers are expected to undergo localized oscillations as a result of the interplay between nonlinear and dispersive effects. On the other hand, when parameters are not picked from those areas, the plane wave solutions will be said to be stable under modulation and will not experience any perturbation.

III.2.2 MI of coupled waves in MTs networks of an electrical transmission line model

In order to perform the MI study here, we assume the set of Eqs.(65) to have the plane wave solutions $B_q\left(\xi, T_2\right) = B_{q0}e^{i\varpi_q T_2}$, where ϖ_q and B_{q0}, with $q = 1, 2$, are, respectively, the angular frequencies and the complex constant amplitudes of the carrier waves satisfying the dispersion relations

$$\begin{aligned} \varpi_1 &= \sigma_1|B_{10}|^2 + \rho_1|B_{20}|^2 - i\gamma_1, \\ \varpi_2 &= \sigma_2|B_{20}|^2 + \rho_2|B_{10}|^2 - i\gamma_2. \end{aligned} \tag{120}$$

We slightly perturb the amplitudes of these initial plane waves in such a way that $B_1\left(\xi, T_2\right) = B_{10}(1+\varepsilon \times g_1(\xi, T_2))e^{i\varpi_1 T_2}$ and $B_2\left(\xi, T_2\right) = B_{20}\left(1 + \varepsilon g_2(\xi, T_2)\right)e^{i\varpi_2 T_2}$, where $\varepsilon \ll 1$ and $g_j(\xi, T_2)$, with $j = 1, 2$, are the modulated amplitudes of perturbation.

Inserting the above perturbed amplitudes into the system Eqs.(65) and linearizing around the unperturbed plane waves, the equations describing the perturbed fields are given by

$$\begin{aligned} &i\frac{\partial g_1}{\partial T_2} - S_1\frac{\partial^2 g_1}{\partial \xi^2} - 2iS_1k_1\frac{\partial g_1}{\partial \xi} - \sigma_1|B_{10}|^2\left(g_1 + g_1^*\right) - \rho_1|B_{20}|^2\left(g_2 + g_2^*\right) = 0 \\ &i\frac{\partial g_2}{\partial T_2} - S_2\frac{\partial^2 g_2}{\partial \xi^2} - 2iS_2k_2\frac{\partial g_2}{\partial \xi} - \sigma_2|B_{20}|^2\left(g_2 + g_2^*\right) - \rho_2|B_{10}|^2\left(g_1 + g_1^*\right) = 0. \end{aligned} \tag{121}$$

Solutions for the above system are then considered to be

$$\begin{aligned} g_1\left(\xi, T_2\right) &= d_1e^{i(\lambda\xi - \delta T_2)} + d_2^*e^{-i(\lambda\xi - \delta^* T_2)}, \\ g_2\left(\xi, T_2\right) &= d_3e^{i(\lambda\xi - \delta T_2)} + d_4^*e^{-i(\lambda\xi - \delta^* T_2)}, \end{aligned} \tag{122}$$

where d_1, d_2, d_3 and d_4 are complex constant amplitudes, λ and δ represent, respectively, the wave number and the frequency of the perturbation, with the asterisk denoting complex conjugation. Applying these solutions to Eqs. (121) and using the standard procedure of linear stability analysis lead to the following homogeneous system of equations in terms of d_1, d_2, d_3 and d_4

$$\begin{pmatrix} Q_{11} + \delta & Q_{12} & Q_{13} & Q_{14} \\ Q_{21} & Q_{22} - \delta & Q_{23} & Q_{24} \\ Q_{31} & Q_{32} & Q_{33} + \delta & Q_{34} \\ Q_{41} & Q_{42} & Q_{43} & Q_{44} - \delta \end{pmatrix} \begin{pmatrix} d_1 \\ d_2 \\ d_3 \\ d_4 \end{pmatrix} = \begin{pmatrix} 0 \\ 0 \\ 0 \\ 0 \end{pmatrix}, \tag{123}$$

where the elements of the matrix $(\mathcal{M})$ are given by

$$\begin{aligned}
&Q_{11} = S_1\lambda^2 - \sigma_1|B_{10}|^2, \;\; Q_{13} = -\rho_1|B_{20}|^2, \;\; Q_{22} = S_1\lambda^2 - \sigma_1^*|B_{10}|^2,\\
&Q_{21} = Q_{23} = Q_{12} = Q_{14} = Q_{32} = Q_{34} = Q_{41} = Q_{43} = 0,\\
&Q_{24} = -\rho_1^*|B_{20}|^2, \;\; Q_{31} = -\rho_2|B_{10}|^2,\\
&Q_{33} = S_2\lambda^2 - \sigma_2|B_{20}|^2, \;\; Q_{42} = -\sigma_2^*|B_{20}|^2, \;\; Q_{44} = S_2\lambda^2 - \sigma_2^*|B_{20}|^2.
\end{aligned} \tag{124}$$

For the above system Eqs.(123) to admit non-trivial solutions, its determinant should be null, i.e. $\mathrm{Det}(\mathcal{M}) = 0$. The dispersion relation, which determines δ, is then obtained by solving the homogeneous matrix equation when its determinant of the coefficient matrix vanishes, which leads to

$$\delta^4 + \eta_3\delta^3 + \eta_2\delta^2 + \eta_1\delta + \eta_0 = 0. \tag{125}$$

Eq.(125) is a four order equation for the perturbation frequency obtained by taking determinant of the matrix null, with η_0, η_1, η_2 and η_3 given to appendix B1.(170).

Solving Eq. (125), we can obtain the following four analytical solutions

$$\begin{aligned}
\delta_{1,2} &= -\frac{\eta_3}{4} - \frac{1}{2}\sqrt{\frac{1}{4}\eta_3^2 - \frac{2}{3}\eta_2 + \Lambda} \pm \frac{1}{2}\sqrt{-\frac{4}{3}\eta_2 + \frac{1}{2}\eta_3^2 - \Lambda + \frac{\eta_3^3 - 4\eta_3\eta_2 + 8\eta_0}{4\sqrt{\frac{1}{4}\eta_3^2 - \frac{2}{3}\eta_2 + \Lambda}}},\\
\delta_{3,4} &= -\frac{\eta_3}{4} + \frac{1}{2}\sqrt{\frac{1}{4}\eta_3^2 - \frac{2}{3}\eta_2 + \Lambda} \pm \frac{1}{2}\sqrt{-\frac{4}{3}\eta_2 + \frac{1}{2}\eta_3^2 - \Lambda - \frac{\eta_3^3 - 4\eta_3\eta_2 + 8\eta_0}{4\sqrt{\frac{1}{4}\eta_3^2 - \frac{2}{3}\eta_2 + \Lambda}}},
\end{aligned} \tag{126}$$

where

$$\Lambda = \frac{1}{3}\left(\sqrt[3]{\frac{\Delta_1 + \sqrt{\Delta_1^2 - 4\Delta_0^3}}{2}} + \frac{\Delta_0}{\sqrt[3]{\frac{\Delta_1 + \sqrt{\Delta_1^2 - 4\Delta_0^3}}{2}}}\right)$$

and $\Delta_0 = \eta_2^2 - 3\eta_3\eta_1 + 12\eta_0$, $\Delta_1 = 2\eta_2^3 - 9\eta_3\eta_2\eta_1 + 27\eta_3^2\eta_0 + 27\eta_1^2 - 72\eta_2\eta_0$. There exists a domain of the wavenumber λ for which the spectrum of the growth rate of MI $G(\lambda, k_1) = 2\mathrm{Im}(\delta_{1,2,3,4})$ can take a positive or a negative value. The system remains stable under modulation if the indicated MI growth rate value is negative and this because of the vanishing long term of the growth rate $|\mathrm{Im}(\delta_{1,2,3,4})|$, exponentially over time. On the other hand, for positive gain values, there is possibility of instabilities. We therefore witness a divergence of the perturbation as time t increases and the system is said to be modulationally unstable. Therefore, necessary information on the onset of instability will be extracted using the maximum MI growth rate $G(\lambda, k_1) = 2[|\mathrm{Im}(\delta_{1,2,3,4})|]_{max}$ which is obtained by comparing the four solutions of the nonlinear dispersion relation (125) given in Eqs.(126). Obviously, the MI growth rate is strongly influenced by the physical parameter β_0 on the one hand, and α on the other hand. To remind, α is the parameter linking the wavenumbers k_1 and k_2. The MI growth rate is illustrated in the $(k_1, \lambda)-$plane in Fig. 24, where β_0 takes increasing values. In general, versus λ, the growth rate spectrum comprises two symmetric lobes of instability. Values of the wavenumber k_1 that give rise to instability are well-limited, while $k_1 = 0$ is not supposed to support instability, with the maximum

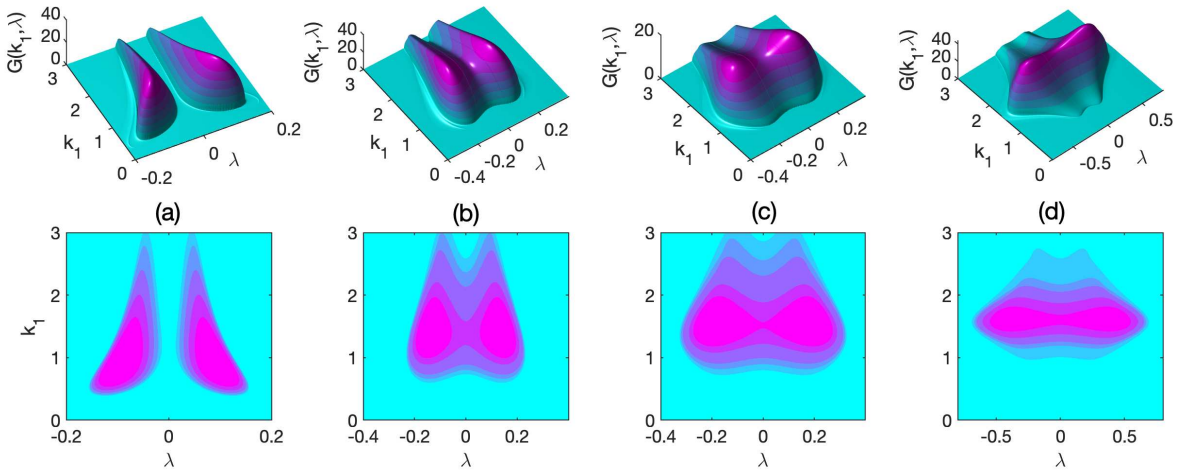

Figure 24: The MI growth rate features versus the perturbation wavenumber λ and the wavenumber of the plane wave k_1, with $k_2 = \alpha k_1$ and $\alpha = 0.5$. The panels (a), (b), (c) and (d) correspond to the respective values 0.06, 0.3, 0.5 and 0.7 of the dissipative coefficient β_0.

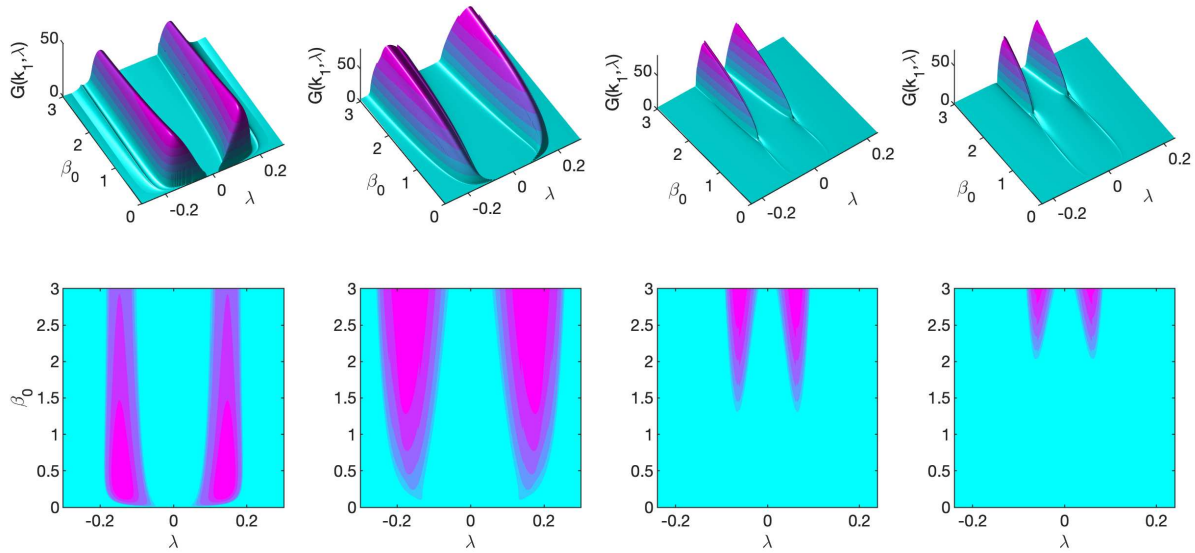

Figure 25: The MI growth rate spectrum in the $(\lambda, \beta_0)-$plane for $k = k_1 = 1$ and $k_2 = \alpha k_1$, with α taking the values 0.1, 0.2, 0.35 and 0.5 corresponding to the respective panels (a), (b), (c) and (d).

growth rate being situated around, including, $k_1 = 1$. With increasing β_0, the bandgap between the two lobes tends to disappear, leading the two lobes of instability to merge into one, under strong symmetry around $\lambda = 0$. Regions where $G \neq 0$ are indeed regions of instability that may support the disintegration of the plane wave solutions into trains of solitonic objects. To further explore the behaviors of the MI growth rate under the influence of β_0, G is plotted in Fig. 25 in the $(\lambda, \beta_0)-$plane, with α changing, so that $k_2 = \alpha k_1$. While the growth rate is an increasing function of the parameter α, the MI spectrum generally displays two symmetric lobes of instability. For $\alpha = 0.1$ and $\alpha = 0.2$, one clearly notices an amplification of the instability, and areas of λ giving rise to the maximum growth rate get expanded [compare Figs. 25(a) and 25(b)]. However, with further increasing α, such intervals shrink,

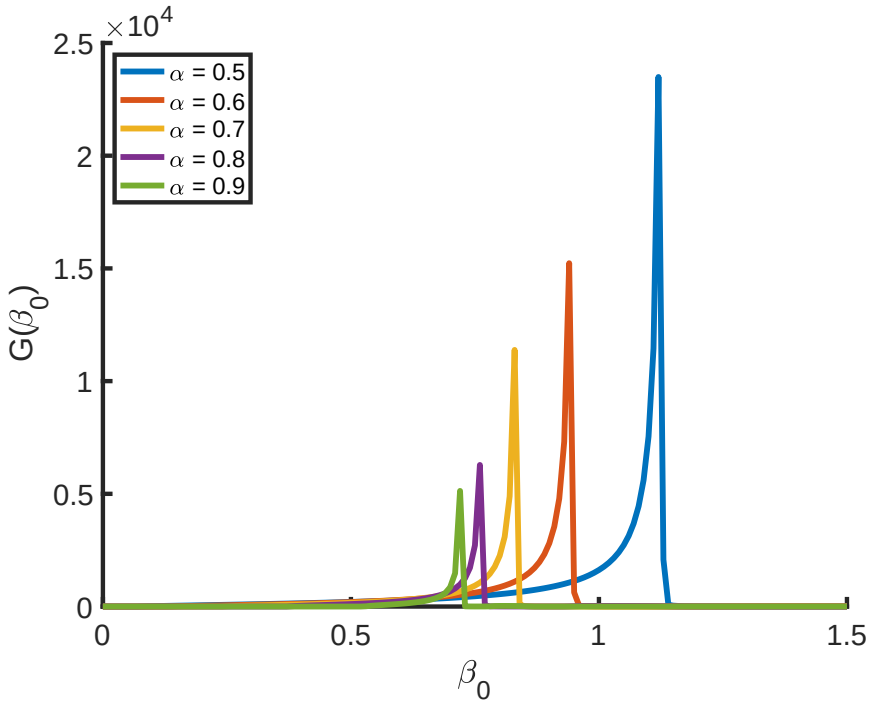

Figure 26: Plot of the MI growth rate versus the dissipation coefficients β_0, with α taking the respective values 0.5, 0.6, 0.7, 0.8, $k_1 = 1$, $k_2 = \alpha k_1$ and $\lambda = 0.15$.

and regions of β_0 that support instability are restricted to higher values. This is once more obvious in Fig. 25(c), where $\alpha = 0.35$. We should stress a change of behaviors in the MI growth rate when $\alpha \geq 0.5$. Another observation of the instability gain $G(\beta_0)$ in Fig.26 shows that for the fixed values of wavenumbers $k_1 = 1$ and $\lambda = 0.001$ taken arbitrarily in the instability interval, $G(\beta_0)$ increases with the parameter α. Likewise, this growth of α induces the instability region in our biological network. Ultimately and globally, the region of instability thus detected is the one likely to contain the oscillations of modulated localized waves with an intensification around the perturbed wavenumber $\lambda = 0$ and capable of provoking the destitution or reconstitution of tubulin dimers to allow them to transport energy or information favorable to the normal accomplishment of their cellular functions. According to the above, there is a straight relationship between MI and soliton formation under a suitable balance between nonlinearity and dispersion.

III.3 Nonlinear mode excitations in φ-model of MTs

Through the MI, we shows that our coupled system equations could admit a broad range of solutions and that mixing of solitary waves is possible in the models under our study. Then, the main purpose here is to obtain exact soliton solutions of two system of coupled NLS equations using the Jacobian elliptic function method already introduced. But we have chosen to start the study by decoupling the systems of Eqs.(52) and (53) and (77) of motion.

III.3.1 The single mode excitations

III.3.1.1 Analytical solutions

♣ **Case with minimized cytoplasmic viscosity effect**

The single mode excitation implies that only one of the two equations is considered, while the other component in turn to zero, i.e., only one NLS equation remains.

• For example, taking $\psi_1 \neq 0$ and $\psi_2 = 0$ leads to the following NLS equation for the lower cut-off mode

$$i\frac{\partial \psi_1}{\partial t} + H_1 \frac{\partial^2 \psi_1}{\partial x^2} + \zeta_{11}|\psi_1|^2\psi_1 = 0. \tag{127}$$

The above equation (127) is well known in nonlinear physics and have even been obtained recently by Zdravković et $a\ell$ [81] in the present model of MTs dynamics. Solutions for such equations depend on the sign of $H_1 \times \zeta_{11}$. From Fig. 19, its obvious that this product is positive, leading to the solution

$$\psi_1(x,t) = K\sqrt{\frac{2H_1}{\zeta_{11}}}sech\left(Kx + 2H_1KK_1\right)e^{i[K_1x - H_1(K_1^2 - K^2)t]}, \tag{128}$$

for Eq.(127). K and K_1 are two free parameters. For this first case, the angular displacement of the dimer at the position n is globally given by the solution

$$\psi_1(x,t) = 2K\sqrt{\frac{2H_1}{\zeta_{11}}}sech\left(Knl + 2H_1KK_1\right)cos[K_1nl - (\omega_0 - H_1(K_1^2 - K^2))t]. \tag{129}$$

One can see, form the above expression, that the dimer oscillations are described by a breather solution.

• The upper cut-off mode implies that $\psi_2 = 0$ and $\psi_2 \neq 0$, so that only the decoupled equation:

$$i\frac{\partial \psi_2}{\partial t} - H_2 \frac{\partial^2 \psi_1}{\partial x^2} + \zeta_{22}|\psi_1|^2\psi_1 = 0, \tag{130}$$

is obtained. Its solution can also easily be found by JEF approach. From Fig. 19, $H_2 \times \zeta_{22}$ is positive, but because of the (-) -sign that appears in Eq.(130), its solution is written as:

$$\psi_2(x,t) = K\sqrt{-\frac{2H_2}{\zeta_{22}}}tanh\left(Kx - 2H_2KK_2\right)e^{i[K_2x - H_2(K_2^2 + 2K^2)t]}, \tag{131}$$

with K and K_2 being two free parameters. Therefore, the following solution for dimer oscillation can be obtained:

$$\psi_1(x,t) = 2(-1)^n K\sqrt{-\frac{2H_2}{\zeta_{22}}}tanh\left(Knl - 2H_2KK_2\right)cos[K_2nl - (\omega_{max} + H_2(K_2^2 + 2K^2))t]. \tag{132}$$

This time, contrary to the lower cut-off mode, one see form the above expression, that the dimer oscillations are also described by a kink soliton solution.

♣ Case with intense cytoplasmic dampening and transport memory effect

In this subpart, It is necessary for the coefficients P_1, P_2, Q_1, Q_2, R_1, and R_2 of the CCNLS equations and their combinations to meet certain conditions. As above, by assuming that either $V_2 = 0$ and $V_1 \neq 0$ or $V_1 = 0$ and $V_2 \neq 0$, we can separate our CCNLS equation system (77) into two independent CNLS equations. Solving each equation will lead also to wave propagation in either frequency mode ω_1 or ω_2. The solutions to this particular case are straightforward and depend on the sign of the products $P_1 \times Q_{1r}$ and $P_2 \times Q_{2r}$ of the two vibrational modes, namely ω_1 and ω_2. In the meantime, by setting $V_2 = V_1 = V$, which transforms the coupled system (77) into an uncoupled one of two still equivalent Schrödinger equations. These last two equations differ just in their dispersion and nonlinearity coefficients. One with $P_{11} = P_1$ and $Q_{11} = Q_1 + R_1$, and the other with $P_{22} = P_2$ and $Q_{22} = Q_2 + R_2$. We have chosen to solve one of them, namely the one with the coefficients P_{11} and Q_{11}. This amounts to the following integration:

$$i\frac{\partial V}{\partial \tau} + P_{11}\frac{\partial^2 V}{\partial \xi^2} + Q_{11}|V|^2 V = 0, \tag{133}$$

where

$$Q_{11} = Q_{1r} - R_{1r} + i\left(Q_{1i} - R_{1i}\right).$$

Eq.(133) is a complex nonlinear Schrödinger equation, similar to the one used for the description of DNA dynamics with memory effect in the literature [111].

The dispersion coefficient P_{11} is real, while the nonlinearity coefficient Q_{11} is complex. Therefore, it is possible to describe the dynamics of the localized soliton wave in our angular MTs model using the complex NLS equation.

In doing so, the cytoplasm of the cell is a medium with several entities, some of which screen the signal transmission, the form of the solution that verifies Eq.(133) can be [120, 191]:

$$V = V_0 e^{-S_i \tau}\left[\operatorname{sech}\left(\frac{1}{N}\xi\right)\right]^{(1+i\delta_0)} e^{iS_r\tau}, \tag{134}$$

where the coefficients V_0, N, δ_0 and the pair (S_r, S_i) represent the amplitude, width, chirp and, real and imaginary parts of the soliton phase, respectively. It represents the signal that could propagate along the MTs.

By introducing Eq.(134) into Eq.(133), we find by simple solution of the resulting linear system of equations, the expressions for the coefficients:

$$S_r = N_0^2 P_{11}\left(1-\delta_0^2\right), \quad S_i = 2N_0^2 P_{11}\delta_0, V_0 = N_0\sqrt{\frac{P_{11}\left(2-\delta_0^2\right)}{Q_{11r}}}, \delta_0^{\pm} = \frac{-3Q_{11r} \pm \sqrt{9Q_{11r}^2 + 8Q_{11i}^2}}{2Q_{11i}}, \tag{135}$$

with

$$N_0 = \frac{1}{N}, \quad Q_{11r} = Q_{1r} - R_{1r} \quad \text{and} \quad Q_{11i} = Q_{1i} - R_{1i}.$$

In our biophysical system, the coefficients P_{11}, Q_{11r}, and their product $P_{11} \times Q_{11r}$ hold great signif-

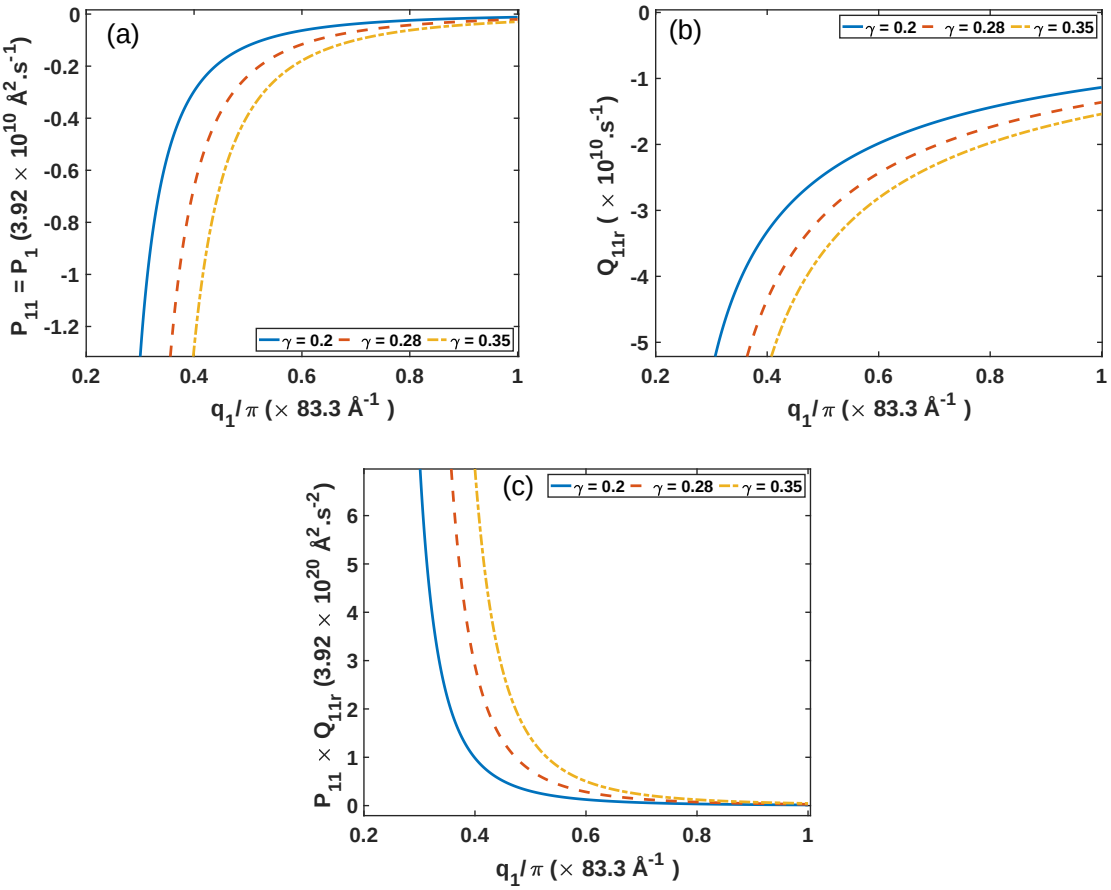

Figure 27: Evolution curves of the parameters P_{11}, Q_{11r} and the $P_{11}\times Q_{11r}$ as a function of the wavenumber q_1, for $\eta = 0.002$ with changing of the memory constant γ.

icance in determining the form of the propagating solution.

Therefore, if $P_{11} \times Q_{11r} > 0$, Eq.(134) represents a localized soliton of the breather type. The variations of these solitons against the wavenumber q_1 are depicted in Fig. 27. The diagrams depicted in Figs. 27(a), 27(b), and 27(c) illustrate how the memory constant γ affects the real coefficients of dispersion P_{11}, nonlinearity Q_{11r}, and the Benjamin-Feir criterion $P_{11} \times Q_{11r} > 0$ of the plane wave grating. It is evident that P_{11} and Q_{11r} are on the rise but still hold negative values. In contrast, their product $P_{11} \times Q_{11r}$ is decreases and shows a positive trend. The increase in the parameter γ is evident in all three figures, and it results in a significant expansion of the forbidden zone for wavenumber q_1, which now ranges from 0 to q_s. It is worth noting that the instability criterion $P_{11} \times Q_{11r} > 0$ indicates the range of wavenumber values in which unstable excitations may occur within the MTs network. As a result, the propagation of plane waves in this region of instability is expected to result in trains of localized structures. It is observed that the memory constant greatly affects this product. An increase in the value of γ causes the threshold wavenumber to rise from 0.31π to 0.4π. For instance, if $\gamma = 0.2$ in the uncoupled NLS equation scenario, selecting a wavenumber q_1 within the range of $[0.31\pi; \pi]$ will likely result in localized wave structures. To determine the width of the soliton, the process outlined in Refs. [111, 192] must be followed. It is shown that in a perfect biological wave propagation medium (without any influence or zero viscosity, denoted by $\delta_0 = 0$), the solution to Eq.(133) has a particular

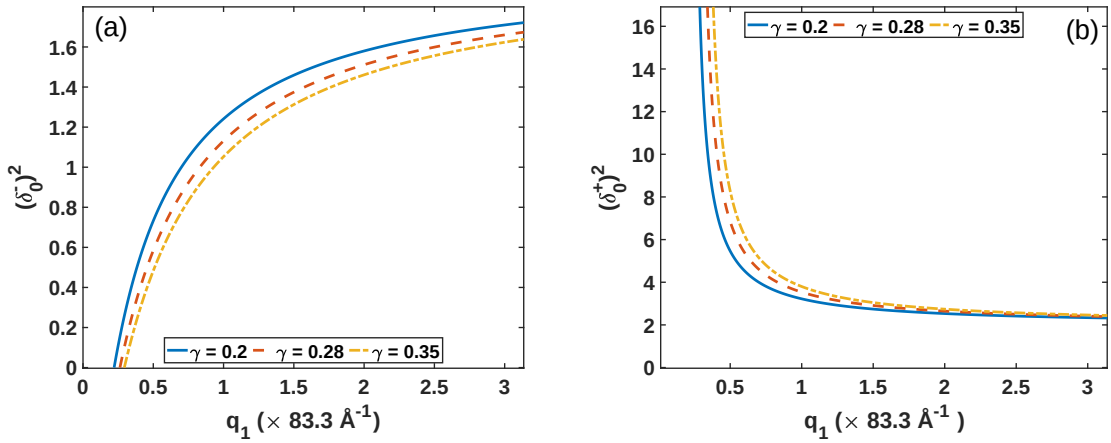

Figure 28: Representation of the chirp evolution of the simple soliton-solution as a function of the wavenumber q_1, for $\eta = 0.002$ and with the changing memory constant γ.

form

$$V = V_e \left[\operatorname{sech}\left(L_e \xi\right)\right] \exp\left[i \frac{u_e}{2P_e}\left(\xi - u_c \tau\right)\right], \tag{136}$$

where

$$L_e = \frac{\sqrt{u_e^2 - 2u_e u_c}}{2P_e} \quad \text{and} \quad V_e = \sqrt{\frac{u_e^2 - 2u_e u_c}{2P_e Q_e}}, \tag{137}$$

with $P_e = P_{11(\delta_0=0)}$, $Q_e = Q_{11r(\delta_0=0)}$ and, u_e and u_c free velocity constants with the relation $u_c = \Xi u_e$ ($\Xi \in [0, 0.5[$). By considering the shielding effects and viscosity ($\delta_0 \neq 0$) that affect the signal transmission along the MTs, we can use Eqs.(137) to derive the width and amplitude of the soliton:

$$N = \frac{\left(2 - \delta_0^2\right) P_{11}}{u_e \sqrt{1 - 2\Xi}} \quad \text{and} \quad V_0 = u_e \sqrt{\frac{1 - 2\Xi}{\left(2 - \delta_0^2\right) P_{11} Q_{11r}}}, \tag{138}$$

whose variation is important for the evolution of the soliton under the memory constant, along with an additional existing condition $\delta_0 < \sqrt{2}$.

Understanding biological systems is inherently complex as they undergo nonlinear evolution in dispersive and dissipative media. To improve our comprehension of the motion of tubulin dimers, we have refined a descriptive angular model that was previously developed in Ref. [14]. It is worth noting that a higher chirp in biological systems often leads to a reduced perception of information in a given area, meaning the information-carrying signal is highly chirped. Crucial information can be obtained from the plot of the chirp parameters δ_0^+ and δ_0^- of the soliton-breather solution of the uncoupled case as a function of the wavenumber q_1, as shown in Fig. 28. We can disregard the chirp δ_0^+ and instead use δ_0^-. This is because the positive product $P_{11} \times Q_{11r}$ is only applicable to certain accessible q_1 values and for the condition $\delta_0 < \sqrt{2}$. By analyzing Fig. 28(b), we can see that despite the agreement with the q_1 wavenumber, the chirp $(\delta_0^+)^2$ is greater than 2. In contrast, Fig. 28(a) shows that the chirp δ_0^2 meets both the wavenumber and upper limit conditions of $\sqrt{2}$. It can be concluded that the soliton-breather in this scenario must have a slight chirp in order to propagate in the medium. Additionally, the growth

of the transport memory constant may have a positive effect in certain areas by reducing the impact of the chirp on the transported information during energy transfer.

Eqs.(134), (68) and (66) ultimately result in a solitary evolution that spans both time and space. This serves as the solution to Eq.(32) for the motion of tubulin dimers within the MT network, accounting for the transport memory effect:

$$\varphi(x,t) = 2\varepsilon V_0 e^{-\left(\varepsilon^2 S_i - \omega_{1i}\right)t} \operatorname{sech}\left[\varepsilon\left(\frac{x - V_{g1}t}{N}\right)\right] \times \cos\left[q_1 x + \left(\varepsilon^2 S_r - \omega_{1r}\right)t + \delta_0 Log\left(\operatorname{sech}\left(\varepsilon\frac{x - V_{g1}t}{N}\right)\right)\right]. \tag{139}$$

According to the solution Eq.(139), the excitation profile in the cell cytoplasm along the MTs is influ-

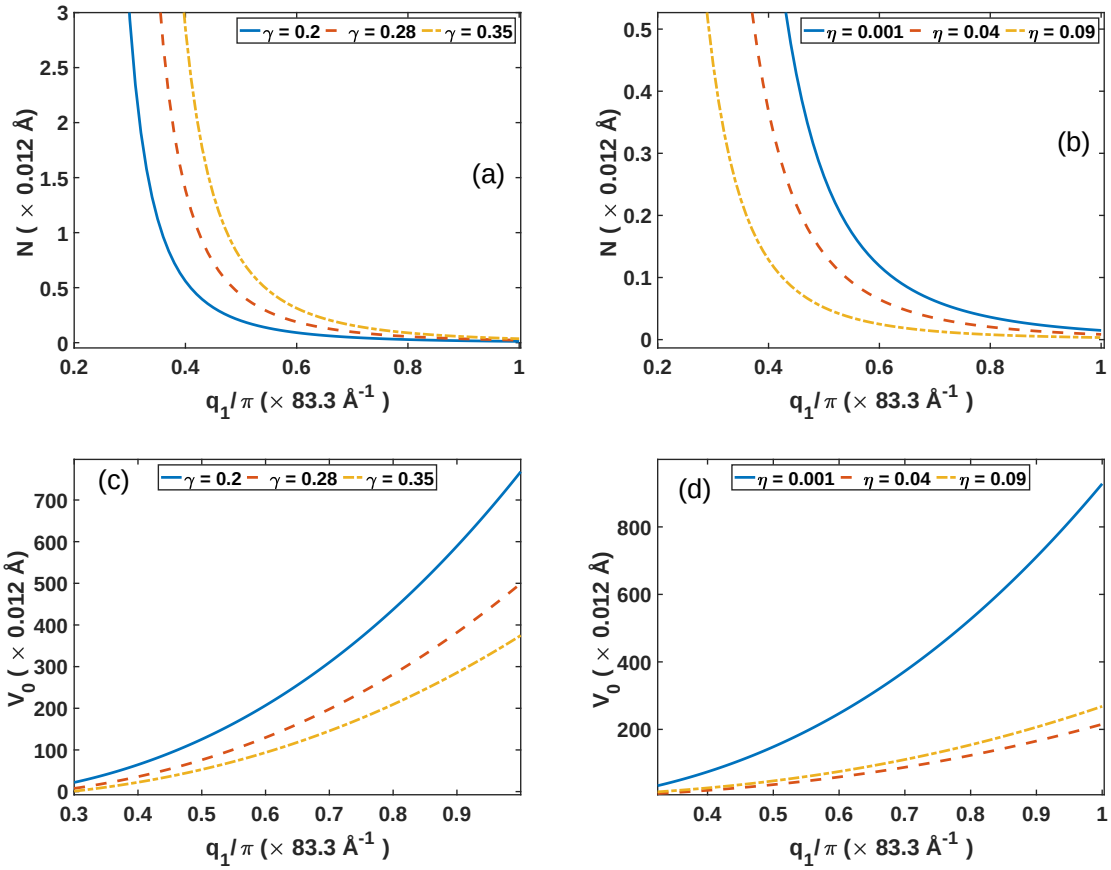

Figure 29: Variation of the soliton-solution width N and the amplitude V_0 as a function of the wavenumber q_1, for three values of the memory constant γ and the nonlinearity rate constant η.

enced by crucial parameters, including the amplitude, which is affected by the nature of the propagation medium, impacting V_0 and the width N. To demonstrate this, we have shown the changes in N and V_0 at various values of the memory constant γ and the rate of nonlinearity η, as a function of the wavenumber q_1 in Fig. 29. Figs. 29(a) and (c) are obtained by setting $\eta = 0.002$ while the dashed lines (see Figs. 29(b) and (d)) are plotted for $\gamma = 0.2247$, with the other constants being taken as $u_e = 1$ and $\Xi = 0.2$. Based on the four graphs, it is evident that N decreases but does not cancel out while V_0 increases as q_1 varies. The impact of the constants γ and η is noticeable in all cases. As γ evolves from 0.2 to 0.35, the width N increases (see Fig. 29(a)), causing the signal to disperse spatially, and the amplitude

V_0 to decrease (see Fig. 29(c)). Over the same width N, the impact of the rate η has the opposite effect to that of γ. It can be seen that changing η from 0.001 to 0.09 leads to the decrease of N (see Fig. 29(b)), while the amplitude V_0 (see Fig. 29(d)) shows the same behaviour as observed previously for the case of Fig. 29(c). By analyzing the scenario of uncoupled dynamics, we can forecast that the impact of transport memory can result in an energy-damping force that moves through the MTs network when the wavenumber q_1 falls within the range of $[0.31\pi; \pi]$, and γ lies between 0.2 and 0.35.

III.3.1.2 Numerical solutions

♣ Case with minimized cytoplasmic viscosity effect

In order to see if the above solutions (129) and (132) are stable at the time of the propagation along the MTs, we have studied its spatiotemporal behavior by direct integrating Eq.(19) using the fourth order Runge-Kutta computational scheme with periodic boundary conditions.

- Firstly for the lower cut-off mode, the time step has been chosen as $\Delta t = 10^{-4}$ns and the initial condition is solution (129). The effect of the dipolar potential energy has been studied (Fig. 30). As a matter of fact, the breather soliton has been proposed recently in MTs [81], but its true biological implications still remain unmasked. However, encouraging is the truth that breather solitons emerge in systems where nonlinear and dispersive effect are coupled. In biological systems in general, breather are always presented to be at the onset of important biological processes. In DNA for example, they are at the onset of transcription [193, 194], while they can be perceived as the triggering signals for motor proteins to start moving along MTs. Their role in the regulation of neural activities should not also be ignored, as they are situated inside the axons of nerve cells. In that respect, it has been shown that MTs are specialized entities in signal transmission within the cell, via dipole interactions in axonal MTs [195, 196]. Importantly, the spatiotemporal behaviors of such structures depend on system parameters as it is obvious that the dipolar potential energy modifies its characteristics. In Figure. 30, simulations have been done for $pE = 0.2$ eV (Fig. 30(a)) to $pE = 0.8$ eV (Fig. 30(d)). As a first remark, increasing pE considerably reduces the amplitude of the wave.

- Using the same numerical procedure as previously, we get the results of Figure. 31, with the initial condition (132). The spatiotemporal evolution of a kink envelope is displayed for different values of the dipolar energy pE, which respectively takes the values 0.2 eV (Fig. 31(a)), 0.4 eV (Fig. 31(b)), 0.6 eV (Fig. 31(c)) and 0.8 eV (Fig. 31(d)). Over the time, the solution evolves into trains of solitonic objects, which diminish with increasing pE.

In general, the single modes solutions (129) and (132) give an idea on the behavior of the coupled wave solution under the influence of the electric field. Solitons are or various types, depending on their meaning and mode of generation in nonlinear systems.

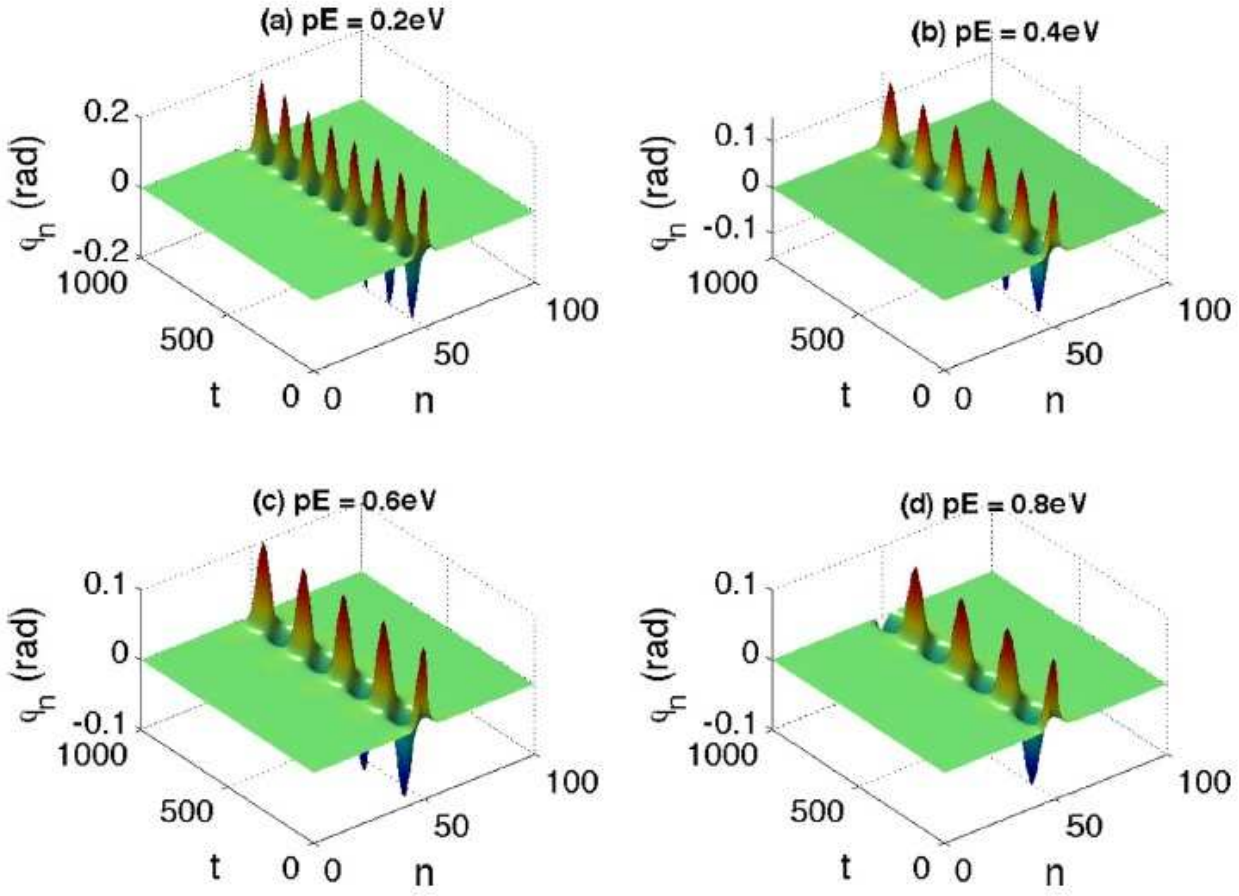

Figure 30: Spatiotemporal evolution of the lower cut-off solution for different values of the dipolar energy pE. The number of objects decreases along with the amplitude with increasing pE.

♣ Case with intense cytoplasmic dampening and transport memory effect

In this other part with the consideration of a highly damped dimer displacement, others specific parameters come into play. To assess the stability of the obtained solutions and the accuracy of the proposed parametric predictions, Eq.(32) is numerically integrated as it contains the memory term that is of importance in this work. We examine the scenario where the initial condition is uncoupled, given by Eq.(139). In doing so, the fourth-order Runge-Kutta computational scheme is utilized, with spatial and temporal step sizes being $\Delta x = \Delta t = 0.01$, under periodic boundary conditions. The final normalized time is set to $t = 1000$, while 201 dimers are considered spatially. It is clear from Eq.(32) that the parameters γ and η have an impact on the propagation of excitations along the MTs, reflecting the effects of transport memory and the degree of nonlinearity, respectively. The initial signal of Eq.(139) is expected to be affected by changes in such parameters, which is confirmed in Figs. 27-29. We aim to identify the conditions under which this soliton solution can describe communication between two dimers in the cell without disappearing. For an objective analysis, via the same parameter limits used to obtain Figs. 27-29, we numerically generate Figs. 32 and 33 with a focus on the amplitude and width of the single-mode soliton solution.

Fig. 32(a) shows the space-time representation of solution (136), while Fig. 32(b) shows a spatial cross-section of such a solution at time $t = 800$. The full breather solution (139) is shown in Fig. 32(c) at

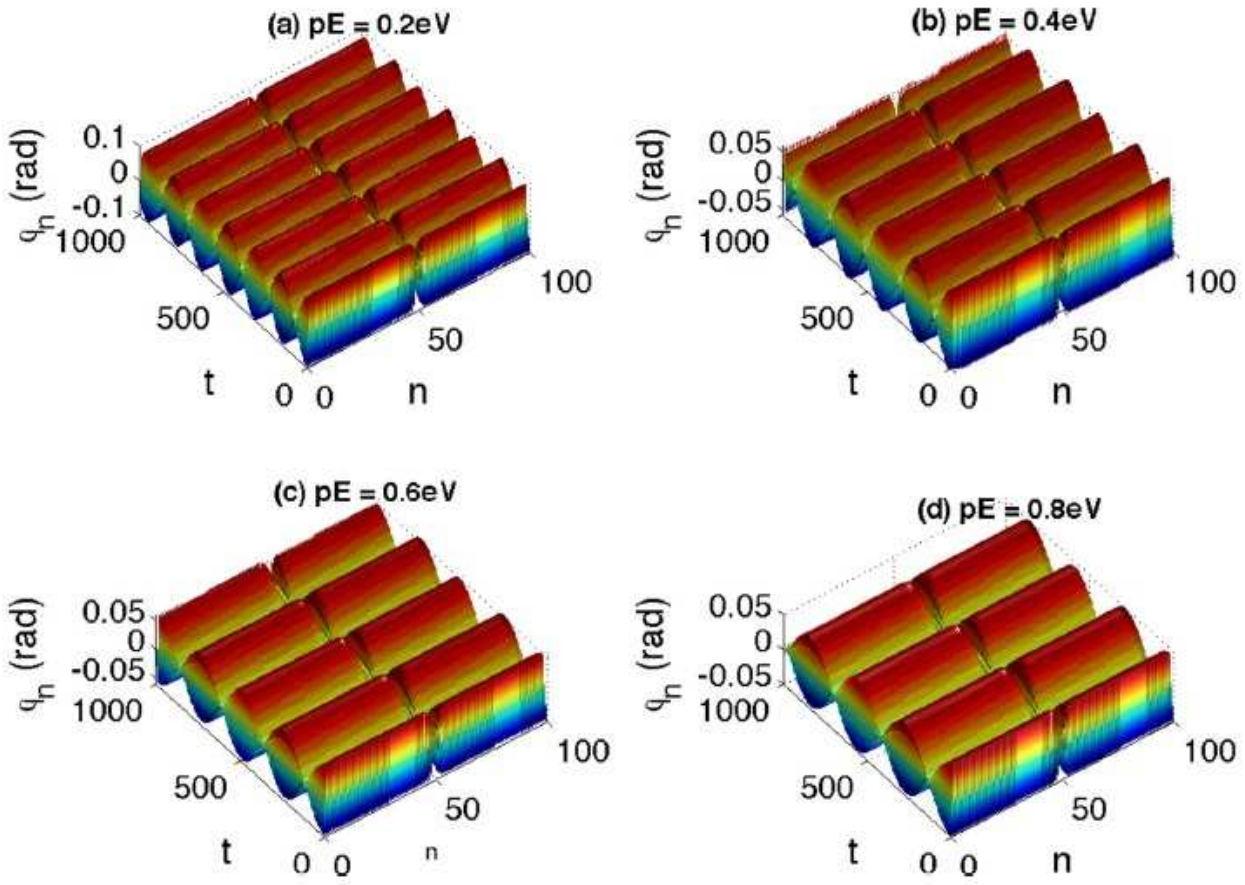

Figure 31: Numerical solution corresponding to the upper cut-off frequency solution, under the influence of the dipolar energy. Similarly to the previous case, the number of solitonic objects and the amplitude decrease when pE grows, giving rise to more larger structures.

time $t = 800$, and more better in dimension three representation on the Fig. 32(d), under full numerical simulations for a memory constant value $\gamma = 0.2247$. Precision should be made that all the panels of Fig. 32 have been obtained at the order $\epsilon = 0.01$, with the wavenumber $q_1 = 0.36\pi$. They show the type of soliton excitation propagated in the studied MT array, which shows indeed a breather structure. Additionally, the profiles in Fig. 33 highlight the qualitative and quantitative influence of the constants γ and η during the propagation of single-breather solution, since the main goal of these numerical simulations is to verify the capacity of the improved model under study to support the obtained analytical solution. In that direction, panels $(aj)_{j=1,2,3}$ show the influence of changing the memory parameter γ. In general, such an increase of the transport memory constant γ not only spatially expands the breathing structure to more dimers but also reduces the amplitude of the localized solitonic object. In particular, under normalized time and space, the width of the oscillating soliton increases from about $x = 90$ units for $\gamma = 0.21$ to $x = 200$ units for $\gamma = 0.35$, while the amplitude increases from $\varphi = 12.5\text{rad}$ ($\gamma = 0.21$) to $\varphi = 1.125\text{rad}$ ($\gamma = 0.35$). Along the same line, we also note that the nonlinear character of the wave is proven, as increasing the degree η can change the wave from a breather-structure to a solitary pulse, thus decreasing its amplitude and width as shown in Figs. 33$(bj)_{j=1,2,3}$. These numerical results in the non-coupled mode are, once more, in agreement with the analytical predictions of Figs. 29(a)-(d). As a whole, it is obvious that for ranges of values of the constants $\gamma \in [0.21; 0.35]$ and $\eta \in [0.001; 0.09]$,

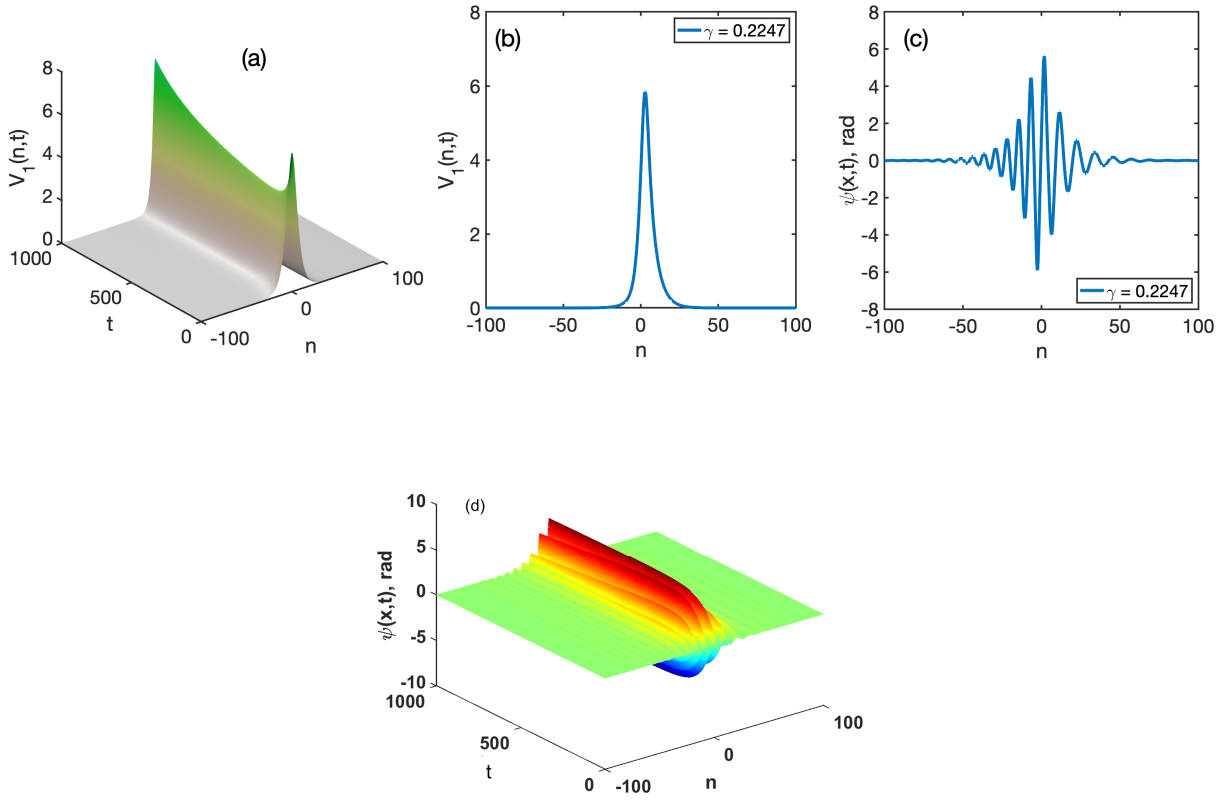

Figure 32: (a) and (b) display the space-time and spatial profiles of the decoupled solution (136), while panel (c) and (d) display the resulting breather solution (139) obtained from numerical simulations, in spatial profiles at time $t = 800$ and 3D at time t respectively, under the parameter values $\gamma = 0.2247$ and $\eta = 0.002$.

the effects of transport memory as a function of nonlinearity can potentially lower the height by increasing the solitonic width of the dimer protein filament vibrations in the cell. Therefore, these effects would behave in the chosen constant ranges as constraints that affect conformational changes in MT's vibrational motion. The same spectrum of behaviors has been reported in other studies. In many other biological systems such as the study of cell invasion through soft biological tissues [197], DNA dynamics [80, 111, 127] and nerve cell networks [148, 198–200], breather waves play important roles in understanding how these processes work. In MTs, some results have reported that breathers may be responsible for triggering the mobility of motor proteins [13, 81]. The studies carried out in the last two references considered negligible damping effects. However, we conducted these investigations believing that stronger damping effects of transport memory would yield satisfying results. As shown in Fig. 33(b3), our assumption proved to be correct, with the soliton pulse being a crucial feature of excitable media, such as brain cells, where the MT is in constant motion. These solitary impulses are generally associated with chemical excitations propagating quickly at the subcellular level [201, 202].

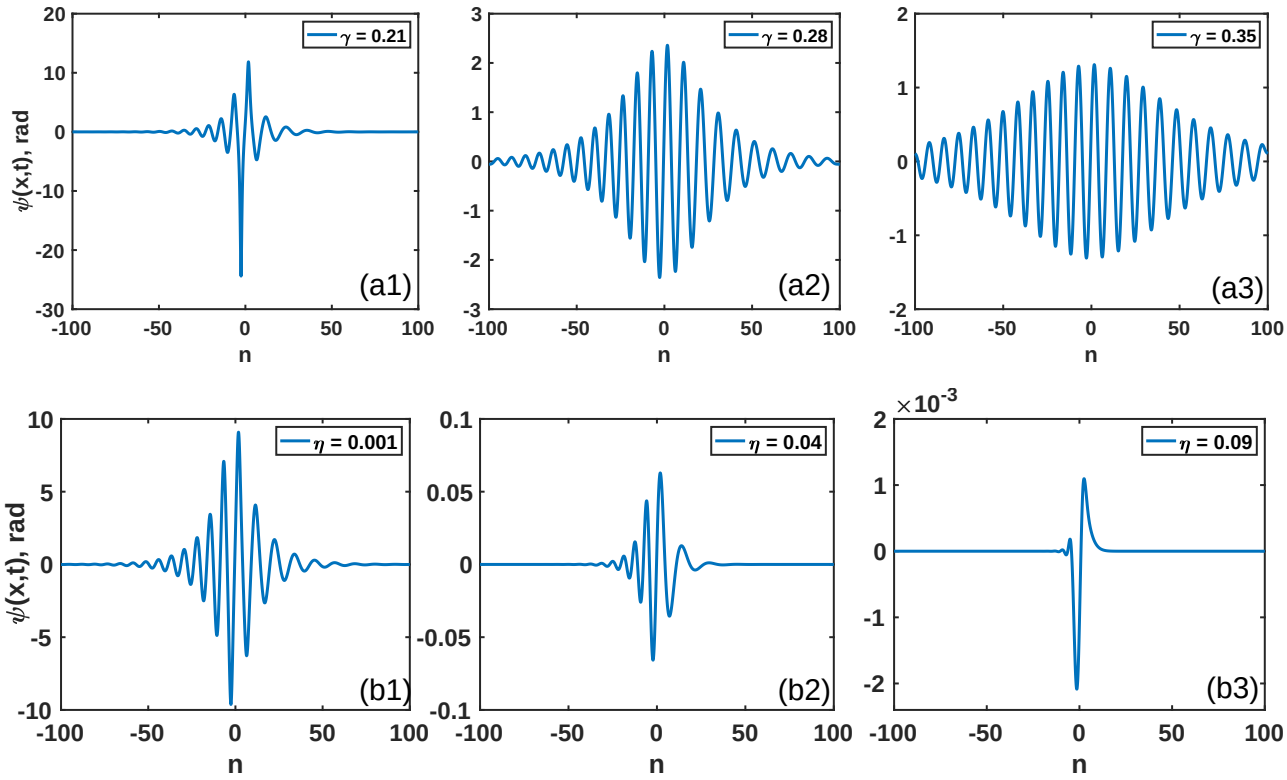

Figure 33: Direct numerical simulations using solution (139) as initial condition. Panels (aj)$_{j=1,2,3}$ display the single breather excitation under the effect of increasing the transport memory constant γ at time $t = 800$ for $\eta = 0.002$. Panels (bj)$_{j=1,2,3}$ show the effect of increasing the the nonlinearity rate η at the same instant $t = 800$, with $\gamma = 0.2247$.

III.3.2 The coupled mode excitations

III.3.2.1 Analytical solutions

♣ **Case with minimized cytoplasmic viscosity effect**

In this subsection, our main purpose is to describe dynamics of radial φ-model through the coupled mode. So in the coupled mode none of the two amplitude is switched to zero, and the nonlinear coupling between them is maintained. That is to say requires us to solve the system of CNLS equations (52) and (53) with $\psi_1 \neq 0$ and $\psi_2 \neq 0$. Exact solutions are established by making the transformations [203]:

$$\psi_1(t,x) = g(\mu_1)e^{i\nu_1} \quad \text{and} \quad \psi_2(t,x) = f(\mu_2)e^{i\nu_2}, \tag{140}$$

where $\mu_1 = Kx + 2H_1KK_1t$, $\mu_2 = Kx + 2H_2KK_2t$, $\nu_1 = K_1x - \Omega_1t$ and $\nu_2 = K_2x - \Omega_2t$ with Ω_1 and Ω_2 the constants to be determined. f and g can be dependent of the any Jacobian elliptical functions $sn(s)$, $dn(s)$ and $cn(s)$. Now, focusing our choice on the following expressions

$$g(\mu_1) = A_{01} + A_1dn(\mu_1) \quad \text{and} \quad f(\mu_2) = A_{02} + A_2sn(\mu_2), \tag{141}$$

with A_{01}, A_1, A_{02} and A_2 the constants to be determined, we substitute the relations of (140) into the system of (52) and (53). Their solving depends on the sign of the coefficients [137,203]:

$$\Delta_1 = \frac{H_2\zeta_{12} + H_1\zeta_{22}}{\zeta_{11}\zeta_{22} - \zeta_{12}\zeta_{21}}, \qquad \Delta_2 = -\frac{(H_2\zeta_{11} + H_1\zeta_{21})}{\zeta_{11}\zeta_{22} - \zeta_{12}\zeta_{21}}. \tag{142}$$

From the modulus $m \to 1$ and for $A_{01} = A_{02} = 0$, the sign of $\Delta_1 > 0$ and $\Delta_2 < 0$ allow us to the solutions for the two equations:

$$\psi_1(t,x) = A_1 sech(Kx + 2H_1KK_1t)e^{i(K_1x - \Omega_1 t)} \tag{143}$$

$$\psi_2(t,x) = A_2 tanh(Kx - 2H_2KK_2t)e^{i(K_2x - \Omega_2 t)}, \tag{144}$$

where

$$\begin{aligned} &A_1^2 = \frac{2K^2\,(H_2\zeta_{12} + H_1\zeta_{22})}{\zeta_{11}\zeta_{22} - \zeta_{12}\zeta_{21}}, \qquad A_2^2 = \frac{2K^2\,(H_2\zeta_{11} + H_1\zeta_{21})}{\zeta_{11}\zeta_{22} - \zeta_{12}\zeta_{21}}, \\ &\Omega_1 = -H_1(K^2 - K_1^2) - \zeta_{12}A_2 \quad , \quad \Omega_1 = -H_2(2K^2 + K_1^2) - \zeta_{21}A_1 \quad , \\ &K_1 = -\frac{H_2}{H_1}k_2. \end{aligned} \tag{145}$$

Eqs.(143), (144), (45) and (40) leads to the global solution for the MT dimer radial displacement is given by:

$$\begin{aligned} \varphi_n(t) =& 2A_1 sech\,(Knl + 2H_1KK_1)\cos[K_1nl - (\omega_0 + \Omega_1)t] \\ &+ 2(-1)^n A_2 tanh\,(Knl - 2H_2KK_2t)\cos[K_2nl - (\omega_{max} + \Omega_2)t]. \end{aligned} \tag{146}$$

At first observation, the components of the above general solution are seen as the solutions found to the cases of simple modes. Except that each parameter of the latter includes the coefficients of the two CNLS equations, which is interesting and would certainly bring something new to this studied φ-radial model. Then we clearly see on two parts of this coupled solution, the breather soliton solution part in $sech$ function and the kink part in $tanh$ function.

♣ Case with intense cytoplasmic dampening and transport memory effect

In this next phase of the coupled mode analysis, we extend our approach also by taking into account the fact that V_1 and V_2 as the solutions of the system of Eqs.(77), are not equal to zero and then proceed to search for analytical pulse-like solitons. These solitons are of the same type as those described in Ref. [204,205]. Whether or not the final coupled solution, as supported by Eq.(32), exists is contingent upon the sign of certain newly introduced parameters (Λ_1, Λ_2, and δ) that are derived from the coefficients of the system (77), as previously described. Assuming that there are microorganisms in the cytoplasm of the cell that can disturb the reception of the information carried by the soliton pulse along

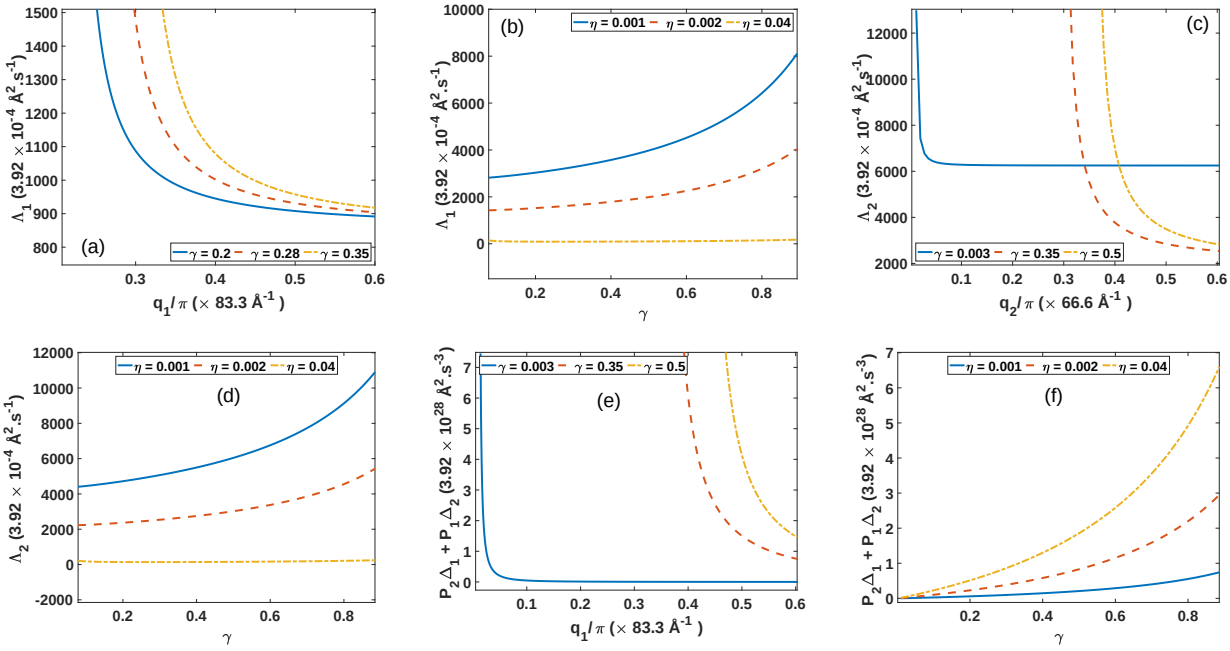

Figure 34: Graphical representations of the coupled soliton-solution coefficients. Panels (a), (c) and (e) as a function of the wavenumbers q_1 and q_2 ($q_2 = 0.8q_1$), for different values of the γ. Panels (b) and (d) as a function of the memory constant γ, for different values of the nonlinearity constant.

the microtubules, the exact solutions are taken to be

$$\begin{aligned} V_1 &= V_{10} e^{-S_{1i}\tau} [\mathrm{sech}\,(\beta\xi)]^{(1+i\delta_1)} e^{iS_{1r}\tau}, \\ V_2 &= V_{20} e^{-S_{2i}\tau} [\mathrm{sech}\,(\beta\xi)]^{(1+i\delta_2)} e^{iS_{2r}\tau}, \end{aligned} \tag{147}$$

where the pair (V_{10}, V_{20}) are real amplitudes, (S_{1r}, S_{2r}) and (S_{1i}, S_{2i}) the real and imaginary parts of the phases of the excitations. The coefficients (δ_1, δ_2) , present in the two solitary pulses V_1 and V_2 take into account the bad reception of information and are called chirps. β is a free parameter while all the others are parameters to be determined. To make the calculations less cumbersome, we have chosen the soliton phases as the only complexes here.

Introducing relations (147) into the CCNLS equations system (77), leads to the linear set consisting of the algebraic equations of unknowns V_{10}, V_{20}, S_{1r}, S_{2r}, S_{1i}, S_{2i}, δ_1, δ_2 and β given to the appendix B2.(171) to B2.(176). To solve these above linear equations, we take into account the microorganisms present around the tubulin dimers in the cell. These microorganisms may have a negative impact on the reception of information carried by soliton signals along these proteins. We conclude that the chirps in both vibration modes are identical, and therefore $\delta_1 = \delta_2 = \delta$.

Eqs.B2.(171) and B3.(174) give :

$$\begin{aligned} S_{1r} &= P_1\beta^2\left(1-\delta^2\right), \quad S_{1i} = 2P_1\beta^2\delta, \\ S_{2r} &= P_2\beta^2\left(1-\delta^2\right), \quad S_{2i} = 2P_2\beta^2\delta. \end{aligned} \tag{148}$$

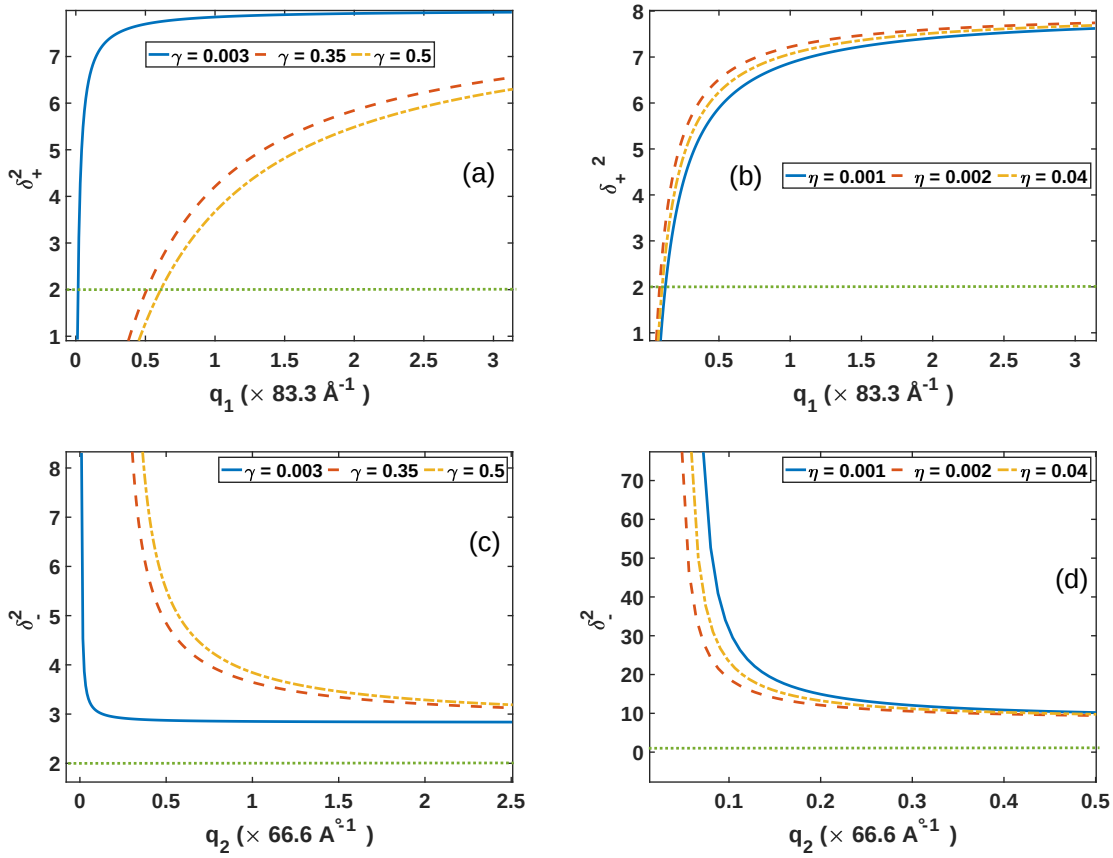

Figure 35: Variations of the chirp of the coupled soliton solution as a function of the wavenumbers q_1 and q_2 ($q_2 = 0.8q_1$). Panels (a) and (c), for different values of γ; panels (b) and (d), for different values of the nonlinearity rate constant.

Then from Eqs.B2.(172) and B2.(175), we obtain the following amplitudes of expressions:

$$V_{10} = \beta\sqrt{\Lambda_1\,(2-\delta^2)}; \quad V_{20} = \beta\sqrt{\Lambda_2\,(2-\delta^2)}, \tag{149}$$

$$\text{where} \quad \Lambda_1 = \frac{P_1Q_{2r} - P_2R_{1r}}{\Lambda} \quad \text{and} \quad \Lambda_2 = \frac{P_2Q_{1r} - P_1R_{2r}}{\Lambda},$$

$$\text{with} \quad \Lambda = Q_{1r}Q_{2r} - R_{1r}R_{2r}.$$

Finally, solving equations B2.(173) and B2.(176) gives the result of the chirp:

$$\delta_{\pm} = \pm\frac{1}{P_1\Delta_2 + P_2\Delta_1}\left[3P_1\Lambda + \sqrt{9P_1^2\Lambda^2 + 8(P_1\Delta_2 + P_2\Delta_1)^2}\right], \tag{150}$$

where $\Delta_1 = R_{1i}Q_{1r} - R_{1r}Q_{1i}$ and $\Delta_2 = Q_{1i}Q_{2r} - R_{1i}R_{2r}$.

As mentioned at the beginning of this section, the real constant β is taken arbitrarily while the other parameters of the soliton envelopes V_1 and V_2 are well determined. The latter includes new coefficients that provide information on the very existence of these pulse waves.

In order to describe the angular displacement profiles of cellular tubulin dimers taking into account the transport memory effects of the medium in the coupling, the parameters obtained in Eqs.(148)-(150)

included in the soliton solutions (147) must therefore fulfil some necessary or sufficient conditions. Thus, to observe the evolution of the soliton pulse coupled by V_1 and V_2 with the influence of the transport memory and nonlinear constant, the amplitudes V_{10}, V_{20} and the chirp δ must be real and nonzero. To achieve this, the main conditions on these constants are such that:

$$\begin{aligned} &\Lambda_1 > 0, \quad \Lambda_2 > 0, \quad \delta < \sqrt{2} \quad \text{or} \quad \Lambda_1 < 0, \quad \Lambda_2 < 0, \\ &\delta > \sqrt{2} \quad \text{and} \quad P_1\Delta_2 + P_2\Delta_1 \neq 0. \end{aligned} \tag{151}$$

The graphical representations of some of the obtained coefficients allow to discuss the different parameter regions necessary for describing the dynamics of the MTs with the impact of its immediate environment. In Figs. 34 and 35, the plots of the characteristic parameters Λ_1, Λ_2, δ and $P_1\Delta_2 + P_2\Delta_1$ of the coupled solution are observed. The graphs in Figs. 34(a), 34(b) and 34(c) represent the variations of three of these parameters as functions of the wavenumbers q_1 and q_2 for three values of the constant γ and those in Figs. 34(b), (d) and (f) show the variations of the same parameters but as a function of the memory constant γ for three values of the nonlinearity rate η with $q_1 = 0.36\pi$. These satisfy one of the conditions given in relation (151), as the parameters are positive for specific regions of q_1, q_2, γ and η. Fig. 35 allows us to discuss the second condition for the existence of the same coupled breather solution. It illustrates the evolution of the chirp $\delta_{\pm}^2$ as a function of the wavenumbers q_1 and q_2 for three values of γ and η, respectively. The square of δ_+ shows increasing behaviors (see Figs. 35(a) and (b)) in contrast to δ_- which decreases (see Figs. 35(c) and (d)). It can be seen that the chirp whose part of values fulfil the condition $\delta < \sqrt{2}(\delta^2 < 2)$ is δ_+. Thus, the coupled breather solution, weakly chirped, can propagate along the MT within the intervals $\gamma \in [0.003; 0.5]$, $q_1 \in [0.01\pi; 0.6\pi]$, with $\eta = 0.002$, and $\Xi = 0.2$. We can notice that, in general, the dynamics of the MT described by a single equation or a system of CCNLS equations show how the energy, after being emitted (e.g. by the hydrolysis of GTP), would propagate in the biological environment of the MT under several constraints such as dispersion, nonlinearity, friction with other particles and chirp effects.

Starting from the previous calculations, we can return to the systems's initial coordinates. The global solution (66) of the equation of motion of the tubulin dimers Eq.(32), with transport memory and nonlinearity effects, in a cell is written as:

$$\begin{aligned} \varphi(x,t) =& 2V_{10}\mathrm{sech}\left[\varepsilon\beta\left(x - V_{g1}t\right)\right] e^{-\left(\varepsilon^2 S_{1i} - \omega_{1i}\right)t} \times \cos\left[q_1 x + \left(\varepsilon^2 S_{1r} - \omega_{1r}\right)t\right. \\ &\left. + \delta Log\left(\mathrm{sech}\varepsilon\beta\left(x - V_{g1}t\right)\right)\right] + 2V_{20}\mathrm{sech}\left[\varepsilon\beta\left(x - V_{g1}t\right)\right] e^{-\left(\varepsilon^2 S_{2i} - \omega_{1i}\right)t} \\ &\times \cos\left[\left(\varepsilon D_1 - q_1\right)x - \left(\varepsilon^2 S_{2r} + \varepsilon D_1 V_{g1} - \varepsilon^2 D_2 \ - \omega_{2r}\right)t + \delta Log\left(\mathrm{sech}\varepsilon\beta\left(x - V_{g1}t\right)\right)\right], \end{aligned} \tag{152}$$

with $D_1 = \frac{D}{2P_2\varepsilon}$ and $D_2 = \frac{D^2}{4P_2}$

Obviously, Eq.(152) comprises two wave packets of complex frequencies ω_1 and ω_2 with imaginary $\omega_{1i} = \omega_{2i}$ and, real parts $\omega_{1r} and \omega_{2r}$ respectively. It should be noted that the imaginary parts refer directly to the physiological dissipative character of biological media. Since the energy allowing the

cellular cytoskeletal filaments to play each its role efficiently comes from the hydrolysis of GTP, the coupled solution (152) would represents the initial energetic excitation received by the dimers on one of the ends of the PF, which is going to be transmitted from near to near all along the MT. In order to numerically appreciate the stable propagation of the coupled energy pulse signal through the entire MT network, Eq.(152) is used as initial input signal. At first sight of this solution, one might think of a solitary wave structure with modulations.

III.3.2.2 Direct numerical simulations of the coupled solutions

♣ **Case with minimized cytoplasmic viscosity effect**

While combined the two monomodes as in Eq.(146) , we have the features presented in Fig. 36 after direct simulation of Eq.(19). Obviously, the kink-envelope soliton is strongly modified by the presence of the electric field E. In fact, its amplitude decreases with increasing pE and the separation between the two sides gives rise to a hole. Kink-envelope being of the soliton-type, solitons are capable of carrying energy, and that energy, in the present context, might give rise to the mechanism of polymerization and depolymerization. Interests have been given recently to soliton collision, where energy is shared for the better achievement of these processes. However, one of the most important issues is how that energy is

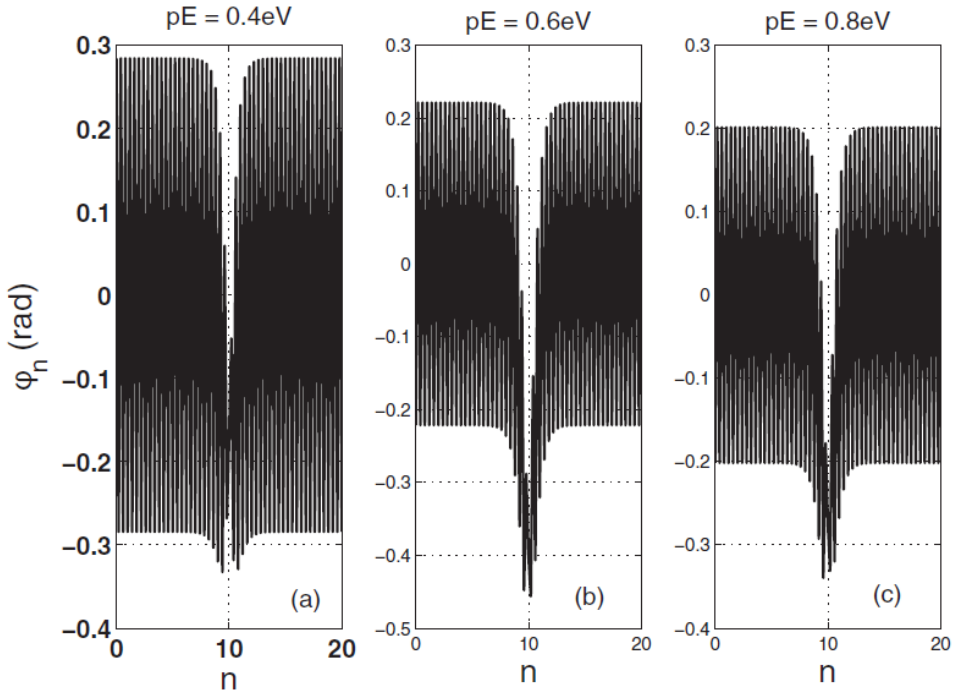

Figure 36: Snapshots of the coupled solution (146) for different values of the dipolar energy pE. Increasing the later reduces the amplitude of the Kink-envelope solution. The kink-antikink character of the solution is visible through the two-humped structure that becomes obvious with increasing pE.

initiated and carried by solitonic structures. At the same time, if the energy released by the hydrolysis of GTP is not sufficient, there will be no dislocation and the state of the tubulin dimer will not be altered. Coupled wave generation could then be a way to boost that energy, so that a strong dislocation could be initiated and followed by the process of polymerization/depolymerization. Furthermore, for motor-

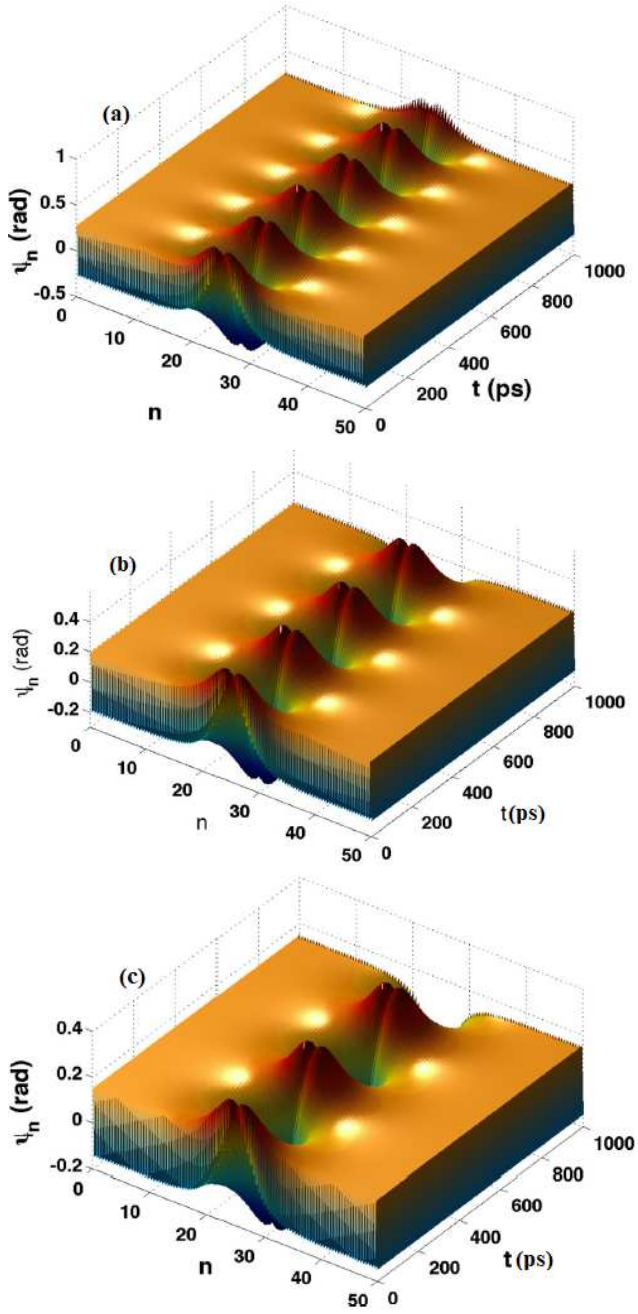

Figure 37: The panels show the space-time evolution of the coupled solutions. Simulations have been made for different values of pE : (a) $pE = 0.4$ eV, (b) $pE = 0.6$ eV and (c) $pE = 0.8$ eV. Over time, the initial condition (146) keeps its shape and characteristics, except that the number of breathing objects decreases along with the wave amplitude with increasing pE.

proteins to start moving, enough energy should be available, which might be brought by the coupled solution. This then implies that the solution should be robust and conserve its form and characteristic for an optimal energy transport. We have for example tested this through the direct numerical integration of Eq.(19), with the initial condition (146). The corresponding spatiotemporal results are displayed in Figure. 37, with changing the dipolar energy. Spatially, the soliton keeps its shape with increasing pE, but temporally, the number of elements diminishes, replaced by more expanded structures. Under the influence of high electric field, the collection of energy is rather ensured by more bigger structures, in order to ensure a permanent release of energy that is capable to provoke the motion of heterodimers

in MTs. This is mediated by an energy rich cap (where GTP is not hydrolyzed) that is formed at the end of the tubulin [206], that will be hydrolyzed in such a way that a considerable quantity of energy is released for a specific process, while the rest is stored in the MT lattice for other specific mechanisms to be achieved. Solitonic structures can then be excited with strong influence on bond length and conformation changes of tubulin heterodimers [11, 81]. Otherwise, there is always energy that is supplied to the vibrations or for motor proteins to move along the MT and transferred to the MT as localized excitation of vibrations, which sufficiently justifies the evidence of coupled mode of vibration in MTs.

♣ Case with intense cytoplasmic dampening and transport memory effect

The coupled-excitation regime is studied here, where one combines two wave packets (ω_1, q_1) and (ω_2, q_2). Then, under also periodic boundary conditions and, with spatial and temporal step sizes being $\Delta x = \Delta t = 0.01$, the fourth-order Runge-Kutta computational scheme is against used for the integration of Eq.(32). This is based on the initial condition Eq.(152), which results from an extended breathing wave made of a train of three breathers, as shown in Fig. 38 with $\gamma = 0.02247$, $\eta = 0.002$ and $\beta = 0.1$, by considering the same parameter limits used to obtain Figs. 34 and 35. In a biophysical context, the coupling of two breathers would allow the transport of a wider range of information via the MTs. It should be mentioned that the obtained results are not an isolated case, as some works in other biological processes have known more enlightened explanations thanks to the coupled signals of breathers. Among others, we can mention the phenomenon of transcription in DNA physics [148, 193, 194], the dynamics of negative ions in plasma [131], the process of disassembly and vesicular and organelle transport in MTs [155, 160]. The transport memory constant γ, the nonlinearity rate η and the free parameter β are, however, expected to bring about more new features that will help to comprehend the various activities induced by wave propagation in the MT lattices within a living cell. More explicitly, one can control how tubulin dimers move to perform their cellular functions by making a suitable choice of γ, η and β. From the panels of Figs. 39 at time $t = 800$, with $\eta = 0.002$ and $\beta = 0.1$, for example, one notices that the memory effect can act in two ways on the motion of the MTs. To be more precise, Figs. 39(aj)$_{j=1,2,3}$ show that the amplitude of the coupled signal increases for values of γ, while higher values of the memory effects, as shown in Figs. 39(bj)$_{j=1,2,3}$, reduces such an amplitude and preserves the solitonic width. Along the same line, under increasing values of η, the wave amplitude drastically decreases as depicted in Fig. 40, where the nonlinearity rate takes the successive values $\eta = 0.001$, $\eta = 0.08$, and $\eta = 0.02$. The free coefficient β mainly affects its width and amplitude as displayed in Fig. 41 at time $t = 800$, with $\eta = 0.002$ and $\gamma = 0.02247$. Obviously, such a parameter can efficiently be used to transit from multiple-breathing structures to single-breathing patterns, therefore adapting the solitonic width to specific cellular functions. It should be noted that the studied physical model has undergone significant improvements, particularly in its responsiveness to coupled and uncoupled excitations. The movement of tubulin dimers may vary in speed, depending on the constant γ responsible for the transport memory effects. However, it is important to note that the nonlinearity in both cases remains a

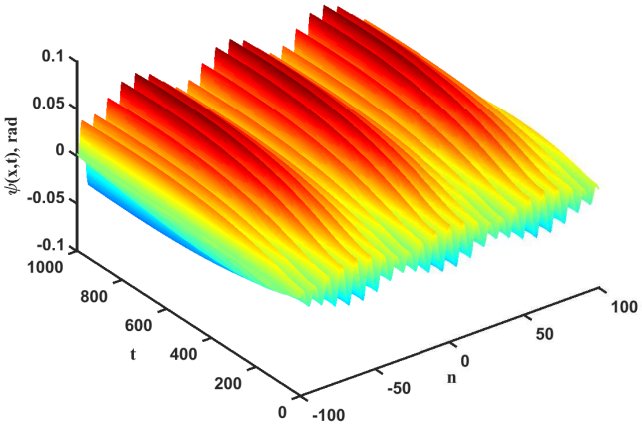

Figure 38: Direct numerical simulations of Eq.(32) using solution (152) as initial condition and integrating the transport memory effect, for $\eta = 0.002$ and $\beta = 0.1$.

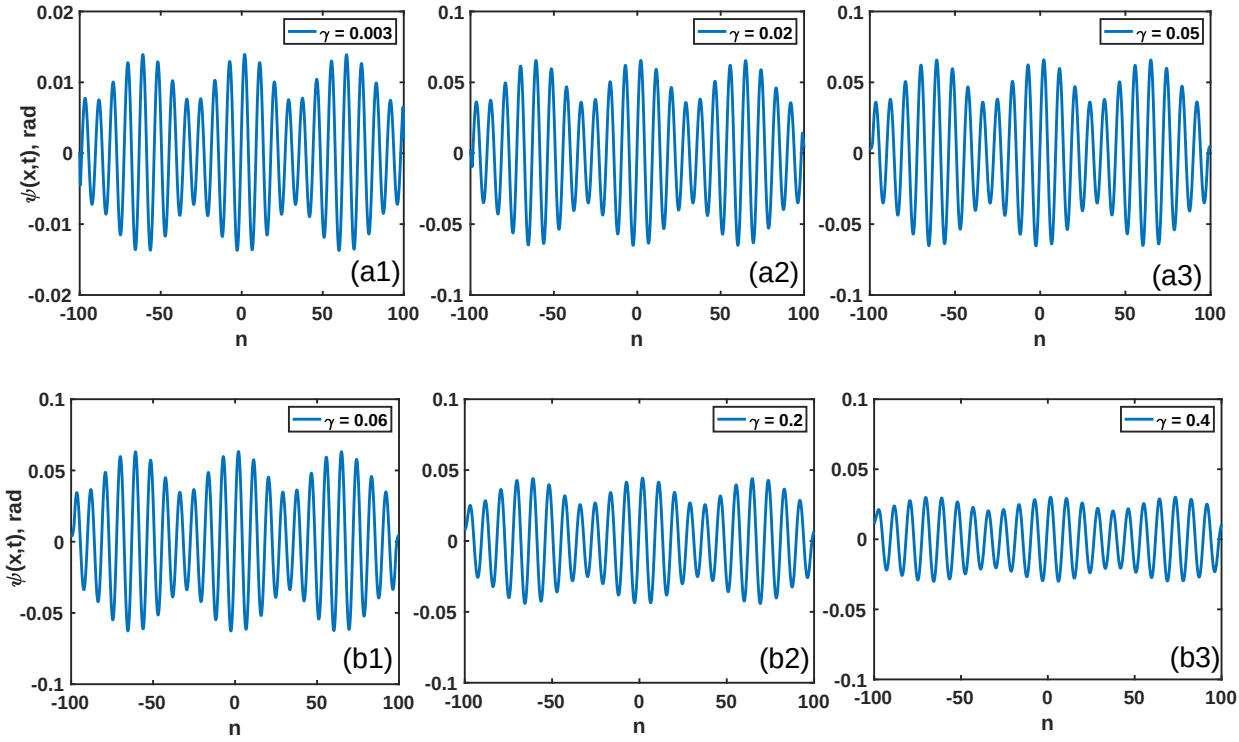

Figure 39: Direct numerical simulations using solution (152) as initial condition. The panels show the impact of the transport memory constant γ on the coupled breather-soliton solution along the MTs, for $\eta = 0.002$ and $\beta = 0.1$.

deamplification factor. From our observations within the selected value ranges, it behaves solely as an attenuating factor. We believe that our results can be replicated in real-world physical experiments as long as the model parameters of Eq.(32) are set to allow for stable spatiotemporal evolutions of nonlinear wave patterns. Within the cell cytoplasm, MTs undergo continuous conformational changes due to physiological mechanisms such as GTP hydrolysis. It has been suggested that the communication necessary for the movement of molecular motors (dynein and kinesin) is facilitated by soliton-breathers.

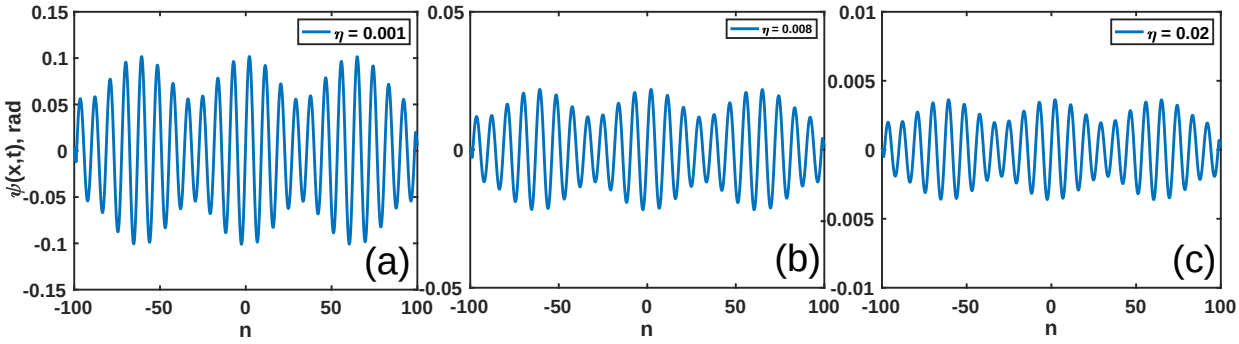

Figure 40: Direct numerical simulations using solution (152) as initial condition. The panels show the impact of the nonlinearity rate η on the coupled breather-soliton solution along the MTs for $\gamma = 0.02247$ and $\beta = 0.1$, at time $t = 800$.

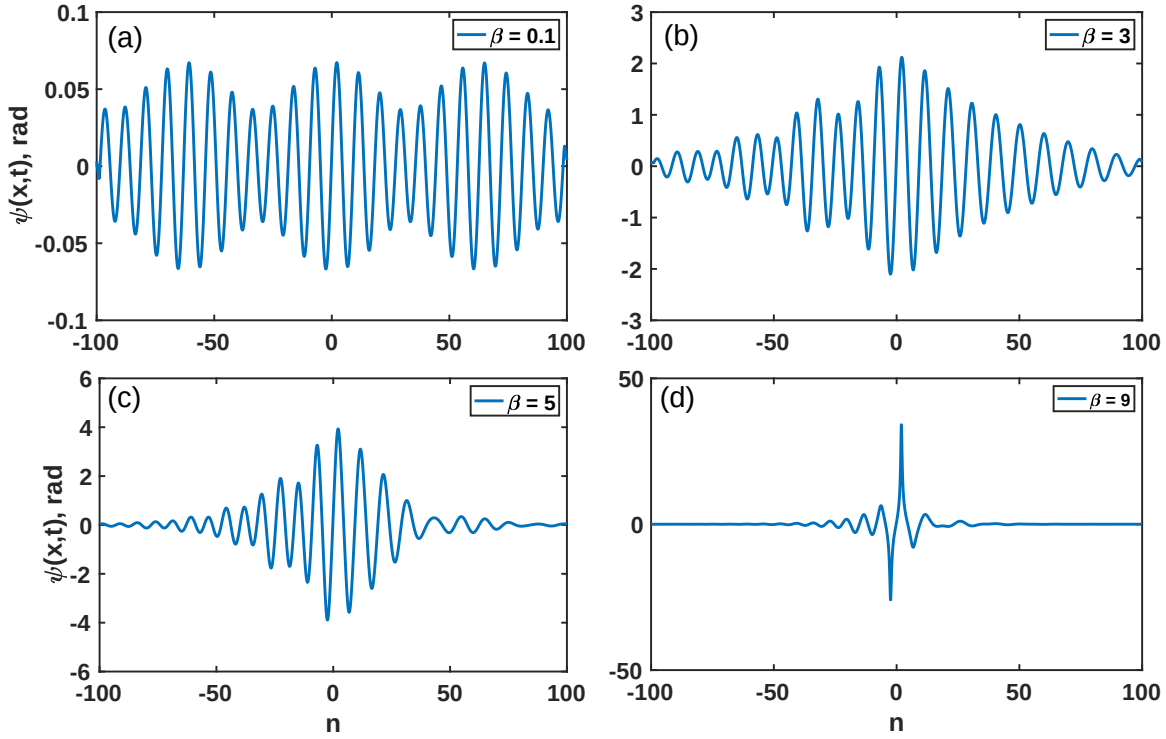

Figure 41: Direct numerical simulations using solution (152) as initial condition. The panels display the impact of the free parameter β taking into account the inverse of the width of the soliton on the coupled breather-solution envelop along the MTs for $\eta = 0.002$ and $\gamma = 0.02247$, at time $t = 800$.

Given the diverse and complex nature of intracellular transport, similar to information processing in neuronal networks, we believe that the coupled breather is essential for addressing any communication deficiencies within the cell. The MT vibrations shown in Figs. 33 and 39 are interesting due to their modulated and localized wave profiles. However, when considering their spatial spread, it becomes clear that the coupled soliton-breather mode would better facilitate the collection, transport, and redistribution of cellular cargoes through MT dynamics. This could especially be true when certain model parameters are varied, resulting in changes to the speed, number, and distribution of dimers in the cytoplasmic environment as they carry out their biological functions. We discussed earlier how MTs with an overdamped movement may display transport memory effects. This idea is motivated by the

contribution of Sahu et al [207], which reveals that MTs have multilevel memory traits. Their scanning tunnelling microscope experiments showed that memory states were linked to the orientations of tilted dipoles (dimers). We argue that these tilts would cause depolymerization followed by polymerization, leading to the attachment of kinesin/dynein via signaling relayed by the coupled breather excitation. This would enable the movement of suitable and useful cargo. Additionally, this would provide valuable insight into the nonlinear dynamics of MTs in the brain. Therefore, by understanding the behavior of a molecular motor along the axonal PF at a certain point in the network, we can predict and control it at the previous point. When two neurons exchange information, the optimal way to observe the memory transfer is through the soliton-breather coupling. This process involves consistent parameters such as η and β. The behavior of the coupled vibration alternates between amplification and deamplification. Amplification is associated with the collection and transfer of a large amount of information, while deamplification results in a loss of energy. This can disrupt the work of motor proteins that supply certain cell sites with energy. The way information is perceived in the brain, which is overseen by MTs at the level of neuronal axons, may lead to reduced neuronal activities. This, in turn, can cause neurodegenerative conditions like Parkinson's and Alzheimer's diseases [208, 209]. We can currently understand how tubulin dimers move in a cytoplasmic environment that is over-damped and scrambled (chirp) when coupled or uncoupled breathing excitations take place. This understanding may contribute to our knowledge of important cellular biological phenomena that are regulated by MT dynamics, including mitosis, mitochondrial motility, and cognitive and memory processes in the brain.

III.4 Nonlinear coupled waves in an electrical circuit model for MTs

III.4.1 Analytical soliton solutions of the CCGL equations

The strong relationship between wave modulation and soliton formation has given rise to a broad range of contributions using several resolution methods of nonlinear equations. Using the modified Hirota's method, the coupled cubic-quintic CGL equations were solved analytically for counter-propagating waves by Zakeri and Yomba [210]. Following a similar procedure to solve a set of coupled Eqs.(65), we first consider the following modified Hirota's linear operators:

$$\left(D_x^m D_t^n\right)_{p_j}(G.F) = \left[\frac{\partial}{\partial x} - \left(\frac{1}{2} + ip_j\right)\frac{\partial}{\partial x'}\right]^m \times \left[\frac{\partial}{\partial t} - \left(\frac{1}{2} + ip_j\right)\frac{\partial}{\partial t'}\right]^n \times G(x,t)\, F\left(x',t'\right)\big|_{x=x',t=t'}, \tag{153a}$$

$$\Lambda_j(F.F) = \left(\frac{1}{2} + ip_j\right)\left(\frac{3}{2} + ip_j\right) \times \left(FF_{xx} - F_x^2\right), \quad j = 1,2 \tag{153b}$$

where p_j (j=1,2) are real parameters, n,m are positive integers and $G(x,t)$, $H(x,t)$ and $F(x,t)$ are assumed to be real-valued functions. Considering $T_2 = t$ and $X_1 = x$, we rewrite the set of Eqs. (65) as:

$$\begin{aligned} i\frac{\partial B_1}{\partial t} - S_1\frac{\partial^2 B_1}{\partial x^2} - \sigma_1|B_1|^2B_1 - \rho_1|B_2|^2B_1 = iA_1B_1 \\ i\frac{\partial B_2}{\partial t} - S_2\frac{\partial^2 B_2}{\partial x^2} - \sigma_2|B_2|^2B_2 - \rho_2|B_1|^2B_2 = iA_2B_2, \end{aligned} \tag{154}$$

whose exact solutions can be obtained using the transformations

$$B_1 = \frac{\eta G e^{i(q_1x-\Omega_1t)}}{F^{\left(\frac{1}{2}+ip_1\right)}}, \qquad B_2 = \frac{\mu H e^{i(q_2x-\Omega_2t)}}{F^{\left(\frac{1}{2}+ip_2\right)}}, \tag{155}$$

where q_1, q_2 and Ω_1, Ω_2, are, respectively, wavenumbers and angular frequencies of envelopes, and assumed real while $\eta = \eta_r + i\eta_i$ and $\mu = \mu_r + i\mu_i$ are complex. Substituting Eqs.(155) into (154), we obtain the following system of bilinear equations, functions of the modified derivatives of Hirota's linear operators (153):

$$\begin{aligned} &\left[\Omega_1 + q_1^2S_1 - iA_1 + iD_{p_1,t} - 2iq_1S_1D_{p_1,x} - S_1D_{p_1,x}^2 + 4\ell_1\right](G.F) = 0, \\ &S_1\Lambda_1\,(F.F) - |\eta|^2\,(\sigma_{1r} + i\sigma_{1i})\,G^2 - |\mu|^2\,(\rho_{1r} + i\rho_{1i})\,H^2 = 0, \\ &\left[\Omega_2 + q_2^2S_2 - iA_2 + iD_{p_2,t} - 2iq_2S_2D_{p_2,x} - S_2D_{p_2,x}^2 + 4\ell_2\right](H.F) = 0, \\ &S_2\Lambda_2\,(F.F) - |\mu|^2\,(\sigma_{2r} + i\sigma_{2i})\,H^2 - |\eta|^2\,(\rho_{2r} + i\rho_{2i})\,G^2 = 0, \end{aligned} \tag{156}$$

with $|\eta|^2 = \eta_r^2 + \eta_i^2$ and $|\mu|^2 = \mu_r^2 + \mu_i^2$, ℓ_1 and ℓ_2 being constants of decoupling. In addition, the normalization condition $F/|F|^{\left(\frac{1}{2}+ip_1\right)} = F/|F|^{\left(\frac{1}{2}+ip_2\right)} = 1$ is used. There are several families of soliton solutions among which, the impulse, frontal and dark solitons [210]. Such solutions are often obtained from the modified bilinear operators (153). However, we pay particular attention to pulse-like solutions because of their numerous applications in microtubular networks in terms of signal processing and information transport. Therefore, the functions G, H, and F are assumed to be in the following forms:

$$\begin{aligned} G = H = e^{\frac{1}{2}(Rx+\omega t)}, \\ F = 1 + de^{(Rx+\omega t)} + Pe^{2(Rx+\omega t)}, \end{aligned} \tag{157}$$

where ω, R, d and L are taken to be real constant. Substituting the above into Eqs. (156) leads to

$$\begin{aligned} \Omega_1 &= S_1\left(\frac{1}{4}R^2 - q_1^2\right), \quad \Omega_2 = S_2\left(\frac{1}{4}R^2 - q_2^2\right), \\ \omega &= 2\left(A_1 + S_1q_1R\right), \quad p_1 < 0, \quad p_2 < 0, \quad \ell_1 = \ell_2 = 0, \\ |\eta|^2 &= \frac{S_1R^2d\left[\rho_{1i}\left(\frac{3}{4} - p_1^2\right) - 2p_1\rho_{1r}\right]}{\sigma_{1r}\rho_{1i} - \sigma_{1i}\rho_{1r}}, \\ q_2 &= \frac{S_1q_1R + A_1 - A_2}{S_2R}, \\ |\mu|^2 &= \frac{S_1R^2d\left[\sigma_{1i}\left(p_1^2 - \frac{3}{4}\right) + 2p_1\sigma_{1r}\right]}{\sigma_{1r}\rho_{1i} - \sigma_{1i}\rho_{1r}}, \quad R^2 = -\frac{A_1}{p_1S_1}, \end{aligned} \tag{158}$$

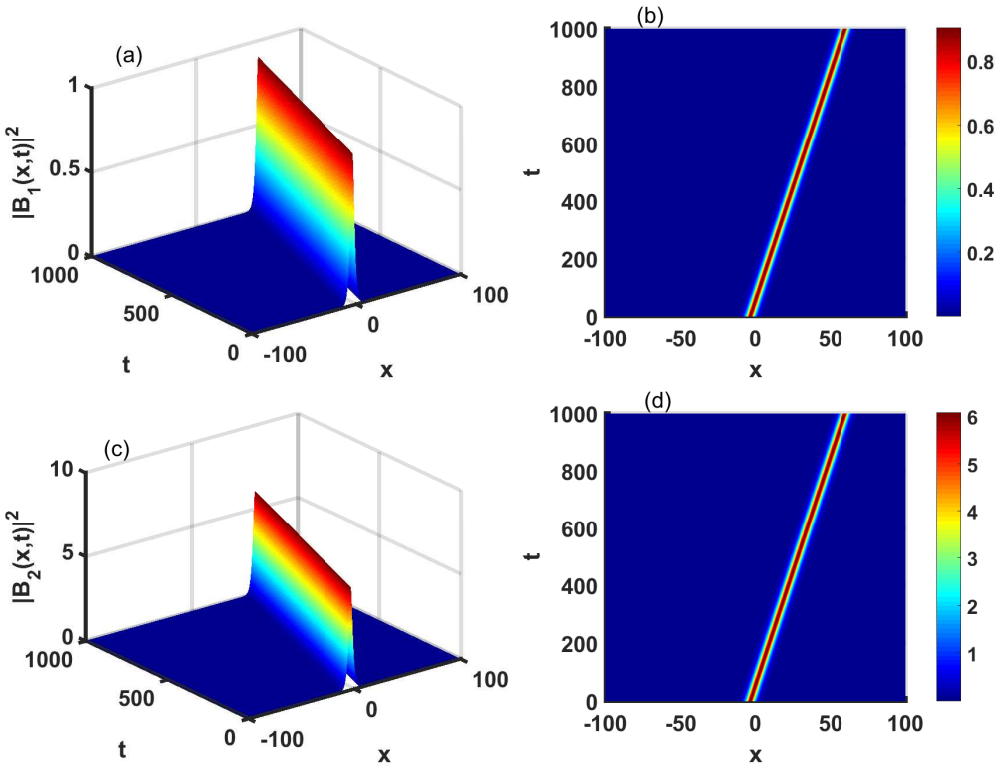

Figure 42: Spatiotemporal evolution of pulse-soliton amplitudes B_1 [panels (a) and (b)] and B_2 [panels (c) and (d)] from Eqs.(160) and (161).

with $d \neq 0$ and $P \neq 0$. In order to further proceed, the constraints in appendix B3.(177) are adopted, which leads to the following solutions, giving the complex amplitude B_1 and B_2:

$$\begin{aligned} B_1(x,t) &= \frac{\eta e^{\frac{1}{2}(Rx+\omega t)+i(q_1 x-\Omega_1 t)}}{\left[1+de^{(Rx+\omega t)}+Pe^{2(Rx+\omega t)}\right]^{\left(\frac{1}{2}+ip_1\right)}}, \\ B_2(x,t) &= \frac{\mu e^{\frac{1}{2}(Rx+\omega t)+i(q_2 x-\Omega_2 t)}}{\left[1+de^{(Rx+\omega t)}+Pe^{2(Rx+\omega t)}\right]^{\left(\frac{1}{2}+ip_2\right)}}, \end{aligned} \tag{159}$$

with their squared norms being given by:

$$|B_1(x,t)|^2 = \frac{|\eta|^2 \left|e^{(Rx+\omega t)}\right|}{\left|1+de^{(Rx+\omega t)}+Pe^{2(Rx+\omega t)}\right|}, \tag{160}$$

$$|B_2(x,t)|^2 = \frac{|\mu|^2 \left|e^{(Rx+\omega t)}\right|}{\left|1+de^{(Rx+\omega t)}+Pe^{2(Rx+\omega t)}\right|}. \tag{161}$$

The panels of Fig. 42 illustrate well the spatiotemporal evolution of such amplitudes, which represent bright-soliton amplitudes. Using Eqs. (159), it is possible to rewrite the spatiotemporal formula of the voltage $V_n(t)$ given by relation (58). It describes the calcium wave propagation through the network of

cellular microtubules and it is given by:

$$V_n(t) = \frac{2\varepsilon}{F}\left[\eta_r G\cos(\Phi_1) + \mu_r H\cos(\Phi_2)\right] + \frac{2\varepsilon^2\eta^2 G^2 F^{-1}}{\omega_1^2 - \omega_0^2\sin^2(k_1)}\left[\alpha_1\omega_1^2\cos(2\Phi_1)\right.$$
$$\left.-\frac{1}{2}\omega_1\left(\beta_0\alpha_1 + 4\beta_2\sin^2(k_1)\right)\sin(2\Phi_1)\right] + \frac{2\varepsilon^2\mu^2 H^2 F^{-1}}{\omega_2^2 - \omega_0^2\sin^2(k_2)}\left[\alpha_1\omega_2^2\cos(2\Phi_2)\right. \quad (162)$$
$$\left.-\frac{1}{2}\omega_2\left(\beta_0\alpha_1 + 4\beta_2\sin^2(k_2)\right)\sin(2\Phi_2)\right],$$

where $\Phi_1 = (q_1 + k_1)\,x - (\Omega_1 + \omega_1)\,t - p_1\ln F$ and $\Phi_2 = (q_2 + k_2)\,x - (\Omega_2 + \omega_2)\,t - p_2\ln F$. This coupled solution comprising the two frequency modes ω_1 and ω_2 will be used as the initial condition in the next section dedicated to numerical analysis of wave propagation in the microtubule network. More precisely, at the initial time ($t = 0$), the signal originating from the hydrolysis of guanosine triphosphate and which is to propagate along the MTs is then given in form (162). In general, interactions of waves can give rise to radiations or generate other types of solitons, especially when other system-related factors such as management and inhomogeneities are included [211]. This can involve bright-bright or bright-dark solitons, leading to more complex and exotic structures potentially full of interest, with possible practical applications. Therefore, In view of solution (162) the reader should notice that the generalized solution has a breather form, which implies the possibility of getting modulated waves.

III.4.2 Numerical simulations of the CCGL equations

Numerical simulations here are carried out in the generic discrete Eq.(37) describing the signal processing in an electrical transmission line of MTs. Obviously, Eq.(37) contains several terms and their corresponding coefficients that may significantly affect wave propagation in the model under study. Among such parameters, particular importance has been given to dissipative effects brought by the coefficients β_0 and β_1. Even at the sub-cellular level, most biological processes are sequenced by an initiation, triggered in the present case by the hydrolysis of GTP, execution, and termination, which is indubitably related to the attenuation of the propagating signal under dissipative effects. However, it should be indicated that other biological factors may contribute to amplifying the signal against dissipation to complete a given process until complete information is transported to the receiver. A failure of such, the case of neuronal microtubules, for example, may lead to a multitude of neuronal disorders such also anxiety [212]. From the physical point of view, dissipative effects significantly modify the intrinsic dynamic equilibrium between nonlinearity and dispersion, consequently affecting the stable information and energy transport in MTs. This shows the straightforward interdependence between the structural role of MTs and their essential function in ionic signal processing at the sub-cellular level, under controlled input from dissipative elements inherent to biological environments.

This study of ionic signal transport along the MT electrical network is based on the direct simulation of Eq.(37) via the well-known Runge-Kutta computational scheme, under periodic boundary conditions and a step over time, $dt = 10^{-2}$ns. As said so far, the input signal is the modulated impulse of Eq.(162), over 201 lattice cells, with two coupled oscillation modes characterized by (k_1, ω_1)

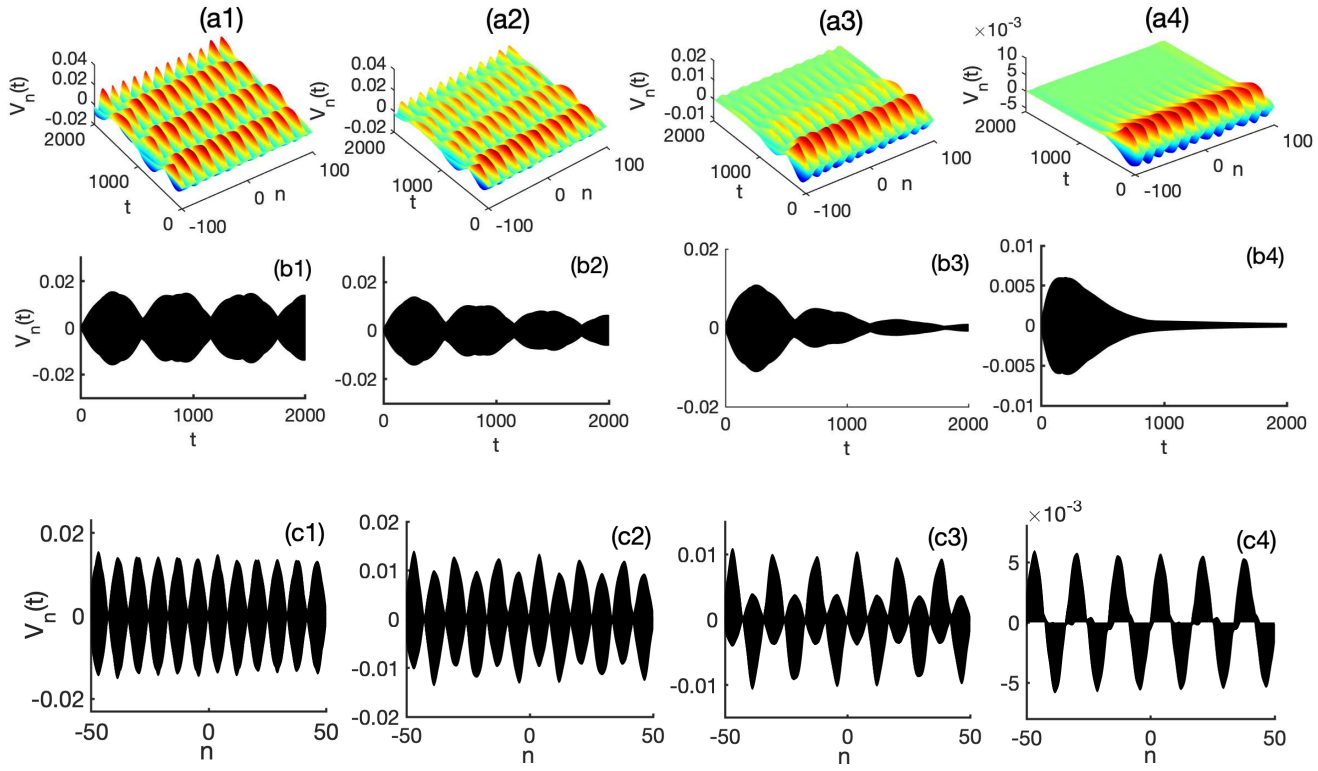

Figure 43: Spatiotemporal evolution of the coupled solution [panels (aj)$_{j=1,2,3,4}$] along with their corresponding time series [panels (bj)$_{j=1,2,3,4}$] and spatial evolution [panels (cj)$_{j=1,2,3,4}$] for the parameters $k_1 = 0.13$, $k_2 = 0.35k_1$. Moreover, from left to right, columns correspond to the respective values $\beta_0 = 0.00009$, $\beta_0 = 0.0009$, $\beta_0 = 0.003$ and $\beta_0 = 0.01$ of the dissipative coefficient.

and (k_2, ω_2), with $k_2 = \alpha k_1$. To remind, the amplitudes of individual modes, shown in Fig. 42, display bell-shaped solitary impulses. Indubitably, the coupled mode results in a robust envelope soliton, already known in several biological settings. The role of coupled bright soliton in neuronal networks was debated in the context of information transport and signal processing [213]. Under the conditions described above, the results for numerical study are shown in Fig. 43. Clearly, the panels of Fig. 43 give a comparison between the spatiotemporal evolution of the coupled solitary wave to its corresponding time series and wave profile, under different values of dissipative coefficients. Obviously, in space and time, the propagation of the coupled mode gives rise to modulated trains of patterns. In panel (a1) of Fig. 43, precisely, the spectrum of behavior is such that the wave structure keeps its stable and periodic state over time and repeats the same propagation events. This assumes that localized excitations of ionic waves are accessible to the electrical network, and the corresponding localized signals present solitary modulated solutions with a regular periodic background. Spatially, the movement of the signal repeats after about 15 unit cells of MTs while temporally, its period is about 1300ns materialized by two alternations. In the same panel (a1), tiger amplitude of oscillations can be noticed, which stands for areas where the energy carried by the voltage wave is maximum. This corresponds to the precise moment when the ionic signal gets more accelerated, inducing the microtubular activities. As for the dark peaks of the signal, the energy would be minimal and would not allow a good appreciation of the desired biological phenomenon, while the moments of respite, where the voltage soliton wave is

zero, would rather be those of the transition between two phases of the process under study. Additionally, there is an amplification of the excitatory signal in the network whose profile is plotted in Fig. 43(b1). The signal propagates in the form of a train of small amplitude with a short wavelength, with each component of the train having the shape of a soliton object. This proves the robustness of the coupled-wave solutions, which corroborates predictions from the linear stability analysis of MI. One of the primary outcomes of the studied model is its sensitivity to model parameters such as dissipation, which is evident in Fig. 43(a2) and Fig. 43(b2). In this context, the spatiotemporal behavior of the ionic waves is still supported by coherent structures whose amplitude goes down as time increases. Interestingly, the time series of Fig. 43(b2) shows that increasing the values of β_0 considerably attenuates wave propagation and even affects the spatial distribution of the obtained patterns. Corresponding values for β_0 are such that $\beta_0 = 0.0009$ for Fig. 43(a2), $\beta_0 = 0.003$ for the case of Fig. 43(a3) and $\beta_0 = 0.01$, which corresponds to the patterns of Fig. 43(a4). We should stress remind that in the process, we have related the value of β_1 to the one of β_0 so that the change in the latter directly affects variation in β_1. Therefore, It is noticeable that the two dissipation coefficients β_0 and β_1 have a common effect on the propagation of the envelope of coupled soliton pulses, except that the action of one, β_0, is more aggressive and quicker than that on the other, β_1, which is proportional to β_0. More precisely, increasing β_0 changes the characteristics of the wave structure more quickly. As a whole, controlling and maintaining small acceptable values of the dissipative parameters would allow good energy propagation in our biomolecular filament network. Due to the strong dissipation of the biological medium studied and to the fact that the supplied energy could suddenly be dissipated and therefore be insufficient for the MTs to perform their cellular functions optimally, the coupled solitary bursting signal would therefore be an excellent option to remedy and promote the release of a large amount of compensatory energy and which would propagate stably and permanently throughout the biological network. The energy and information transport that originates from a hydrolysis of GTP in cellular MTs would then be possible via the envelope solution of coupled voltage pulses of the soliton-type supported by the discrete model of transmission line studied. The inherent electric nature of neurons points out the effectivity and potential functions of the MT cytoskeleton that conveys electric information. Although no direct experiment has been realized showing the evidence and contribution of MT in signal conduction in neurons, it remains scientifically verified that MT contributes importantly to higher cognitive processes, among which neuronal signal processing. A broad range of oscillatory modes has been reported recently, where Tabi and co-workers [148, 149, 199, 214] showed that neuronal waves and action potentials might rely on frequency distribution, depending on the physiological process to be achieved. Indubitably, the transmission line elements, such as the intrinsic resistance and capacitance, play a crucial role in the spatiotemporal spreading of the wave. This is finely illustrated by the different scenarios depicted in Fig. 43(cj)$_{j=1,2,3,4}$, where panels from left to right correspond to increasing values of β_0, the dissipative coefficient. Importantly, such structures have been reported in many contributions as being caused by the activation of MI. Noticeably, increasing the resistance in the system contributes to generating asymmetric solitonic objects while the amplitude decreases. Although the precise mechanism

is not fully clear yet [88], it may involve diffusion through the central channel [215] and ion redistribution along the microtubule resulting from the variations in cation (Na^+; K^+; Ca^{2+})migration through nanopores along the microtubule wall [216]. In that direction, several contributions have demonstrated charge centers with corresponding counter ion clouds along the axis of the microfilament allowing ionic waves to propagate along its axis [17,217,218]. The described phenomenon was already reported by Lin et $a\ell$ [89], who further confirmed electrical signal via soliton waves in actin filaments. However, against dissipation, it was shown recently that microtubules are capable of amplifying ionic signal waves [90] which may importantly contribute to the regulation of voltage-dependent anion channel in the mitochondria [219] with considerable implications in exchanges involving the extracellular matrix [220] that facilitates permanent dynamics and information exchange between the cytoskeleton and extracellular environment.

III.5 Conlusion

The studies carried out in this chapter relate to some crucial fact that provide a better understanding of the complex functioning of biological MT networks during the collection, transport and transfer of information or energy in a cellular environment. These fact, namely, the coupling of two frequency modes, MI, dipole energy variation, the effect of transport memory and dissipation, have given satisfactory results for the propagation of nonlinearly coupled waves along MTs.

The MI phenomenon, due to the combined effects of the nonlinearity and dispersion of the systems explored, has led to realize that information transport and transfer can be achieved by robust coupled soliton waves, thus consolidating the theory that the soliton retains its properties as it moves. Clearly, thanks to the plane wave solutions, an expression for the growth rate of the MI has been proposed, from which a complete parametric analysis of the MI has been carried out on the two models studied. In particular, we have shown and discussed the impact of dipole energy and dissipation on the parametric expansion of unstable regions in the angular and electrical line models. It is worth mentioning that localized coupled structures such as envelope solitons of kinks, breathers and light pulses are found in the modulationally unstable domain. The construction of these results analytically was done by means of the solving methods of Jacobian Elliptic Functions and Bilinear Modified Hirota, with the obtaining of new envelopes of exact solutions coupled by two frequency modes.

The numerical test confirmed that the dynamics of tubulin dimers could be described by nonlinear models of solitonic trains, whose characteristics are sensitive to changes in the parameters of the system, mainly, dipole energy, dissipation and transport memory. Indeed, the amplitude of the kinks envelope decreases with increasing dipole energy, but more extended structures are obtained. We also showed that the over damped character of MTs during their movement in the cytoplasmic environment mainly gives rise to transport memory effects. Thus, the effect of transport memory acts slightly by lowering or increasing the large amount of information that could be conveyed, for example, by motor proteins (kinesin or dynein) from one site to another via the envelope of coupled breathers soliton.

On the other hand, the solitary impulses obtained during the process help to explain the operating mechanism of the protein filaments studied in excitable environments such as neurons. As for the dissipation phenomenon, we noted that over time the dissipation coefficient had an impact on the amplitude of the coupled ionic voltage wave, while spatially other interesting characteristics were obtained that justify the diversity of oscillatory ionic movements across the MT network. This could provide an explanation for the variation and migration of K^+, Na^+ and Ca^{2+} ions across the nanopores present between the tubulin dimers of neighbouring PFs. This could lead to a better understanding of the redistribution of ions throughout the MT during neuronal excitation. These valuable electrical properties may benefit to the neuronal signal processing and to the key process of energy transport and transfer along the MT network, given the direct relationship between electrical behaviour and network deformation for specific biological functions of MTs to be fulfilled under normal physiological conditions.

GENERAL CONCLUSION AND PERSPECTIVES

A. Summary and Contributions

The exploration of nonlinear waves in biological environments is of growing interest and now covers a wide range of biophysical systems, including muscular tissue, MTs, neuronal networks and many others. The study carried out in this thesis focused on the nonlinear dynamics of coupled waves in two mathematical models of microtubules. The primary objective of the work was to reveal that the dynamics of MTs could be studied through the existence and propagation of new classes of soliton train structures, under some optimal circumstances and parametric conditions. Moreover, there was also a strong interest in extending the investigations made by Satarić to more improved models. In more improved considerations, an individual tubulin dimer protein constitutes on the one hand, a dipolar molecule under the influence of other microparticles of the cytoplasm and on the other hand, an electrical cell with capacitive, inductive and resistive components, linked to the polyelectrolyte character of the MT in the cytosol. To achieve these main objectives, the work in this thesis has been divided into three chapters.

The First Chapter presented a general biological overview of microtubules, including a description of their anatomy and physiology, with a focus on their role in the electrical activity of excitable cells such as neurons. We found that MTs are highly dynamic filamentous molecules and that a multitude of physical mathematical models have been introduced in an attempt to explain and understand their complex functioning. These models with biophysically acceptable results were then reviewed and, the transmission electrical line and angular models in particular caught our attention given the geometry and behaviour of an individual tubulin dimer, which is close to the reality of things in the biological environment. They were therefore adopted for this work.

The Second Chapter was devoted to describing the analytical and numerical methods used for the investigations. Thus, after a few important physio-anatomical reminders of the MT in its biotope, we first showed the various modifications on which this research focused and then presented the main analytical methods in turn, such as the expansion of multiple scales, the analysis of modulational instability, Jacobian Elliptic Functions, the semi-discrete approximation and the Modified Hirota Bilinear Method. The fourth-order Runge-Kutta numerical scheme for a direct simulation of the initial equations of motion was also presented. We also showed how to reduce the discrete and continuous models to their coupled amplitude equations. Thus the angular model led to the CNLS and CCNLS systems of equations, respectively, with the absence of cytoplasm damping and the presence of intense friction for the production of transport memory effects. The transmission line model was used to derive a system of nonlinear dissipative CCGL equations.

The Third Chapter has been reserved to the main results reported in this thesis. In particular, their

presentations, each accompanied by a discussion. We began by analyzing the modulation instability in the models explored. This made it possible to realize that the transport and transfer of information can be ensured by soliton-type wave structures in the MT environment. Clearly, thanks to the plane wave solutions, an expression for the growth rate of the MI was proposed, from which a complete parametric analysis of the MI was carried out on the two models studied. In the angular model, the influence of dipole energy on the emergence of unstable modes was discussed and two parameter regions were found to support the formation of non-linear modulated waves, under intense electric field. In a similar process in the transmission line model, we analyzed the impact of dissipative elements on the parametric expansion of unstable regions, in which ionic excitations with solitonic characteristics would also exist. On this basis, the Jacobian Elliptic Function method and the Modified Hirota Bilinear Method were used to construct solutions for breathers, impulses and kinks. All these analytical solutions were found in simple and combined frequency modes. In all cases, a test of stable propagation was carried out by direct numerical simulations of the various equations of the discrete or continuous model, and confirmed for certain well-fixed values of system parameters. Structures with soliton characteristics were obtained, but particular attention was paid to the coupled modes, which proved to be the solutions that best described energy harvesting. The angular model led to robust coupled soliton structures modulated by kink and breathers envelopes, while the electrical model led to a coupled and localized bright light pulse soliton envelope. Interesting observations were made during the study of the effects of the specific parameters used in the MI analysis on the propagation of these non-linear excitations. Firstly, it was found that the kink envelope soliton is strongly modified under an intense electric field through the increase in dipole energy. Subsequently, on over damped movements of tubulin dimers, analysis of the memory constant on the coupled breather's soliton showed that the effect of transport memory would act in two ways by slightly reducing or amplifying the large amount of information traffic that could be carried from one site to another via the MTs. Finally, we noted that the ion current dynamics described by localized non-linear modes of ion soliton envelope trains are sensitive to changes in system parameters, mainly dissipation. In the course of the studies, solitary pulses were obtained. This would justify the diversity of oscillatory movements in the MTs network and, together with other observations, explain the operating mechanism of this filamentous network in eukaryotic cells in general, of which neurons are a part. We have seen that the MTs of neurite extensions (axon and dendrite) are more stable than those of other cells in the body of a living being. The energy collection mechanism should therefore be stronger. During oscillatory movements in neurons, an increase in the concentration of Ca^{2+} ions outside the MT during neuronal excitation would break down the free energy barrier preventing the migration of certain ions such as potassium K^+ or sodium Na^+ towards the inside of the MT. This would lead to a redistribution of ions throughout the MT network. Given the direct relationship between ion displacement and deformation of the protofilament network, the valuable properties observed may be beneficial to neuronal electrical signal processing and to the key process of energy transport along MTs in general. Consequently, the robust and broad soliton envelopes generated and the coupled frequencies would best present the characteristics of a serious candidate for the process of collection, transport and transfer of energy released by GTP hydrolysis. We have argued that such solutions to the case of protofilament dynamics can be justified by the presence of the two different modes of vibration [221]. This could have interesting biological meanings and enrich the family of solitons describing the oscillations of tubulin dimers as in reference [222]. We also argued that by relying on systematic control of certain effects of the cytoplasmic environment, including transport

memory, chirp, electric field and dissipation, the specific biological functions of MTs could be fulfilled under normal physiological conditions. Among these specific functions, the initiation of the polymerization /depolymerization process, the electrical activity of neurons and intracellular trafficking can be mentioned.

B. Open problems and future directions

The work in this thesis has helped to improve our understanding of the complex operation of the nonlinear dynamics of MTs in the cellular environment by means of the mathematical models studied above. Most of the research carried out was aimed at studying multi-mode wave propagation phenomena as a function of certain parameters, the number of which is not exhaustive. This is why we are exploring other points of interest that may be resolved in the future :

1 – The idea that MTs can act as complex subcellular nanopores remains an open question, although it has recently received considerable attention [88]. To our knowledge, appropriate models for this have not been sufficiently explored and are a serious concern in terms of the possible efficiency of charge carriers and their robustness against dissipative effects. However, we believe that ion fluxes and permeability can relay the communication of cellular information to the nucleus as an instantaneous response to a high concentration Ca^{2+} ion pulse.

2 – Since there are other models that deal with the nonlinear dynamics of MTs, such as the longitudinal model in which the movement of the tubulin dimer is assumed to be rectilinear, we can admit the presence of two types of simultaneous movement (rotation and translation) for the same dimer. This opens up a new field of exploration in two directions, with the effects of memory on structural movement and intracellular transport being taken into account in a more generalized model of MT dynamics.

3 – It could also be interesting to approach the two-dimensional version by studying the particularities of each mode, in terms of dissipative solitons, and to see their biological implications.

4 – From a theoretical point of view, it is known that the stability and lifetime of localized structures are very sensitive to properties of thermal fluctuations such as the effect of temperature. In the cell, the MT is in permanent contact with the thermal bath of the cytosol. Consequently, thermal forces play an important role in its internal dynamics. It is therefore necessary to explore the role of thermal noise in the formation of localized structures in the models studied in this thesis.

APPENDIX

Main results

Appendix A1: Respective real and imaginary parts of the coefficients (σ_1, σ_2) and (ρ_1, ρ_2) of the system of Coupled Complex Ginzburg-Landau equations given in Eqs.(65)

$$\begin{aligned}
\sigma_{1r} &= \frac{3}{2}\omega_1\left[\alpha_2 + \frac{2\alpha_1^2\omega_1^2 - \left(\alpha_1\beta_0 + 4\beta_2\sin^2\left(\frac{k_1h}{2}\right)\right)\left(\alpha_1\beta_0 + 4\beta_2\sin^2\left(k_1h\right)\right)}{3\left(\omega_1^2 - \omega_0^2\sin^2\left(\frac{k_1h}{2}\right)\right)}\right],\\
\sigma_{1i} &= \frac{3}{2}\left[\alpha_2\beta_0 + 4\beta_3\sin^2\left(\frac{k_1h}{2}\right) + \frac{3\alpha_1^2\omega_1^2\beta_0 + 4\alpha_1\beta_2\omega_1^2\left(\sin^2\left(k_1h\right) + 2\sin^2\left(\frac{k_1h}{2}\right)\right)}{3\left(\omega_1^2 - \omega_0^2\sin^2\left(\frac{k_1h}{2}\right)\right)}\right],\\
\sigma_{2r} &= \frac{3}{2}\omega_2\left[\alpha_2 + \frac{2\alpha_1^2\omega_2^2 - \left(\alpha_1\beta_0 + 4\beta_2\sin^2\left(\frac{k_2h}{2}\right)\right)\left(\alpha_1\beta_0 + 4\beta_2\sin^2\left(k_2h\right)\right)}{3\left(\omega_2^2 - \omega_0^2\sin^2\left(\frac{k_2h}{2}\right)\right)}\right],\\
\sigma_{2i} &= \frac{3}{2}\left[\alpha_2\beta_0 + 4\beta_3\sin^2\left(\frac{k_2h}{2}\right) + \frac{3\alpha_1^2\omega_2^2\beta_0 + 4\alpha_1\beta_2\omega_2^2\left(\sin^2\left(k_2h\right) + 2\sin^2\left(\frac{k_2h}{2}\right)\right)}{3\left(\omega_2^2 - \omega_0^2\sin^2\left(\frac{k_2h}{2}\right)\right)}\right],\\
\rho_{1r} &= 2\alpha_2\omega_1,\ \rho_{1i} = 3\left(\alpha_2\beta_0 + 4\beta_3\sin^2\left(\frac{k_1h}{2}\right)\right),\ \rho_{2r} = 2\alpha_2\omega_2,\ \rho_{2i} = 3\left(\alpha_2\beta_0 + 4\beta_3\sin^2\left(\frac{k_2h}{2}\right)\right).
\end{aligned} \tag{163}$$

Appendix A2: Respective real and imaginary parts of the coefficients (Q_1, Q_2) and (R_1, R_2) of the system of Coupled Complex Nonlinear Schrödinger Equations given in Eqs.(77)

$$\begin{aligned}
Q_{1r} &= \frac{3\omega_0^2\eta_2 + \eta_1\omega_i}{2\omega_{1r}}, \quad Q_{2r} = \frac{3\omega_0^2\eta_2 + \eta_1\omega_i}{2\omega_{2r}}, \quad Q_{1i} = Q_{2i} = -\frac{\eta_1}{2}\\
R_{1r} &= \frac{3\omega_0^2\eta_2 + \eta_1\omega_i}{\omega_{1r}}, \quad R_{2r} = \frac{3\omega_0^2\eta_2 + \eta_1\omega_i}{\omega_{2r}}, \quad R_{1i} = R_{2i} = -\eta_1
\end{aligned} \tag{164}$$

Appendix A3: Details of calculations on the derivation of the system of Coupled Nonlinear Schrödinger Equations (50) and (51) from the angular model

By letting $j = 2$ in equation (43), using the result obtained in equation(45), we have the second-order approximation equation :

$$\begin{aligned}
\left(\frac{\partial^2}{\partial t^2} + \omega_g^2\right)\varphi_{n,n}^{(2)} - C\left(\varphi_{n,n+1}^{(2)} + \varphi_{n,n-1}^{(2)}\right) =& 2\mu\frac{\partial^2\varphi_{n,n}^{(1)}}{\partial t\partial\xi_n} + Cl\frac{\partial}{\partial\xi_n}\left(Q_1(T,\xi_n)e^{-i\omega_g t}\right.\\
&- (-1)^n Q_2(T,\xi_n)e^{-i\omega_{\max}t} + cc - Q_1(T,\xi_n)e^{-i\omega_g t}\\
&\left.+ (-1)^n Q_2(T,\xi_n)e^{-i\omega_{\max}t} - cc\right),
\end{aligned} \tag{165}$$

then, using the solvability condition $\mu = 0$, we obtain

$$\left(\frac{\partial^2}{\partial t^2} + \omega_g^2\right)\varphi_{n,n}^{(2)} - C\left(\varphi_{n,n+1}^{(2)} + \varphi_{n,n-1}^{(2)}\right) = 0. \tag{166}$$

We now consider the case $j = 3$ in equation (43). Using the results obtained in equations (45) and (49), one has:

$$\begin{aligned}
\left(\frac{\partial^2}{\partial t^2} + \omega_g^2\right)\varphi_{n,n}^{(3)} - C\left(\varphi_{n,n+1}^{(3)} + \varphi_{n,n-1}^{(3)}\right) =& Cl\frac{\partial}{\partial \xi_n}\Big(B_1(T,\xi_n)e^{-i\omega_g t} - (-1)^n B_2(T,\xi_n)e^{-i\omega_{\max} t} + cc \\
&- B_1(T,\xi_n)e^{-i\omega_g t} + (-1)^n B_2(T,\xi_n)e^{-i\omega_{\max} t} - cc\Big) \\
&+ \frac{Cl^2}{2}\frac{\partial^2}{\partial \xi_n^2}\Big(Q_1(T,\xi_n)e^{-i\omega_g t} - (-1)^n Q_2(T,\xi_n)e^{-i\omega_{\max} t} + cc \\
&+ Q_1(T,\xi_n)e^{-i\omega_g t} - (-1)^n Q_2(T,\xi_n)e^{-i\omega_{\max} t} + cc\Big) \\
&- \alpha\omega_g^2\Big(\left|Q_1\right|^2 Q_1 e^{-i\omega_g t} + (-1)^n\left|Q_2\right|^2 Q_2 e^{-i\omega_{\max} t} \\
&+ 2\left|Q_1\right|^2 Q_1 e^{-i\omega_g t} + 2(-1)^n\left|Q_1\right|^2 Q_2 e^{-i\omega_{\max} t} \\
&+ 2\left|Q_2\right|^2 Q_1 e^{-i\omega_g t} + 2(-1)^n\left|Q_2\right|^2 Q_2 e^{-i\omega_{\max} t} \\
&+ cc + \text{higher harmonics}\Big) \\
=& Cl^2\frac{\partial^2 Q_1}{\partial \xi_n^2}e^{-i\omega_g t} - (-1)^n\frac{\partial^2 Q_2}{\partial \xi_n^2}e^{-i\omega_{\max} t} + 2i\omega_g\frac{\partial Q_1}{\partial T}e^{-i\omega_g t} \\
&+ 2i(-1)^n\omega_{\max}\frac{\partial Q_2}{\partial T}e^{-i\omega_{\max} t} - \alpha\omega_g^2\Big(3\left|Q_1\right|^2 Q_1 e^{-i\omega_g t} \\
&+ 2(-1)^n\left|Q_1\right|^2 Q_2 e^{-i\omega_{\max} t} + 2\left|Q_2\right|^2 Q_1 e^{-i\omega_g t} \\
&+ 3(-1)^n\left|Q_2\right|^2 Q_2 e^{-i\omega_{\max} t} + cc + \text{higher harmonics}\Big),
\end{aligned} \tag{167}$$

In so going,

$$\begin{aligned}
\left(\frac{\partial^2}{\partial t^2} + \omega_g^2\right)\varphi_{n,n}^{(3)} - C\left(\varphi_{n,n+1}^{(3)} + \varphi_{n,n-1}^{(3)}\right) =& \Big(2i\omega_g\frac{\partial Q_1}{\partial T} + Cl^2\frac{\partial^2 Q_1}{\partial \xi_n^2} - 3\alpha\omega_g^2\left|Q_1\right|^2 Q_1 \\
&- 2\alpha\omega_g^2\left|Q_2\right|^2 Q_1\Big)e^{-i\omega_g t} + \Big(2i\omega_{\max}\frac{\partial Q_2}{\partial T} - Cl^2\frac{\partial^2 Q_2}{\partial \xi_n^2} \\
&- 3\alpha\omega_g^2\left|Q_2\right|^2 Q_2 - 2\alpha\omega_g^2\left|Q_1\right|^2 Q_2\Big)(-1)^n e^{-i\omega_{\max} t} \\
&+ cc + \text{higher harmonics}.
\end{aligned} \tag{168}$$

We note that the term proportional to $e^{-i\omega_g t}$ and $e^{-i\omega_m axt}$ on the right-hand side of equation (168) is a secular term that must be eliminated in order for the theory to be valid [171, 173]. Removal these secular term in equation above, we obtain the CNLS equation for the envelope functions $Q_1(T,\xi_n)$ and $Q_2(T,\xi_n)$:

$$\begin{aligned}
2i\omega_g\frac{\partial Q_1}{\partial T} + Cl^2\frac{\partial^2 Q_1}{\partial \xi_n^2} - 3\alpha\omega_g^2\left|Q_1\right|^2 Q_1 - 2\alpha\omega_g^2\left|Q_2\right|^2 Q_1 = 0 \\
2i\omega_{\max}\frac{\partial Q_2}{\partial T} - Cl^2\frac{\partial^2 Q_2}{\partial \xi_n^2} - 3\alpha\omega_g^2\left|Q_2\right|^2 Q_2 - 2\alpha\omega_g^2\left|Q_1\right|^2 Q_2 = 0
\end{aligned} \tag{169}$$

Like this, we obtain the system of equation (52) and (53).

Appendix B1: Coefficients η_0, η_1, η_2 and η_3 of the fourth degree perturbed dispersion equation (125) in the microtubular model of electrical transmission line

$$\begin{aligned}
\eta_3 &= Q_{11} - Q_{22} + Q_{33} - Q_{44} \\
\eta_2 &= -Q_{11}Q_{22} - Q_{31}Q_{13} - Q_{42}Q_{24} - Q_{33}Q_{44} \\
&\quad + Q_{11}Q_{33} + Q_{22}Q_{44} - Q_{11}Q_{44} - Q_{22}Q_{33}, \\
\eta_1 &= Q_{22}Q_{33}Q_{44} + Q_{31}Q_{13}Q_{44} - Q_{42}Q_{24}Q_{33} \\
&\quad - Q_{11}Q_{33}Q_{44} - Q_{11}Q_{42}Q_{24} - Q_{11}Q_{22}Q_{33} \\
&\quad + Q_{11}Q_{22}Q_{44} + Q_{31}Q_{13}Q_{22}, \\
\eta_0 &= Q_{11}Q_{22}Q_{33}Q_{44} + Q_{31}Q_{13}Q_{42}Q_{24} \\
&\quad - Q_{31}Q_{13}Q_{22}Q_{44} - Q_{11}Q_{42}Q_{24}Q_{33}.
\end{aligned} \tag{170}$$

Appendix B2: Linear set consisting of the algebraic equations of unknowns V_{10}, V_{20}, S_{1r}, S_{2r}, S_{1i}, S_{2i}, δ_1, δ_2 and β in solution (152)

$$P_1\beta^2 - S_{1r} - P_1\beta^2\delta_1^2 - i\left(S_{1i} - 2P_1\beta^2\delta_1\right) = 0, \tag{171}$$
$$P_1\beta^2\left(\delta_1^2 - 2\right) + V_{10}^2 Q_{1r} + V_{20}^2 R_{1r} = 0, \tag{172}$$
$$-3P_1\beta^2\delta_1 + V_{10}^2 Q_{1i} + V_{20}^2 R_{1i} = 0, \tag{173}$$
$$P_2\beta^2 - S_{2r} - P_2\beta^2\delta_2^2 + i\left(-S_{2i} + 2P_2\beta^2\delta_2\right) = 0, \tag{174}$$
$$P_2\beta^2\left(\delta_2^2 - 2\right) + V_{20}^2 Q_{2r} + V_{10}^2 R_{2r} = 0, \tag{175}$$
$$-3P_2\beta^2\delta_2 + V_{20}^2 Q_{2i} + V_{10}^2 R_{2i} = 0. \tag{176}$$

Appendix B3: Constraints arising from the modified Hirota's bilinear operators when determining B_1 and B_2 complex amplitudes in Eqs. (159)

$$\begin{aligned}
\rho_{2r} &= \frac{S_2\left(\frac{3}{4} - p_2^2\right)\left(\sigma_{1r}\rho_{1i} - \sigma_{1i}\rho_{1r}\right)}{S_1\left[\sigma_{1i}\left(p_1^2 - \frac{3}{4}\right) + 2p_1\sigma_{1r}\right]} \\
&\quad - \frac{\left[\rho_{1i}\left(\frac{3}{4} - p_1^2\right) - 2p_1\rho_{1r}\right]\sigma_{2r}}{\left[\sigma_{1i}\left(p_1^2 - \frac{3}{4}\right) + 2p_1\sigma_{1r}\right]} \\
\rho_{2i} &= \frac{2p_2S_2\left(\sigma_{1r}\rho_{1i} - \sigma_{1i}\rho_{1r}\right)}{S_1\left[\sigma_{1i}\left(p_1^2 - \frac{3}{4}\right) + 2p_1\sigma_{1r}\right]} \\
&\quad - \frac{\left[\rho_{1i}\left(\frac{3}{4} - p_1^2\right) - 2p_1\rho_{1r}\right]\sigma_{2i}}{\left[\sigma_{1i}\left(p_1^2 - \frac{3}{4}\right) + 2p_1\sigma_{1r}\right]}, \\
A_2 &= \frac{p_2S_2}{p_1S_1}A_1, \\
S_2 &= S_1\frac{p_2}{p_1}\left[\frac{R\left(12p_1^2 + 1\right) - 16p_1q_1}{R\left(12p_2^2 + 1\right) - 16p_2q_2}\right].
\end{aligned} \tag{177}$$

References

[1] Avila J., Microtubule proteins. *1st Ed. Taylor and Francis Group*; (1990).

[2] Wijeratne S.S., Marchan M.F., Tresback J.S., and Subramanian R., Atomic force microscopy reveals distinct protofilament-scale structural dynamics in depolymerizing microtubule arrays. *PNAS*, 119:e2115708119 (2022).

[3] Nasrin S.R., Ganser C., Nishikawa S., Sada K., Yamashita T., Ikeguchi M., Uchihashi T., Hess H., Kakugo A., and Kabir A.M.d.R., Deformation of microtubules regulates translocation dynamics of kinesin. *Sci Adv.*, 7:eabf2211 (2021).

[4] Tuszyński J.A., Brown J.A., Crawford E., Carpenter E.J., Nip M.L.A., Dixon J.M., and Satarić M.V., Molecular dynamics simulations of tubulin structure and calculations of electrostatic properties of microtubules, *Math. Comput. Model.*, 41:1055 (2005).

[5] Audenaert R., Engelborghs Y., Heremans L., and Heremans K., Secondary structure analysis of tubulin and microtubules with Rarnan spectroscopy. *Biochim. Biophys. Acta*, 996:110 (1989)

[6] Dutcher S.K., The tubulin fraternity: alpha to eta. *Curr Opin Cell Biol*, 13:49(2001).

[7] Job D., Valiron O., Oakley B., Microtubule nucleation. *Curr Opin Cell Biol*, 15:111(2003).

[8] Harrison B.C., Marchese-Ragona S.P., Gilbert S.P., Cheng N., Steven A.C., Johnson K.A., Decoration of the microtubule surface by one kinesin head per tubulin heterodimer. *Nature*, 362:73(1993).

[9] Mandelkow E., Schultheiss R., Mandelkow E.M., Reconstructions of tubulin protofilaments: different appearances of the same structure. *Ultramicroscopy*, 13:125(1984).

[10] Margolis R.L., Wilson L., Opposite end assembly and disassembly of microtubules at steady state in vitro. *Cell* 13:1(1978).

[11] Satarić M.V., Tuszyński J.A., and Žakula R.B., Kinklike excitations as an energy-transfer mechanism in microtubules. *Phys Rev E.*, 48:589 (1993).

[12] Zdravković S., Kavitha L., Satarić M.V., Zeković S., and Petrović J., Modified extended tanh-function method and nonlinear dynamics of microtubules, *Chaos, Solitons and Fractals*, 45:1378 (2012).

[13] Zdravković S., Zeković S., Bugay A.N. and Satarić M.V., Localized modulated waves and longitudinal model of microtubules. *Appl. Maths. Comput.*, 285:248 (2016).

[14] Zdravković S., Satarić M.V., Maluckov A., and Balaž A., A nonlinear model of the dynamics of radial dislocations in microtubules, *Appl. Math. Comput.*, 237:227 (2014).

[15] Zdravković S., Satarić M.V., and Zeković S., Nonlinear dynamics of microtubules - A longitudinal model. *EuroPhy Lett.*, 102:38002 (2013)

[16] Alexander I.N., Mónica F.R., Gennady P.B., and Nick E.M., Nonlinear dynamics of dipoles in microtubules: Pseudospin model, *Phys Rev E.*, 93:062412 (2016)

[17] Tuszyński J.A., Portet S., Dixon J.M., Luxford C., and Cantiello H.F., Ionic Wave Propagation along Actin Filaments. *Biophys. J.*, 86:1890 (2004).

[18] Tabi C.B., Ekobena H.P.F., Mohamadou A. and Kofané T.C., Wave propagation of coupled modes in the DNA double helix. *Phys Scr*, 83:035802 (2011).

[19] Dustin P., Microtubules, *2nd edition Springer-Verlag, Berlin*, (1984).

[20] Hyams J. S. and Lloyd C. W., Microtubules in Modern cell Biology. *J B Harford, Editor Wiley-Liss, New York*, 1:439 (1993).

[21] Chrétien D. and Wade R.H., New data on the microtubule surface lattice. *Biology of the cell / under the auspices of the European Cell Biology Organization*, 71:161 (1991).

[22] Ledbetter M.C. and Porter K.R., Morphology of Microtubules of Plant Cell. *Science (New York, N.Y.)*, 144:872 (1964).

[23] Tilney L.G., Bryan J. and Bush D.J., Microtubules evidence for 13 protofilaments. *Journal of Cell Biology*, 59:267 (1973).

[24] Evans L., Mitchison T. and Kirschner M., Influence of the centrosome on the structure of nucleated microtubules. *Journal of Cell Biology*, 100:1185 (1985).

[25] Raynaud-Messina B. and Merdes A. Gamma-tubulin complexes and microtubule organization. *Curr Opin Cell Biol*, 19:24 (2007).

[26] Belmont L.D., Hyman A.A., Sawin K.E., Mitchison T.J., Realtime visualization of cell cycle-dependent changes in microtubule dynamics in cytoplasmic extracts. *Cell,* 62:579 (1990).

[27] Mitchison T.J., Polewards microtubule flux in the mitotic spindle: Evidence from photoactivation of fluorescence. *Journal of Cell Biology*, 109:637 (1989).

[28] Mitchison T. and Kirschner M., Dynamic instability of microtubule growth. *Nature*, 312:237 (1984).

[29] Akhmanova A. and Steinmetz M.O., Tracking the ends: a dynamic protein network controls the fate of microtubule tips. *Nature reviews. Molecular cell biology*, 9:309 (2008).

[30] Akhmanova A. and Steinmetz M.O., Control of microtubule organization and dynamics: two ends in the limelight. *Nature reviews. Molecular cell biology*, 16:711 (2015).

[31] Nogales E., Wolf S.G. and Downing K.H., Electron Crystallography. *Nature*, 391:199 (1998).

[32] Mitchison T.J., Localization of an exchangeable GTP binding site at the plus end of microtubules. *Science (New York, N.Y.)*, 261:1044 (1993).

[33] Nogales E., Structural insights into microtubules functions. *Annual review of biochemistry*, 69:277 (2000).

[34] Nogales E, Whittaker M., Milligan R.A. and Downing K.H., High-resolution model of the microtubule. *Cell,* 96:79 (1999).

[35] Alushin G.M., High-Resolution microtubule structures reveal the structural transitions in gamma-tubulin upon GTP hydrolysis. *Cell*, 157:1117 (2014).

[36] Desai A. and Mitchison T.J., Microtubule Polymerization Dynamics. *Annual Review of Cell and Developmental Biology*, 13:83 (1997).

[37] Cassimeris L., Accessory protein regulation of microtubule dynamics throughout the cell cycle. *Curr Opin Cell Biol*, 11:134 (1999).

[38] Kline-Smith S.L. and Walczak C.E., The Microtubule-destabilizing Kinesin XKCM1 Regulates Microtubule Dynamic Instability in Cells. *Molecular biology of Cell*, 13:2718 (2002).

[39] Moore A.T., MCAK associates with the tips of polymerizing microtubules. *Journal of Cell Biology*, 169:391 (2005).

[40] Mallik R. and Gross S.P., Molecular motors: strategies to get along. *Curr Biol*, 14:971 (2004).

[41] Schliwa M. and Woehlke G., Molecular motors. *Nature*, 422:759 (2003).

[42] Sablin H.P., Kinesins and microtubules: their structures and motor mechanisms. *Curr Opin Cell Biol*, 12:35 (2000).

[43] Hafezparast M., Klocke R., Ruhrberg C., Russ A.P., Stumm G., Martin J.E. and Fisher E.M., Mutations in dynein link motor neuron degeneration to defects in retrograde transport. *Science*, 300:808 (2003).

[44] Williams R., The Control Of Neuron Number. *Annu. Rev. Neurosci.*, 11:423 (1988).

[45] Herrup, K. and Yang Y., Cell cycle regulation in the postmitotic neuron: oxymoron or new biology? *Nat. Rev. Neurosci.*, 8:368 (2007).

[46] Hirai S., Cui D.F., Miyata T., Ogawa M., Kiyonari H., Suda Y., Aizawa S., Banda Y. and Ohno S., The c-Jun N-terminal kinase activator dual leucine zipper kinase regulates axon growth and neuronal migration in the developing cerebral cortex. *J. Neurosci.*, 26:11992 (2006).

[47] Connors B.W. and Long M.A., Electrical synapses in the mammalian brain. *Annu. Rev. Neurosci.*, 27:393 (2004).

[48] Baas P.W., Pienkowski T.P., Cimbalnik K.A., Toyama K., Bakalis S., Ahmad F.J. and Kosik K.S., Tau confers drug stability but not cold stability to microtubules in living cells. *J Cell Sci*, 107:135 (1994).

[49] Webb B.C. and Wilson L. Cold-stable microtubules from brain. *Biochemistry*, 19:1993 (1980).

[50] Black M.M., Baas P.W., Humphries S., Dynamics of alpha-tubulin deacetylation in intact neurons. *J Neurosci*, 9:358 (1989).

[51] Ahmad J., Pienkowski T.P. and Baas P.W., Regional Differences in Microtubule and in the Axon. 73:856 (1993).

[52] Goldstein L.S.B. and Gunawardena S. Flying Through the Drosophila Cytoskeletal Genome. *Cell*, 150:63 (2000).

[53] Alberts B.e.a., Molecular Biology of the Cell, *Garland Science*, (2002).

[54] Manning A.L. and Compton D.A., Structural and regulatory roles of nonmotor spindle proteins. *Curr Opin Cell Biol*, 20:101 (2008).

[55] Wittmann T. and Hyman A., The spindle: a dynamic assembly of microtubules and motors. *Nat Cell Biol*, 3:28 (2001).

[56] Huang K., Yanai A., Kang R., Arstikaitis P., Singaraja R.R., Metzler M., Mullard A., Haigh B., Gauthier C.C., Gutekunst C.A., Hayden M.R., El-Husseini A., Huntingtin-interacting protein HIP14 is a palmitoyl transferase involved in palmitoylation and trafficking of multiple neuronal proteins. *Neuron*, 44:977 (2004).

[57] Mandell J.W. and Banker G.A., The microtubule cytoskeleton and the development of neuronal polarity. *Neurobiol Aging*, 16:229 (1995).

[58] Baas P.W., Slaughter T. and Brown A., Black MM. Microtubule dynamics in axons and dendrites. *J Neurosci Res*, 30:134 (1991).

[59] Hirokawa N., Kinesin and dynein superfamily proteins and the mechanism of organelle transport. *Science (New York, N.Y)*, 279:519 (1998).

[60] Przedborski S., Vila M. and Jackson-Lewis V., Neurodegeneration : What is it and where are we? *J. Clin. Invest.*, 111:3 (2003).

[61] Kim Y., Hwang O. and Kim D.J. Pathology of Neurodegenerative Diseases. Brain Damage - Bridg. *Between Basic Res. Clin.*, 5:111 (2012).

[62] Mandelkow E. and Mandelkow E.M., Microtubules and microtubule-associated proteins. *Curr Opin Cell Biol*, 7:72 (1995).

[63] Garcia M.L. and Cleveland D.W., Going new places using an old MAP: tau, microtubules and human neurodegenerative disease. *Curr. Opin. Cell Biol.*, 13:41 (2001).

[64] Frôhlich H., The Biological Effects of Microwaves and Related Questions. *Adv. Electr. Electr. Phys.*, 53:85 (1980).

[65] Satarić M.V., Koruga D., Ivić Z. and Žakula R.B., The detachment of dimers in the tube of microtubulin as a result of a solitonic mechanism. *J. Mol. Electron.*, 6:63 (1990).

[66] Currie J.F., Blumen A., Collins M.A. and Ross J., Dynamics of domain walls in ferrodistortive materials II. Applications to $Pb_5Ge_3O_11$- and SbSI-type ferroelectrics. *Phys. Rev. B*, 19:3645 (1979).

[67] Hakim M.B., Lindsay S.M. and Powell J., The speed of sound in DNA. *Biopolymers*, 23:1185 (1984).

[68] Fatuzzo E., Theoretical considerations on the switching transient in ferroelectrics. *Phys. Rev.*, 127:1999 (1962).

[69] Germann K.H, Optical anisotropy measurements in multidomain samples. *Phys. Status Solidi. A*, 38:8l (1976).

[70] Satarić M.V., Žakula R.B., lvić Z. and Tuszyński J.A., Influence of a solitonic mechanism on the process of chemical catalysis. *J. Mol. Electron*, 7:39 (1991).

[71] Kirschner M. and Mitchison T., Beyond self-assembly: from microtubules to morphogenesis. *Cell.*, 45:329 (1986).

[72] Kivshar Y.S., and Malomed B.A., Dynamics of solitons in nearly integrable systems. *Rev. Mod. Phys.*, 61:763 (1989).

[73] Gross S.P., Hither and yon, a review of bi-directional microtubule based transport. *Phys. Biol.*, 1:11 (2004).

[74] Satarić M.V., Petkovic B.L., Lončarević L. and Tuszyńsky J.A., Modeling the role of intrinsic electric fields in microtubules as an additional control mechanism of bi-directional intracellular transport. *Cell Biochem Biophys*, 52:113-24 (2008).

[75] Satarić M.V, Kozmidis-Luburić U., Petkovic B.L. and Lončarević L., Intrinsic electric field as a control mechanism of intracellular transport along microtubules. *J Comput Theor Nanosci*, 6:721-31 (2009).

[76] Pampaloni F. and Florin E.L., Microtubule Architecture:inspiration for novel carbon nanotube-based biomimetic materials. *Trends Biotechnol*, 26:302 (2008).

[77] Satarić M.V., Matsson L., and Tuszyński J.A., Complex movements of motor protein relay helices during the power stroke. *Phys. Rev. E*, 74 : 051902 (2006).

[78] Davydov A.S., Solitons in Molecular Systems, Mathematics and its Applications, *D. Reidel Publishing Company, Dordrecht*, 1985.

[79] Kudryashov N.A. and Loguinova N.B., Extended simplest equation method for nonlinear differential equations. *Appl. Math. Comput.*, 205:396 (2008).

[80] Dauxois T., Dynamics of breather modes in a nonlinear helicoidal model of DNA. *Phys. Lett. A*, 159:390 (1991).

[81] Zdravković S., Bugay A.N., Aru G.F., and Maluckov A., Localized modulated waves in microtubules. *Chaos*, 24:023139 (2014).

[82] Hodgkin A.L. and Huxley A. F., A quantitative description of membrane current and its application to conduction and excitation in nerve. *J. Physiol.*, 117:500 (1952).

[83] Havelka D. , M. Cifra M. and Kučera O., Appl. Phys. Lett. 104:243702 (2014).

[84] Havelka D., Cifra M., Kučera O., Pokorný J. and Vrba J., High-frequency electric field and radiation characteristics of cellular microtubule network. *J. Theor. Biol.*, 286:31 (2011).

[85] Cifra M., Pokorný J., Havelka D. and Kučera O., Electric field generated by axial longitudinal vibration modes of microtubule. *BioSystems*, 100:122 (2010).

[86] Drabik P., Gusarov S. and Kovalenko A., Microtubule Stability Studied by Three-Dimensional Molecular Theory of Solvation. *Biophys. J.*, 92:394 (2007).

[87] Schoutens J.E., Dipole-Dipole Interactions in Microtubules, *J. Biol. Phys.*, 31:35 (2005).

[88] Satarić M.V., Ilić D.I., Ralević N. and Tuszyński J.A., A nonlinear model of ionic wave propagation along microtubules. *Eur Biophys J*, 38:637 (2009).

[89] Lin E.C., Cantiello H.F., A novel method to study the electrodynamic behavior of actin filaments. Evidence for cable-like properties of actin. *Biophys J*, 65:1371 (1993).

[90] Priel A., and Tuszyński J.A., A nonlinear cable-like model of amplified ionic wave propagation along microtubules. *EPL*, 83:68004 (2008).

[91] Jimenez M.A., Evangelio J.A., Aranda C. and Lopez-Brauet A., Helicity of alpha (404-451) and beta (394-445) tubulin C-terminal recombinant peptides. *Protein Sci*, 8:788 (1999).

[92] Minoura I. and Muto E., Dielectric measurement of individual microtubules using the electroorientation method. *Biophys J.*, 90:3739 (2006).

[93] Wang B.G., Zhao X.A., Wang J., and Guo H., Nonlinear quantum capacitance. *Appl Phys Lett*, 74:2887 (1999).

[94] Albriton N.L., Meyer T. and Stryer L., Range of messenger activation of calcium ions and IP3. *Science*, 258:1812 (1992).

[95] Wang K., Rappel W.J. and Levine H., Cooperativity can reduce stochasticity in intracellular calcium dynamics. *Phys Biol*, 1:27 (2004).

[96] Pokorny L.J., Hašek J. and Jelínek F., Electromagnetic field of microtubules: effects of transfer of mass particles and electrons. *J Biol Phys*, 31:501 (2005)

[97] Satarić M.V. and Tuszyński J.A., Relationship between the nonlinear ferroelectric and liquid crystal models for microtubules. *Phys Rev E*, 67:011901 (2003).

[98] Amos L.A. and Schlieper D., Microtubules and maps, *Adv. Propein Chem.*, 71:254 (2005).

[99] Watts N.R., Cheng N., W West, Steven A.C. and Sacket D.L., The cryptophycin-tubulin ring structure indicates two points of curvature in the tubulin dimer. *Biochemistry*, 41:12662 (2002).

[100] Pokorný J., Jelinek F., Trkal V., Lamprecht I., and Hölzel R., Vibrations in microtubules. *Astrophys. Space Sci.*, 23:171 (1997).

[101] Pokorný J., Excitation of vibrations in microtubules in living cells. *Bioelectrochemistry*, 63:321 (2004).

[102] Tabi C.B., Mohamadou A. and Kofané T.C., Modulated wave packets in DNA and impact of viscosity. *Chin. Phys. Lett.*, 26:068703 (2009).

[103] Rubinstein S.M., Cohen G., and Fineberg J., Contact areameasurements reveal loading-history dependence of static friction. *Phys. Rev. Lett.*, 96:256103 (2006).

[104] Dillavou S. and Rubinstein S.M., Nonmonotonic aging and memory in a frictional interface. *Phys. Rev. Lett.*, 120:224101 (2018).

[105] Kovacs A.J., Transition vitreuse dans les polymères amorphes, Etude phénoménologique. *Adv. Polym. Sci.*, 3:394 (1964).

[106] Sun Y., Salamon M.B., Garnier K., and Averback R.S., Memory effects in an interacting magnetic nanoparticle system, *Phys. Rev. Lett.*, 91:167206 (2003).

[107] Mvogo A. and Kofané T.C., Fractional formalism to DNA chain and impact of the fractional order on breather dynamics, *Chaos*, 26:123120 (2016).

[108] Mvogo A., Ben-Bolie G. H., and Kofané T.C., Fractional nonlinear dynamics of DNA breathing, *Commun. Nonlinear Sci. Numer. Simul.*, 48:258 (2017).

[109] Nigmatullin R.R. and Baleanu D., Is it possible to derive Newtonian equations of motion with memory?, *Int. J. Theor. Phys.*, 49:701 (2010).

[110] Guimfack B.A., Mbakob R.Y., Tabi C.B. and Kofané T. C., On stochastic response of fractional-order generalized birhythmic van der Pol oscillator subjected to delayed feedback displacement and Gaussian white noise excitation, *Chaos Solit. Fract.*, 157:111936 (2022).

[111] Okaly J.B., Ndzana F. II, Woulaché R.L., Tabi C.B., and Kofané T.C., Base pairs opening and bubble transport in damped DNA dynamics with transport memory effects, *Chaos*, 29:093103 (2019);

[112] Abramson G., Bishop A.R., and Kenkre V.M., Effects of transportmemory and nonlinear damping in a generalized Fisher's equation. *Phys. Rev. E*, 64:066615 (2001).

[113] Manne K.K., Hurd A.J., and Kenkre V.M., Nonlinear waves in reactiondi fusion systems: The effect of transport memory. *Phys. Rev. E*, 61:4177 (2000).

[114] Kenkre V.M., Memory formalism, nonlinear techniques, and kinetic equation approaches, *AIP Conf. Proc.*, 658:63 (2003).

[115] Kenkre V.M., Scott J.E., Pease E., and Hurd A. J., Nonlocal approach to the analysis of the stress distribution in granular systems. I. Theoretical framework, *Phys. Rev. E,*, 57:5841 (1998).

[116] Gradshteyn I.S. and Ryzhik I.M., Table of Integrals, Series, and Products, 7th ed. *Elsevier Academic Press*, p. 21 (2007).

[117] Kar S., Banik S.K., and Ray D. S., Exact solutions of Fisher and Burgers equations with fnite transport memory. *J. Phys. A Math. Gen.* 36:2771 (2003).

[118] Murray J.D., Mathematical Biology, *2nd corrected ed. Springer, Berlin,* (1993).

[119] Remoissenet M, Low-amplitude breather and envelope solitons in quasi-onedimensional physical models. *Phys. Rev. B*, 33:2386 (1986).

[120] Okaly J.B., Mvogo A., Woulaché R.L. , and Kofané T.C., Nonlinear dynamics of DNA systems with inhomogeneity effects. *Chin. J. Phys.*, 56:2613 (2018).

[121] Johnson B.D, Byerly L., and Pfugers arch., Ca^{2+} channel Ca^{2+}-dependent inactivation in a mammalian central neuron involves the cytoskeleton. *Eur J Physiol.*, 439:14 (1994).

[122] Kaech S., Parmar H., Roelandse M., Bornmann C., and Matus A., Cytoskeletal microdifferentiation: A mechanism for organizing morphological plasticity in dendrites. *PNAS*, 98:7086 (2001).

[123] Manning G.S., Limiting laws and counterion condensation in polyelectrolyte solutions I. Colligative properties. *J. Chem. Phys.*, 51:924 (1969).

[124] Huang G., Soliton excitations in one-dimensional diatomic lattices. *Phys. Rev. B*, 51:12347 (1995).

[125] Huang G. and Hu B., Asymmetric gap soliton modes in diatomic lattices with cubic and quartic nonlinearity. *Phys. Rev. B*, 57:5746 (1998).

[126] Peyrard M. and Bishop A.R., Statistical mechanics of a nonlinear model for DNA denaturation. *Phys. Rev. Lett.*, 62:2755 (1989).

[127] Dauxois T., Peyrard M. and Bishop A.R., Dynamics and thermodynamics of a nonlinear model for DNA denaturation. *Phys. Rev. E*, 47:684 (1993).

[128] Manakov S.V., On the theory of two-dimensional stationary self-focusing of electromagnetic waves. *Sov Phys JETP*, 38:248 (1974).

[129] Tsurui A., Wave Modulations in Anharmonic Lattices. *Prog. Theor. Phys.*, 48:1196 (1972).

[130] Kawahara T., The Derivative-Expansion Method and Nonlinear Dispersive Waves. *J. Phys. Soc. Jpn.*, 35:1537 (1973).

[131] Tabi C.B., Panguetna C.S, Motsumi T.G. and Kofané T.C., Modulational instability of coupled waves in electronegative plasmas. *Phys. Scr.*, 95:075211 (2020).

[132] Tabi C.B., Etémé A.S., Kofané T.C., Unstable cardiac multi-spiral waves in a FitzHugh-Nagumo soliton model under magnetic flow effect. *Nonlinear Dyn.*, 100:3799 (2020).

[133] Okaly J.B., Mvogo A., Tabi C.B., Ekobena F.H.P. and Kofané T.C., Base pair opening in a damped helicoidal Joyeux-Buyukdagli model of DNA in an external force field. *Phys Rev E.*, 102:062402 (2020).

[134] Kourakis I., Shukla P.K. and Morfill G., Modulational instability and localized excitations involving two nonlinearly coupled upper-hybrid waves in plasmas. *New J Phys.*, 7:153 (2005).

[135] Kengne E, and Abdourahman A., Ahmed L., Interacting signal packets in a lossless nonlinear transmission network with linear dispersion. *Chin J Phys.*, 63:271 (2020).

[136] Yemélé D. and Kofané T.C., Suppression of the fast and slow modulated waves mixing in the coupled nonlinear discrete LC transmission lines. *J Phys D.*, 39:4504 (2006).

[137] Kofané T.C., Zebaze M. and Zibi A., Non-linear wave modulation on a coupled transmission line. *J Phys D Appl Phys.*, 23:764 (1990).

[138] Otlaadisa P., Tabi C.B., Kofané T.C., Modulation instability in helicoidal spin-orbit coupled open Bose-Einstein condensates. *Phys Rev E.*, 103:052206 (2021).

[139] Tabi C.B., Veni S., and Kofané T.C., (2+1)-dimensional unstable matter waves in self-interacting pseudospin-1/2 BECs under combined Rashba and Dresselhaus spin-orbit couplings. *Phys Lett A.*, 442:128192 (2022).

[140] Ndebele K.K., Tabi C.B. and Kofané T.C., Modulational instability in nonlinear doped optical fiber induced by the cubic-quintic-septic complex Ginzburg-Landau equation with higher-order dispersions. *J Opt Soc Am B.*, 37:214 (2020).

[141] Djazet A., Tabi C.B., Fewo S.I. and Kofané T.C., Vector dissipative light bullets in optical laser beam. *Appl Phys B*: Lasers Optics., 126:74 (2020).

[142] Djazet A., Fewo S.I., Tabi C.B. and Kofané T.C., Dynamics of moving cavity solitons in two-level laser system from symmetric gaussian input: vectorial cubic-quintic complex Ginzburg-Landau equation. *Appl Phys B*: Lasers Optics., 127:151 (2021).

[143] Abemgnigni N.M., Tabi C.B. and Kofané T.C., Few-cycle optical pulses in negative index materials with dispersive permittivity and permeability . *J Opt Soc Am B.*, 37:331 (2020).

[144] Megne T.L., Tabi C.B. and Kofané T.C., Modulation instability in nonlinear metamaterials modeled by a cubic-quintic complex Ginzburg-Landau equation beyond the slowly varying envelope approximation. *Phys Rev E.*, 102:042207 (2020).

[145] Zanga D., Fewo S.I., Tabi C.B. and Kofané T.C., Generation of dissipative solitons in a doped optical fiber modeled by the higher-order dispersive cubic-quintic-septic complex Ginzburg-Landau equation. *Phys Rev A.*, 105:023502 (2022).

[146] Ndjomatchoua F.T., Tchawoua C., Kakmeni F.M.M., Le R.B.P. and Tonnang H.E.Z., Waves transmission and amplification in an electrical model of microtubules. *Chaos.*, 26:053111 (2016).

[147] Guemkam G.P., Tameh B.J.T. and Moukam K.F.M., Ionic wave propagation and collision in an excitable circuit model of microtubules. *Chaos.*, 28:023106 (2018).

[148] Tabi C.B., Etémé A.S. and Mohamadou A., Frequency mode excitations in two-dimensional Hindmarsh-Rose neural networks. *Physica A*, 474:186 (2017).

[149] Etémé A.S., Tabi C.B. and Mohamadou A., Synchronized nonlinear patterns in electrically coupled Hindmarsh-Rose neural networks with long-range diffusive interactions. *Chaos Solitons and Fractals* , 104:813 (2017).

[150] Ndebele K.K., Tabi C.B., Tiofack L.C.G., and Kofané T.C., Higher-order dispersion and nonlinear effects of optical fibers under septic self-steepening and self-frequency shift. *Phys Rev E.*, 104:044208 (2021).

[151] Akhmediev N., Soto-Crespo J.M. and Town G., Pulsating solitons, chaotic solitons, period doubling, and pulse coexistence in mode-locked lasers: Complex Ginzburg-Landau equation approach. *Phys Rev E.*, 63:056602 (2001).

[152] Soto-Crespo J.M. and Akhmediev N., Soliton as Strange Attractor: Nonlinear Synchronization and Chaos. *Phys Rev Lett.*, 95:024101 (2005).

[153] Weber A., Kramer L., Aranson I.S. and Aranson L., Stability limits of traveling waves and the transition to spatiotemporal chaos in the complex Ginzburg-Landau equation. *Phys D.*, 61:279 (1992).

[154] Tabi C.B., Etémé A.S., Mohamadou A. and Kofané T.C., Mohamadou A. and Kofané T.C., Oscillationg two-dimensional C_a^{2+} wawes in cell networks with directional paracrine signaling. *Waves Rand Compl Media.*, 31:1028 (2019).

[155] Tankou E., Tabi C.B., Kofané T.C., Soliton-mediated ionic pulses and coupled ionic excitations in a dissipative electrical network model of microtubules. *Chaos, Solitons and Fractals*, 162:112446 (2022).

[156] Legoya P., Etémé A. S., Tabi C. B., Mohamadou A., and Kofané T. C., Frequency modes of unstable spiral waves in two-dimensional Rosenzweig-MacArthur ecological networks. *Chaos Solit. Fract.*, 146:112599 (2022).

[157] Bansi Kamdem C. D., Ndjawa Yomi P. A., Tabi C. B., and Mohamadou A., Modulated blood waves in the coupled complex Ginzburg-Landau equations of Jeffrey fluids in arteries. *Eur. Phys. J. Plus.,* 138:176 (2023).

[158] Edouma Biloa B. P., Tabi C. B., Ekobena Fouda H. P., and Kofané T. C., Nonlinear dissipative wave trains in a system of self-propelled particles. *Phys. Scr.*, 98:115230 (2023).

[159] Bansi C.D., Tabi C.B. and Mohamadou A., Dissipative Mayer's waves in fluid-filled viscoelastic tubes. *Chaos, Solitons and Fractals*, 109:170 (2018).

[160] Tabi C.B., Tankou E. and Mohamadou A., Nonlinear coupled mode excitations in microtubules. *Chaos Solit Fract.*, 95:187 (2017).

[161] Essimbi B.Z. and Kofané T.C., Physica Scripta Coupling of stationary nonlinear modes in an electrical lattice. *Phys. Scr.*, 76:480 (2007).

[162] Benjamin T.B. and Feir J.E., The disintegration of wave trains on deep water Part 1. Theory. *J. Fluid. Mech.*, 27:417 (1967).

[163] Bespalov V.I. and Talanov V.I., On thread-like structure of light beams in a nonlinear liquid. *Pisma JETP*, 3:471 (1966).

[164] Kourakis I. and Shukla P.K., Modulated wavepackets associated with longitudinal dust grain oscillations in a dusty plasma crystal. *Phys. Plasmas*, 11:1384 (2004).

[165] Agrawal G.P., Nonlinear Fiber Optics, Optics and Photonics. *4th ed., Academic Press, New York*, (2009).

[166] Ndzana F. II, Mohamadou A., and Kofané T.C., Discrete Lange-Newell criterion for dissipative systems. *Phys. Rev. E*, 79:056611 (2009).

[167] Tabi C.B., Mohamadou A. and Kofané T.C., Discrete instability in the DNA double helix. *Chaos*, 19:043101 (2009).

[168] Ondoua R.Y., Tabi C.B., Ekobena F.H.P., Mohamadou A. and and Kofané T.C., Discrete energy transport in the perturbed Ablowitz-Ladik equation for Davydov model of α-helix proteins. *Eur. Phys. J. B*, 85:318 (2012).

[169] Mimshe F.J.C., Tabi C.B., Edongue H., Ekobena F.H.P. and Kofané T.C., Wave patterns in α-helix proteins with interspine coupling. *Phys. Scr.*, 87:025801 (2013).

[170] Mvogo A., Ben-Bolie G.H. and and Kofané T.C., Discrete energy transport in collagen molecules. *Chin. Phys. B*, 23:098701 (2014).

[171] Ablowitz M. and Segur H., Solitons and the Inverse Scattering Transform. *Philadelphia: SIAM*, (1985).

[172] Pickering A., A new truncation in Painleve analysis. *J. Phys. A: Math. Gen.*, 26:4395 (1993).

[173] Tabi C.B., Mohamadou A. and Kofané T.C., Soliton-like excitation in a nonlinear model of DNA dynamics with viscosity. *Math. Biosci. Eng.*, 5:205 (2008).

[174] Yomba E. and and Kofané T.C., Solutions of the Lowest Order Complex Ginzburg-Landau Equation. *J. Phys. Soc. Jpn*, 69:1027 (2000).

[175] Wamba E., Matter waves of Bose-Einstein condensates with two-and three-body interaction, *PhD thesis, University of Yaounde I*, (2013)

[176] Havelka D., M Cifra M. and Vrbra J., What is more important for radiated power from cellssize or geometric? *J.Phys:Conf. Ser. Lett.*, 102:012014 (2011).

[177] Wahlquist H.D. and Estabrook F.B., Bäcklund Transformation for Solutions of the Korteweg-de Vries Equation. *Phys. Lett. A*, 31:1386 (1973).

[178] Remoissenet M., Waves Called Solitons *(Berlin, Heidelberg: Springer-Verlag)*, (1989).

[179] Scott A., Nonlinear Science Emergence and Dynamics of Coherent Structures, *(Moscow: Fizmatlit in Russian)*, (2007).

[180] Zdravković S. and Tabi C.B., Two Possible Approaches in Peyrard-Bishop-Dauxois Model of DNA Dynamics. *J. Comput. Theor. Nanosci.*, 7:1 (2010).

[181] Hirota R., Bullough R.K. and Candrey P.J., Direct Methods in Soliton Theory, in Solitons. *(Tapies in Current Physics 17, Springer Verlag)*, (1980).

[182] Nozaki K. and Bekki N., Exact Solutions of the Generalized Ginzburg-Landau Equation. *J. Phys. Soc. Jpn.*, 53:1581 (1984).

[183] Tat-Leung Yee, Dynamics of Coherent Structures in the Coupled Complex Ginzburg-Landau Equations. *J. Math. Stat.*, 8:413 (2012).

[184] Newell A.C. and Whitehead J.A., Finite bandwidth, finite amplitude convection. *J. Fluid Mech.*, 38:279 (1969).

[185] Ballagh R.J., Partial Differential Equation Algorithm: Conceptual *unpublished personal papers*, (1995).

[186] Caradoc-Davies B.M., Ballagh R.J. and Burnett K., Coherent Dynamics of Vortex Formation in Trapped Bose-Einstein Condensates. *Phys. Rev. Lett.*, 83:895 (1999).

[187] Ballagh R.J. Computational methods for nonlinear partial differential equations. *Lectures given at the Institute for Theoretical Physics, Innsbruck University*, 176 (2000).

[188] Caradoc-Davies B.M., Ballagh R.J. and Blakies P. B., Three-dimensional vortex dynamics in Bose-Einstein condensates *Phys. Rev. A*, 62:011602 (2000).

[189] Agrawal G., Nonlinear Fiber Optics,*3rd edition, Academic Press, San Diego*, (2001).

[190] Tabi C.B., Mohamadou A. and Kofané T.C., Modulational instability of charge transport in the Peyrard-Bishop-Holstein model. *J Phys Condens Matter*, 21:335101 (2009).

[191] Englander S.W., Kallenbach N.R., Heeger A.J., Krumhansl J.A. and Litwin S., Nature of the open state in long polynucleotide double helices: possibility of soliton excitations. *Proc. Natl. Acad. Sci. U.S.A.*, 77:7222 (1980).

[192] Toko D., Mohamadou A., Tabi C.B. and Kofané T.C., Coherent modes and parameter selection in DNA models with finite stacking enthalpy. *J. Comput. Theor. Nanosci.*, 9:97 (2012).

[193] Tabi C.B., Mohamadou A. and Kofané T.C., Wave propagation of nonlinear modes and formation of bubble in a two-component helicoidal lattice. *Eur Phys J D*, 50:307 (2008).

[194] Tabi C.B. , Ekobena H.P.F., and Kofané T.C., Protein-DNA Interaction: Effect of Helicity on Bubble Size. *J. Comput. Theor. Nanosci.*, 8:2220 (2011).

[195] Brown J.A. and Tuszyński J.A., Dipole interactions in axonal microtubules as a mechanism of signal propagation. *Phys. Rev. E.*, 56:5834 (1997).

[196] Gundersen G.G. and Cook T.A., Microtubules and signal transduction. *Curr Opin Cell Biol*, 11:81 (1999).

[197] Domgno W.K. and Mohamadou A., Management of invasive cells in soft biological tissues through modulated nonlinear excitations: Long-range effects. *Com. Non. Scie. Numer. Simul.*, 110:106360 (2022).

[198] Tankou A.S.T., Takembo C.N., Ben-Bolie H.G. and Ateba O.P., Localized nonlinear excitations in diffusive memristor-based neuronal networks. *PLoS One*, 14:0214989 (2019).

[199] Tabi C.B., Etémé A.S., Mohamadou A. and Kofané T.C., Unstable discrete modes in Hindmarsh-Rose neural networks under magnetic flow effect. *Chaos Solit Fract.*, 123:116 (2019).

[200] Takembo C.N., Mvogo A., Ekobena H.P.F. and Kofané T.C., Localized modulated wave solution of diffusive FitzHugh-Nagumo cardiac networks under magnetic flow effect. *Nonlinear Dynam.*, 95:1079 (2019).

[201] Deneke V.E. and Talia S. Di, Chemical waves in cell and developmental biology. *J. Cell. Biol.*, 217:1193 (2018).

[202] Kuwayama H. and Ishida H., Biological soliton in multicellular movement. *Sci. Rep.*, 3:2272 (2013).

[203] Bhakta J.C., A pair of coupled equations for high frequency Langmuir and dispersive ion-acoustic waves with collisional damping. *Plasma Phys. Control. Fusion*, 29:245 (1987).

[204] Hocking L.M. and Stewartson K., *Proc. R. Soc. London, Ser. A*, 326:289 (1972);

[205] Pereira N.R. and Stenflo L., Nonlinear Schrödinger equation including growth and damping. *Phys. Fluids*, 20:1733 (1977).

[206] Caplow M. and Shanks J., Evidence that a single monolayer tubulin-GTP cap is both necessary and sufficient to stabilize microtubules. *Molec Biol Cell*, 7:663 (1996).

[207] Sahu S., Ghosh S., Hirata K., Fujita D. and Bandyopadhyay A., Multi-level memory-switching properties of a single brain microtubule. *Appl. Phys. Lett.*, 102:123701 (2013).

[208] Gabor D., Theory of communication. Part 1: The analysis of information. *J Inst Electr Eng.*, 93:429 (1946).

[209] Boashash B., Estimating and interpreting the instantaneous frequency of a signal. I. Fundamentals. *Proc IEEE.*, 80:520 (1992).

[210] Zakeri G.A. and Yomba E., Dissipative Solitons in a Generalized Coupled Cubic-Quintic Ginzburg-Landau Equations. *J Phys Jpn.*, 82:084002 (2013).

[211] Yang D-Yu, Tian B., Zhang C-R., Chen Su-Su and Wei C-C., Lax pair, conservation laws, Darboux transformation and localized waves of a variable-coefficient coupled Hirota system in an inhomogeneous optical fiber. *Chaos Solit Fract.*, 150:110487 (2021).

[212] Berman J.I., Liu S., Bloy L., Blaskey L., Roberts T.P. and Edgar J.C., Alpha-to-gamma phase-amplitude coupling methods and application to autism spectrum disorder. *Brain connectivity*, 5:80 (2012).

[213] Nfor N.O., Ghomsi P.G. and Moukam K.F.M., Dynamics of coupled mode solitons in bursting neural networks. *Phys Rev E.*, 97:022214 (2018).

[214] Etémé A.S., Tabi C.B. and Mohamadou A., Firing and synchronization modes in neural network under magnetic stimulation. *Commun Nonl Sci Numer Simul.*, 72:432 (2019).

[215] Odde D., Diffusion inside microtubules. *Eur Biophys J.*, 27:514 (1998).

[216] Shen C. and Guo W., Ion permeability of a microtubule in neuron environment. *J Phys Chem Lett.*, 9:2009 (2018).

[217] Patolsky F., Weizmann Y. and Willner I., Actin-based metallic nanowires as bio-nanotransporters. *Nat Mater.*, 3:692 (2004).

[218] Hunley C., Uribe D. and Marucho M., A multi-scale approach to describe electrical impulses propagating along actin filaments in both intracellular and in vitro conditions. *RSC Adv.*, 8:12017 (2018).

[219] Rostovtseva T.K. and Bezrukov S.M., VDAC inhibition by tubulin and its physiological implications. *Biochim Biophys Acta (BBA)-Biomembranes*, 1818:1526 (2012).

[220] Putnam A.J., Schultz K. and Mooney D.J., Control of microtubule assembly by extracellular matrix and externally applied strain. *Am J Physiol Cell Physiol.*, 280:556 (2001).

[221] Portet S., Tuszyński J.A., Hogue C.W.V. and Dixon J.M., Elastic vibrations in seamless microtubules. *Eur Biophys J*, 34:912 (2005).

[222] Tabapsi K.R., Belobo B.D., Bansi K.C.D., Dang K.A., Tabi C.B. and Kofané T.C., Nonlinear dynamics effect of viscosity of cytosol into the microtubules and exact solutions. *Commun. Nonlinear. Sci. Numer. Simult.*, 143:108615 (2025).

List of Publications

1- Tabi C.B., **Tankou E.**, and Mohamadou A., **Nonlinear coupled mode excitations in microtubules**. *Chaos, Solitons and Fractals*, 95:187 (2017).

2- **Tankou E.**, Tabi C.B., and Kofané T.C., **Soliton-mediated ionic pulses and coupled ionic excitations in a dissipative electrical network model of microtubules**. *Chaos, Solitons and Fractals*, 162:112446 (2022)

3- **Tankou E.**, Tabi C.B., Mohamadou A., and Kofané T.C., **Transport memory effects on coupled nonlinear waves in microtubule dynamics**. *Chaos, Solitons and Fractals*, 181:114717 (2024).

Chaos, Solitons and Fractals 95 (2017) 187–194

Contents lists available at ScienceDirect

Chaos, Solitons and Fractals

Nonlinear Science, and Nonequilibrium and Complex Phenomena

journal homepage: www.elsevier.com/locate/chaos

Nonlinear coupled mode excitations in microtubules

Conrad Bertrand Tabi[a,b,c,*], Eric Tankou[a], Alidou Mohamadou[d]

[a] Laboratory of Biophysics, Department of Physics, Faculty of Science, University of Yaoundé I, P.O. Box 812, Yaoundé, Cameroon
[b] Botswana International University of Science and Technology, P/Bag 16 Palapye, Botswana
[c] The African Institute for Mathematical Sciences, 6-8 Melrose Rd, Muizenberg 7945, South Africa
[d] Department of Physics, Faculty of Science, University of Maroua, P.O. Box 814, Maroua, Cameroon

ARTICLE INFO

Article history:
Received 4 March 2016
Accepted 16 December 2016

Keywords:
Microtubules
Solitons
Energy transport

ABSTRACT

The dynamics of coupled nonlinear waves is addressed in the framework of the angular model of microtubules. The semi-discrete approximation is used to write the dynamics of the lower and upper cutoff modes in the form of coupled nonlinear Schrödinger equations. The linear stability analysis of modulational instability is used to confirm the existence of soliton solutions, and the growth-rate of instability is shown to be importantly influenced by the dipolar energy. Single mode solutions are found as breathers and resonant kink, while the coupled mode introduces a kink envelope solution, whose characteristics are discussed with respect to the dipolar energy. The found solution is shown to be robust, which is important for energy transport in the Polymerization/depolymerization mechanism of protofilaments.

1. Introduction

Microtubules (MTs) are found in every eukaryotic cell, where they play a broad range of roles such as maintaining and protecting the cell structure, and are even involved in key biological processes such as cell division. Besides, evidences that they serve as network for motor proteins are now well established [1]. While many experimental methods progressively reveal the structures of MTs, they all agree that a MT is made of protofilaments (PFs), arranged on a hollow cylinder in elementary units called dimers, whose constituent parts are α and β tubulins, denoting positively and negatively charged sides, respectively.

Wave propagation along MTs is of fundamental concern in many cellular functions and relies on the hydrolysis of guanosine triphosphate (GTP), which releases energy. According to recent investigations, the idea that such energy travels along MTs as a solitary wave has become effective [2]. Solitons arise in continuum as well as in discrete nonlinear systems as the results of the concomitant effects of dispersion and nonlinearity [3–5]. They are classified in two categories known as topological and non-topological and have been used to explain a broad range of phenomena in biological settings such as DNA [5,6], hemodynamics [7], energy transport in proteins [8], just to name a few. In microtubules, Chou et al. [9] investigated kinks and pulses and showed that their propagation is facilitated by the coupling between the elastic states of tubulin dimers. Recent contributions, to substantially support the proposal of Satarić et al. [10], have further proposed kink solitons to be responsible for the transfer of the chemical energy brought by GTP hydrolysis [11,12]. A more recent, but different, model introduces a single angular displacement per dimer in order to describe conformational distortion of discretely coupled dimers in radial direction [13]. As this model has been shown to support kink soliton propagation, new directions have led to the conclusion that localized modulated waves could be of importance in MT nonlinear dynamics [14]. On this background, it is clear that the problem of finding proper solutions to describe microtubules vibrations remains open. On the other hand, these different classes of waves could coexist just like in many other biological systems. In DNA for example, different classes of waves have been detected, each corresponding to a specific biological process. Tabi et al. [3] have, in that direction, shown that breather solitons could be used to explain the initiation of transcription, whilst pulse solitons are suitable for the description of the open states observed during the reading of the genetic code by the messenger-RNA. In blood flow, there are pulses that describe normal blood pressure and Mayer's waves that refer to the arterial pressure oscillations [7], slower than respiration, that exhibit the strongest, significant coherence with oscillations of sympathetic nervous activity. In this work, we intend to show that coupled waves can also coexist in microtubules. We adopt the method of Ref. [15] and we argue that except the breather and kink solitons already discussed in the literature, new types of solitons can come out of the coupled mode with pertinent biological implications. In Section 2, we present the model and we discuss the coexistence of the lower and upper cut-off mode

* Corresponding author at: Laboratory of Biophysics, Department of Physics, Faculty of Science, University of Yaoundé I, P.O. Box 812, Yaoundé, Cameroon.
E-mail address: conrad@aims.ac.za (C.B. Tabi).

http://dx.doi.org/10.1016/j.chaos.2016.12.019
0960-0779/

excitations. We use the multiple-scale expansion to show that the system can be described by a set of coupled nonlinear Schrödinger (CNLS) equations. In section 3, the modulational instability (MI) of a plane wave is discussed and we bring out the effect of the dipolar potential energy on the growth rate of instability. In Section 4, we propose solutions for the single and coupled modes and still, we discuss the effect of the dipolar potential energy. Section 5 is devoted to some concluding remarks.

2. Model and amplitude equations

2.1. Model

The Hamiltonian considered in Ref. [14] describes the dynamics of a single PF, since interactions between dimers from the same PFs are stronger than the ones between dimers form different PFs. However, interactions between dimers form different PFs are introduced through an electric field. On this background, only one degree of freedom is considered per dimer, namely the angular displacement ψ_n of the dimer at position n. The resulting Hamiltonian therefore contains a kinetic energy $T = \frac{I}{2}\dot{\varphi}_n^2$, the stacking potential, $V = \frac{k}{2}(\varphi_{n+1} - \varphi_n)^2$, between adjacent dimers, and the dipolar potential energy $U = -\vec{p}.\vec{E} = -pE\cos\varphi_n$. The dot means a first derivative with respect to time and $I = \frac{ml^2}{12}$ is a moment of inertia of the single dimer of mass $m = 1.8 \times 10^{-22}$ kg [16], $k =$ 0.1 eV [14] is the inter-dimer bonding interaction within the same PF, originating from the link between the corresponding protruding loops [17]. $p = 1.13 \times 10^{-27}$ [18] Cm is an electric dipole moment, and E is the intrinsic electric field strength.

The equation for the nth dimer can be derived from the above described Hamiltonian in the form

$$\ddot{\varphi}_n - C(\varphi_{n+1} + \varphi_{n-1} - 2\varphi_n) + \omega_0^2 \sin\varphi_n = 0 \tag{1}$$

or, after a series expansion of the sine term,

$$\ddot{\varphi}_n - C(\varphi_{n+1} + \varphi_{n-1} - 2\varphi_n) + \omega_0^2\left(\varphi_n - \alpha\varphi_n^3\right) = 0, \tag{2}$$

with $C = \frac{k}{I}$, $\omega_0^2 = \frac{pE}{I}$ and $\alpha = -\frac{1}{6}$. The dispersion relation for the linear vibrations of PFs can be found by considering only linear terms in Eq. (2). This is given by

$$\omega^2 = \omega_0^2 + 4C\sin^2\left(\frac{ql}{2}\right), \tag{3}$$

with q being the wavelength and $l = 8$ nm the tubulin dimers spacing. $\omega_{\min} = \omega_0$ is the lower cut-off frequency, while $\omega_{\max} = \sqrt{\omega_0^2 + 4C}$ is the upper cut-off frequency. The corresponding dispersion curve is depicted in Fig. 1, where ω_0 and $\omega_{\max}$ are clearly indicated. However, ω is found to be very sensitive to the variations of pE. It is in fact evident that ω_0 and $\omega_{\max}$ are increasing functions of pE, which shows the importance of the dipolar potential in the dynamics of MTs. We then assume $\omega_0^2 \gg 4C$ because of the discreteness of the PF lattice. Furthermore, it has been argued that the viscous damping brought by the cytoplasm viscosity is minimized by the ion density around the MT [19], that is the reason why damping effects will not be considered in this work.

2.2. Multiple scale expansion and amplitude equations

As demonstrated in Ref. [15], each of the cutoff modes can support soliton solutions, but their type and characteristics depends on the system that is studied. The richest behaviors usually come form the coupling between ω_0 and $\omega_{\max}$ modes, as pointed out by Tabi et al. [15] within the Peyrard-Bishop model of DNA. For that to be possible, they derived a set of coupled NLS equations. Nevertheless, The equation from our Hamiltonian can be solved exactly

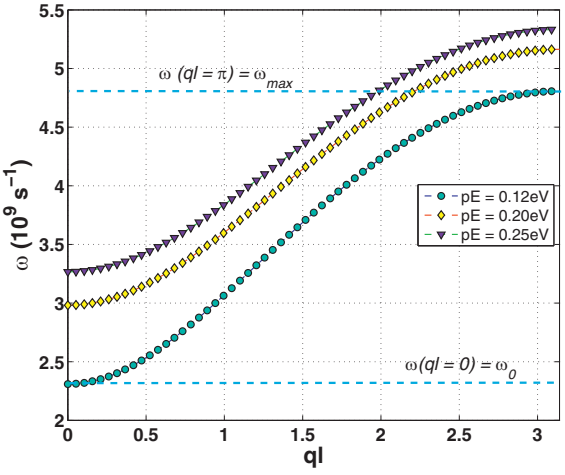

Fig. 1. The panel shows the dispersion relation (3) under the influence of the dipolar energy pE. While the upper and lower cutoff frequencies are indicated, they also increase with pE, with the parameter values $m = 1.8 \times 10^{-22}$ kg and $k = 0.1$ eV.

as it is the celebrated sine-Gordon equation, but the context of the present work calls for an expansion of the sine term for a better use of the quasi-discrete approximation. This asymptotic expansion has the merit to combine dispersive and strong nonlinear effects. It implies a trial solution of the form [20]

$$\varphi_n = \epsilon\varphi_{n,n}^{(1)} + \epsilon^2\varphi_{n,n}^{(2)} + \epsilon^3\varphi_{n,n}^{(3)} + \cdots = \sum_{j=1}^{\infty}\epsilon^j\varphi_{n,n}^{(j)}, \tag{4}$$

with $\varphi_{n,m}^{(j)} = \varphi^{(j)}(\xi_n, T, \theta_{0,m}(t), \theta_{max,m}(t))$, where the subscripts n and m represent ξ_n and $\theta_{0,\,m}(t)$ (or $\theta_{max,\,m}(t)$), respectively. ϵ is a small parameter denoting the relative amplitude of the excitation; $\xi_n = \epsilon(nl - \mu t)$ and $T = \epsilon^2 t$ are the multiple scale slow variables. μ is a small variable that will be determined by a solvability condition. This implies the use of the derivative $\frac{d}{dt} = \frac{\partial}{\partial t} - \epsilon\mu\frac{\partial}{\partial\xi_n} + \epsilon^2\frac{\partial}{\partial T}$. The fast variables $\theta_{0,\,m}(t)$ and $\theta_{max,\,m}(t)$ represent the phases of two carrier waves. For the discreteness term, the expansion [15,20]

$$\begin{aligned}\varphi_{n\pm1} = {} & \epsilon\varphi_{nn\pm1}^{(1)} + \varepsilon^2\left(\varphi_{nn\pm1}^{(2)} \pm l\frac{\partial\varphi_{nn\pm1}^{(1)}}{\partial\xi_n}\right) \\ & + \epsilon^3\left(\varphi_{nn\pm1}^{(3)} + \frac{l^2}{2}\frac{\partial^2\varphi_{nn\pm1}^{(1)}}{\partial\xi_n^2} \pm l\frac{\partial\varphi_{nn\pm1}^{(2)}}{\partial\xi_n}\right) + \ldots.\end{aligned} \tag{5}$$

can be used. Substituting Eq. (4) into Eq. (5) and comparing the different powers of ϵ , we obtain a hierarchy of equations about $\varphi_{n,n}^{(j)}$ $(j = 1, 2, 3, \ldots)$. The whole problem, through this procedure, reduces to the set of equations

$$\left(\frac{d^2}{dt^2} + \omega_1^2\right)\varphi_{n,n}^{(j)} - C\left(\varphi_{n+1}^{(j)} - \varphi_{n-1}^{(j)}\right) = M_{n,n}^{(j)}, \quad j = 1, 2, 3, \ldots, \tag{6}$$

with $\omega_1^2 = \omega_0^2 + 2C$, and $M_{n,n}^{(j)}$ being given by

$$\begin{aligned}M_{n,n}^{(1)} &= 0, \\ M_{n,n}^{(2)} &= 2\mu\frac{\partial^2\varphi_{n,n}^{(1)}}{\partial t\partial\xi_n} + Cl\frac{\partial}{\partial\xi_n}\left(\varphi_{n+1}^{(1)} - \varphi_{n-1}^{(1)}\right), \\ M_{n,n}^{(3)} &= 2\mu\frac{\partial^2\varphi_{n,n}^{(2)}}{\partial t\partial\xi_n} - \mu^2\frac{\partial^2\varphi_{n,n}^{(1)}}{\partial\xi_n^2} - 2\frac{\partial^2\varphi_{n,n}^{(1)}}{\partial t\partial T} + Cl\frac{\partial}{\partial\xi_n}\left(\varphi_{n+1}^{(2)} - \varphi_{n-1}^{(2)}\right) \\ &\quad + \frac{Cl^2}{2}\frac{\partial^2}{\partial\xi_n^2}\left(\varphi_{n+1}^{(1)} + \varphi_{n-1}^{(1)}\right) - \omega_0^2\alpha\left(\varphi_{n,n}^{(1)}\right)^3, \\ &\ldots\end{aligned} \tag{7}$$

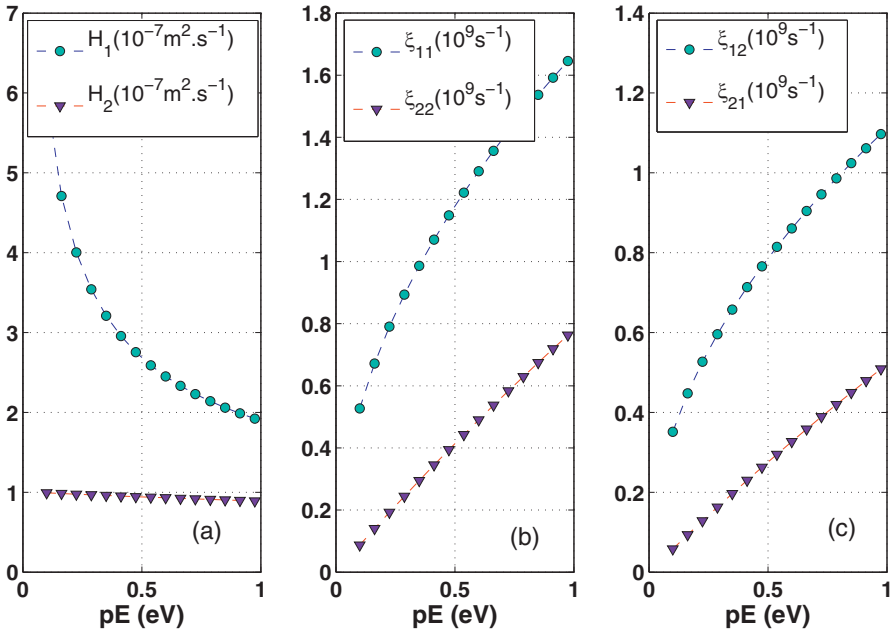

Fig. 2. The panels show the parameters for the set of coupled NLSE versus pE. Panel (a) clearly shows how H_1 and H_2 are decreasing functions of pE, while panels (b) and (c) show that ξ_{jj} and ξ_{ij} are increasing functions of pE.

In order to describe the possibility of wave mixing during the radial dislocations in MTs, Eq. (6) is solved step by step at different orders, where for $j = 1$, the solution of the system can be assumed to be of the form

$$\varphi_{n,n}^{(1)} = Q_1(T, \xi_n)e^{i\theta_{0,n}(t)} + Q_2(T, \xi_n)e^{i\theta_{max,n}(t)} + c.c., \tag{8}$$

where c.c. stands for complex conjugates. Q_1 and Q_2 are two undetermined envelope functions. For both cut-off modes, we have $\theta_{0,n}(t) = \omega(q = 0)t = -\omega_0 t$ and $\theta_{max,n}(t) = \pi n - \omega(q = \frac{\pi}{l})t = \pi n - \omega_{\max} t$, and $\varphi_{n,n}^{(1)}$ becomes

$$\varphi_{n,n}^{(1)} = Q_1(T, \xi_n)e^{-i\omega_0 t} + (-1)^n Q_2(T, \xi_n)e^{-i\omega_{max} t} + c.c. \tag{9}$$

By letting $j = 2$, the solvability condition imposes $\mu = 0$ and $\xi_n = \epsilon nl$, and we have the second-order approximation equation $(\frac{\partial^2}{\partial t^2} + \omega_1^2)\varphi_{n,n}^{(2)} - C(\varphi_{n+1}^{(2)} - \varphi_{n-1}^{(2)}) = 0$, which admits plane wave solutions that can be written in the general form $\varphi_{n,n}^{(2)} = B_1 e^{-i\omega_0 t} + B_2 e^{-i\omega_{\max} t} + c.c.$, with B_1 and B_2 being two constant amplitudes. Besides, we can assume $B_1 = B_2 = 0$, which leads to $\varphi_{n,n}^{(2)} = 0$, a solution with no impact on the nonlinear and dispersive behaviors of the model under study. When $j = 3$, the solvability conditions leads to the following set of equations in Q_1 and Q_2

$$i\frac{\partial Q_1}{\partial T} + H_1\frac{\partial^2 Q_1}{\partial \xi_n^2} + (\zeta_{11}|Q_1|^2 + \zeta_{12}|Q_2|^2)Q_1 = 0 \tag{10}$$

$$i\frac{\partial Q_2}{\partial T} - H_2\frac{\partial^2 Q_2}{\partial \xi_n^2} + (\zeta_{21}|Q_1|^2 + \zeta_{22}|Q_2|^2)Q_2 = 0, \tag{11}$$

where $H_1 = \frac{Cl^2}{2\omega_0}$, $H_2 = \frac{Cl^2}{2\omega_{\max}}$, $\zeta_{11} = -\frac{3\alpha\omega_0}{2}$, $\zeta_{12} = -\alpha\omega_0$, $\zeta_{21} = -\frac{\alpha\omega_0^2}{\omega_{\max}}$, $\zeta_{22} = -\frac{3\alpha\omega_0^2}{2\omega_{\max}}$. The above set of equations can be rewritten using the original variables by letting $(\psi_1, \psi_2) = \epsilon(Q_1, Q_1)$, along with the change of variables $\xi_n = \epsilon nl$ and $T = \varepsilon^2 t$, so that

$$i\frac{\partial \psi_1}{\partial t} + H_1\frac{\partial^2 \psi_1}{\partial x^2} + (\zeta_{11}|\psi_1|^2 + \zeta_{12}|\psi_2|^2)\psi_1 = 0 \tag{12}$$

$$i\frac{\partial \psi_2}{\partial t} - H_2\frac{\partial^2 \psi_2}{\partial x^2} + (\zeta_{21}|\psi_1|^2 + \zeta_{22}|\psi_2|^2)\psi_2 = 0, \tag{13}$$

where $x = nl$. The above set of CNLS equations is coupled nonlinearly through the coefficients ζ_{12} and ζ_{21}. When these coefficients are equal and $H_2 = -H_1$, the Manakov's system is recovered [21]. Otherwise, these equations will be decoupled if $\zeta_{12} = \zeta_{21} = 0$, leading to individual NLS equations. The solutions for Eqs. (12) and (13) depend on the sign of their coefficients, plotted in Fig. 2. Obviously, H_1 and H_2 are positive dispersion terms with respect to pE (Fig. 2(a)). The§same is observed for ζ_{11} and ζ_{22} (Fig. 2(b)) and for ζ_{12} and ζ_{21} (Fig. 2(c)). However, H_1 and H_2 decrease with increasing pE, while ζ_{ii} and $\zeta_{ij}(j \neq i)$ are increasing functions of the dipolar energy pE.

3. MI of coupled waves in microtubules.

One of the direct mechanisms solitonic structures emerge in nonlinear systems is through MI. In order to investigate the possibility of wave mixing in the set of Eqs. (12) and (13), we assume the plane waves $\psi_j = \psi_{j0}e^{i\omega_j t}$ as solutions, where the real constants $\omega_j (j = 1, 2)$, and the complex constant amplitudes ψ_{j0} are characterized by the dispersion relations

$$\omega_j = \zeta_{jj}|\psi_{j0}|^2 + \zeta_{jk}|\psi_{k0}|^2, j, k = 1, 2 \quad \text{with} \quad k \neq j. \tag{14}$$

The stability of these plane wave solutions can be investigated by slightly perturbing their amplitudes as $\psi = (\psi_{j0} + \epsilon\psi_j)e^{i\omega_j t}$ [22]. After some linearization around the unperturbed solutions and using condition (14), we write $\psi_j = u_j + iv_j$, $\psi_{j0} = a_j + ib_j$, which leads to the following real and imaginary parts for Eqs. (12) and (13)

$$H_1\frac{\partial^2 u_1}{\partial x^2} - \frac{\partial v_1}{\partial t} + \zeta_{11}\left(2a_1^2u_1 + 2a_1b_1v_1\right) + \zeta_{12}(2a_1a_2u_2 + 2a_1b_2v_2) = 0 \tag{15}$$

$$H_1\frac{\partial^2 v_1}{\partial x^2} + \frac{\partial u_1}{\partial t} + \zeta_{11}\left(2a_1b_1u_1 + 2b_1^2v_1\right) + \zeta_{12}(2a_2b_1u_2 + 2b_1b_2v_2) = 0 \tag{16}$$

$$H_2\frac{\partial^2 u_2}{\partial x^2} - \frac{\partial v_2}{\partial t} + \zeta_{21}(2a_1a_2u_1 + 2a_2b_1v_1) + \zeta_{22}\left(2a_2^2u_2 + 2a_2b_2v_2\right) = 0 \tag{17}$$

$$H_2\frac{\partial^2 v_2}{\partial x^2}+\frac{\partial u_2}{\partial t}+\zeta_{21}(2b_1b_2v_1+2a_1b_2u_1)$$
$$+\zeta_{22}\left(2a_2b_2u_2+2b_2^2v_2\right)=0. \quad (18)$$

Furthermore, from the previous assumption, inserting $u_j=u_{j0}e^{i(\lambda x-\Omega t)}+c.c.$ and $v_j=v_{j0}e^{i(\lambda x-\Omega t)}+c.c.$ into Eqs. (15)–(18), where λ and Ω are the perturbation wavenumber and the frequency, respectively, which are much smaller than those of the carrier wave, and c.c. stands for the complex conjugate, we obtain an homogeneous system for u_{j0} and v_{j0} as follows

$$\begin{pmatrix} -i\Omega+2\zeta_{11}a_1b_1 & -H_1\lambda^2+2\zeta_{11}b_1^2 & 2\zeta_{12}a_2b_1 & 2\zeta_{12}b_1b_2 \\ -H_1\lambda^2+2\zeta_{11}a_1^2 & i\Omega+2\zeta_{11}a_1b_1 & 2\zeta_{12}a_1a_2 & 2\zeta_{12}a_1b_2 \\ 2\zeta_{21}a_1b_2 & 2\zeta_{21}b_2b_1 & -i\Omega+2\zeta_{22}a_2b_2 & -H_2\lambda^2+2\zeta_{22}b_2^2 \\ 2\zeta_{21}a_1a_2 & 2\zeta_{21}b_1a_2 & -H_2\lambda^2+2\zeta_{22}a_2^2 & i\Omega+2\zeta_{22}a_2b_2 \end{pmatrix}$$
$$\times\begin{pmatrix} u_{10} \\ v_{10} \\ u_{20} \\ v_{20} \end{pmatrix}=\begin{pmatrix} 0 \\ 0 \\ 0 \\ 0 \end{pmatrix} \quad (19)$$

The condition for the above system to have nontrivial solutions is obtained by setting its determinant to zero, which leads to the nonlinear dispersion relation

$$\Omega^4-R\Omega^2+S=0, \quad (20)$$

where

$$R=\left(H_1^2+H_2^2\right)\lambda^4-2\left(H_1\zeta_{11}|\psi_{10}|^2+H_2\zeta_{22}|\psi_{20}|^2\right)\lambda^2$$
$$S=H_1^2H_2^2\lambda^8-2H_1H_2\left(H_2\zeta_{11}|\psi_{10}|^2+H_1\zeta_{22}|\psi_{20}|^2\right)\lambda^6$$
$$+4H_1H_2|\psi_{10}|^2|\psi_{20}|^2(\zeta_{11}\zeta_{22}-\zeta_{12}\zeta_{21})\lambda^4$$

• For the system to be stable under modulation, the conditions $R>0$, $S>0$ and $\Delta=R^2-4S>0$ should be fulfilled. Eq. (20) admits two solutions as

$$\Omega_+^2=\frac{1}{2}\left[R+\sqrt{R^2-4S}\right], \quad \Omega_-^2=\frac{1}{2}\left[R-\sqrt{R^2-4S}\right]. \quad (21)$$

In this framework, the instability is a purely growing mode and we have the growth rate of instability $\Gamma=\sqrt{-\Omega_-^2}$.

• On the other hand, if $\Delta=R^2-4S<0$, there exists a domain of the wavenumber λ for which Ω^2 is negative. In this range, the solution of (20) are complex and so that Ω^2 has a nonvanishing imaginary part. The plane wave will be unstable if this imaginary part of Ω is positive, leading the perturbation to grow exponentially. Then, the plane wave tends to self-modulate with a wavenumber λ corresponding to the growth rate

$$\Gamma=\mathrm{Im}(\Omega_\pm^2)=\pm\frac{1}{2}\sqrt{4S-R^2}. \quad (22)$$

The above growth rate of instability implies that the condition $\sqrt{4S-R^2}>0$ should be satisfied for wave instability to take place. The corresponding growth rate of instability is plotted versus the wavenumbers of perturbation, λ, in Fig. 3. On studying the influence of the dipolar energy on the behavior of the of the growth rate of instability, one sees that for $pE=0.15$ eV, there is only one region of instability, where modulated waves are expected. That region is situated in the interval $0<\lambda<0.30\pi$, and gets expanded for $pE=0.20$ eV. Wave instability now spans in the interval $0<\lambda<0.55\pi$. However, beyond that value of the dipolar energy, there emerges another region of instability $0.35\pi<\lambda<0.45\pi$ for $pE=0.60$ eV. Further increasing the later also expands the two regions of parameter for MI to develop gets large as well. Regions of instability are those where the dimers are expected to undergo localized oscillations as a result of the interplay between nonlinear and dispersive effects. On the other hand, when parameters are not picked from those areas, the plane wave solutions will be said to be stable under modulation and will not experience any perturbation.

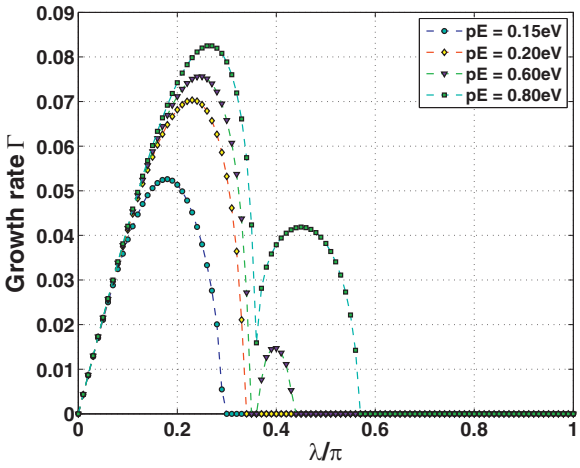

Fig. 3. The growth rate of MI is plotted for the coupled mode versus the perturbation wavenumber λ. It is obvious that increasing the dipolar energy contributes to expand the instability region. There also appears another region of instability, where nonlinear waves in protofilaments.

4. Single and coupled mode excitations

4.1. Single mode excitations

The single mode excitation implies that only one of the two equations is considered, while the other component in turn to zero, i.e., only one NLS equation remains.

• For example, taking $\psi_2=0$ leads to the following NLS equation for the lower cut-off mode:

$$i\frac{\partial\psi_1}{\partial t}+H_1\frac{\partial^2\psi_1}{\partial x^2}+\zeta_{11}|\psi_1|^2\psi_1=0. \quad (23)$$

The above equation is well known in nonlinear physics and have even been obtained recently by Zdravković et al. [14] in the present model of MTs dynamics. Solutions for such equations depend on the sign of $H_1\times\zeta_{11}$. From Fig. 1, its obvious that this product is positive, leading to the solution

$$\psi_1(x,t)=K\sqrt{\frac{2H_1}{\zeta_{11}}}\mathrm{sech}(Kx+2H_1KK_1t)e^{i[K_1x-H_1(K_1^2-K^2)t]} \quad (24)$$

for Eq. (23). K and K_1 are two free parameters. For this first case, the angular displacement of the dimer at the position n is globally given by the solution

$$\psi_n(t)=2K\sqrt{\frac{2H_1}{\zeta_{11}}}\mathrm{sech}(Knl+2H_1KK_1t)\cos[K_1nl$$
$$-(\omega_0+H_1(K_1^2-K^2))t]. \quad (25)$$

One can see, form the above expression, that the dimer oscillations are described by a breather solution. We have studied its spatiotemporal behavior by integrating Eq. (1) using the fourth-order Runge-Kutta computational scheme with periodic boundary conditions. The time step has been chosen as $\Delta t=10^{-4}$ ns and the initial condition is solution (25). The effect of the dipolar potential energy has been studied. As a matter of fact, the breather soliton has been proposed recently in MTs [14], but its true biological implications still remain unmasked. However, encouraging is the truth that breather solitons emerge in systems where nonlinear and dispersive effect are coupled. In biological systems in general, breather are always presented to be at the onset of important biological processes. In DNA for example, they are at the onset of transcription [3,23], while they can be perceived as the triggering signals for motor proteins to start moving along MTs. Their role in the regulation of neural

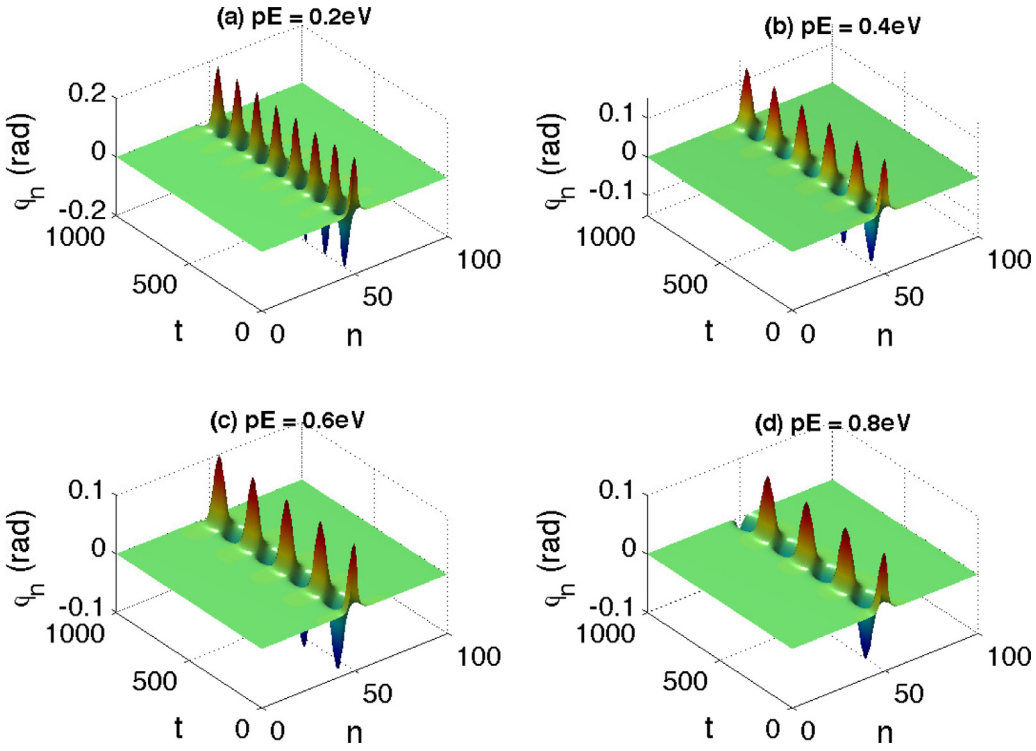

Fig. 4. Spatiotemporal evolution of the lower cutoff solution for different values of the dipolar energy *pE*. The number of objects decreases along with the amplitude with increasing *pE*.

activities should not also be ignored, as they are situated inside the axons of nerve cells. In that respect, it has been shown that MTs are specialized entities in signal transmission within the cell, via dipole interactions in axonal MTs [24,25]. Importantly, the spatiotemporal behaviors of such structures depend on system parameters as it is obvious that the dipolar potential energy modifies its characteristics. In Fig. 4, simulations have been done for $pE = 0.2$ eV (panel (a)) and for $pE = 0.8$ eV. As a first remark, increasing *pE* considerably reduces the amplitude of the wave.

- The upper cut-off mode implies that $\psi_1 = 0$ and $\psi_2 \neq 0$, so that only the decoupled equation

$$i\frac{\partial \psi_2}{\partial t} - H_2\frac{\partial^2 \psi_2}{\partial x^2} + \zeta_{22}|\psi_2|^2\psi_2 = 0 \tag{26}$$

is obtained. Its solution can also easily be found. From Fig. 1, $H_2 \times \zeta_{22}$ is positive, but because of the $(-)$-sign that appears in Eq. (26), its solution is written as

$$\psi_2(x,t) = K\sqrt{-\frac{2H_2}{\zeta_{22}}}\tanh(Kx - 2H_2KK_2t)e^{i[K_2x - H_2(K_2^2+2K^2)t]}, \tag{27}$$

whith K and K_2 being two free parameters. Therefore, the following solution for dimer oscillation can be obtained

$$\begin{aligned}\psi_n(t) \quad &= 2(-1)^n K\sqrt{-\tfrac{2H_2}{\zeta_{22}}}\tanh(Knl - 2H_2KK_2t) \\ &\times \cos[K_2nl - (\omega_{max} + H_2(K_2^2 + 2K^2))t].\end{aligned} \tag{28}$$

Using the same numerical procedure as previously, we get the results of Fig. 5, with the initial condition (27). The spatiotemporal evolution of a kink envelope is displayed for different values of the dipolar energy *pE*, which respectively takes the values 0.2 eV (Fig. 5(a)), 0.4 eV (Fig. 5(b)), 0.6 eV(Fig. 5(c)) and 0.8 eV (Fig. 5(d)). Over the time, the solution evolves into trains of solitonic objects, which diminish with increasing *pE*.

In general, the single modes solutions (25) and (28) give an idea on the behavior of the coupled wave solution under the influence of the electric field. Solitons are or various types, depending on their meaning and mode of generation in nonlinear systems.

4.2. The coupled-mode excitations

In the coupled mode none of the two amplitude is switched to zero, and the nonlinear coupling between them is maintained. In this framework, solving the set of Eqs. (13)–(14) depends on the sign of the coefficients [26,27]

$$\Delta_1 = \frac{H_1\zeta_{22} + H_2\zeta_{12}}{\zeta_{11}\zeta_{22} - \zeta_{21}\zeta_{12}}, \quad \text{and} \quad \Delta_2 = -\frac{H_2\zeta_{11} + H_1\zeta_{21}}{\zeta_{11}\zeta_{22} - \zeta_{21}\zeta_{12}} \tag{29}$$

that we have plotted in Fig. 5. Since $\Delta_1 > 0$ and $\Delta_2 < 0$, the solutions for the two equations are found to be

$$\psi_1(x,t) = A_1\,\mathrm{sech}(Kx + 2H_1KK_1t)e^{i(K_1x - \Omega_1t)}, \tag{30}$$

$$\psi_2(x,t) = A_2\tanh(Kx + 2H_2KK_2t)e^{i(K_2x - \Omega_2t)}, \tag{31}$$

where

$$\begin{aligned}&A_1^2 = \frac{2K^2(H_2\zeta_{12} + H_1\zeta_{22})}{\zeta_{11}\zeta_{22} - \zeta_{12}\zeta_{21}}, \quad A_2^2 = \frac{2K^2(H_2\zeta_{11} + H_1\zeta_{21})}{\zeta_{11}\zeta_{22} - \zeta_{12}\zeta_{21}}, \\ &\Omega_1 = -H_1(K^2 - K_1^2) - \zeta_{12}A_2, \\ &\Omega_1 = -H_2(2K^2 + K_2^2) - \zeta_{21}A_1, \quad K_2 = -\frac{H_1}{H_2}K_1.\end{aligned} \tag{32}$$

The global solution for the MT dimer radial displacement is given by

$$\begin{aligned}\psi_n(t) &= 2A_1\,\mathrm{sech}(Knl + 2H_1KK_1t)\cos[K_1nl - (\omega_0 + \Omega_1)t] \\ &+ 2(-1)^nA_2\tanh(Knl - 2H_2KK_2t)\cos[K_2nl - (\omega_{max} + \Omega_2)t].\end{aligned} \tag{33}$$

The above solution has two parts. We clearly see the breather soliton solution part in sech and the kink part in tanh. While combined, we have the features presented in Fig. 6. Obviously, the

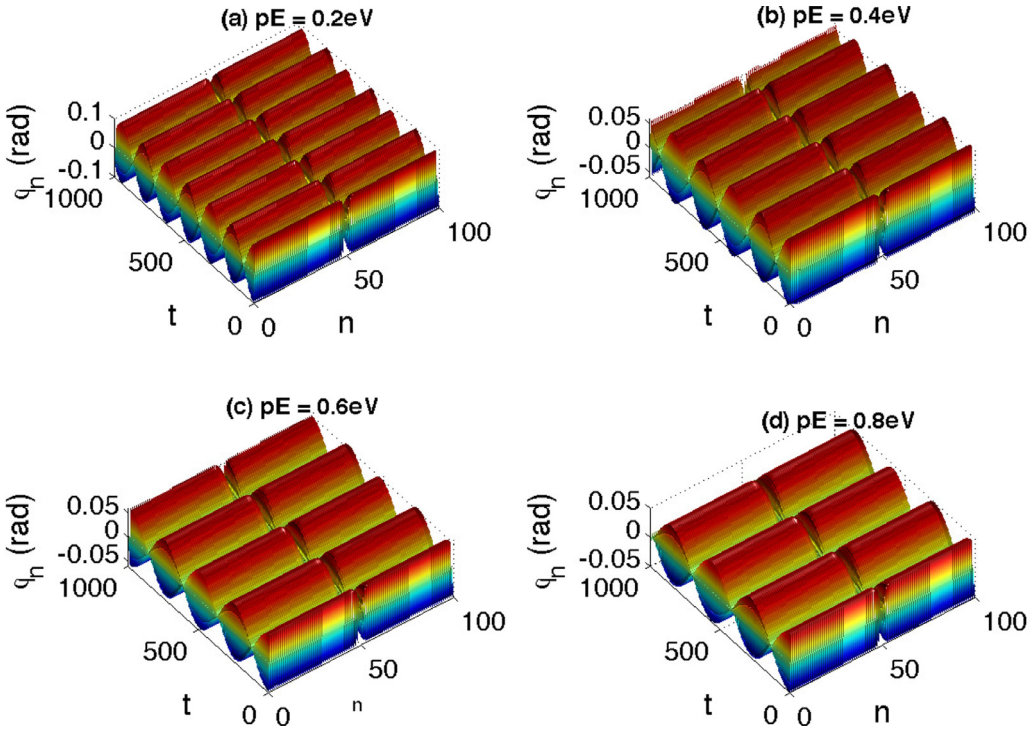

Fig. 5. Numerical solution corresponding to the upper cutoff frequency solution, under the influence of the dipolar energy. Similarly to the previous case, the number of solitonic objects and the amplitude decrease when *pE* grows, giving rise to more larger structures.

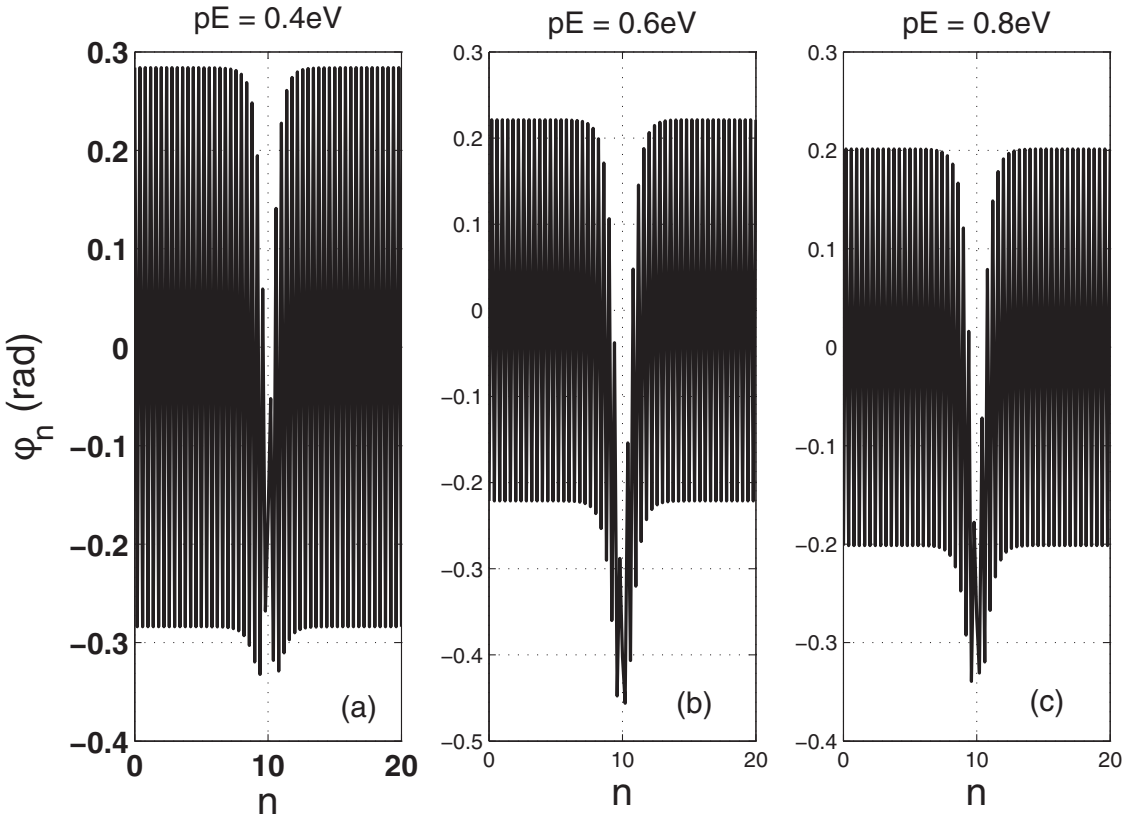

Fig. 6. Snapshots of the coupled solution (33) for different values of the dipolar energy *pE*. Increasing the later reduces the amplitude of the Kink-envelope solution. The Kink-antiKink character of the solution is visible through the two-humped structure that becomes obvious with increasing *pE*.

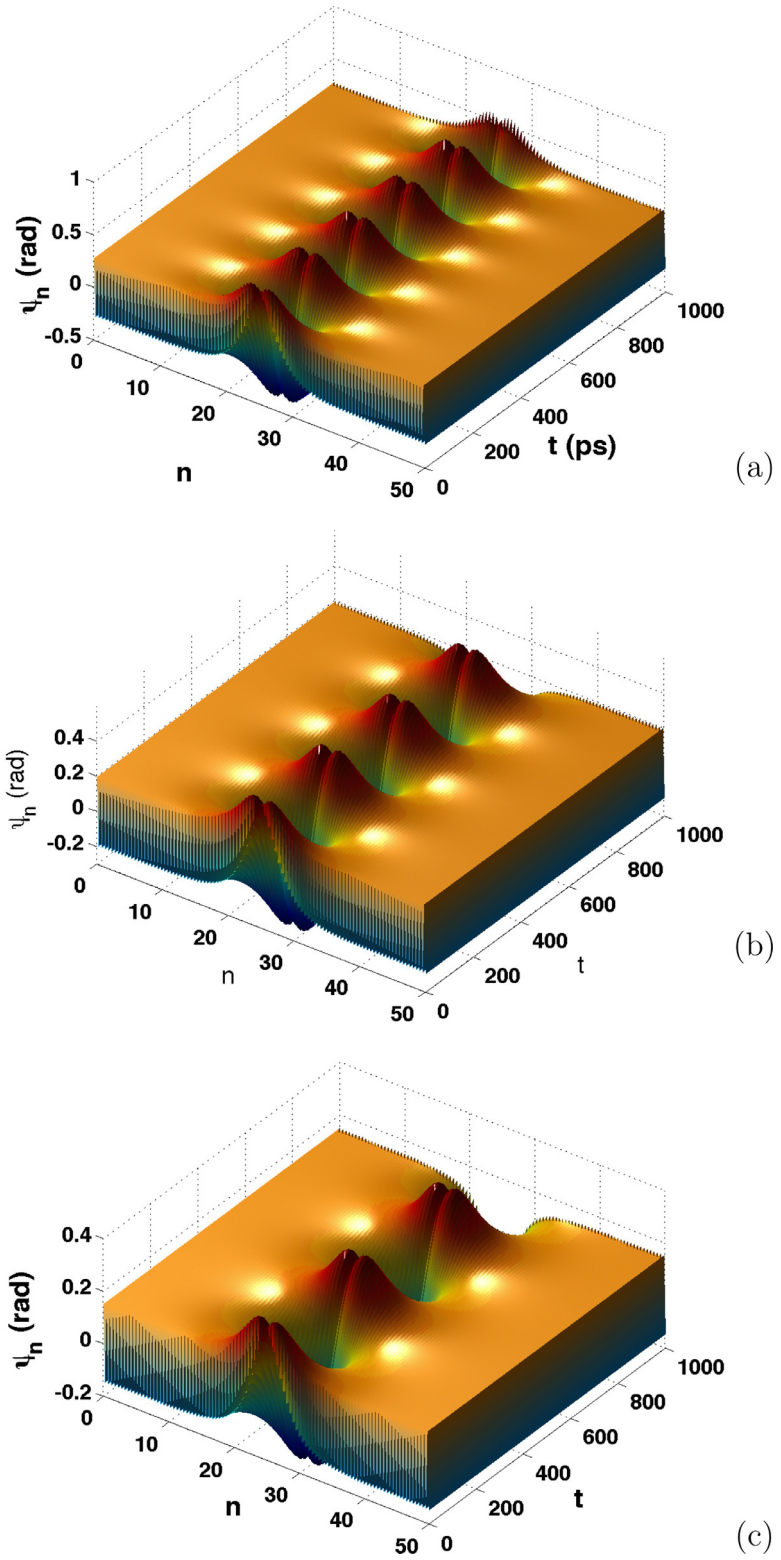

Fig. 7. The panels show the space-time evolution of the coupled solutions. Simulations have been made for different values of pE: (a) $pE = 0.4$ eV, (b) $pE = 0.6$ eV and (c) $pE = 0.8$ eV. Over time, the initial condition (33) keeps its shape and characteristics, except that the number of breathing objects decreases along with the wave amplitude with increasing pE.

kink-envelope soliton is strongly modified by the presence of the electric field E. In fact, its amplitude decreases with increasing pE and the separation between the two sides gives rise to a hole. Solitons are capable of carrying energy, and that energy, in the present context, might give rise to the mechanism of polymerization and depolymerization. Interests have been given recently to soliton collision, where energy is shared for the better achievement of these processes. However, one of the most important issues is how that energy is initiated and carried by solitonic structures. At the same time, if the energy released by the hydrolysis of GTP

is not sufficient, there will be no dislocation and the state of the tubulin dimer will not be altered. Coupled wave generation could then be a way to boost that energy, so that a strong dislocation could be initiated and followed by the process of polymerization-depolymerization. Furthermore, for motor-proteins to start moving, enough energy should be available, which might be brought by the coupled solution. This then implies that the solution should be robust and conserve its form and characteristic for an optimal energy transport. We have for example tested this through the direct numerical integration of Eq. (1), with the initial condition (33). The corresponding spatiotemporal results are displayed in Fig. 7, with changing the dipolar energy. Spatially, the soliton keeps its shape with increasing pE, but temporally, the number of elements diminishes, replaced by more expanded structures. Under the influence of high electric field, the collection of energy is rather ensured by more bigger structures, in order to ensure a permanent release of energy that is capable to provoke the motion of heterodimers in MTs. This is mediated by an energy rich cap (where GTP is not hydrolyzed) that is formed at the end of the tubulin [28], that will be hydrolyzed in such a way that a considerable quantity of energy is released for a specific process, while the rest is stored in the MT lattice for other specific mechanisms to be achieved. Solitonic structures can then be excited with strong influence on bond length and conformation changes of tubulin heterodimers [10,14]. Otherwise, there is always energy that is supplied to the vibrations or for motor proteins to move along the MT and transferred to the MT as localized excitation of vibrations, which sufficiently justifies the evidence of coupled mode of vibration in MTs.

5. Conclusion

The present work was dedicated to the dynamics of MTs relying on a radial model. The studied nonlinear lattice equation has been reduced, through the semi-discrete multiple scaling expansion, to a set of nonlinearly CNLS equations. These equations are in fact due to the coupling between lower and upper cut-off frequencies. The corresponding single modes have been studied, but particular attention has been given to the coupled mode which better describes energy collection for the intake of polymerization/depolymerization mechanism. The activation of MI has been addressed in this particular mode, and the influence of the electric field on the emergence of unstable modes has been discussed. Two regions of parameters have been found to support the formation of nonlinear modulated waves, under strong electric field. On this background, the analytical treatment of the coupled mode was also made and it has been found to be a kink-envelope solution. We have argued that such solutions for the dynamics of MT protofilaments may be justified by the presence of different modes of vibration [29], which might be efficient in the collection and transport of the energy released by the GTP hydrolysis, responsible for the initiation of the dislocation motion along the protofilaments. Accordingly, the robustness of the proposed coupled mode has been investigated through numerical simulations. This is important in the process of energy storage and transport in biological settings, and particularly in MTs as said so far. This analysis therefore suggests that due to the coexistence of different frequencies of vibration [29], it might be interesting to address the two dimensional version of this model and study the particularities of each mode, in terms of solitons, and differentiate low to high frequency excitations, and their biological implications regarding the motion of motor proteins, for example. Calculations in that direction are being addressed and will be published elsewhere.

References

[1] Alberts B, Bray D, Lewis J, Raff M, Roberts K, Watson J. Molecular biology of the cell. New York and London: Garland publishing,; 2005.
[2] Satarić MV, Kormidis-Luburić U, Budinski-Petković L, Loncarević I. J Comput Theor Nanosci 2009;6:721.
[3] Tabi CB, Mohamadou A, Kofané TC. Eur Phys J D 2008;50:307.
[4] Hennig D, Archilla JFR, Agrawal J. Physica D 2003;180:256.
[5] Koko AD, Tabi CB, Ekobena HPF, Mohamadou A, Kofané TC. Chaos 2012;22:043110.
[6] Zdravkovic` S, Sataric` MV. Europhys Lett 2007;80:38003.
[7] Mefire GRY, Tabi CB, Mohamadou A, Ekobena HPF, Kofané TC. Chaos 2013;23:033128.
[8] Tabi CB, Mimshe JCF, Ekobena HPF, Mohamadou A, Kofané TC. Eur Phys J B 2013;86:374.
[9] Chou KC, Zhang CT, Maggiora GM. Biopolymers 1994;34:143.
[10] Sataric` MV, Tuszyński JA, Zakula RB. Phys Rev E 1993;48:589.
[11] Zdravković S, Kavitha L, Satarić MV, Zeković S, Petrović J. Chaos Solitons Fract 2012;45:1378.
[12] Zdravković S, Satarić MV, Zeković S. Europhys Lett 2013;102:38002.
[13] Zdravković S, Satarić MV, Maluckov A, Balaz A. Appl Math Comput 2014;237:227.
[14] Zdravković S, Bugay AN, Aru GF, Maluckov A. Chaos 2014;24:023139.
[15] Tabi CB, Ekobena HPF, Mohamadou A, Kofané TC. Phys Scr 2011;83:035802.
[16] Pokorný J., Jelinek F., Trkal V., Lamprecht I., Hölzel R., Astrophys Space Sci1997. 23, 171.
[17] Pampaloni F, Florin EL. Trends Biotechnol 2008;26:302.
[18] Schoutens JE. J Biol Phys 2005;31:35.
[19] Pokorny J. Bioelectrochemistry 2004;63:321.
[20] Huang G. Phys Rev B 1995;51:12347.
[21] Manakov SV. Sov Phys JETP 1974;38:248.
[22] Tabi CB, Mohamadou A, Kofané TC. J Phys Condens Matter 2009;21:335101.
[23] Tabi CB, Ekobena HPF, Kofané TC. J Comput Theor Nanosci 2011;8:2220.
[24] Brown JA, Tuszyński JA. Phys Rev E 1997;56:5834.
[25] Gundersen GG, Cook TA. Curr Opin Cell Biol 1999;11:81.
[26] Bhakta JC. Plasma Phys Control Fusion 1987;29:245.
[27] Kofané TC, Zebaze M, Zibi A. J Phys D Appl Phys 1990;23:764.
[28] Caplow M, Shanks J. Molec Biol Cell 1996;7:663.
[29] Portet S, Tuszyński JA, Hogue CWV, Dixon JM. Eur Biophys 2005;34:912.

Chaos, Solitons and Fractals 162 (2022) 112446

Contents lists available at ScienceDirect

Chaos, Solitons and Fractals

Nonlinear Science, and Nonequilibrium and Complex Phenomena

journal homepage: www.elsevier.com/locate/chaos

Soliton-mediated ionic pulses and coupled ionic excitations in a dissipative electrical network model of microtubules

Eric Tankou [a], Conrad Bertrand Tabi [b,c,*], Timoléon Crépin Kofané [b,d]

[a] Laboratory of Biophysics, Department of Physics, Faculty of Science, University of Yaoundé I, P.O. Box 812, Yaoundé, Cameroon
[b] Department of Physics and Astronomy, Botswana International University of Science and Technology, Private Mail Bag 16, Palapye, Botswana
[c] Kavli Institute for Theoretical Physics (KITP), University of California at Santa Barbara, Santa Barbara, CA 93106, USA
[d] Laboratory of Mechanics, Department of Physics, Faculty of Science, University of Yaoundé I, P.O. Box 812, Yaoundé, Cameroon

ARTICLE INFO

Article history:
Received 26 February 2022
Received in revised form 3 June 2022
Accepted 11 July 2022
Available online xxxx

Keywords:
Microtubules
Electrical transmission line
Dissipative bright-bright soliton
Modulational instability

ABSTRACT

Many cellular activities are mediated by microtubules (MTs), with most electrophysiological processes depending on ionic flow through MT cylinders. This paper addresses such conductive features by representing the MT as a nonlinear electrical transmission line composed of capacitive and dissipative properties. Thanks to the semi-discrete approximation near the continuum limit, coupled ionic pulses flowing along cellular microtubules are described by a set of coupled cubic complex Ginzburg-Landau (CGL) equations whose one of the solutions is a plane wave. The stability of the latter is checked, under weak modulation, using an explicit analytical expression for the modulational instability (MI) growth rate. The parametric analysis of the instability growth rate allows detecting parameter regions where ionic conductivity, through modulated waves, in the MT network is likely to occur. Dissipative bright-bright pulse soliton solutions for the nonlinearly coupled cubic CGL equations are constructed using a modified Hirota's bilinear method. A generalized coupled mode for the discrete ionic signal is proposed and used as the initial condition to be propagated in the nonlinear electrical transmission lattice of MT under direct numerical simulations. The ionic pulse transfer, mediated by the nonlinear interaction between oscillatory modes, is manifested by the formation of trains of modulated waves whose behaviors depend on the right choice of system parameters. Those results theoretically suggest that coupled ionic signals may facilitate information processing involving MTs.

1. Introduction

The structure of all eukaryotic cells is defined by networking filamentous protein polymers that form the cytoskeleton [1]. The cytoskeleton is made up of three different types of filamentary structures that include actin-based microfilaments (MFs), intermediate filaments (IFs) (e.g., neurofilaments, keratin), and tubulin-based microtubules (MTs). They are organized into networks, interconnected through numerous particular proteins, and have specific roles in the cell's functioning. The cytoskeletal networks are primarily involved in the organization of different directed movements in cell migration, cell division, or the internal transport of materials. Polymerization of MFs is responsible for cell migration and the remodeling of the leading edge of cells [2,3]. Molecular motors are protein complexes associated with the cytoskeleton and drive organelles along MTs and MFs in a vectorial transport. Microtubules are the main organizers of the cytoskeleton. They are formed by cylindrical structures (with a diameter of about 25 nm) composed of 13 (or 14) protofilaments (PFs) which are one-dimensional chains of heterodimer tubulin molecules [2,3]. A tubulin molecule comprises two globular proteins α and β tubulins, each of which has a relative molecular mass of about 55,000 ('molecular weight' in daltons), but the masses are not equal. The heterodimer molecule can change conformation from the α state (nontilted) to the β state (tilted by 29 degrees from the microtubule axis) [4]. The heterodimer molecule is an electric dipole [5–7]. As a result, the MTs are polar structures with the plus end (fast-growing) and the minus end (slow-growing) embedded in the centrosome. The half-lifetime of a microtubule is about 10 min. Guanosine triphosphate (GTP) molecules are bound to both tubulins in a heterodimer. After polymerization, when the heterodimer is attached to the microtubule, the GTP bound to the β-tubulin is hydrolyzed to guanosine diphosphate (GDP). The majority of the hydrolysis energy is not released but stored in the MT [8,9]. Note that MTs are some of the most basic and most critical cytoskeletal elements in the

* Corresponding author at: Department of Physics and Astronomy, Botswana International University of Science and Technology, Private Mail Bag 16, Palapye, Botswana.
E-mail address: tabic@biust.ac.bw (C.B. Tabi).

https://doi.org/10.1016/j.chaos.2022.112446
0960-0779/

morphological scheme of neurons. As for the case of cytochalasins in actin structures, the addition of microtubular modifying agents was first used to assess the role of MTs in axon elongation. Microtubular disrupting agents affect axons first and have no early effects on growth cones and filopodia, suggesting that MTs support the axon. Conversely, the microtubular invasion may be critical in forming neurite projections. Initially expanded lamellipodia first undergo segmentation at certain spots where MTs accumulate in an ordered array [10–12] and gradually migrate away from the cell body. Thus, MTs are essential for neurite development. One particular aspect of microtubular involvement in neurite outgrowth is vesicular transport. Most membrane insertion occurs at the growth cone of axons [13,14]. It has become apparent that neurons might utilize MT networks in cognitive processes via associated proteins (MAPs), including MAP-tau and MAP2, in neuronal processes such as learning and memory [15,16]. MTs are also linked to the regulation of several ion channels, thus contributing to the electrical activity of excitable cells [17]. Therefore, MTs may play a fundamental role in processing electrical signals within the neuron. Structural reorganization of the cytoskeletal may reflect changes in neural circuits in response to learning and experience, and they must involve highly dynamic regulatory mechanisms.

According to the previous research, the idea of examining MTs in the context of polyelectrolyte features was inspired by the experimental and theoretical results obtained for actin filaments by Lin and Cantiello [18] and Tuszynski et al. [19], where they later develop a physical model of microtubule systems based on a nonlinear RLC transmission line. Along the same line, Sataric et al. [20] investigated the conditions enabling MTs to act as electrical transmission lines for ion flows along their lengths and showed that MTs could support the propagation of localized waves. On this background, energy loss-free transport along MTs has been shown possible [21,22] as a result of nonlinear excitations, or solitons, as an energy-transfer mechanism in MTs. Priel et al. [23] experimentally demonstrated that MTs are excellent conductors of electrical signals and can amplify an electrical current stimulated by a pulse of applied voltage. More recently, Ndzana and Mohamadou [24] present analytical studies for the generation of exact solitary wavelike solutions in a nonlinear electrical MT transmission line. They have shown that modulated waves emerge in a nonlinear electrical microtubule transmission line using modulational instability (MI) and also show the effects of the dissipation of the electrical components [24]. Indubitably, one of the factors capable of contributing to signal amplification is the combination of several modes. This was shown in DNA dynamics to enhance the energy needed to initiate the key phenomena known as replication and transcription [25]. In neural networks, it was demonstrated by Eteme et al. [26,27] that coupled modes could help to differentiate high from low-frequency oscillation modes, as well as the subsequent categories of the involved solitary waves. More recently, to further prove the existence of electrical oscillations in MT bundles, direct measurements were made in neurons, from which spontaneous changes of oscillatory behaviors were noticed, therefore shading lights on the existence of various spontaneous electrophysiological oscillatory regimes [28]. So far, no electrical model of MTs, to the best of our knowledge, has substantially addressed such a problem that could be fundamental in understanding the mechanism underlying optimal energy transport and information processing at the sub-cellular scale. Moreover, one of the fundamental and still open questions that are exclusively reported in this paper is the contribution of dissipative elements to such processes. We explicitly discuss the conditions required for ionic signals to flow under such circumstances, especially when two or more modes are involved along the MT. In the process, one shows that coupled excitable modes are described by a set of nonlinearly coupled cubic complex Ginzburg-Landau (CGL) equations. A comprehensive parametric analysis to predict MI allows qualitatively evaluating the dissipative effects on the formation of modulated waves in the MT nonlinear electrical network. The analytical derivation of the input signal through a modified Hirota's bilinear method allows us to confirm our predictions from MI via direct numerical simulations, where electrical signal propagation is manifested through the appearance of trains of modulated waves whose behaviors are sensitive to variations in dissipative coefficients.

The rest of the paper comprises Section 2, where the electrical network of MTs is introduced, followed by the derivation of the coupled cubic CGL equations via the semi-discrete approximations. In Section 3, the linear stability analysis of MI is carried out, and an expression for the MI growth rate is derived. A parametric study of MI is proposed, emphasizing the impact of dissipative elements. Section 4 uses a modified Hirota's bilinear method to propose analytic pulse soliton solutions for the proposed model, followed by direct numerical simulation to confirm our analytical predictions. Section 5 is devoted to some concluding remarks.

2. Model and derivation of the coupled cubic complex Ginzburg-Landau equations

2.1. Model

In order to derive the model equation, we consider a discrete nonlinear mono-inductance transmission line of microtubule whose unit is shown in Fig. 1. The studied discrete model of MTs is made of a succession of such N adjacent unit cells, which individually contain a linear inductance L in series with a linear resistance r_1, a cylindrical capacitor C_0 connected in series with a transversal resistivity r_2. The capacitor is biased by a constant voltage V_0 and depends on the voltage V_n, for low voltage, at the nth section so that

$$Q_n = C_0\left(V_n - \alpha_1 V_n^2 - \alpha_2 V_n^3\right), \tag{1}$$

where C_0 is the capacitance in the linear regime, with α_1 and α_2 being positive parameters that account for nonlinearities in the charge. We introduce the discrete potential in one unit section of the MT, where Kirchhoff's laws for the currents and voltages are applied. The idea is to develop a spatiotemporal equation for the potential over the capacitance as a function of the model's parameters. For the calculations of this work, the parameter values [19] used are: $L = 0.8 \times 10^{-15}\mathrm{H}, r_1 = 10^9\Omega, r_2 = 7 \times 10^6\Omega, C_0 = 0.13 \times 10^{-14}\mathrm{F}, \alpha_1 = 0.03\ \mathrm{Volts}^{-1}, \alpha_2 = 0.0019\ \mathrm{Volts}^{-2}$. From these Kirchhoff's laws based on Fig. 1, we get the following from segment MN:

$$u_n - u_{n+1} = r_1 I_n + L\frac{dI_n}{dt}. \tag{2}$$

The relation between the current entering segment MO and the current across the capacitance is given by:

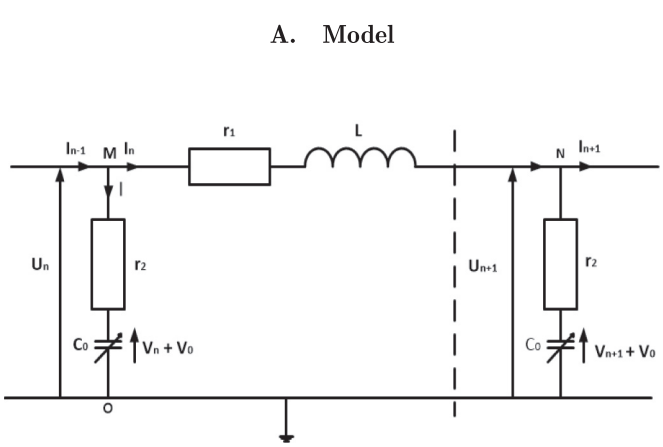

Fig. 1. Schematic representation of the dissipative nonlinear electrical transmission line describing the electronic analog of the microtubule model.

$$I_{n-1}-I_n=\frac{dQ_n}{dt}. \tag{3}$$

The voltage across the input to the elementary section, u_n, may be written in the following form:

$$u_n=r_2(I_{n-1}-I_n)+(V_n+V_0), \tag{4}$$

where V_n is the potential over the capacitance and V_0, the bias voltage of the capacitor. Combining the previous relations (1), (2), (3) and (4), it is easy to show that the spatiotemporal evolution of the waves' voltage $V_n(t)$ within the microtubule network is governed by the following equation:

$$\begin{aligned}&\frac{d^2V_n}{dt^2}-\omega_0^2(V_{n+1}+V_{n-1}-2V_n)\\&+\beta_0\frac{dV_n}{dt}-\beta_1\frac{d}{dt}(V_{n+1}+V_{n-1}-2V_n)-\beta_0\frac{d}{dt}\left(\alpha_1V_n^2+\alpha_2V_n^3\right)\\&-\frac{d^2}{dt^2}\left(\alpha_1V_n^2+\alpha_2V_n^3\right)+\beta_2\frac{d}{dt}\left(V_{n+1}^2+V_{n-1}^2-2V_n^2\right)\\&+\beta_3\frac{d}{dt}\left(V_{n+1}^3+V_{n-1}^3-2V_n^3\right)=0,\end{aligned} \tag{5}$$

where $\omega_0^2=\frac{1}{LC_0},\beta_0=\frac{r_1}{L},\beta_1=\frac{r_2}{L},\beta_2=\alpha_1\beta_0,\beta_3=\alpha_2\beta_1$ and $n=1,2,\ldots,N$ (N being the number of cells considered). By considering the dissipative coefficients β_0 and β_1 in the order of ε^3, the dispersion relation for the linear vibrations of PFs can be found by taking only linear terms in Eq. (5). This is given by:

$$\omega^2-4\omega_0^2\sin^2\left(\frac{k}{2}\right)=0, \tag{6}$$

where ω_0 is the characteristic frequency of the elementary cell, k being the wavelength. Under these conditions, the propagation without absorption of a wave for real k is only possible if $\omega\leq 2\omega_0$. The system therefore exhibits a low-pass type behavior. At the wave number $k=0$, the eigenfrequency spectrum has a lower cutoff $\omega_{\min}=0$, corresponding to direct current part, while for $k=\pi,\omega_{\max}=2\omega_0$, the alternating current part is the upper cut-off frequency. It is therefore sufficient to restrict the study of the $\omega(k)$ function to the $[0,\pi]$ interval of the values of k in order to fully describe the dynamic behavior of the tubulin dimer chain in MTs. The linear spectrum then has a gap $[0,2\omega_0]$ due to the discrete effects of the network. From the previous relation (5), we deduce the group speed

$$V_g=\frac{\partial\omega}{\partial k}=\frac{\omega_0^2\sin(k)}{\omega}. \tag{7}$$

We see that this group speed is not constant but depends on the frequency $\omega(k)$, which obviously implies a dispersive behavior of the system. It is good to know that the group velocity V_g is a physical speed; it corresponds to the speed of energy propagation and to the rate of information transport, and therefore cannot exceed the speed of light. The shapes of curves of the dispersion relation (6) and the group velocity (7) are plotted in Fig. 2, where they clearly show the interval in which the values of the wavenumber k are restricted. The coming part of this work will be used in the search for a given solution of Eq. (5). We will obtain the coupled cubic CGL equations whose solutions are generally of soliton type.

2.2. Multiple-scale expansion and derivation of the coupled complex Ginzburg-Landau equations

In general, solving the discrete Eq. (5) is not an easy task. Moreover, the present work's main purpose is to study solitons made up of carrier waves modulated by an envelope signal, also called envelope solitons; it is suitable to use the multiple-scale expansion, which can be applied to

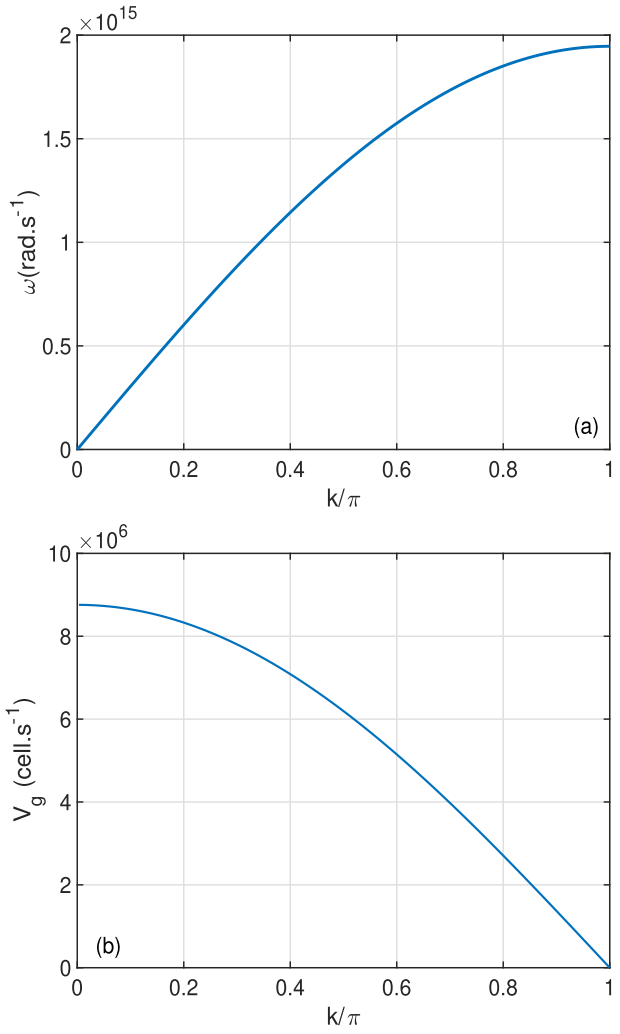

Fig. 2. Panel (a) shows the dispersion relation (6) and panel (b) displays the group velocity , both versus the wavenumber k of the plane wave signal along the protofilaments, with .

the semidiscrete approximation. To proceed, we consider that β_0 and β_1 are perturbed parameters of order ϵ^3. Through this process, the nonlinear Eq. (5) is transformed into two coupled cubic CGL equations that describe the amplitudes of the oscillations of nonlinear coupled impulses along microtubules. In the interval of frequencies $[0,2\omega_0]$, we choose to couple any two packets of waves centered (k_1,ω_1) and (k_2,ω_2) with $k_2=\alpha k_1(\alpha\in[0,1])$ for our study, and we assume the following solution for Eq. (5):

$$\begin{aligned}V_n(t)&=\varepsilon\left(B_1e^{i\theta_1}+B_2e^{i\theta_2}\right)\\&+\varepsilon^2\left(B_{30}+B_3e^{2i\theta_1}+B_{40}+B_4e^{2i\theta_2}\right)+c.c.,\end{aligned} \tag{8}$$

where $\theta_1=k_1n-\omega_1t$ and $\theta_2=k_2n-\omega_2t$, with k_1 and k_2 being the normal mode wavenumbers and ω_1 and ω_2 their associated frequencies. In the semi-discrete approximation, the undetermined envelope functions $B_q(q=1,2,3,4)$ are supposed to be independent from the fast variables t and n. This otherwise implies that they are functions of the slow variables $X_j=\varepsilon^jx$ and $T_j=\varepsilon^jt$, with $j\geq 1$. This implicitly means that a continuum limit approximation is made with the wave amplitudes, while the discrete nature of the phase is preserved. Moreover, taking into account the asymmetry of the charge-voltage relation given by Eq. (1), the direct terms $B_{30}(X_1,T_1,T_2),B_{40}(X_1,T_1,T_2)$ and the second harmonic terms $B_3(X_1,T_1,T_2),B_4(X_1,T_1,T_2)$ are added to the fundamental ones B_1

(X_1, T_1, T_2) and $B_2(X_1, T_1, T_2)$, respectively. Inserting Eq. (8) into Eq. (5) and using the following Taylor's expansions

$$B_{j,n\pm1} = B_j \pm \varepsilon h\left(\frac{\partial B_j}{\partial X_1}\right) + \varepsilon^2\frac{h^2}{2!}\left(\frac{\partial^2 B_j}{\partial X_1^2}\right) \pm \varepsilon^3\frac{h^3}{3!}\left(\frac{\partial^3 B_j}{\partial X_1^3}\right) + \cdots, j = 1,2,3,4, \tag{9}$$

yield, after some standard calculations, a series of inhomogeneous equations at different orders of perturbation parameter ε. The first orders of perturbation $(\varepsilon, e^{i\theta_1})$ and $(\varepsilon, e^{i\theta_2})$ lead to the dispersion relations of linear waves for the two wave packets (k_1, ω_1) and (k_2, ω_2) taken into the interval of frequencies $[0, 2\omega_0]$:

$$\begin{aligned}\omega_1^2 - 4\omega_0^2 \sin^2\left(\frac{k_1}{2}\right) = 0,\\ \omega_2^2 - 4\omega_0^2 \sin^2\left(\frac{k_2}{2}\right) = 0.\end{aligned} \tag{10}$$

They are identical to the expression given by Eq. (6). The second orders of perturbation $(\varepsilon^2, e^{i\theta_1})$ and $(\varepsilon^2, e^{i\theta_2})$, lead to

$$\begin{aligned}\frac{\partial B_1}{\partial T_1} = -V_{g1}\frac{\partial B_1}{\partial X_1}, \quad \text{with} \quad V_{g1} = \frac{\partial \omega_1}{\partial k_1} = \frac{\omega_0^2 \sin(k_1)}{\omega_1},\\ \frac{\partial B_2}{\partial T_1} = -V_{g2}\frac{\partial B_2}{\partial X_1}, \quad \text{with} \quad V_{g2} = \frac{\partial \omega_2}{\partial k_2} = \frac{\omega_0^2 \sin(k_2)}{\omega_2}.\end{aligned} \tag{11}$$

Form Eq. (11), the non-zero solutions B_1 and B_2 can be written in the forms $B_1 = B_1(\xi, T_2)$ and $B_2 = B_2(\xi', T_2)$, where $\xi = X_1 - V_{g1}T_1$ and $\xi' = X_2 - V_{g2}T_2$.

At orders $(\varepsilon^2, e^{2i\theta_1})$ and$(\varepsilon^2, e^{2i\theta_2})$, we find the relations

$$\begin{aligned}B_{30} = B_{40} = 0,\\ B_3 = \frac{\alpha_1\omega_1^2 + \frac{1}{2}i\omega_1(\beta_0\alpha_1 + 4\beta_2 \sin^2(k_1))}{\omega_1^2 - \omega_0^2 \sin^2(k_1)}B_1^2,\\ B_4 = \frac{\alpha_1\omega_2^2 + \frac{1}{2}i\omega_2(\beta_0\alpha_1 + 4\beta_2 \sin^2(k_2))}{\omega_2^2 - \omega_0^2 \sin^2(k_2)}B_2^2.\end{aligned} \tag{12}$$

Finally, at the third orders $(\varepsilon^3, e^{i\theta_1})$ and $(\varepsilon^3, e^{i\theta_2})$, using relation expressions (12) we recover the group velocities (11), while the slow envelope evolution of the solitonic ionic waves in microtubules are described by the coupled equations

$$i\frac{\partial B_1}{\partial T_2} - S_1\frac{\partial^2 B_1}{\partial \xi^2} - \sigma_1|B_1|^2B_1 - \rho_1|B_2|^2B_1 = iA_1B_1, \tag{13}$$

$$i\frac{\partial B_2}{\partial T_2} - S_2\frac{\partial^2 B_2}{\partial \xi'^2} - \sigma_2|B_2|^2B_2 - \rho_2|B_1|^2B_2 = iA_2B_2. \tag{14}$$

Further introducing the change of variables $\xi' = X_1 - V_{g2}T_1 = \xi + (V_{g1} - V_{g2})T_2$, Eq. (14) becomes

$$i\frac{\partial B_2}{\partial T_2} + \left(\frac{V_{g2} - V_{g1}}{\epsilon}\right)\frac{\partial B_2}{\partial \xi} - S_2\frac{\partial^2 B_2}{\partial \xi^2} - \sigma_2|B_2|^2B_2 - \rho_2|B_1|^2B_2 = iA_2B_2. \tag{15}$$

By using the dependent variable transformation $B_2 \to B_2 \exp\{-i(\frac{\Delta V_g}{2S_2}\xi + \frac{\Delta V_g^2}{4S_2}T_2)\}$, with $\Delta V_g = \frac{V_{g1} - V_{g2}}{\epsilon}$, the above Eq. (15) becomes

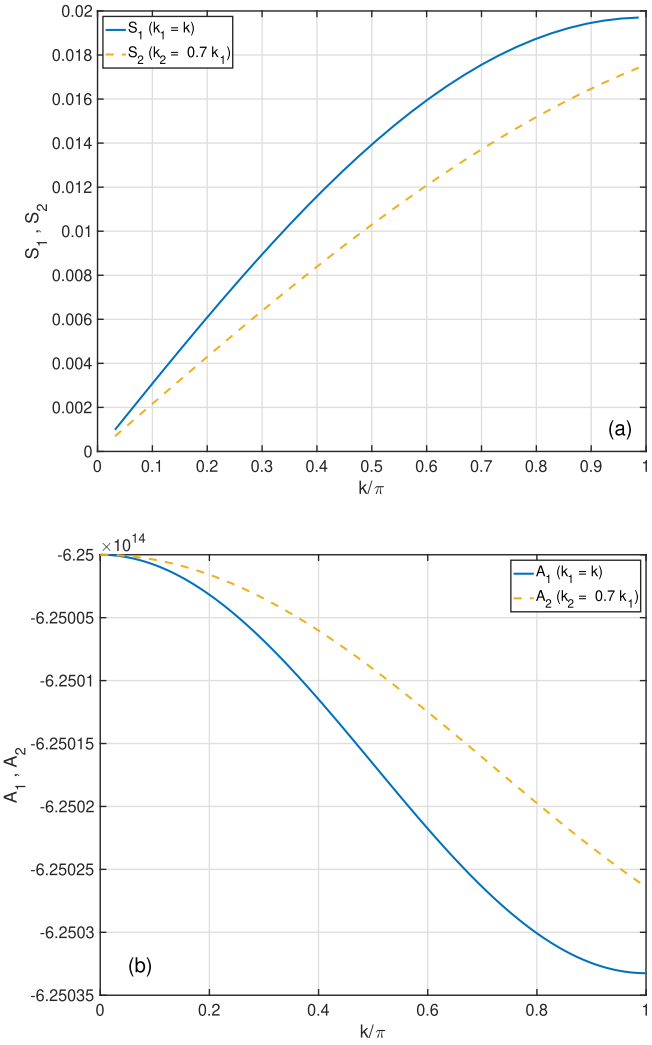

Fig. 3. Panel (a) shows the dispersion coefficients and of Eqs. (13) and (16), while panel (b) displays the dissipative coefficients and of the coupled cubic CGL equations versus the wavenumber k, with and , so that (yellow dashed line) corresponds to and , functions of . (For interpretation of the references to colour in this figure legend, the reader is referred to the web version of this article.)

$$i\frac{\partial B_2}{\partial T_2} - S_2\frac{\partial^2 B_2}{\partial \xi^2} - \sigma_2|B_2|^2B_2 - \rho_2|B_1|^2B_2 = iA_2B_2, \tag{16}$$

which forms a set of CGL equations with Eq. (13), whose coefficients $S_1, S_2, A_1, A_2, \rho_1, \rho_2, \sigma_1$ and σ_2 are given in the appendix. According to the plots of Fig. 3(a), the dispersion coefficients S_1 and S_2 are all positively increasing with respect to k, while Fig. 3(b) shows the dissipative coefficients A_1 and A_2 that are negatively decreasing functions of the wavenumber $k = k_1$, with $k_2 = \alpha k_1$. Along the same line, the complex self-phase modulation nonlinear coefficients σ_1 and σ_2, and the coupling coefficients ρ_1 and ρ_2 parameters, responsible for cross-phase modulation are complex parameters and the variations of their real and imaginary parts are summarized in Fig. 4 versus the wavenumber k. We should, however, stress that if the ρ_1 and ρ_2 are set to null, we obtain two decoupled cubic CGL equations. The CGL equations finds applications in many context and has actually been useful in physical systems related to biophysics [25,29–31], plasma physics [32], electrical lattices [33–35], Bose-Einstein condensation [36,37], nonlinear optics, lasers and metamaterials [38–42], to cite a few. Most of the studied systems probe the

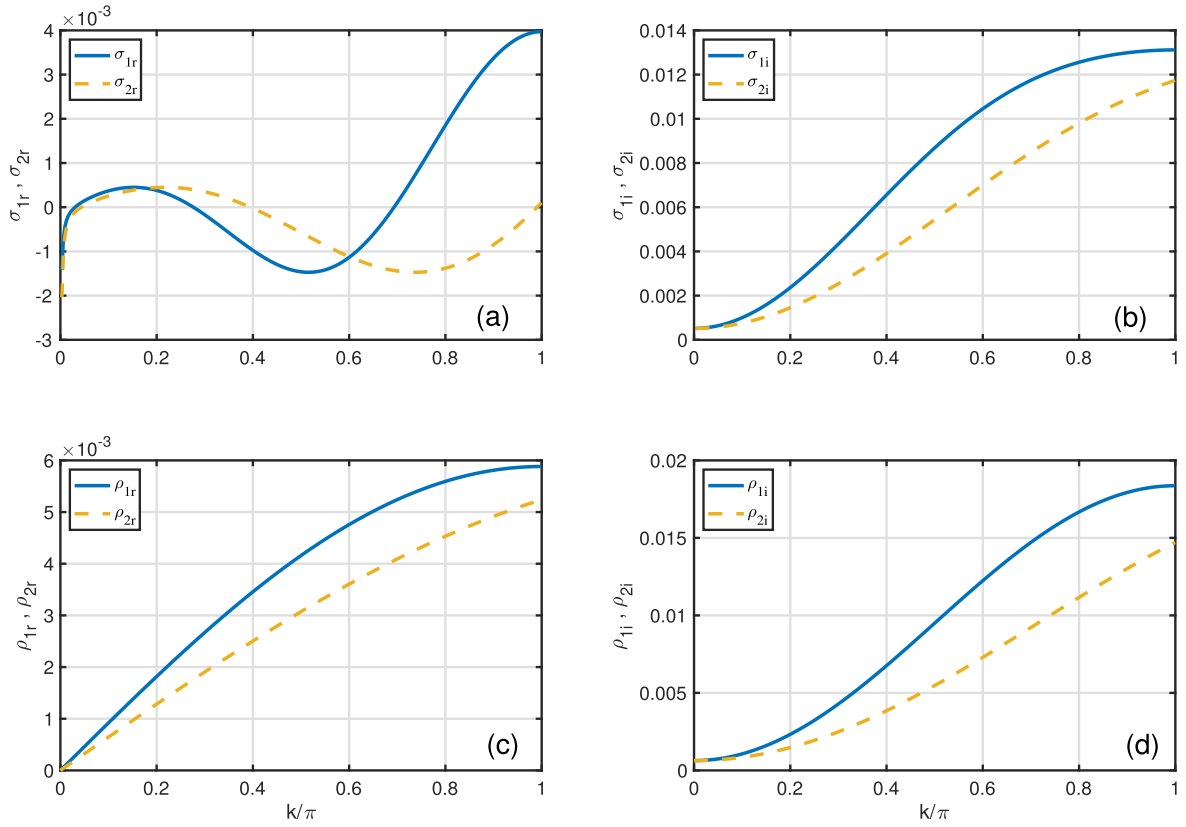

Fig. 4. Panels (a) and (b) show, respectively the real and imaginary part of the coefficients and of Eqs. (13) and (16) versus the wavenumber k. Panels (c) and (d) display plots of the coefficients and versus the wavenumber k, with and .

efficiency of the CGL equation in signal processing with good example being ionic waves transmission and amplification in neuronal microtubule networks [44,45], neural networks [26,27], along with pattern formation in many other physical systems. Interestingly, one of the techniques that have been widely used in characterizing pattern formation in the CGL equation is the MI mechanism, a consequence of the competition between nonlinearity and dispersion [38,41–43,46]. In relation to MI phenomenon, spatiotemporal chaos has been identified in the CGL equation [47,48]. Weber et al. [49] also reported transition to spatiotemporal turbulence from traveling waves resulting from instabilities, while solutions such as spiral waves were found [50].

3. Modulational instability analysis

In order to perform the MI study, we assume the set of Eqs. (13) and (16) to have the plane wave solutions $B_q(\xi,T_2)=B_{q0}e^{i\varpi_q T_2}$, where ϖ_q and B_{q0}, with $q=1,2$, are, respectively, the angular frequencies and the complex constant amplitudes of the carrier waves satisfying the dispersion relations

$$\begin{aligned}\varpi_1&=\sigma_1|B_{10}|^2+\rho_1|B_{20}|^2-i\gamma_1,\\ \varpi_2&=\sigma_2|B_{20}|^2+\rho_2|B_{10}|^2-i\gamma_2.\end{aligned}\tag{17}$$

In order to investigate the stability of the initial plane waves, we slightly perturb their amplitudes in such a way that $B_1(\xi,T_2)=B_{10}(1+\varepsilon g_1(\xi,T_2))e^{i\varpi_1 T_2}$ and $B_2(\xi,T_2)=B_{20}(1+\varepsilon g_2(\xi,T_2))e^{i\varpi_2 T_2}$, where $\varepsilon\ll 1$ and $g_j(\xi,T_2)$, with $j=1,2$, are the modulated amplitudes of perturbation. Inserting the above into Eqs. (13) and (16) and linearizing around the unperturbed plane waves, the equations describing the perturbed fields are given by

$$\begin{aligned}&i\frac{\partial g_1}{\partial T_2}-S_1\frac{\partial^2 g_1}{\partial\xi^2}-2iS_1k_1\frac{\partial g_1}{\partial\xi}-\sigma_1|B_{10}|^2(g_1+g_1^*)\\&\qquad-\rho_1|B_{20}|^2(g_2+g_2^*)=0\\&i\frac{\partial g_2}{\partial T_2}-S_2\frac{\partial^2 g_2}{\partial\xi^2}-2iS_2k_2\frac{\partial g_2}{\partial\xi}-\sigma_2|B_{20}|^2(g_2+g_2^*)\\&\qquad-\rho_2|B_{10}|^2(g_1+g_1^*)=0.\end{aligned}\tag{18}$$

Solutions for the above system are then considered to be

$$\begin{aligned}g_1(\xi,T_2)&=d_1e^{i(\lambda\xi-\delta T_2)}+d_2^*e^{-i(\lambda\xi-\delta^* T_2)},\\ g_2(\xi,T_2)&=d_3e^{i(\lambda\xi-\delta T_2)}+d_4^*e^{-i(\lambda\xi-\delta^* T_2)},\end{aligned}\tag{19}$$

where d_1,d_2,d_3 and d_4 are complex constant amplitudes, λ and δ represent, respectively, the wave number and the frequency of the perturbation, with the asterisk denoting complex conjugation. Applying these solutions to Eq. (18) and using the standard procedure of linear stability analysis lead to the following homogeneous system of equations in terms of d_1,d_2,d_3 and d_4:

$$\begin{pmatrix}Q_{11}+\delta & Q_{12} & Q_{13} & Q_{14}\\ Q_{21} & Q_{22}-\delta & Q_{23} & Q_{24}\\ Q_{31} & Q_{32} & Q_{33}+\delta & Q_{34}\\ Q_{41} & Q_{42} & Q_{43} & Q_{44}-\delta\end{pmatrix}\begin{pmatrix}d_1\\ d_2\\ d_3\\ d_4\end{pmatrix}=\begin{pmatrix}0\\0\\0\\0\end{pmatrix}\tag{20}$$

where the elements of the matrix are given in the appendix. For the above system to admit non-trivial solutions, its determinant should be null, i.e., $Det(\mathscr{M})=0$. The dispersion relation, which determines Ω, is then obtained by solving the homogeneous matrix equation when its determinant of the coefficient matrix vanishes, which leads to

$$\delta^4+\eta_3\delta^3+\eta_2\delta^2+\eta_1\delta+\eta_0=0. \tag{21}$$

Eq. (21) is a four order equation for the perturbation frequency obtained by taking determinant of the matrix null, with

$$\begin{aligned}
\eta_3 &= Q_{11}-Q_{22}+Q_{33}-Q_{44}\\
\eta_2 &= -Q_{11}Q_{22}-Q_{31}Q_{13}-Q_{42}Q_{24}-Q_{33}Q_{44}\\
&\quad +Q_{11}Q_{33}+Q_{22}Q_{44}-Q_{11}Q_{44}-Q_{22}Q_{33},\\
\eta_1 &= Q_{22}Q_{33}Q_{44}+Q_{31}Q_{13}Q_{44}-Q_{42}Q_{24}Q_{33}\\
&\quad -Q_{11}Q_{33}Q_{44}-Q_{11}Q_{42}Q_{24}-Q_{11}Q_{22}Q_{33}\\
&\quad +Q_{11}Q_{22}Q_{44}+Q_{31}Q_{13}Q_{22},\\
\eta_0 &= Q_{11}Q_{22}Q_{33}Q_{44}+Q_{31}Q_{13}Q_{42}Q_{24}\\
&\quad -Q_{31}Q_{13}Q_{22}Q_{44}-Q_{11}Q_{42}Q_{24}Q_{33}.
\end{aligned} \tag{22}$$

Solving Eq. (21), we can obtain the following four analytical solutions:

$$\begin{aligned}
\delta_{1,2} &= -\frac{\eta_3}{4}-\frac{1}{2}\sqrt{\frac{1}{4}\eta_3^2-\frac{2}{3}\eta_2+\Lambda}\pm\frac{1}{2}\sqrt{-\frac{4}{3}\eta_2+\frac{1}{2}\eta_3^2-\Lambda+\frac{\eta_3^3-4\eta_3\eta_2+8\eta_0}{4\sqrt{\frac{1}{4}\eta_3^2-\frac{2}{3}\eta_2+\Lambda}}},\\
\delta_{3,4} &= -\frac{\eta_3}{4}+\frac{1}{2}\sqrt{\frac{1}{4}\eta_3^2-\frac{2}{3}\eta_2+\Lambda}\pm\frac{1}{2}\sqrt{-\frac{4}{3}\eta_2+\frac{1}{2}\eta_3^2-\Lambda-\frac{\eta_3^3-4\eta_3\eta_2+8\eta_0}{4\sqrt{\frac{1}{4}\eta_3^2-\frac{2}{3}\eta_2+\Lambda}}},
\end{aligned} \tag{23}$$

where

$$\Lambda=\frac{1}{3}\left(\sqrt[3]{\frac{\Delta_1+\sqrt{\Delta_1^2-4\Delta_0^3}}{2}}+\frac{\Delta_0}{\sqrt[3]{\frac{\Delta_1+\sqrt{\Delta_1^2-4\Delta_0^3}}{2}}}\right)$$

and $\Delta_0=\eta_2^2-3\eta_3\eta_1+12\eta_0, \Delta_1=2\eta_2^3-9\eta_3\eta_2\eta_1+27\eta_3^2\eta_0+27\eta_1^2-72\eta_2\eta_0$. There exists a domain of the wavenumber λ for which the spectrum of the growth rate of MI $G(\lambda,k_1)=2Im(\delta_{1,2,3,4})$ can take a positive or a negative value. The system remains stable under modulation if the indicated MI growth rate value is negative and this because of the vanishing long term of the growth rate $|\ Im(\delta_{1,2,3,4})\ |$, exponentially over time. On the other hand, for positive gain values, there is possibility of instabilities. We therefore witness a divergence of the perturbation as time t increases and the system is said to be modulationally unstable. Therefore, necessary information on the onset of instability will be extracted using the maximum MI growth rate $G(\lambda,k_1)=2[|Im(\delta_{1,2,3,4})|\ ]_{max}$ which is obtained by comparing the four solutions of the nonlinear dispersion relation (21). Obviously, the MI growth rate is strongly influenced by the physical parameter β_0 on the one hand, and α on the other hand. To remind, α is the parameter linking the wavenumbers k_1 and k_2. The MI growth rate is illustrated in the $(k_1,\lambda)-$plane in Fig. 5, where β_0 takes increasing values. In general, versus λ, the growth rate spectrum comprises two symmetric lobes of instability. Values of the wavenumber k_1 that give rise to instability are well-limited, while $k_1=0$ is not supposed to support instability, with the maximum growth rate being situated around, including $k_1=1$. With increasing β_0, the bandgap between the two lobes tends to disappear, leading the two lobes of instability to merge into one, under strong symmetry around $\lambda=0$. Regions where $\zeta\neq0$ are indeed regions of instability that may support the disintegration of the plane wave solutions into trains of solitonic objects. To further explore the behaviors of the MI growth rate under the influence of β_0,ζ is plotted in Fig. 3 in the $(\lambda,\beta_0)-$plane, with α changing, so that $k_2=\alpha k_1$. While the growth rate is an increasing function of the parameter α, the MI spectrum generally displays two symmetric lobes of instability. For $\alpha=0.1$ and $\alpha=0.2$, one clearly notices an amplification of the instability, and areas of λ giving rise to the maximum growth rate get expanded [compare Figs. 6(a) and 6(b)]. However, with further increasing α, such intervals shrink, and regions of β_0 that support instability are restricted to higher values. This is once more obvious in Fig. 6(c), where $\alpha=0.35$. We should stress a change of behaviors in the MI growth rate when $\alpha\geq0.5$. Another observation of the instability gain $G(\beta_0)$ in Fig. 7 shows that for the fixed values of wavenumbers $k_1=1$ and $\lambda=0.001$ taken arbitrarily in the instability interval, $G(\beta_0)$ increases with the parameter α. Likewise, this growth of α induces the instability region in our biological network. Ultimately and globally, the region of instability thus detected is the one likely to contain the oscillations of modulated localized waves with an intensification around the perturbed wavenumber $\lambda=0$ and capable of provoking the destitution or reconstitution of tubulin dimers to allow them to transport energy or information favorable to the normal accomplishment of their cellular functions. According to the above, there is a straight relationship between MI and soliton formation under a suitable balance between nonlinearity and dispersion.

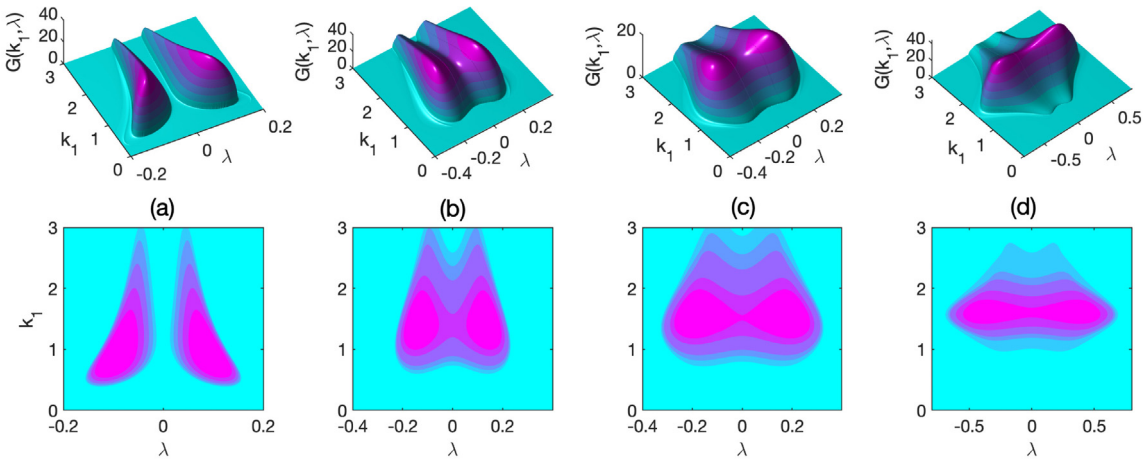

Fig. 5. The MI growth rate features versus the perturbation wavenumber λ and the wavenumber of the plane wave , with and . The panels (a), (b), (c) and (d) correspond to the respective values 0.06, 0.3, 0.5 and 0.7 of the dissipative coefficient .

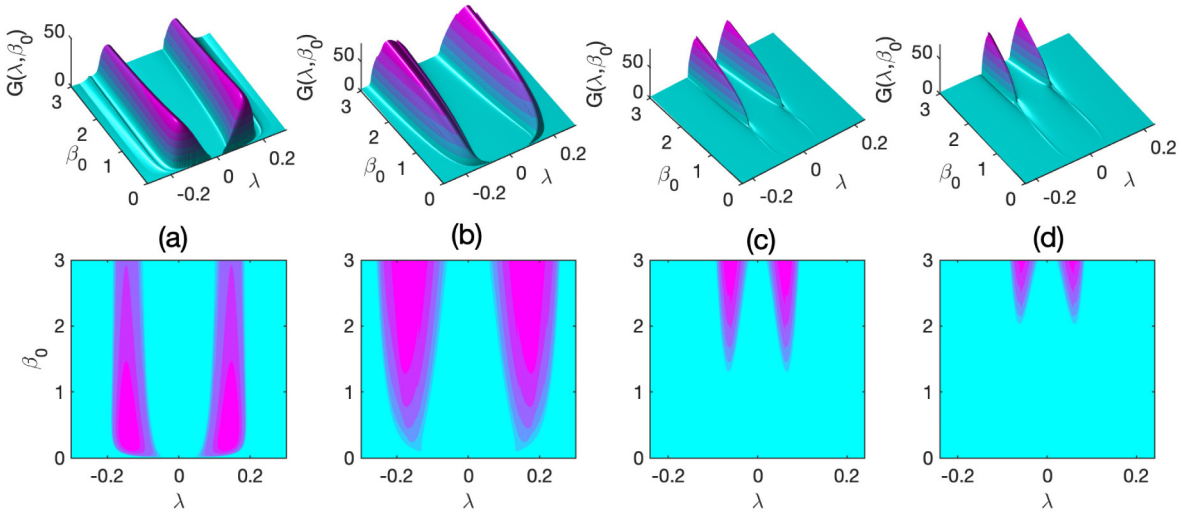

Fig. 6. The MI growth rate spectrum in the plane for and , with α taking the values 0.1, 0.2, 0.35 and 0.5 corresponding to the respective panels (a), (b), (c) and (d).

4. Nonlinear propagation of coupled modulated waves

4.1. Coupled solution for ionic waves in MTs electrical lattice

The strong relationship between wave modulation and soliton formation has given rise to a broad range of contributions using several resolution methods of nonlinear equations. Improved nonlinear physics models have triggered the elaboration of more sophisticated methods of resolution. Such methods include the auto-Bäcklund transformation method, used to find soliton solutions for a multi-component optical fiber [53], and the hetero-Bäcklund transformation method applied to water-wave phenomena [54]. Multi-dimensional water waves were also recently studied via a symbolic computation bringing together the hetero-Bäcklund transformation and similarity reduction [55]. Let us also mention the possibility of simultaneously using the scaling transformation, the hetero-Bäcklund transformation, and the bilinear forms to find nonlinear solutions [54], which otherwise confirms the possibility to combine the linear forms to other methods such as the Hirota's one. Particularly, the Hirota method has been intensively adopted among the useful resolution schemes since it does not require the inverse scattering method, which seems more complex. Simply, the Hirota bilinear method is based on the use of the Hirota's operator,

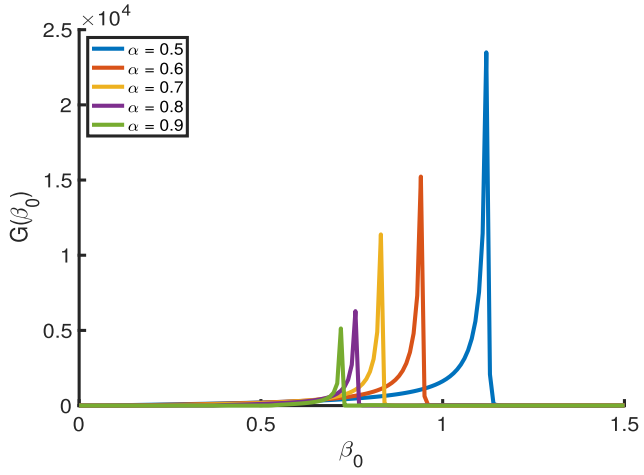

Fig. 7. Plot of the MI growth rate versus the dissipation coefficients , with α taking the respective values 0.5, 0.6, 0.7, 0.8, and .

which reduces the nonlinear equation to be solved into several coupled bilinear equations. Depending on the problem at hand, the method has been improved over the years to derive a larger class of nonlinear wave solutions. Accordingly, the coupled cubic-quintic CGL equations were solved analytically for counter-propagating waves by Zakeri and Yomba [56]. Following a similar procedure to solve Eq. (13), we first consider the following modified Hirota's linear operators:

$$\begin{aligned}(D_x^m D_t^n)_{p_j}(G.F) &= \left[\frac{\partial}{\partial x}-\left(\frac{1}{2}+ip_j\right)\frac{\partial}{\partial x'}\right]^m \\ &\times\left[\frac{\partial}{\partial t}-\left(\frac{1}{2}+ip_j\right)\frac{\partial}{\partial t'}\right]^n \\ &\times G(x,t)F(x',t')\big|_{x=x',t=t'},\end{aligned} \tag{24a}$$

$$\begin{aligned}\Lambda_j(F.F) &= \left(\frac{1}{2}+ip_j\right)\left(\frac{3}{2}+ip_j\right) \\ &\times\left(FF_{xx}-F_x^2\right), \quad j=1,2\end{aligned} \tag{24b}$$

where p_j $(j=1,2)$ are real parameters, n,m are positive integers and $G(x,t)$, $H(x,t)$ and $F(x,t)$ are assumed to be real-valued functions. Considering $T_2 = t$ and $X_1 = x$, we rewrite the set of Eq. (13) as

$$\begin{aligned}i\frac{\partial B_1}{\partial t}-S_1\frac{\partial^2 B_1}{\partial x^2}-\sigma_1|B_1|^2B_1-\rho_1|B_2|^2B_1 &= iA_1B_1 \\ i\frac{\partial B_2}{\partial t}-S_2\frac{\partial^2 B_2}{\partial x^2}-\sigma_2|B_2|^2B_2-\rho_2|B_1|^2B_2 &= IA_2B_2,\end{aligned} \tag{25}$$

whose exact solutions can be obtained using the transformations

$$B_1 = \frac{\eta G e^{i(q_1x-\Omega_1t)}}{F^{\left(\frac{1}{2}+ip_1\right)}}, \qquad B_2 = \frac{\mu H e^{i(q_2x-\Omega_2t)}}{F^{\left(\frac{1}{2}+ip_2\right)}}, \tag{26}$$

where q_1, q_2 and Ω_1, Ω_2, are, respectively, wavenumbers and angular frequencies of envelopes, and assumed real while $\eta = \eta_r + i\eta_i$ and $\mu = \mu_r + i\mu_i$ are complex. Substituting Eqs. (26) into (25), we obtain the following system of bilinear equations, functions of the modified derivatives of Hirota's linear operators (24a) and (24b):

$$\begin{aligned}&[\Omega_1 + q_1^2S_1 - iA_1 + iD_{p_1,t} - 2iq_1S_1D_{p_1,x} - S_1D_{p_1,x}^2 + 4\not{\prime}_1](G.F) \\ &= 0, S_1\Lambda_1(F.F) - |\eta|^2(\sigma_{1r}+i\sigma_{1i})G^2 - |\mu|^2(\rho_{1r}+i\rho_{1i})H^2 \\ &= 0, [\Omega_2 + q_2^2S_2 - iA_2 + iD_{p_2,t} - 2iq_2S_2D_{p_2,x} - S_2D_{p_2,x}^2 + 4\not{\prime}_2](H.F) \\ &= 0, S_2\Lambda_2(F.F) - |\mu|^2(\sigma_{2r}+i\sigma_{2i})H^2 - |\eta|^2(\rho_{2r}+i\rho_{2i})G^2 = 0,\end{aligned} \tag{27}$$

with $|\eta|^2=\eta_r^2+\eta_i^2$ and $|\mu|^2=\mu_r^2+\mu_i^2$, $\curlyvee_1$ and $\curlyvee_2$ being constants of decoupling. In addition, the normalization condition $F/|F|^{(\frac{1}{2}+ip_1)}=F/|F|^{(\frac{1}{2}+ip_2)}=1$ is used. There are several families of soliton solutions among which, the impulse, frontal and dark solitons [56]. Such solutions are often obtained from the modified bilinear operators (24). However, in the rest of this paper, we pay particular attention to pulse-like solutions because of their numerous applications in microtubular networks in terms of signal processing and information transport. Therefore, the functions G, H, and F are assumed to be in the following forms:

$$\begin{aligned} G &= H = e^{\frac{1}{2}(Rx+\omega t)}, \\ F &= 1+de^{(Rx+\omega t)}+Pe^{2(Rx+\omega t)}, \end{aligned} \tag{28}$$

where ω, R, d and L are taken to be real constant. Substituting the above into Eq. (27) leads to

$$\begin{aligned} \Omega_1 &= S_1\left(\frac{1}{4}R^2-q_1^2\right), \quad \Omega_2=S_2\left(\frac{1}{4}R^2-q_2^2\right), \\ \omega &= 2(A_1+S_1q_1R), \quad p_1<0, \quad p_2<0, \quad \curlyvee_1=\curlyvee_2=0, \\ |\eta|^2 &= \frac{S_1R^2d\left[\rho_{1i}\left(\frac{3}{4}-p_1^2\right)-2p_1\rho_{1r}\right]}{\sigma_{1r}\rho_{1i}-\sigma_{1i}\rho_{1r}}, q_2=\frac{S_1q_1R+A_1-A_2}{S_2R}, \\ |\mu|^2 &= \frac{S_1R^2d\left[\sigma_{1i}\left(p_1^2-\frac{3}{4}\right)+2p_1\sigma_{1r}\right]}{\sigma_{1r}\rho_{1i}-\sigma_{1i}\rho_{1r}}, R^2=-\frac{A_1}{p_1S_1}, \end{aligned} \tag{29}$$

with $d\neq 0$ and $P\neq 0$. In order to further proceed, the following constraints are adopted:

$$\begin{aligned} \rho_{2r} &= \frac{S_2\left(\frac{3}{4}-p_2^2\right)(\sigma_{1r}\rho_{1i}-\sigma_{1i}\rho_{1r})}{S_1\left[\sigma_{1i}\left(p_1^2-\frac{3}{4}\right)+2p_1\sigma_{1r}\right]}-\frac{\left[\rho_{1i}\left(\frac{3}{4}-p_1^2\right)-2p_1\rho_{1r}\right]\sigma_{2r}}{\left[\sigma_{1i}\left(p_1^2-\frac{3}{4}\right)+2p_1\sigma_{1r}\right]} \\ \rho_{2i} &= \frac{2p_2S_2(\sigma_{1r}\rho_{1i}-\sigma_{1i}\rho_{1r})}{S_1\left[\sigma_{1i}\left(p_1^2-\frac{3}{4}\right)+2p_1\sigma_{1r}\right]}-\frac{\left[\rho_{1i}\left(\frac{3}{4}-p_1^2\right)-2p_1\rho_{1r}\right]\sigma_{2i}}{\left[\sigma_{1i}\left(p_1^2-\frac{3}{4}\right)+2p_1\sigma_{1r}\right]}, \\ A_2 &= \frac{p_2S_2}{p_1S_1}A_1, S_2=S_1\frac{p_2}{p_1}\left[\frac{R(12p_1^2+1)-16p_1q_1}{R(12p_2^2+1)-16p_2q_2}\right], \end{aligned} \tag{30}$$

which leads to the following solutions, giving the complex amplitude B_1 and B_2:

$$\begin{aligned} B_1(x,t) &= \frac{\frac{1}{\eta e^2}(Rx+\omega t)+i(q_1x-\Omega_1t)}{\left[1+de^{(Rx+\omega t)}+Pe^{2(Rx+\omega t)}\right]^{\left(\frac{1}{2}+ip_1\right)}}, \\ B_2(x,t) &= \frac{\mu e^{\frac{1}{2}(Rx+\omega t)+i(q_2x-\Omega_2t)}}{\left[1+de^{(Rx+\omega t)}+Pe^{2(Rx+\omega t)}\right]^{\left(\frac{1}{2}+ip_2\right)}}, \end{aligned} \tag{31}$$

with their squared norms being given by

$$|B_1(x,t)|^2=\frac{|\eta|^2\left|e^{(Rx+\omega t)}\right|}{\left|1+de^{(Rx+\omega t)}+Pe^{2(Rx+\omega t)}\right|}, \tag{32}$$

$$|B_2(x,t)|^2=\frac{|\mu|^2\left|e^{(Rx+\omega t)}\right|}{\left|1+de^{(Rx+\omega t)}+Pe^{2(Rx+\omega t)}\right|}. \tag{33}$$

The panels of Fig. 8 illustrate well the spatiotemporal evolution of such amplitudes, which represent bright-soliton amplitudes. Using Eq. (31), it is possible to rewrite the spatiotemporal formula of the voltage $V_n(t)$ given by relation (8). It describes the calcium wave propagation through the network of cellular microtubules and it is given by

$$\begin{aligned} V_n(t) &= \frac{2\varepsilon}{F}\left[\eta_rG\cos(\Phi_1)+\mu_rH\cos(\Phi_2)\right] \\ &+\frac{2\varepsilon^2\eta^2G^2F^{-1}}{\omega_1^2-\omega_0^2\sin^2(k_1)}\left[\alpha_1\omega_1^2\cos(2\Phi_1)-\frac{1}{2}\omega_1(\beta_0\alpha_1+4\beta_2\sin^2(k_1))\sin(2\Phi_1)\right] \\ &+\frac{2\varepsilon^2\mu^2H^2F^{-1}}{\omega_2^2-\omega_0^2\sin^2(k_2)}\left[\alpha_1\omega_2^2\cos(2\Phi_2)-\frac{1}{2}\omega_2(\beta_0\alpha_1+4\beta_2\sin^2(k_2))\sin(2\Phi_2)\right], \end{aligned} \tag{34}$$

where $\Phi_1=(q_1+k_1)x-(\Omega_1+\omega_1)t-p_1\ln F$ and $\Phi_2=(q_2+k_2)x-(\Omega_2+\omega_2)t-p_2\ln F$. This coupled solution comprising the two frequency modes ω_1 and ω_2 will be used as the initial condition in the next section dedicated to numerical analysis of wave propagation in the microtubule network. More precisely, at the initial time ($t=0$), the signal originating from the hydrolysis of GTP and which is to propagate along the MTs is then given in form (34). Phenomena related to wave interaction have become an attractive research direction. Applications of such are found in areas like nonlinear optics [57,58], atmospheric physics [59], hydrodynamics [60], and many more. In general, interactions of waves can give rise to radiations or generate other types of solitons, especially when other system-related factors such as management and inhomogeneities are included [57]. This can involve bright-bright or bright-dark solitons, leading to more complex and exotic structures potentially full of interest, with possible practical applications. Therefore, in view of solution (34) the reader should notice that the generalized solution has a breather form, which implies the possibility of getting modulated waves.

4.2. Ionic wave propagation and generation of wave trains

Numerical simulations are carried out in the generic discrete Eq. (5) describing the signal processing in an electrical transmission line of MTs. Obviously, Eq. (5) contains several terms and their corresponding coefficients that may significantly affect wave propagation in the model under study. Among such parameters, particular importance has been given to dissipative effects brought by the coefficients β_0 and β_1. Even at the sub-cellular level, most biological processes are sequenced by an initiation, triggered in the present case by the hydrolysis of GTP, execution, and termination, which is indubitably related to the attenuation of the propagating signal under dissipative effects. However, it should be indicated that other biological factors may contribute to amplifying the signal against dissipation to complete a given process until complete information is transported to the receiver. A failure of such, the case of neuronal microtubules, for example, may lead to a multitude of neuronal disorders such as neurodegenerative disease (Alzheimer), Parkinson's [61,62] and anxiety [63], to name a few. From the physical point of view, dissipative effects significantly modify the intrinsic dynamic equilibrium between nonlinearity and dispersion, consequently affecting the stable information and energy transport in MTs. This shows the straightforward interdependence between the structural role of MTs and their essential function in ionic signal processing at the sub-cellular level, under controlled input from dissipative elements inherent to biological environments.

The numerical study of signal transport along the MT electrical network is based on the direct integration of Eq. (5) via the well-known Runge-Kutta computational scheme, under periodic boundary conditions and a step over time, $dt=10^{-2}$ns. As said so far, the input signal is the modulated impulse of Eq. (34), over 201 lattice cells, with two coupled oscillation modes characterized by (k_1,ω_1) and (k_2,ω_2), with $k_2=\alpha k_1$. To remind, the amplitudes of individual modes, shown in Fig. 8, display bell-shaped solitary impulses. Indubitably, the coupled

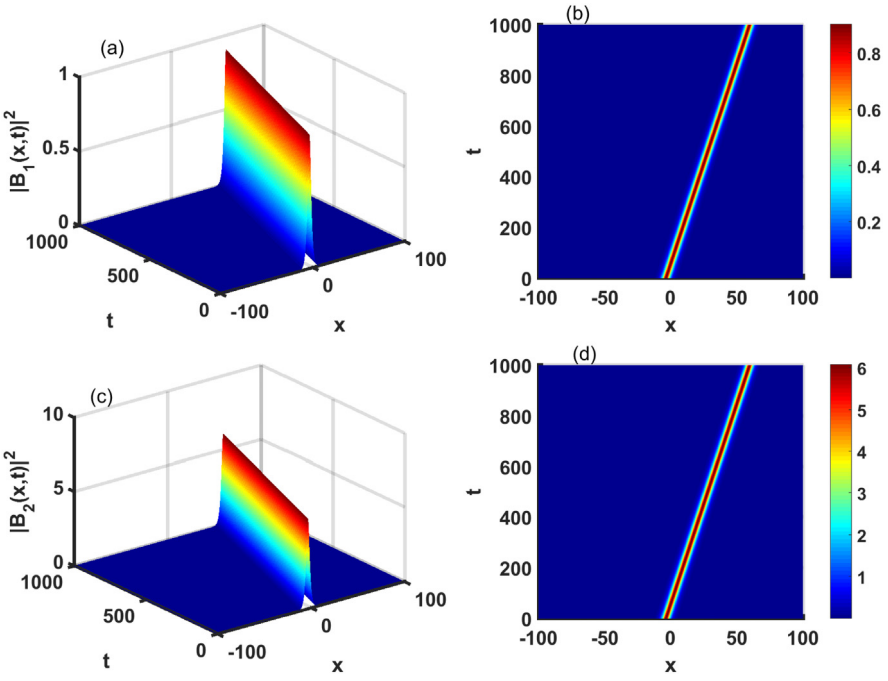

Fig. 8. Spatiotemporal evolution of pulse-soliton amplitudes [panels (a) and (b)] and [panels (c) and (d)] from Eqs. (32) and (33).

mode results in a robust envelope soliton, already known in several biological settings. In DNA dynamics, for example, coupled breather solitons were proposed to describe the initiation process of transcription [25,64,65]. Coupled breathing waves were also shown to be at the origin of angular dislocation of tubulin dimers and the transport of organelles by motor proteins along MTs [29]. The role of coupled bright soliton in neuronal networks was debated in the context of information transport and signal processing [66].

Under the conditions described above, the results for numerical simulations are shown in Fig. 9. Clearly, the panels of Fig. 9 give a comparison between the spatiotemporal evolution of the coupled solitary wave to its corresponding time series and wave profile under different values of dissipative coefficients. Obviously, in space and time, the propagation of the coupled mode gives rise to modulated trains of patterns. In panel (a1), precisely, the spectrum of behavior is such that the wave structure keeps its stable and periodic state over time and repeats the same propagation events. This assumes that localized excitations of ionic waves are accessible to the electrical network, and the corresponding localized signals present solitary modulated solutions with a regular periodic background. Spatially, the movement of the signal repeats after about 15

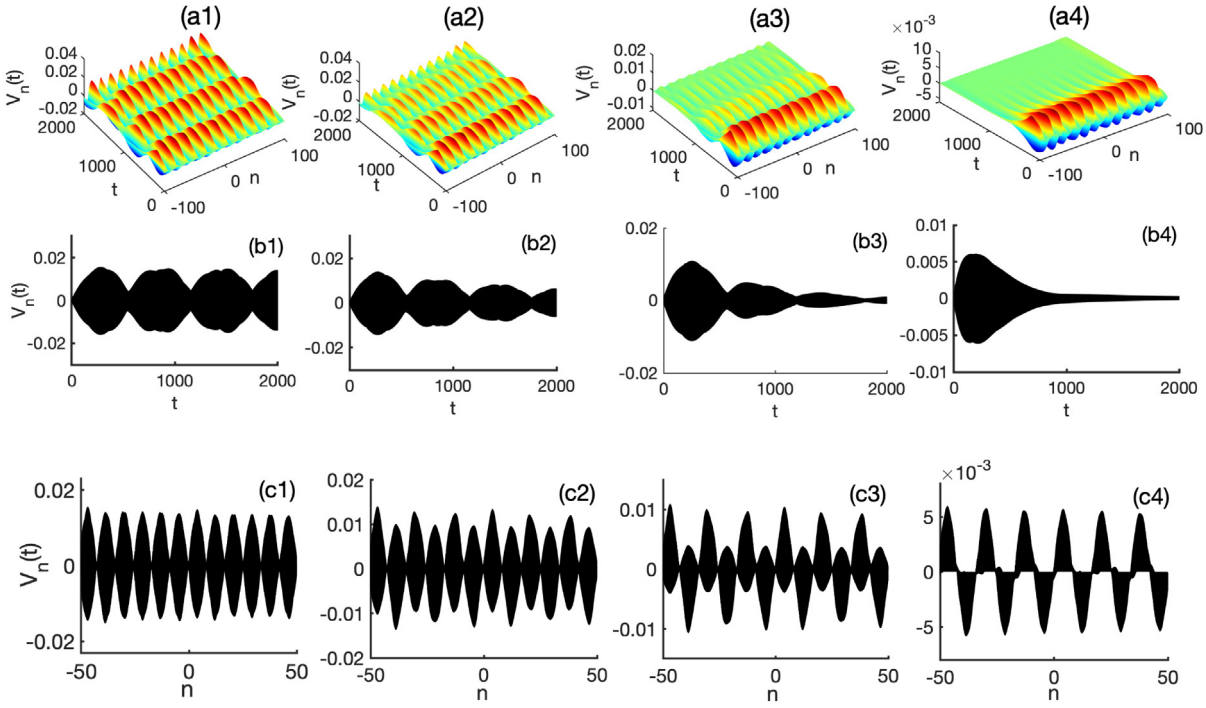

Fig. 9. Spatiotemporal evolution of the coupled solution [panels] along with their corresponding time series [panels] and spatial evolution [panels] for the parameters Moreover, from left to right, columns correspond to the respective values and of the dissipative coefficient.

unit cells of MTs, while temporally, its period is about 1300 ns materialized by two alternations. In panel (a1) of Fig. 9, tiger amplitude of oscillations can be noticed, which stands for areas where the energy carried by the voltage wave (which originates from the hydrolysis of GTP) is maximum. This corresponds to the precise moment when the signal gets more accelerated, inducing the polymerization/depolymerization phenomenon. As for the dark peaks of the signal, the energy would be minimal and would not allow a good appreciation of the desired biological phenomenon, while the moments of respite, where the voltage soliton wave is zero, would rather be those of the transition between two phases of the process under study. Additionally, there is an amplification of the excitatory signal in the network, whose profile is plotted in Fig. 9(b1). The signal propagates in the form of a train of small amplitude with a short wavelength, with each component of the train having the shape of a soliton object. This proves the robustness of the coupled-wave solutions, which corroborate predictions from the linear stability analysis of MI. One of the primary outcomes of the studied model is its sensitivity to model parameters such as dissipation, which is evident in Fig. 9(a2) and (b2). In this context, the spatiotemporal behavior of the ionic waves is still supported by coherent structures whose amplitude goes down as time increases. Interestingly, the time series of Fig. 9(b2) shows that increasing the values of β_0 considerably attenuates wave propagation and even affects the spatial distribution of the obtained patterns. Corresponding values for β_0 are such that $\beta_0 = 0.0009$ for Fig. 9 (a2), $\beta_0 = 0.003$ for the case of Fig. 9(a3) and $\beta_0 = 0.01$, which corresponds to the patterns of Fig. 9(a4). We should stress remind that in the process, we have related the value of β_1 to the one of β_0 so that the change in the latter directly affects variation in β_1. Therefore, it is noticeable that the two dissipation coefficients β_0 and β_1 have a common effect on the propagation of the envelope of coupled soliton pulses, except that the action of one, β_0, is more aggressive and quicker than that on the other, β_1, which is proportional to β_0. More precisely, increasing β_0 changes the characteristics of the wave structure more quickly. As a whole, controlling and maintaining small acceptable values of the dissipative parameters would allow good energy propagation in our biomolecular filament network. Due to the strong dissipation of the biological medium studied and to the fact that the supplied energy could suddenly be dissipated and therefore be insufficient for the MTs to perform their cellular functions optimally, the coupled solitary bursting signal would therefore be an excellent option to remedy and promote the release of a large amount of compensatory energy and which would propagate stably and permanently throughout the biological network. The energy and information transport that originates from the hydrolysis of GTP in cellular MTs would then be possible via the envelope solution of coupled voltage pulses of the soliton-type supported by the discrete model of the transmission line studied. The inherent electric nature of neurons points out the effectivity and potential functions of the MT cytoskeleton that conveys electric information. Although no direct experiment has been realized showing the evidence and contribution of MT in signal conduction in neurons, it remains scientifically verified that MT contributes importantly to higher cognitive processes, among which neuronal signal processing. A broad range of oscillatory modes has been reported recently, where Tabi and co-workers [26,27,51,52] showed that neuronal waves and action potentials might rely on frequency distribution, depending on the physiological process to be achieved. Indubitably, the transmission line elements, such as the intrinsic resistance and capacitance, play a crucial role in the spatiotemporal spreading of the wave. This is finely illustrated by the different scenarios depicted in Fig. 9$(\mathrm{cj})_{j=1,2,3,4}$, where panels from left to right correspond to increasing values of β_0, the dissipative coefficient. Importantly, such structures have been reported in many contributions as being caused by the activation of MI. Noticeably, increasing the resistance in the system contributes to generating asymmetric solitonic objects while the amplitude decreases. Although the precise mechanism is not fully clear yet [20], it may involve diffusion through the central channel [67] and ion redistribution along the microtubule resulting from the variations in cation (Na^+, K^+, Ca^{2+}) migration through nanopores along the microtubule wall [68]. In that direction, several contributions have demonstrated charge centers with corresponding counter ion clouds along the axis of the microfilament allowing ionic waves to propagate along its axis [18,19,69,70]. The described phenomenon was already reported by Cantiello et al. who further confirmed electrical signal via soliton waves [18] in actin filaments. However, against dissipation, it was shown recently that microtubules are capable of amplifying ionic signal waves [71] which may importantly contribute to the regulation of voltage-dependent anion channel in the mitochondria [72] with considerable implications in exchanges involving the extracellular matrix [73] that facilitates permanent dynamics and information exchange between the cytoskeleton and extracellular environment.

5. Conclusion

The study of nonlinear waves in excitable media is of growing interest and nowadays covers a broad range of biophysical systems, including the muscular tissues, the hearth, and the neural networks. The study carried out in this paper addresses the circumstances and the conditions under which MTs may act as nonlinear dissipative electrical transmission lines for ions to migrate through their pseudohelical cylinders. In such an electrical transmission line model, an individual tubulin dimmer protein constitutes an electric cell that comprises capacitive, inductive, and resistive components related to polyelectrolyte features of MTs in the cytosol. The important issue of multimode propagation of ionic current has been addressed using a set of nonlinearly coupled cubic CGL equations derived from the generic electrical transmission line equation through the semi-discrete approximation, each corresponding to a mode of oscillation with distinct frequencies. Thanks to the linear stability analysis of plane wave solutions, a MI growth rate expression has been proposed, from which a comprehensive parametric analysis of MI has been carried out. In the process, we have discussed the impact of dissipative elements on the parametric expansion of unstable regions, where the plane wave input is expected to break into modulated ionic waves with solitonic features. The analysis of MI has also pointed out that the behaviors of the instability windows for the model under study strongly depend on the interdependence between the two modes via their wavenumbers. Dissipation can be used as a tool to control the occurrence of MI under the combined mode. It should be noted that exact bright envelope solitons are found in the modulationally unstable domain. Confirmation of such results has been obtained via direct derivation, through the modified Hirota bilinear method, of the exact envelope solution of the coupled modes. Indeed, under direct numerical simulation, with the input signal being the found solution, the dynamics of ionic current was found to be described by nonlinear patterns of solitonic trains, with features being susceptible to changes in system parameters, mainly dissipation. Over time, dissipative coefficients have been found to impact the ionic wave amplitude under a strong background of the polarization-repolarization process. Spatially, interesting features of nonlinear wave propagation have been obtained, which justifies the diversity of oscillatory ionic movement across the MT lattice, relayed by nanopores present between neighboring tubulin dimers, through which K^+ and Na^+ ions can easily migrate in the microtubule wall. In the process, a higher free energy barrier prevents Ca^{2+} ions from migrating, and an increase in the Ca^{2+} concentration outside the MT during neuronal excitation will cause K^+ and Na^+ ions to be driven into the MT, leading to ion redistribution throughout the MT. Such valuable electrical properties, relying on the ion-permeability of MTs, may be beneficial to neural signal processing and the key energy transport process along the MT lattice, given the straightforward relationship between ionic transport and lattice deformation for specific biological functions of MTs to be fulfilled under normal physiological conditions. The idea that MTs can play the role of complex subcellular nanowires remains an open question as it has recently drawn

considerable attention. To the best of our knowledge, suitable models, in that regard, have not been sufficiently explored and constitute a serious concern about the possible efficient charge carriers and their robustness under dissipative effects. We, however, believe that ion flows and permeability may relay communication of cellular information to the nucleus as an instant response to high centration Ca^{2+} pulse.

CRediT authorship contribution statement

E. Tankou: Conceptualization, Methodology, Software C. B. Tabi: Conceptualization, Data curation, Writing- Original draft preparation, Visualization, Investigation. T. C. Kofane: Supervision, Writing-Reviewing, Editing, Validation.

Data availability

Data will be made available on request.

Declaration of competing interest

The authors of the manuscript "Soliton-mediated ionic pulses and coupled ionic excitations in a dissipative electrical network model of microtubules", certify that they have NO affiliations with or involvement in any organization or entity with any financial interest (such as honoraria; educational grants; participation in speakers' bureaus; membership, employment, consultancies, stock ownership, or other equity interest; and expert testimony or patent-licensing arrangements), or non-financial interest (such as personal or professional relationships, affiliations, knowledge or beliefs) in the subject matter or materials discussed in this manuscript.

Acknowledgements

CBT thanks the Kavli Institute for Theoretical Physics (KITP), University of California Santa Barbara (USA), where this work was supported in part by the National Science Foundation Grant no. NSF PHY-1748958, NIH Grant no. R25GM067110, and the Gordon and Betty Moore Foundation Grant no. 2919.01.

Appendix A. Coefficients of the coupled cubic CGL Eqs. (13) and (16)

$$S_1=\frac{{V_{g1}}^2-\omega_0^2\cos(k_1)}{2\omega_1},S_2=\frac{{V_{g1}}^2-\omega_0^2\cos(k_2)}{2\omega_2},$$
$$A_1=-\frac{1}{2}\left(\beta_0+4\beta_3\sin^2\left(\frac{k_1}{2}\right)\right),\quad A_2=-\frac{1}{2}\left(\beta_0+4\beta_3\sin^2\left(\frac{k_2}{2}\right)\right), \tag{A.35}$$
$$\sigma_1=\sigma_{1r}+i\sigma_{1i},\sigma_2=\sigma_{2r}+i\sigma_{2i},\rho_1=\rho_{1r}+i\rho_{1i},\quad \rho_2=\rho_{2r}+i\rho_{2i},$$

$$\sigma_{1r}=\frac{3}{2}\omega_1\left[\alpha_2+\frac{2\alpha_1^2\omega_1^2-\left(\alpha_1\beta_0+4\beta_2\sin^2\left(\frac{k_1}{2}\right)\right)(\alpha_1\beta_0+4\beta_2\sin^2(k_1))}{3\left(\omega_1^2-\omega_0^2\sin^2\left(\frac{k_1}{2}\right)\right)}\right],$$

$$\sigma_{1i}=\frac{3}{2}\left[\alpha_2\beta_0+4\beta_3\sin^2\left(\frac{k_1}{2}\right)+\frac{3\alpha_1^2\omega_1^2\beta_0+4\alpha_1\beta_2\omega_1^2\left(\sin^2(k_1)+2\sin^2\left(\frac{k_1}{2}\right)\right)}{3\left(\omega_1^2-\omega_0^2\sin^2\left(\frac{k_1}{2}\right)\right)}\right],$$

$$\sigma_{2r}=\frac{3}{2}\omega_2\left[\alpha_2+\frac{2\alpha_1^2\omega_2^2-\left(\alpha_1\beta_0+4\beta_2\sin^2\left(\frac{k_2}{2}\right)\right)(\alpha_1\beta_0+4\beta_2\sin^2(k_2))}{3\left(\omega_2^2-\omega_0^2\sin^2\left(\frac{k_2}{2}\right)\right)}\right],$$

$$\sigma_{2i}=\frac{3}{2}\left[\alpha_2\beta_0+4\beta_3\sin^2\left(\frac{k_2}{2}\right)+\frac{3\alpha_1^2\omega_2^2\beta_0+4\alpha_1\beta_2\omega_2^2\left(\sin^2(k_2)+2\sin^2\left(\frac{k_2}{2}\right)\right)}{3\left(\omega_2^2-\omega_0^2\sin^2\left(\frac{k_2}{2}\right)\right)}\right],$$

$$\rho_{1r}=2\alpha_2\omega_1,\rho_{1i}=3\left(\alpha_2\beta_0+4\beta_3\sin^2\left(\frac{k_1}{2}\right)\right),\rho_{2r}=2\alpha_2\omega_2,\rho_{2i}=3\left(\alpha_2\beta_0+4\beta_3\sin^2\left(\frac{k_2}{2}\right)\right). \tag{A.36}$$

Appendix B. Matrix elements for system (20)

The matrix Q_{pm}, with $p,m=1,2,3,4$, are given by

$$\begin{aligned}
Q_{11}&=S_1\lambda^2-\sigma_1|B_{10}|^2,\quad Q_{13}=-\rho_1|B_{20}|^2,\quad Q_{22}=S_1\lambda^2-\sigma_1^*|B_{10}|^2,\\
Q_{21}&=Q_{23}=Q_{12}=Q_{14}=Q_{32}=Q_{34}=Q_{41}=Q_{43}=0,\\
Q_{24}&=-\rho_1^*|B_{20}|^2,\quad Q_{31}=-\rho_2|B_{10}|^2,\\
Q_{33}&=S_2\lambda^2-\sigma_2|B_{20}|^2,\quad Q_{42}=-\sigma_2^*|B_{20}|^2,\quad Q_{44}=S_2\lambda^2-\sigma_2^*|B_{20}|^2.
\end{aligned} \tag{A.37}$$

References

[1] Avila J. Microtubule proteins. 1st Ed. Taylor and Francis Group; 1990.
[2] Wijeratne SS, Marchan MF, Tresback JS, Subramanian R. PNAS. 2022.;119: e2115708119.
[3] Nasrin SR, Ganser C, Nishikawa S, Sada K, Yamashita T, Ikeguchi M, Uchihashi T, Hess H, Kakugo A, Kabir AMdR. Sci Adv. 2021.;7:eabf2211.
[4] Gui M, Wang X, Dutcher SK, Brown A, Zhang R. Nat Struct Mol Biol. 2022;29:483.
[5] Satarić MV, Tuszynski JA, Hameroff S, Žakula RB. Neural Netw World. 1994;4:281.
[6] Tuszynski JA, Hameroff S, Satarić MV, Trpisová B, Nip MLA. J Theor Biol. 1995;174: 371.
[7] Tuszynski JA, Trpisová B, Sept D. Neural Netw World. 1995;5:675.
[8] Alberts B, Bray D, Lewis J, Raff M, Roberts K, Watson JD. New York - London: Garland Publishing; 1994.
[9] Caplow M, Ruhlen RL, Shanks J. J Cell Biol. 1994;127:779.
[10] Tang D, Goldberg DJ. Mol Cell Neurosci. 2000;15:303.
[11] Yu W, Ling C, Baas PW. J Neurocytol. 2001;30:861.
[12] Dehmelt L, Smart FM, Ozer RS, Halpain S. J Neurosci. 2003;23:9479.
[13] Craig AM, Wyborski RJ, Banker G. Nature. 1995;375:592.
[14] Dai J, Sheetz MP. Biophys J. 1995;68:988.
[15] Kaech S, Parmar H, Roelandse M, Bornmann C, Matus A. Proc Natl Acad Sci U S A. 2001;98:7086.
[16] Woolf NJ, Zinnerman MD, Johnson GVW. Brain Res. 1999;821:241.
[17] Johnson BD, Byerly L. Pfugers arch. Eur J Physiol. 1994;439:14.
[18] Lin E, Cantiello H. Biophys J. 1993;65:1371.
[19] Tuszynski JA, Portet S, Dixon JM, Luxford C, Cantiello HF. Biophys J. 2004;86:1890.
[20] Satarić MV, Ilić DI, Ralević N, Tuszynski JA. Eur Biophys J. 2009;38:637.
[21] Satarić MV, Tuszynski JA, Zakula RB. Phys Rev E. 1993;48:589.
[22] Trpisova B, Tuszynski JA. Phys Rev E. 1997;55:3288.
[23] Priel A, Ramos JA, Tuszynski JA, Cantiello HF. Biophys J. 2006;90:4639.
[24] Ii Ndzana F, Mohamadou A. Chaos. 2019.;29:013116.
[25] Tabi CB, Ekobena HP, Mohamadou A, Kofané TC. Phys Scr. 2011.;83:035802.
[26] Tabi CB, Etémé AS, Mohamadou A. Physica A. 2017;474:186.
[27] Etémé AS, Tabi CB, Mohamadou A. Chaos Solitons Fractals. 2017;104:813.
[28] del Rocío Cantero M, Villa Etchegoyen C, Perez PL, Scarinci N, Cantiello HF. Sci Rep. 2018;8:11899.
[29] Tabi CB, Tankou E, Mohamadou A. Chaos Solit Fract. 2017;95:187.
[30] Tabi CB, Etémé AS, Kofané TC. Nonlinear Dyn. 2020;100:3799.
[31] Okaly JB, Mvogo A, Tabi CB, Ekobena Fouda HP, Kofané TC. Phys Rev E. 2020.;102: 062402.
[32] Kourakis I, Shukla PK, Morfill G. New J Phys. 2005;7:153.
[33] Kengne E, Abdourahman ALakhssassi. Chin J Phys. 2020;63:271.
[34] Yemélé D, Kofané TC. J Phys D. 2006;39:4504.
[35] Kofané TC, Zebaze M, Zibi A. J Phys D Appl Phys. 1990;23:764.
[36] Otlaadisa P, Tabi CB, Kofané TC. Phys Rev E. 2021.;103:052206.
[37] Tabi CB, Veni S, Kofané TC. Phys Lett A. 2022.;442:128192.
[38] Ndebele KK, Tabi CB, Kofané TC. J Opt Soc Am B. 2020.;37:A214.
[39] Djazet A, Tabi CB, Fewo SI, Kofané TC. Appl Phys B: Lasers Optics. 2020;126:74.
[40] Djazet A, Fewo SI, Tabi CB, Kofané TC. Appl Phys B: Lasers Optics. 2021;127:151.
[41] Abemgnigni Njifon M, Tabi CB, Kofané TC. J Opt Soc Am B. 2020.;37:A331.
[42] Megne Tiam L, Tabi CB, Kofané TC. Phys Rev E. 2020.;102:042207.
[43] Zanga D, Fewo SI, Tabi CB, Kofané TC. Phys Rev A. 2022.;105:023502.
[44] Ndjomatchoua FT, Tchawoua C, Kakmeni FMM, Le Ru BP, Tonnang Henri EZ. Chaos. 2016.;26:053111.
[45] Guemkam Ghomsi P, Tameh Berinyoh JT, Moukam Kakmeni FM. Chaos. 2018.;28: 023106.
[46] Ndebele KK, Tabi CB, Tiofack Latchio CG, Kofané TC. Phys Rev E. 2021.;104:044208.
[47] Akhmediev N, Soto-Crespo JM, Town G. Phys Rev E. 2001.;63:056602.
[48] Soto-Crespo JM, Akhmediev N. Phys Rev Lett. 2005.;95:024101.
[49] Weber A, Kramer L, Aranson IS, Aranson L. Phys D. 1992;61:279.
[50] Tabi CB, Etémé AS, Mohamadou A, Kofané TC. Waves Rand Compl Media. 2019;31: 1028.
[51] Etémé CBTabi, Mohamadou A. Commun Nonl Sci Numer Simul. 2019;72:432.
[52] Tabi CB, Etémé AS, Mohamadou A, Kofané TC. Chaos Solit Fract. 2019;123:116.
[53] Guo Y-J, Shan W-R, Yi Gao X. Appl Math Lett. 2021.;120:107161.
[54] Gao X-Yi, Guo Y-J, Shan W-R. Eur Phys J Plus. 2021;136:893.
[55] Gao X-Yi, Guo Y-J, Shan W-R. Chaos Solit Fract. 2021.;150:111066.
[56] Zakeri GA, Yomba E. J Phys Jpn. 2013.;82:084002.
[57] Yang D-Yu, Tian Bo, Zhang C-R, Chen Su-Su, Wei C-C. Chaos Solit Fract. 2021.;150: 110487.

[58] Wang M, Tian B, Hu C-C, Liu S-H. Appl Math Lett. 2021.;119:106936.
[59] Shen Y, Tian B. Appl Math Lett. 2021.;122:107301.
[60] Gao X-T, Tian B, Shen Y, Feng C-H. Chaos Soliton Fractals. 2021.;151:111222.
[61] Gabor D. J Inst Electr Eng. 1946;93:429.
[62] Boashash B. Proc IEEE. 1992;80:520.
[63] Berman JI, McDaniel J, Liu S, Cornew L, Gaetz W, Roberts TP, Edgar JC. Brain Connect. 2012;2:155.
[64] Tabi CB, Mohamadou A, Kofané TC. Eur Phys J D. 2008;50:307.
[65] Tabi CB, Ekobena HP, Kofané TC. J Comput Theor Nanosci. 2011;8:2220.
[66] Nfor NO, Ghomsi PG, Moukam Kakmeni FM. Phys Rev E. 2018.;97:022214.
[67] Odde D. Eur Biophys J. 1998;27:514.
[68] Shen C, Guo W. J Phys Chem Lett. 2018;9:2009.
[69] Patolsky F, Weizmann Y, Willner I. Nat Mater. 2004;3:692.
[70] Hunley C, Uribe D, Marucho M. RSC Adv. 2018;8:12017.
[71] Priel A, Tuszynski JA. Europhys Lett. 2008;83:68004.
[72] Rostovtseva TK, Bezrukov SM. Biochim Biophys Acta. 2012;1818:1526.
[73] Putnam AJ, Schultz K, Mooney DJ. Am J Physiol Cell Physiol. 2001;280:C556.

Chaos, Solitons and Fractals 181 (2024) 114717

Contents lists available at ScienceDirect

Chaos, Solitons and Fractals

journal homepage: www.elsevier.com/locate/chaos

Transport memory effects on coupled nonlinear waves in microtubule dynamics

Eric Tankou [a,b], Conrad Bertrand Tabi [c,*], Alidou Mohamadou [d], Timoléon Crépin Kofané [c,e]

[a] Laboratory of Biophysics, Department of Physics, Faculty of Science, University of Yaoundé I, P.O. Box 812, Yaoundé, Cameroon
[b] African Centre for Advanced Studies, P.O. Box 4477, Yaounde, Cameroon
[c] Department of Physics and Astronomy, Botswana International University of Science and Technology, Private Mail Bag 16 Palapye, Botswana
[d] National Advanced School of Engineering of Maroua, University of Maroua, P.O. Box 46, Maroua, Cameroon
[e] Laboratory of Mechanics, Department of Physics, Faculty of Science, University of Yaoundé I, P.O. Box 812, Yaoundé, Cameroon

ARTICLE INFO

Keywords:
Nonlinear dynamics
Solitons
Noise
Non equilibrium and quantum processes

ABSTRACT

The paper examines how microtubules (MTs) function in their biological environment, focusing on soliton-breather solutions. These solutions are nonlinear localized excitations that propagate in an angular continuous model of microtubule dynamics. Our model considers competitive effects from transport memory and nonlinearity, which arise due to collisions between tubulin dimers and particulate entities during energy processing in eukaryotic cells due to the hydrolysis of guanosine triphosphate (GTP). Our mathematical approach determines that the angular displacement of a dimer is governed by a modified system of coupled complex nonlinear Schrödinger equations. Analytical solutions are obtained and propagated in the MT lattice through direct numerical simulations, and small variations in coefficients significantly impact energy processing in cytoplasmic MTs.

1. Introduction

In the field of nonlinear science, biological systems are highly valued for their complex nature, both on small and large scales. These systems are typically comprised of vast networks of interconnected biochemical units, known as cells. Cells serve as the foundational building blocks for biological systems, with their structure being key to understanding their function. Specifically, cells consist of a component called the cytoplasm, which is primarily made up of water molecules (roughly 80 per cent). Additionally, eukaryotic cells' cytoplasm contains various protein structures, such as microtubules (MTs). MTs are a crucial component of the cytoskeleton, with a well-known structure that has been extensively studied [1–4]. They are formed by the lateral assembly of protofilaments (PFs), which themselves are composed of dimers of $\alpha-$ and β-tubulins. MTs play a vital role in several essential cellular activities, including material transport, cell motility, cell division, signal transduction, and information processing in nerve cell axons [5–7]. Observations conducted both in vivo and in vitro have confirmed that individual MTs can switch stochastically between assembly and disassembly states, making them highly dynamic structures [8]. It is believed that movements of the MT molecules result from an energetic excitation resulting from the hydrolysis of guanosine triphosphate (GTP) bound to $\beta-$tubulin, which converts it to guanosine diphosphate (GDP) [8]. Numerous models and techniques have been proposed to describe the nonlinear properties of MTs in their cellular environment [9–12]. Comprehending the function of MTs is a significant challenge for molecular biology and nonlinear science. This includes polymerization/depolymerization processes, intracellular transport, and axonal transduction of MTs is crucial. Previous studies have accounted for the low friction between dimers and water molecules in their models. However, the cytoplasmic medium contains other micro-entities that may significantly restrict the movement of MTs. Tabi and colleagues [13] have recently introduced a new approach to explain the dynamical behaviors of MTs. Taking advantage of the φ-angular model proposed in Ref. [14], two modes of excitation were extracted to highlight the coexistence of minimum and maximum cut-off modes excitations. It was additionally suggested that without sufficient energy from GTP hydrolysis, there would be no dislocation of the tubulin dimers. To initiate a strong dislocation, coupled waves could potentially stimulate the required energy, leading to the polymerization/depolymerization mechanism [13]. The initial study on wave coupling along the MTs may have overlooked the impact of frictional effects. However, following the suggestion by Kovacs [15], friction

* Corresponding author.
E-mail addresses: etankou2000@yahoo.fr (E. Tankou), tabic@biust.ac.bw (C.B. Tabi), mohdoufr@yahoo.fr (A. Mohamadou), tckofane@yahoo.com (T.C. Kofané).

https://doi.org/10.1016/j.chaos.2024.114717
Received 13 November 2023; Received in revised form 10 February 2024; Accepted 7 March 2024
Available online 13 March 2024
0960-0779/

surfaces without lubrication may indeed lead to the memory effect. Additionally, experimental studies by Dillavou et al. [16] have shown that intense friction during the collision of two bodies can also produce some memory effects. These findings suggest that frictional effects should not be ignored when considering wave coupling along the MTs. The frictional force may depend on two states of the contact surface: the present state and the state that led to it. Research physicists have made interesting observations on how to characterize viscosity and frictional forces, which can be applied to many physical systems. For instance, in the study of DNA nonlinear dynamics [17], frictional forces exist between nucleotides and solvent particles. Similarly, we believe that frictional forces are present during MT dynamics, particularly at the interfaces between tubulin dimers due to micro entities from the cytoplasmic cytosol.

Our main objective is to show that incorporating viscous forces and transport memory effects brings about new features to the vibrational dynamics of MTs in the context of coupled signal propagation. By doing so, we anticipate that the memory effects will have a significant impact on the parameters of the improved angular model. This will enable a better explanation of the movements of dimers in living cells. Energy transport along the MTs plays a significant role in regulating the cellular functions of these proteins. It is suggested that solitons are ideal for monitoring the development of biophysical or biological systems due to their nonlinear and dispersive nature [18–20]. Solitons have been observed in various biological processes, including DNA [20,21], hemodynamics [22], and energy transport within proteins [23]. In the realm of MTs, kink, pulse, and breather solitons have been theorized to further explain the transfer of chemical energy from GTP hydrolysis [9,10,12,24,25]. These solutions are typically described by simplified nonlinear Schrödinger (NLS) equations with real or complex coefficients (known as Ginzburg–Landau equations) derived from the specific models being studied [9,10,12,26]. In contrast, a study by Tabi et al. [13] found that a system of NLS equations without viscosity effects can support the emergence of kink envelopes. By adding memory effects to the φ-angular model, we were able to develop a new solution with two breather-type solitons sustained by a system of coupled complex nonlinear Schrödinger (CCNLS) equations. It should be noted that pulse soliton solutions of the complex nonlinear Schrödinger (CNLS) or complex Ginzburg–Landau (CGL) equations are of great interest in various fields of physics, including nonlinear optics, Bose–Einstein condensates, hydrodynamics, and reaction–diffusion systems [27–40]. However, extensive reviews indicate that the simplest CGL equation with cubic nonlinearity produces unstable breather or pulse-like analytical solutions [41]. Nevertheless, stable localized soliton solutions can be achieved by introducing a cubic–quintic nonlinearity [42] to the simplest CGL equation with cubic nonlinearity or by linearly coupling the CGL equation with cubic nonlinearity to an additional equation that is predominantly influenced by linear loss [43,44]. We have considered previous contributions and believe that a CCNLSE system can produce solutions such as coupled breathers and multi-breather solitons. These results provide valuable insights into microtubular conformational dynamics within eukaryotic cells. It is crucial to determine the conditions necessary for solitary wave propagation and understand the normal functioning of MTs in their biological environment. Therefore, our primary goal in this paper is to study the impact of transport memory effects and the coupled solution from the angular model introduced in Ref. [14] on the system.

The rest of the paper is organized as follows. In Section 2, a detailed overview of the model is given. The discrete Hamiltonian of the system is introduced from which a differential–difference equation is derived and further reduced to its corresponding continuous version. After incorporating the memory effects in Section 3, we use the derivative-expansion method [45,46] in Section 4 to show that the dynamics of coupled modes in the MT is governed by a set of CCNLS equations. In Section 5, analytical soliton solutions corresponding to the single and coupled vibrational modes are derived under suitable parametric conditions. Numerical experiments are also carried out to assess the stability of the proposed solutions as they propagate in the MT network. Finally, Section 6 gives some concluding remarks.

2. φ-angular model with memory effect

The structure of MTs is well known [2]. They are lateral assemblies of PFs forming hollow cylinders. PFs are designed by series of proteins known as tubulin dimers and are usually 13 in number in a single MT [1]. Due to the α and β ends of the tubulin dimer with physiologically respective negative and positive charges, each dimer has the character of an electrical dipole with dimensions ℓ and the distance between the two opposite charges $d = 4$ nm [25]. A longitudinal component of the electrical dipole moment of the dimer is $p = 337$ Debye [47]. This model, called φ-model, has the particularity of suitably taking into account interactions between the dimers of different PFs. These interactions are introduced into a resulting electric field created by the set of dipoles [14]. The model itself assumes a single radial degree of freedom where the main coordinate φ is an angular displacement in the radial direction of the dimer relative to the direction of the resultant electric field [10]. The dipole energy from a dimer and the other energy components lead to the following Hamiltonian for a single protein PF [14] :

$$H = \sum_n \left[\frac{I}{2}\left(\frac{d\varphi_n}{dt}\right)^2 + \frac{k}{2}\left(\varphi_n - \varphi_{n+1}\right)^2 - pE\cos\varphi_n \right], \tag{1}$$

where I is the moment of inertia of the single tubulin dimer, and k is the parameter characterizing the dimer-dimer interaction of the same protofilament. As in the physiological geometry of MTs, the two subunits, $\alpha-$ and $\beta-$ tubulins confer the dipole character to the dimer. E represents the resulting electric field between a selected dimer and the neighboring PFs. From left to right in Hamiltonian (1), the first and second terms, respectively, represent the kinetic energy of a dimer and the interaction energy between adjacent dimers of the same PF, while the third term is the dipole energy of the dimer. The parameter values for the proposed model are: $m = 1.08\times10^5$ amu [48], $k = 10$ eV. nm^{-2} [14], $E = 1.06\times10^{26}$ eV C^{-1} m^{-1} [10] and $I = \frac{5m\ell^2}{16}$ [49]. Using Hamilton's equations one obtains the discrete equation of motion of a tubulin dimer:

$$I\frac{d^2\varphi_n}{dt^2} - k\left(\varphi_{n+1} + \varphi_{n-1} - 2\varphi_n\right) + pE\sin\varphi_n = 0. \tag{2}$$

Eq. (2) describes the dynamics of the dimer at position n in the presence of the damping brought by the MT surroundings and the effect of certain biological micro entities on the movement of the dimers. Taking into account such effects may result in the single damping term $M_\Gamma = -\Gamma\frac{d\varphi_n}{dt}$, where Γ represents the damping coefficient or viscosity. The dynamics of the dimers at the nth site then takes the form

$$I\frac{d^2\varphi_n}{dt^2} - k\left(\varphi_{n+1} + \varphi_{n-1} - 2\varphi_n\right) + pE\sin\varphi_n = M_\Gamma. \tag{3}$$

As most biological phenomena undergo nonlinear dynamics that are difficult to interpret, but around equilibrium positions, we assumed that tubulin dimers have an anharmonic oscillatory motion around the stable equilibrium points of a two-well potential, usually written as $V_0(\varphi_n) = \frac{\varphi_n^4}{4}A_2^{(1)} - \frac{\varphi_n^2}{2}A_1^{(1)}$ with $A_2^{(1)} > 0$ and $A_1^{(1)} > 0$. This implies a series expansion of the sine term up to the fourth order so that Eq. (3) becomes

$$\begin{aligned} &I\frac{d^2\varphi_n}{dt^2} - k\left(\varphi_{n+1} + \varphi_{n-1} - 2\varphi_n\right) \\ &\quad + pE\left(\varphi_n - \frac{\varphi_n^3}{6}\right) = -\Gamma\frac{d\varphi_n}{dt}. \end{aligned} \tag{4}$$

From the fact that tubulin dimers are very dense along microtubular PFs and have an inter-dimer distance of the order of nanometers, it is possible to switch to the continuum limit approximation of the model equation. In doing so, we assume that $n\ell \to x$ and $\varphi_n(t) \to \varphi(x,t)$, with $\ell = 8$ nm (the interval between two dimers of the same protofilament). The use of the generalized coordinate $\varphi(x,t) = \varphi$ and the Taylor's expansion of the discrete terms φ_{n+1} and φ_{n-1}, i.e.,

$$\varphi_{n\pm1} \to \varphi \pm \ell\frac{\partial\varphi}{\partial x} + \frac{\ell^2}{2}\frac{\partial^2\varphi}{\partial x^2} \pm \frac{\ell^3}{3!}\frac{\partial^3\varphi}{\partial x^3} + \cdots,$$

in Eq. (4), lead to the continuous second-order partial differential equation

$$I\frac{\partial^2\varphi}{\partial t^2} - k\ell^2\frac{\partial^2\varphi}{\partial x^2} + pE\left(\varphi - \frac{\varphi^3}{6}\right) = -\Gamma\frac{\partial\varphi}{\partial t}. \tag{5}$$

Biological systems are affected by solvent molecules like water, which results in low viscosity. Other micro-entities, such as small biological particles, have high damping rates that can cause a significant impact on the movement of MTs. It is important to mention that the viscosity coefficient Γ is a parameter that allows us to quantify and control the degree of damping in the system. It should also be noted that the motion of damped systems, according to several investigations, may induce memory effects as comprehensively demonstrated in the rest of this paper.

3. Dynamics of tubulin dimers with memory effect

To describe mathematically the supposedly highly damped movement of MTs, consisting of tubulin dimers in the cell cytoplasm, Eq. (5) undergoes a series of transformations with the involvement of rescaled time and space variables. Thus, we have from Eq. (5) the following relationship

$$\frac{\partial^2\varphi}{\partial t^2} + \frac{\Gamma}{I}\frac{\partial\varphi}{\partial t} = r_1\frac{\partial^2 v}{\partial x^2} - \frac{pE}{I}\left(\varphi - \frac{1}{6}\varphi^3\right), \tag{6}$$

with $r_1 = \frac{k\ell^2}{I}$ and $\omega_0^2 = \frac{pE}{I}$. From the rescaled variables

$$t \to \frac{\omega_0^2 I}{\Gamma}t \quad \text{and} \quad x \to \left(\frac{\omega_0^2}{r_1}\right)^{\frac{1}{2}}x,$$

Eq. (6) can be rewritten in the form

$$e\frac{\partial^2\varphi}{\partial t^2} + \frac{\partial\varphi}{\partial t} = \frac{\partial^2\varphi}{\partial x^2} - \varphi + \frac{1}{6}\varphi^3, \tag{7}$$

where $e = \omega_0^2 I^2/\Gamma^2$. The expression relating the parameter e to the others in the model shows that as the viscosity coefficient increases the value of e decreases. Therefore, at the strongly damped limit ($\Gamma \to \infty$), e must tend to zero, under such considerations, Eq. (7) reduces to

$$\frac{\partial\varphi}{\partial t} = \frac{\partial^2\varphi}{\partial x^2} - \varphi + \frac{1}{6}\varphi^3, \tag{8}$$

which represents the equation for the dynamics of a dimer in a highly damped environment without transport memory effects. In this work, we consider the effect due to the high viscosity of the cell cytoplasm in which the frictional forces interact with other forces when moving the MT protein PFs.

Among the frictional forces mentioned, those describing strong interactions between particles will induce memory effects on the behavior of the MT system under study [50]. In the context of DNA dynamics, memory effects have been considered to model the vibrational behavior of the DNA molecule in its biological environment [16]. The memory effects have been explained with advanced mathematical and computational techniques [51]. As the fractional parameter gets closer to 1, the behavior of a biological system at a particular point becomes less dependent on its previous point. However, for a small order (close to 0), the memory phenomenon becomes more noticeable and pronounced [52]. On the other hand, these memory effects were exclusively used in the Newtonian equations of motion of a strongly damped particle [53]. More recently, Guimfack et al. [54] investigated the stochastic response of fractional-order generalized biorhythmic Van der Pol oscillator subjected to delayed feedback displacement and Gaussian white noise excitation. This allowed them to bring more insights into understanding memory effects in biological systems, which is intrinsically related to introducing fractional-order derivatives, along with some inherent fluctuations that can be materialized by considering noise effects. In their work, Okaly et al. [17] also introduced memory effects directly into the Peyrard–Bishop–Dauxois model describing the propagation of nonlinear waves in DNA dynamics. They showed that transport memory effects on the dynamics of base pairs could allow physiological control of the amount of energy required to break the hydrogen bonds between the bases that make up the molecule. Following a similar procedure, we introduce transport memory by reformulating Eq. (8) in the following non-local form:

$$\frac{\partial\varphi}{\partial t} = \int_0^t f(t-\tau)\frac{\partial^2\varphi}{\partial x^2}d\tau - \eta\left(\varphi - \frac{1}{6}\varphi^3\right), \tag{9}$$

where η is a constant known as the quadratic growth rate. It accounts for the degree of nonlinearity of the system. $f(t) = \gamma e^{-\gamma t}$ is the transport memory function, which describes the finite nature of the diffusion or inverse diffusion time [55,56]. The diffusion time is the ratio $1/\gamma$, while for the inverse diffusion is simply γ. As the system is not purely diffusive, the function defining the transport memory decreases with finite time. Thus the decay in time indicates the time between different diffusion events [57].

The propagation equation for the rational and modulated excitations of a constant velocity particle in a medium is related to its diffusive incoherent motion by the intermediate Eq. (9). A decay characterizes the diffusion equation in the extreme limits of the parameter γ, with on one side γ tending towards zero and to infinity on the other. Note here that as a function of the time diffusion, with the constant γ taken arbitrarily, Eq. (9) describes an oscillatory motion for very small times, and when the time becomes large, the motion decreases. The continuous integral symbol present in this intermediate Eq. (9) makes it difficult to use. Thus the general mathematical rule of calculation given by [58]

$$\begin{aligned} I\frac{\partial}{\partial t}\left[\int_{b_1(t)}^{b_2(t)} f(t,\tau)\cdot h(x,\tau)d\tau\right] &= \\ \frac{\partial b_2(t)}{\partial t}\left[f\left(t,b_2(t)\right)\cdot h(x,(b_2(t)))\right] &\\ -\frac{\partial b_1(t)}{\partial t}\left[f\left(t,b_1(t)\right)\cdot h(x,(b_1(t)))\right] &\\ + \int_{b_1(t)}^{b_2(t)}\frac{\partial f(t)}{\partial t}h(x,\tau)d\tau, & \end{aligned} \tag{10}$$

is used in differentiation to obtain the equation of the motion for the tubulin dimers in their environment with memory effect and is easily solvable. By differentiating Eq. (9) in time, we obtain the following result:

$$\frac{\partial^2\varphi}{\partial t^2} = \frac{\partial}{\partial t}\left[\int_0^t f(t-\tau)\frac{\partial^2\varphi}{\partial x^2}d\tau\right] + \eta\left(1 - \frac{\varphi^2}{2}\right)\frac{\partial\varphi}{\partial t}. \tag{11}$$

From Eq. (10) we can consider

$$\frac{\partial}{\partial t}\left[\int_0^t f(t-\tau)\frac{\partial^2\varphi}{\partial x^2}d\tau\right] = \frac{\partial}{\partial t}\left[\int_{b_1(t)}^{b_2(t)} f(t,\tau)\,h(x,\tau)d\tau\right], \tag{12}$$

where, by identification, we find the expressions of some inherent functions as follows:

$$\begin{aligned} &b_1(t) = 0, \quad b_2(t) = t, \quad h(x,\tau) = \frac{\partial^2\varphi}{\partial x^2}, \\ &f(t,\tau) = f(t-\tau) = \gamma e^{-\gamma(t-\tau)}. \end{aligned} \tag{13}$$

Using the previous functions in Eqs. (12) and (13) with the application of Eq. (10) into the differentiation of Eq. (11) leads to the crucial equation of motion

$$\begin{aligned} &\frac{\partial^2\varphi}{\partial t^2} + \left(\gamma + \eta - \frac{\eta}{2}\varphi^2\right)\frac{\partial\varphi}{\partial t} \\ &= \gamma\frac{\partial^2\varphi}{\partial x^2} - \eta\gamma\left(\varphi - \frac{\varphi^3}{6}\right), \end{aligned} \tag{14}$$

which represents a second-order differential equation whose solutions explain the dynamics of MTs in the cytoplasm of eukaryotic cells with transport memory effects. In Eq. (14), the term $\left(\gamma + \eta - \frac{\eta}{2}\varphi^2\right)\frac{\partial\varphi}{\partial t}$ accounts for the damping of tubulin dimers as they move through the cell

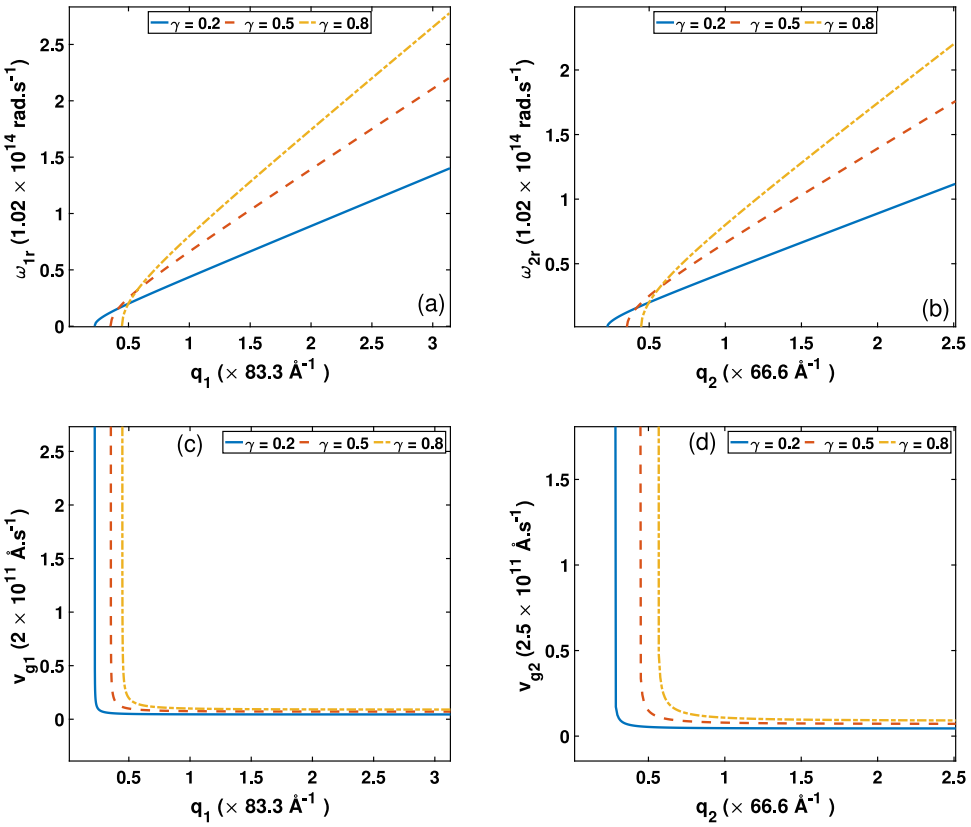

Fig. 1. Representative curves of the real part of the angular pulsation and group velocity of the wave as a function of the wavenumbers q(q_1 and q_2) for $q_2 = 0.8q_1$ and $\eta = 0.002$. Panels (a), (b), (c) and (d) show the influence of the memory constant γ on these quantities.

environment. It depends on the transport memory under consideration. Neglecting the coefficient η, which gives information on the degree of nonlinearity of the system, we find, from relation (14), the classical linear form of one-dimensional D'Alembert wave equations for the damped system. Eq. (14) is known as the generalized Fisher equation and is used to describe damped nonlinear phenomena [55]. The description of hyperbolic reaction–diffusion systems has been greatly improved using the Fisher equation [59,60]. The speed at which the energy transported by the dimer in the homogeneous part of the medium (i.e., between the possible diffusion events) will be given by the uniform quantity $c_0 = \gamma^{\frac{1}{2}}$. On the other hand, the uniform movement of the dimers is no longer observed in the diffusive parts. It will therefore give the impression of being diffuse and must return to the so-called Fisher limit. In most nonlinear phenomena that describe the human environment, concerns frequently arise when solving the model equation. Obviously, obtaining the solutions of Eq. (14) seems very complex. However, some techniques for obtaining exact solutions of the soliton type can be used, and one can have bright, dark, kink/antikink and impulse solitons [60,61], to cite a few. Among these methods, those allowing the use of a special ansatz and the multiple-scale are of interest to us in the rest of this work [62,63].

4. Derivation of the coupled complex nonlinear Schrödinger equations with memory effect

As the size of the MTs in the cell is minimal, we have considered that their movement is of small amplitudes. To derive the coupled amplitude equations for the protein PF network and appreciate the interaction of the solitary solutions, we introduce the change of the dependent variable around its equilibrium point as follows:

$$\varphi(x,t) = \varepsilon\phi(x,t), \tag{15}$$

where $\varepsilon \ll 1$ accounts for the order of the excitation and ϕ, a new physical dependent variable. Applying the change of variable from Eq. (15) into Eq. (14), the equation to be solved reduces to

$$\frac{\partial^2\phi}{\partial t^2} + \left(\eta_0 - \varepsilon^2\eta_1\phi^2\right)\frac{\partial\phi}{\partial t} = \gamma\frac{\partial^2\phi}{\partial x^2} - \omega_0^2\left(\phi - \varepsilon^2\eta_2\phi^3\right), \tag{16}$$

where $\eta_0 = \gamma + \eta$, $\eta_1 = \frac{\eta}{2}$, $\eta_2 = \frac{1}{6}$, and $\omega_0^2 = \eta\gamma$.

To obtain the CCNLS equations whose modulated soliton solutions can explain the transport of energy and information along MTs, we consider the following ansatz that includes two oscillation modes [64]:

$$\phi(x,t) = V_1 e^{i\theta_1} + V_2 e^{i\theta_2} + \text{c.c.} + \varepsilon\left(V_{01} + V_{02} + V_{11}e^{2i\theta_1} + V_{22}e^{2i\theta_2} + \text{c.c.}\right), \tag{17}$$

where $V_j = V_j\left(X_1, X_2, T_1, T_2\right)$, $V_{0j} = V_{0j}\left(X_1, X_2, T_1, T_2\right)$, and $V_{jj} = V_{jj}\left(X_1, X_2, T_1, T_2\right)$, with $j = 1, 2$, are complex amplitudes to be determined. $\theta_j = q_j x - \omega_j t$ $(j = 1, 2)$ are carrier phases, depending on the variables t and x, with q_j and ω_j being, respectively, the wavenumbers and angular frequencies of two wave packets, and c.c. denoting the complex conjugate. The terms V_{0j} and V_{jj} of first and second harmonics added to the fundamental terms V_j are taken as perturbation terms because of the nonlinear character of Eq. (16). The functions V_j, V_{0j} and V_{jj} depend on the slow variables of multiple scales $T_j = \varepsilon^j t$ and $X_j = \varepsilon^j x$ with $j = 1, 2$. Introducing Eq. (17) into Eq. (16), and setting the quantities proportional to the different orders $\left(\varepsilon^j, e^{i\theta_n}\right)$ and $\left(\varepsilon^j, e^{i2\theta_n}\right)$ to zero, with $j = 0, 1, 2$ and $n = 1, 2$, the following results are obtained:

- For $j = 0$ and $n = 1, 2$ at the orders $\left(\varepsilon^0, e^{i\theta_1}\right)$ and $\left(\varepsilon^0, e^{i\theta_2}\right)$, we find the complex equations of unknowns ω_1 and ω_2

$$\begin{aligned} \omega_1^2 + i\eta_0\omega_1 - \omega_0^2 - \gamma q_1^2 = 0, \\ \omega_2^2 + i\eta_0\omega_2 - \omega_0^2 - \gamma q_2^2 = 0, \end{aligned} \tag{18}$$

leading to the linear complex angular frequencies

$$\omega_1 = \omega_{1r} + i\omega_{1i} \quad \text{and} \quad \omega_2 = \omega_{2r} + i\omega_{2i}, \tag{19}$$

where

$$\omega_{1r}^2 = \gamma_1^2 \left[1 - \left(\frac{\eta_0}{2\gamma_1}\right)^2\right],$$
$$\omega_{2r}^2 = \gamma_2^2 \left[1 - \left(\frac{\eta_0}{2\gamma_2}\right)^2\right],$$
$$\omega_{1i} = \omega_{2i} = -\frac{\eta_0}{2},$$

with $\gamma_1 = \sqrt{\omega_0^2 + \gamma q_1^2}$ and $\gamma_2 = \sqrt{\omega_0^2 + \gamma q_2^2}$. While the imaginary parts $\omega_{1i} = \omega_{2i}$ of the angular frequencies are constant, we limit ourselves to plotting the real parts (ω_{1r} and ω_{2r}) as functions of the wavenumbers q_1 and q_2, belonging to the interval $[q_s; \pi]$ for three values of the transport memory constant γ in Fig. 1(a) and (b). In the first panel of Fig. 1, the influence of the memory effect on the propagation of the excitation along the cellular microtubules is clearly perceptible because the growth of the parameter γ implies that of the real angular frequencies ω_{1r} and ω_{2r}. At the same time, we also see that the shapes of these decreasing curves are similar, but with an increase in the threshold value of the wavenumber q_s, which moves further away from zero, thus decreasing the range of choice of wavenumbers q_1 and q_2 of the wave packets, characterized by the pairs of values (ω_{1r}, q_1) and (ω_{2r}, q_2) used in this work. These first results show that for $\eta_0 = 0$, the angular frequencies of both vibration modes become real. Therefore, the damping forces acting on the motion of the MTs cancel out, while the dependence on the memory effect created by these forces remains and is controlled by η, the nonlinearity degree of the system. It also follows from Eq. (20) that the complex angular frequencies given by Eq. (19) only exist from a threshold value q_s of the wavenumber $q \geq q_s$ given by

$$q_s = \sqrt{\frac{1}{\gamma_{1,2}}\left(\frac{\eta_0^2}{4} - \omega_0^2\right)}.$$

• For $j = 1$ and $n = 1, 2$, at the $(\varepsilon^1, e^{i\theta_1})$, $(\varepsilon^1, e^{i\theta_2})$, we obtain, respectively, the differential equations

$$\left(\eta_0 - 2i\omega_1\right)\frac{\partial V_1}{\partial T_1} = 2i\gamma q_1 \frac{\partial V_1}{\partial X_1},$$
$$\left(\eta_0 - 2i\omega_2\right)\frac{\partial V_2}{\partial T_1} = 2i\gamma q_2 \frac{\partial V_2}{\partial X_1}, \tag{20}$$

which lead to the physical velocities of propagation of information along the PFs, also known as group velocities, given by

$$V_{g1} = \frac{\gamma q_1}{\omega_{1r}}, \quad \text{and} \quad V_{g2} = \frac{\gamma q_2}{\omega_{2r}}. \tag{21}$$

Note that, unlike the angular frequencies of Eq. (19) which have real and imaginary parts, the group velocities are real quantities. Fig. 1(c) and (d) also show the influence of the memory effect on group speeds V_{g1} and V_{g2}, plotted as functions of the wavenumbers q_1 and q_2. We observe that for a given value of the constant γ taken between 0 and 0.9, the group velocities decrease with respect to q_1 and q_2, respectively. But in both cases, the minimum limit value of the group velocity increases slightly with the growth of γ. Therefore, the effect of transport memory could contribute to limiting the decrease of the propagation or transport speed of information through the cellular MTs channel.

• For $j = 1$ and $n = 1, 2$, at the orders $(\varepsilon^1, e^{0\times\theta_1})$, $(\varepsilon^1, e^{0\times\theta_2})$, $(\varepsilon^1, e^{i2\theta_1})$, and $(\varepsilon^1, e^{i2\theta_2})$, the first and second harmonics, respectively, lead to

$$V_{01} = V_{02} = 0 \quad \text{and} \quad V_{11} = V_{22} = 0. \tag{22}$$

• Finally, for $j = 2$ and $n = 1, 2$, at the orders $(\varepsilon^2, e^{i\theta_1})$ and $(\varepsilon^2, e^{i\theta_2})$, the complex amplitudes V_1 and V_2 verify the equations

$$\begin{aligned}
&\left(\eta_0 - 2i\omega_1\right)\frac{\partial V_1}{\partial T_2} - 2i\gamma q_1 \frac{\partial V_1}{\partial X_2} + \frac{\partial^2 V_1}{\partial T_1^2} - \gamma \frac{\partial^2 V_1}{\partial X_1^2} \\
&- \left(3\omega_0^2\eta_2 - i\eta_1\omega_1\right)|V_1|^2 V_1 - \left(6\omega_0^2\eta_2 - 2i\eta_1\omega_1\right)|V_2|^2 V_1 = 0, \\
&\left(\eta_0 - 2i\omega_2\right)\frac{\partial V_2}{\partial T_2} - 2i\gamma q_2 \frac{\partial V_2}{\partial X_2} + \frac{\partial^2 V_2}{\partial T_1^2} - \gamma \frac{\partial^2 V_2}{\partial X_1^2} \\
&- \left(3\omega_0^2\eta_2 - i\eta_1\omega_2\right)|V_2|^2 V_2 - \left(6\omega_0^2\eta_2 - 2i\eta_1\omega_2\right)|V_1|^2 V_2 = 0.
\end{aligned} \tag{23}$$

Using the shifted variables $\xi_m = X_m - V_{g1}T_m$, $\xi'_m = X_m - V_{g2}T_m$ and $\tau_m = T_m$, with $m = 1, 2$, Eqs. (20) and (21) are transformed and introduced into the system of Eqs. (23) with the simple combination $\xi'_1 = \xi_1 + \left(V_{g1} - V_{g2}\right)T_1$ $(m = 1)$ to give

$$\begin{aligned}
&i\frac{\partial V_1}{\partial \tau_2} + P_1 \frac{\partial^2 V_1}{\partial \xi_1^2} + Q_1|V_1|^2 V_1 - R_1|V_2|^2 V_1 = 0, \\
&i\frac{\partial V_2}{\partial \tau_2} + P_2 \frac{\partial^2 V_2}{\partial \xi_1^2} + i\left(\frac{V_{g2} - V_{g1}}{\varepsilon}\right)\frac{\partial V_2}{\partial \xi_1} \\
&\qquad + Q_2|V_2|^2 V_2 - R_2|V_1|^2 V_2 = 0.
\end{aligned} \tag{24}$$

To make the second equation of system (24) easy to handle, we cancel the term in $\frac{\partial V_2}{\partial \xi_1}$ via the gauge transformation $V_2 = V_2 \exp\left[-i\left(\frac{D}{2P_2\varepsilon}\xi_1 + \frac{D^2}{4P_2}\tau_2\right)\right]$, with $D = V_{g1} - V_{g2}$. By setting $\tau = \tau_2 = \varepsilon^2 t$ and $\xi = \xi_1 = \varepsilon t$, the set of Eqs. (24) becomes

$$\begin{aligned}
&i\frac{\partial V_1}{\partial \tau} + P_1 \frac{\partial^2 V_1}{\partial \xi^2} + Q_1|V_1|^2 V_1 - R_1|V_2|^2 V_1 = 0, \\
&i\frac{\partial V_2}{\partial \tau} + P_2 \frac{\partial^2 V_2}{\partial \xi^2} + Q_2|V_2|^2 V_2 - R_2|V_1|^2 V_2 = 0,
\end{aligned} \tag{25}$$

where

$$\begin{aligned}
&P_1 = \frac{\gamma - V_{g1}^2}{2\omega_{1r}}, \quad P_2 = \frac{\gamma - V_{g2}^2}{2\omega_{2r}}, \\
&Q_1 = Q_{1r} + iQ_{1i}, \quad Q_2 = Q_{2r} + iQ_{2i}, \\
&R_1 = R_{1r} + iR_{1i}, \quad R_2 = R_{2r} + iR_{2i},
\end{aligned} \tag{26}$$

with the expressions for Q_{1r}, Q_{2r}, Q_{1i}, Q_{2i}, R_{1r}, R_{2r}, R_{1i} and R_{2i} being given by

$$\begin{aligned}
&Q_{1r} = \frac{3\omega_0^2\eta_2 + \eta_1\omega_i}{2\omega_{1r}}, \quad Q_{2r} = \frac{3\omega_0^2\eta_2 + \eta_1\omega_i}{2\omega_{2r}}, \\
&Q_{1i} = Q_{2i} = -\frac{\eta_1}{2}, \quad R_{1r} = \frac{3\omega_0^2\eta_2 + \eta_1\omega_i}{\omega_{1r}}, \\
&R_{2r} = \frac{3\omega_0^2\eta_2 + \eta_1\omega_i}{\omega_{2r}}, \quad R_{1i} = R_{2i} = -\eta_1.
\end{aligned} \tag{27}$$

The set of Eqs. (25) represents two nonlinearly CCNLS equations with real dispersion coefficients P_1 and P_2, and complex coefficients Q_1, Q_2, R_1, and R_2 representing nonlinearity coefficients, with the coupling being ensured by R_1 and R_2. Eqs. (25) can also, but abusively, be called the complex Ginzburg–Landau (CGL) equations due to the complex form of some coefficients. However, compared to the standard CGL equation, an explicit linear dissipative term is absent [65–68]. Examples of similar forms of coupled CGL equations with dissipative terms different from zero allowed Tankou et al. [64] to study the dynamics of ionic waves in a dissipative network of MTs mimicking their electrophysiological behavior, while Bansi et al. [69] used it to study wave propagation in a viscoelastic tube filled with viscous fluid. Note that in addition to the nonexistent dissipative terms, if the imaginary parts of the coupling and nonlinearity coefficients are assumed to be zero, i.e., $R_{1i} = R_{2i} = Q_{1i} = Q_{2i} = 0$, the system of Eqs. (25) reduces to a set of coupled NLS equations [13,70,71]. In the latter, the nonlinear tunneling of soliton was investigated in the presence of higher-order nonlinear effects [72]. A similar study was extended to coupled NLS-Maxwell–Bloch equations for the ultrashort pulse propagation in an

erbium-doped birefringent fiber system, where two-soliton solutions and energy exchange between the modes were further addressed [73]. Moreover, soliton solutions for N-coupled NLS equations were proposed using the Darboux transformation, with, on the background, cascade compression of optical soliton due to multi-nonlinear barriers [74]. Remarkably, the obtained Eqs. (25) has the particularity of having all its six coefficients depending on the memory constant γ and the degree of nonlinearity η. At the same time, its decoupling leads directly to two uncoupled complex NLS equations of the same form, as obtained in Ref. [17] in the context of DNA nonlinear dynamics. It is important to mention that obtaining the analytical solutions of Eqs. (25) is essential for further progress in understanding the propagation of coupled signals in the damped MT network under our study.

5. Analytical single- and coupled-mode soliton solutions and numerical experiments

Several biological phenomena can be described using coupled nonlinear equations, whether they are complex or not, or GL equations. These equations often use hyperbolic solutions, which are generally localized. This localization is a result of the interaction between the nonlinearity effects and the dispersion of the medium being studied. There are many practical applications for these localized excitations in various areas of modern physics. For instance, they are used in electrical networks [75–78], plasma [79], and biophysics [13,70]. In this section, we propose an analytical solution for the system of Eqs. (25) and use it as a starting point for the numerical analysis of the problem.

5.1. Analytical coupled soliton solutions

To find soliton solutions for the set of Eqs. (25), there are various mathematical techniques available. However, in order to obtain impulse solitons, a specific method can be used that relies on the coefficients P_1, P_2, Q_1, Q_2, R_1, and R_2 of the CCNLSEs. It is necessary for these coefficients and their combinations to meet certain conditions. By assuming that either $V_2 = 0$ and $V_1 \neq 0$ or $V_1 = 0$ and $V_2 \neq 0$, we can separate our CCNLS equation system (25) into two independent CNLS equations. Solving each equation will lead to wave propagation in either frequency mode ω_1 or ω_2. The solutions to this particular case are straightforward and depend on the sign of the products $P_1 \times Q_{1r}$ and $P_2 \times Q_{2r}$ of the two vibrational modes, namely ω_1 and ω_2. If $P_1 \times Q_{1r} > 0$ or $P2 \times Q_{2r} > 0$, bright or breathers solitons are typically observed. Conversely, in the opposite scenario where $P_1 \times Q_{1r} < 0$ or $P_2 \times Q_{2r} < 0$, kink/antikink or dark solitons are obtained.

In the meantime, by setting $V_2 = V_1 = V$, which transforms the coupled system (25) into the NLS equation

$$i\frac{\partial V}{\partial \tau} + P_{11}\frac{\partial^2 V}{\partial \xi^2} + Q_{11}|V|^2 V = 0, \tag{28}$$

where $Q_{11} = Q_{1r} - R_{1r} + i\left(Q_{1i} - R_{1i}\right)$. Eq. (28) is a complex NLS equation similar to the one used for the description of DNA dynamics with memory effect [17].

The dispersion coefficient P_{11} is real, while the nonlinearity coefficient Q_{11} is complex. Therefore, it is possible to describe the dynamics of the localized soliton wave in our angular MTs model using the complex NLS equation. In doing so, the cytoplasm of the cell is a medium with several entities, some of which screen the signal transmission, the form of the solution that verifies Eq. (28) can be [63,80]:

$$V = V_0 e^{-S_i \tau}\left[\operatorname{sech}\left(\frac{\xi}{N}\right)\right]^{(1+i\delta_0)} e^{iS_r\tau}, \tag{29}$$

where the coefficients V_0, N, δ_0 and the pair (S_r, S_i) represent the amplitude, width, chirp and real and imaginary parts of the soliton phase, respectively. By introducing Eq. (29) into Eq. (28), we find, by solving the resulting linear system of equations, the expressions for the coefficients:

$$\begin{aligned} &S_r = N_0^2 P_{11}\left(1-\delta_0^2\right), \quad S_i = 2N_0^2 P_{11}\delta_0, \\ &V_0 = N_0\sqrt{\frac{P_{11}\left(2-\delta_0^2\right)}{Q_{11r}}}, \\ &\delta_0^{\pm} = \frac{-3Q_{11r} \pm \sqrt{9Q_{11r}^2 + 8Q_{11i}^2}}{2Q_{11i}}, \end{aligned} \tag{30}$$

with $N_0 = 1/N$, $Q_{11r} = Q_{1r} - R_{1r}$ and $Q_{11i} = Q_{1i} - R_{1i}$. In our biophysical system, the coefficients P_{11}, Q_{11r}, and their product $P_{11} \times Q_{11r}$ hold great significance in determining the form of the propagating solution. Therefore, if $P_{11} \times Q_{11r} > 0$, Eq. (29) represents a localized soliton of the breather type. The variations of these solitons against the wavenumber q_1 are depicted in Fig. 3. The diagrams depicted in Fig. 3(a), (b), and (c) illustrate how the memory constant γ affects the real coefficients of dispersion P_{11}, nonlinearity Q_{11r}, and the Benjamin–Feir criterion $P_{11} \times Q_{11r} > 0$ of the plane wave grating. It is evident that P_{11} and Q_{11r} are on the rise but still hold negative values. In contrast,

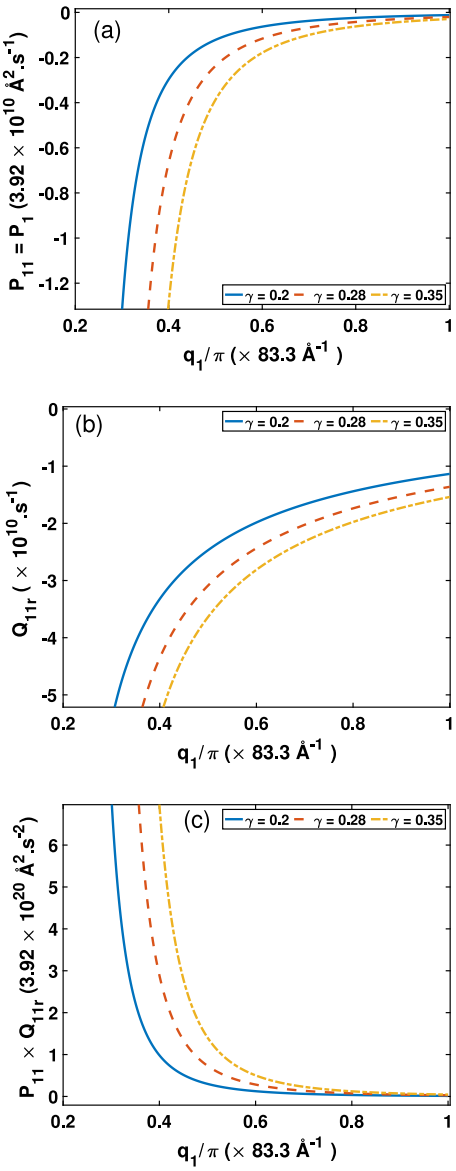

Fig. 2. Representation of the chirp evolution of the simple soliton-solution as a function of the wavenumber q_1, for $\eta = 0.002$ and with the changing memory constant γ.

their product $P_{11} \times Q_{11r}$ is decreases and shows a positive trend. The increase in the parameter γ is evident in all three figures, and it results in a significant expansion of the forbidden zone for wavenumber q_1, which now ranges from 0 to q_s. It is worth noting that the instability criterion $P_{11} \times Q_{11r} > 0$ indicates the range of wavenumber values in which unstable excitations may occur within the MTs network. As a result, the propagation of plane waves in this region of instability is expected to result in trains of localized structures. It is observed that the memory constant greatly affects this product. An increase in the value of γ causes the threshold wavenumber to rise from 0.31π to 0.4π. For instance, if $\gamma = 0.2$ in the uncoupled NLS equation scenario, selecting a wavenumber q_1 within the range of $[0.31\pi; \pi]$ will likely result in localized wave structures. To determine the width of the soliton, the process outlined in Refs. [17,81] must be followed. It is shown that in a perfect biological wave propagation medium (without any influence or zero viscosity, denoted by $\delta_0 = 0$), the solution to Eq. (28) has a particular form

$$V = V_e \,\mathrm{sech}\left(L_e \xi\right) \exp\left[i \frac{u_e}{2P_e}\left(\xi - u_c \tau\right)\right], \tag{31}$$

where

$$L_e = \frac{\sqrt{u_e^2 - 2u_e u_c}}{2P_e} \quad \text{and} \quad V_e = \sqrt{\frac{u_e^2 - 2u_e u_c}{2P_e Q_e}}, \tag{32}$$

with $P_e = P_{11(\delta_0=0)}$, $Q_e = Q_{11r(\delta_0=0)}$ and, u_e and u_c free velocity constants with the relation $u_c = \Xi u_e$ ($\Xi \in [0, 0.5[$). By considering the shielding effects and viscosity ($\delta_0 \neq 0$) that affect the signal transmission along the MTs, we can use Eqs. (32) to derive the width and amplitude of the soliton

$$N = \frac{\left(2 - \delta_0^2\right) P_{11}}{u_e \sqrt{1 - 2\Xi}} \quad \text{and} \quad V_0 = u_e \sqrt{\frac{1 - 2\Xi}{\left(2 - \delta_0^2\right) P_{11} Q_{11r}}}, \tag{33}$$

whose variation is important for the evolution of the soliton under the memory constant, along with an additional existing condition $\delta_0 < \sqrt{2}$.

Understanding biological systems is inherently complex as they undergo nonlinear evolution in dispersive and dissipative media. To improve our comprehension of the motion of tubulin dimers, we have refined a descriptive angular model that was previously developed in Ref. [14]. It is worth noting that a higher chirp in biological systems often leads to a reduced perception of information in a given area, meaning the information-carrying signal is highly chirped. Crucial information can be obtained from the plot of the chirp parameters δ_0^+ and δ_0^- of the soliton-breather solution of the uncoupled case as a function of the wavenumber q_1, as shown in Fig. 2. We can disregard the chirp δ_0^+ and instead use δ_0^+. This is because the positive product $P_{11} \times Q_{11r}$ is only applicable to certain accessible q_1 values and for the condition $\delta_0 < \sqrt{2}$. By analyzing Fig. 2(b), we can see that despite the agreement with the q_1 wavenumber, the chirp $(\delta_0^+)^2$ is greater than 2. In contrast, Fig. 2(a) shows that the chirp δ_0^2 meets both the wavenumber and upper limit conditions of $\sqrt{2}$. It can be concluded that the soliton-breather in this scenario must have a slight chirp in order to propagate in the medium. Additionally, the growth of the transport memory constant may have a positive effect in certain areas by reducing the impact of the chirp on the transported information during energy transfer.

Eqs. (29), (17), and (15) ultimately result in a solitary evolution that spans both time and space. This serves as the solution to Eq. (14) for the motion of tubulin dimers within the MT network, accounting for the transport memory effect

$$\begin{aligned}\varphi(x,t) = {} & 2\varepsilon V_0 e^{-\left(\varepsilon^2 S_i - \omega_{1i}\right)t} \,\mathrm{sech}\left[\varepsilon\left(\frac{x - V_{g1} t}{N}\right)\right] \\ & \times \cos\left[q_1 x + \left(\varepsilon^2 S_r - \omega_{1r}\right) t\right. \\ & \left. + \delta_0 \mathrm{Log}\left(\mathrm{sech}\left(\varepsilon \frac{x - V_{g1} t}{N}\right)\right)\right].\end{aligned} \tag{34}$$

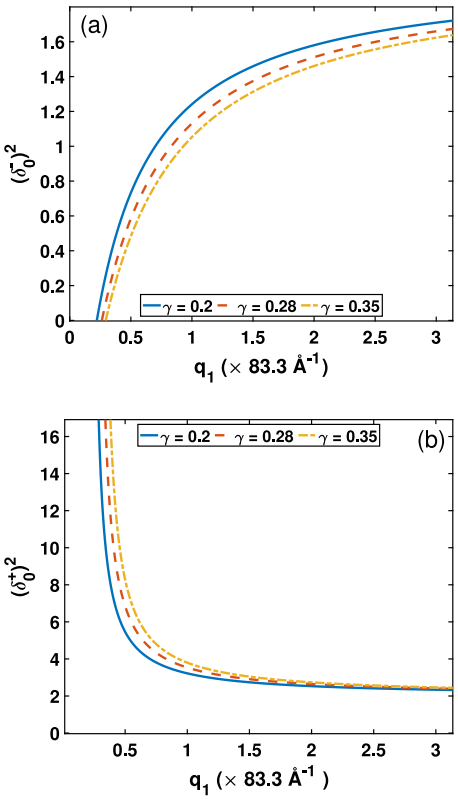

Fig. 3. Evolution curves of the parameters P_{11}, Q_{11r} and the $P_{11} \times Q_{11r}$ as a function of the wavenumber q_1, for $\eta = 0.002$ with changing of the memory constant γ.

According to the solution (34), the excitation profile in the cell cytoplasm along the MTs is influenced by crucial parameters, including the amplitude, which is affected by the nature of the propagation medium, impacting V_0 and the width N. To demonstrate this, we have shown the changes in N and V_0 at various values of the memory constant γ and the rate of nonlinearity η, as a function of the wavenumber q_1 in Fig. 4. Fig. 4(a) and (c) are obtained by setting $\eta = 0.002$ while the dashed lines (see Fig. 4(b) and (d)) are plotted for $\gamma = 0.2247$, with the other constants being taken as $u_e = 1$ and $\Xi = 0.2$. Based on the four graphs, it is evident that N decreases but does not cancel out while V_0 increases as q_1 varies. The impact of the constants γ and η is noticeable in all cases. As γ evolves from 0.2 to 0.35, the width N increases (see Fig. 4(a)), causing the signal to disperse spatially, and the amplitude V_0 to decrease (see Fig. 4(c)). Over the same width N, the impact of the rate η has the opposite effect to that of γ. It can be seen that changing η from 0.001 to 0.09 leads to the decrease of N (see Fig. 4(b)), while the amplitude V_0 (see Fig. 4(d)) shows the same behavior as observed previously for the case of Fig. 4(c). By analyzing the scenario of uncoupled dynamics, we can forecast that the impact of transport memory can result in an energy-damping force that moves through the MTs network when the wavenumber q_1 falls within the range of $[0.31\pi; \pi]$, and γ lies between 0.2 and 0.35.

In the next phase of the coupled mode analysis, we extend our approach by taking into account the fact that V_1 and V_2 are not equal to zero and then proceed to search for analytical pulse-like solitons. These solitons are of the same type as those described in Ref. [41]. Whether or not the final coupled solution, as supported by Eq. (14), exists is contingent upon the sign of certain newly introduced parameters (Λ_1, Λ_2, and δ) that are derived from the coefficients of the system (25), as previously described.

Assuming that there are microorganisms in the cytoplasm of the cell that can disturb the reception of the information carried by the soliton

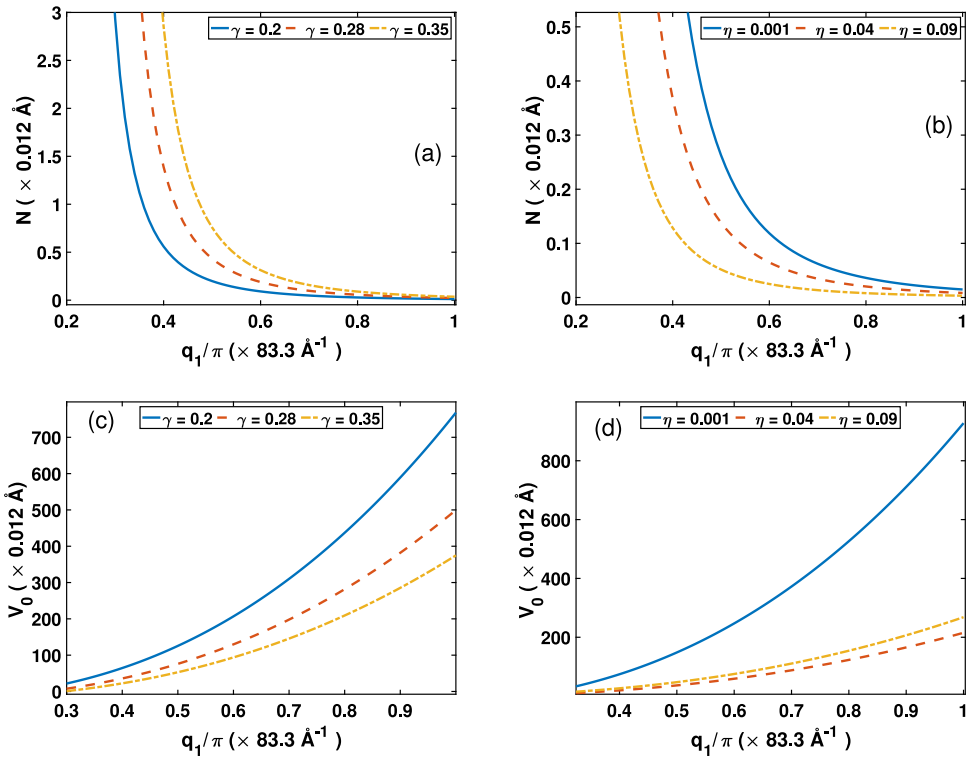

Fig. 4. Variation of the soliton-solution width N and the amplitude V_0 as a function of the wavenumber q_1, for three values of the memory constant γ and the nonlinearity rate constant η.

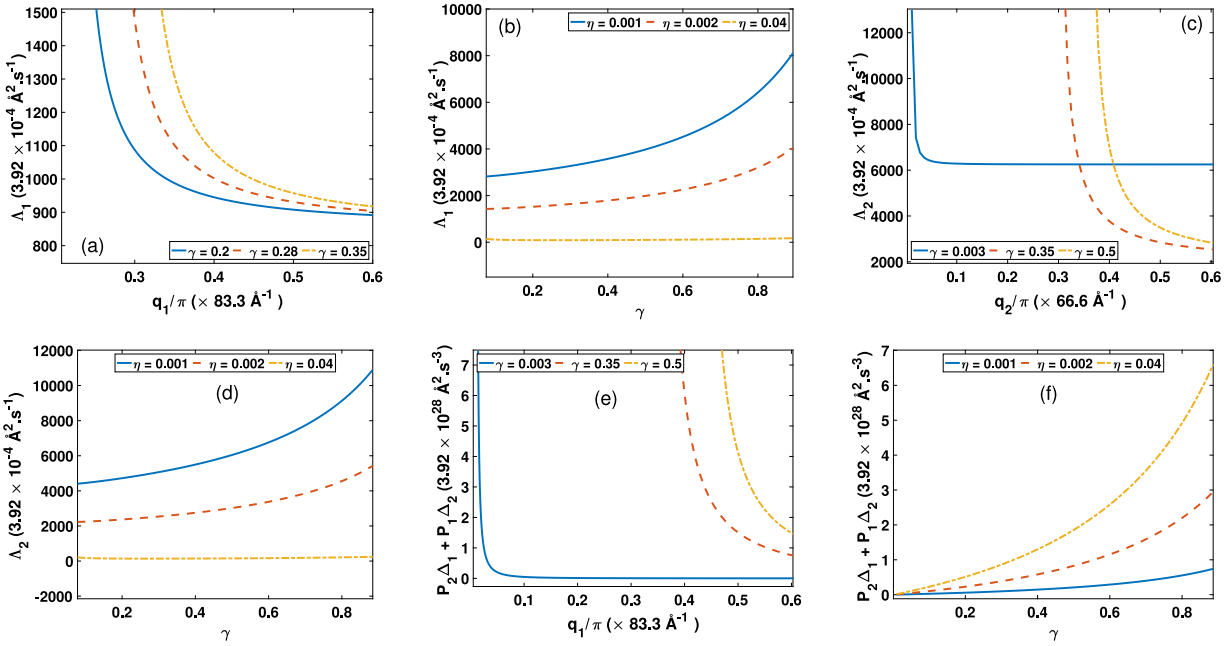

Fig. 5. Graphical representations of the coupled soliton-solution coefficients. Panels (a), (c) and (e) as a function of the wavenumbers q_1 and q_2 ($q_2 = 0.8q_1$), for different values of the γ. Panels (b) and (d) as a function of the memory constant γ, for different values of the nonlinearity constant.

pulse along the microtubules, the exact solutions are taken to be

$$\begin{aligned} V_1 &= V_{10} e^{-S_{1i}\tau} \left[\operatorname{sech}(\beta\xi)\right]^{(1+i\delta_1)} e^{iS_{1r}\tau}, \\ V_2 &= V_{20} e^{-S_{2i}\tau} \left[\operatorname{sech}(\beta\xi)\right]^{(1+i\delta_2)} e^{iS_{2r}\tau}, \end{aligned} \tag{35}$$

where the pair (V_{10}, V_{20}) are real amplitudes, (S_{1r}, S_{2r}) and (S_{1i}, S_{2i}) the real and imaginary parts of the phases of the excitations. The coefficients (δ_1, δ_2), present in the two solitary pulses V_1 and V_2 take into account the bad reception of information and are called Chirps. β is a free parameter while all the others are parameters to be determined. To make the calculations less cumbersome, we have chosen the soliton phases as the only complexes. Introducing relations (35) into the CCNLS equations system (25), leads to the linear set consisting of the algebraic equations of unknowns V_{10}, V_{20}, S_{1r}, S_{2r}, S_{1i}, S_{2i}, δ_1, δ_2 and β given by

$$\begin{aligned}
P_1\beta^2 - S_{1r} - P_1\beta^2\delta_1^2 - i\left(S_{1i} - 2P_1\beta^2\delta_1\right) &= 0,\\
P_1\beta^2\left(\delta_1^2 - 2\right) + V_{10}^2 Q_{1r} + V_{20}^2 R_{1r} &= 0,\\
-3P_1\beta^2\delta_1 + V_{10}^2 Q_{1i} + V_{20}^2 R_{1i} &= 0,\\
P_2\beta^2 - S_{2r} - P_2\beta^2\delta_2^2 + i\left(-S_{2i} + 2P_2\beta^2\delta_2\right) &= 0,\\
P_2\beta^2\left(\delta_2^2 - 2\right) + V_{20}^2 Q_{2r} + V_{10}^2 R_{2r} &= 0,\\
-3P_2\beta^2\delta_2 + V_{20}^2 Q_{2i} + V_{10}^2 R_{2i} &= 0.
\end{aligned} \tag{36}$$

To solve the above linear equations, we take into account the microorganisms present around the tubulin dimers in the cell. These microorganisms may have a negative impact on the reception of information carried by soliton signals along these proteins. We conclude that the chirps in both vibration modes are identical, and therefore $\delta_1 = \delta_2 = \delta$. This leads to

$$\begin{aligned}
S_{1r} &= P_1\beta^2\left(1-\delta^2\right), \quad S_{1i} = 2P_1\beta^2\delta,\\
S_{2r} &= P_2\beta^2\left(1-\delta^2\right), \quad S_{2i} = 2P_2\beta^2\delta.
\end{aligned} \tag{37}$$

and

$$V_{10} = \beta\sqrt{\Lambda_1\left(2-\delta^2\right)}, \quad V_{20} = \beta\sqrt{\Lambda_2\left(2-\delta^2\right)}, \tag{38}$$

where

$$\Lambda_1 = \frac{P_1Q_{2r} - P_2R_{1r}}{\Lambda} \quad \text{and} \quad \Lambda_2 = \frac{P_2Q_{1r} - P_1R_{2r}}{\Lambda},$$

with $\Lambda = Q_{1r}Q_{2r} - R_{1r}R_{2r}$. Solving the same set of equations also gives the chirp

$$\begin{aligned}
\delta = &\pm\frac{1}{P_1\Delta_2 + P_2\Delta_1}\\
&\times\left[3P_1\Lambda + \sqrt{9P_1^2\Lambda^2 + 8\left(P_1\Delta_2 + P_2\Delta_1\right)^2}\right],
\end{aligned} \tag{39}$$

where $\Delta_1 = R_{1i}Q_{1r} - R_{1r}Q_{1i}$ and $\Delta_2 = Q_{1i}Q_{2r} - R_{1i}R_{2r}$. As mentioned earlier, the real constant β is taken arbitrarily, while the other parameters of the soliton envelopes V_1 and V_2 are well determined. The latter includes new coefficients that provide information on the existence of these pulse waves.

In order to describe the angular displacement profiles of cellular tubulin dimers, taking into account the transport memory effects of the medium in the coupling, the parameters obtained in Eqs. (37)–(39) included in the soliton solutions (35) must therefore fulfill some conditions. Thus, to observe the evolution of the soliton pulse coupled by V_1 and V_2 with the influence of the transport memory and nonlinear constant, the amplitudes V_{10}, V_{20} and the chirp δ must be real and nonzero. To achieve this, the main conditions on these constants such that

$$\begin{aligned}
&\Lambda_1 > 0, \quad \Lambda_2 > 0, \quad \delta < \sqrt{2} \quad \text{or} \quad \Lambda_1 < 0, \quad \Lambda_2 < 0,\\
&\delta > \sqrt{2} \quad \text{and} \quad P_1\Delta_2 + P_2\Delta_1 \neq 0.
\end{aligned} \tag{40}$$

The graphical representations of some of the obtained coefficients allow to discuss the different parameter regions necessary for describing the dynamics of the MTs with the impact of its immediate environment.

In Figs. 5 and 6, the plots of the characteristic parameters Λ_1, Λ_2, δ and $P_1\Delta_2 + P_2\Delta_1$ of the coupled solution are observed. The graphs in Fig. 5(a), (b) and (c) represent the variations of three of these parameters as functions of the wavenumbers q_1 and q_2 for three values of the constant γ and those in Fig. 5(b), (d) and (f) show the variations of the same parameters but as a function of the memory constant γ for three values of the nonlinearity rate η with $q_1 = 0.36\pi$. These satisfy one of the conditions given in relation (40), as the parameters are positive for specific regions of q_1, q_2, γ and η. Fig. 6 allows us to discuss the second condition for the existence of the same coupled breather solution. It illustrates the evolution of the chirp $\delta_\pm^2$ as a function of the wavenumbers q_1 and q_2 for three values of γ and η, respectively. The square of δ_+ shows increasing behaviors (see Fig. 6(a) and (b)) in contrast to δ_- which decreases (see Fig. 6(c) and (d)). It can be seen that

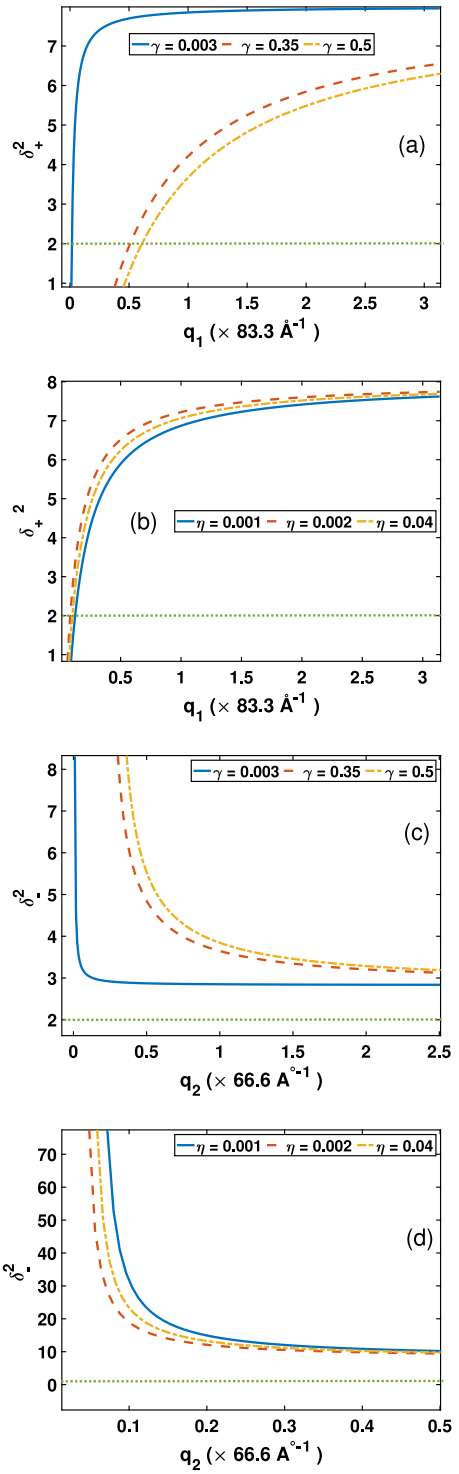

Fig. 6. Variations of the chirp of the coupled soliton solution as a function of the wavenumbers q_1 and q_2 ($q_2 = 0.8q_1$). Panels (a) and (c), for different values of γ; panels (b) and (d), for different values of the nonlinearity rate constant.

the chirp whose part of values fulfill the condition $\delta < \sqrt{2}(\delta^2 < 2)$ is δ_+. Thus, the coupled breather solution, weakly chirped, can propagate along the MT within the intervals $\gamma \in [0.003; 0.5]$, $q_1 \in [0.01\pi; 0.6\pi]$, with $\eta = 0.002$, and $\Xi = 0.2$. We can notice that, in general, the dynamics of the MT described by a single equation or a system of CCNLS equations show how the energy, after being emitted (e.g. by the hydrolysis of GTP), would propagate in the biological environment

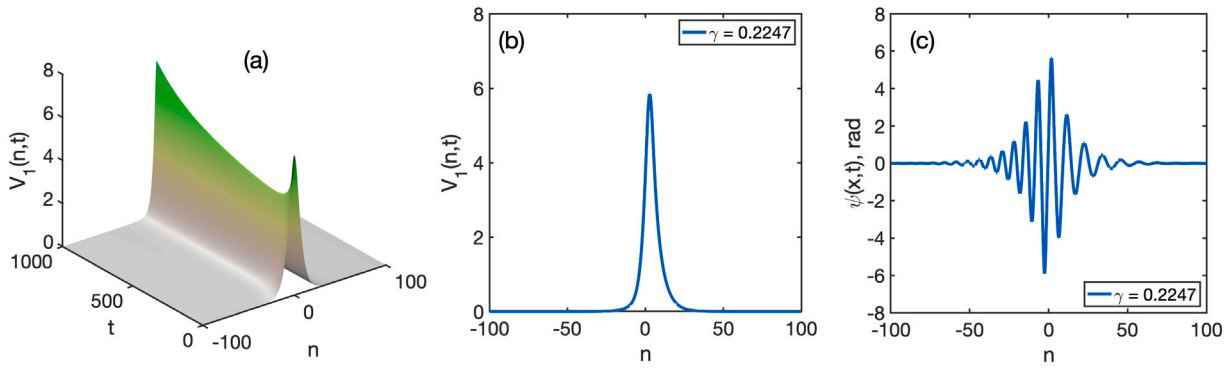

Fig. 7. (a) and (b) display the space–time and spatial profiles of the decoupled solution (31), while panel (c) displays the resulting breather solution (34) obtained from numerical simulations and recorded at time $t = 800$, under the parameter values $\gamma = 0.2247$ and $\eta = 0.002$.

of the MT under several constraints such as dispersion, nonlinearity, friction with other particles and chirp effects.

Starting from the previous calculations, we can return to the systems's initial coordinates. The global solution (15) of the equation of motion of the tubulin dimers Eq. (14), with transport memory and nonlinearity effects, in a cell is written as

$$\begin{aligned}\varphi(x,t) =& 2V_{10}\,\mathrm{sech}\left[\varepsilon\beta\left(x-V_{g1}t\right)\right]e^{-\left(\varepsilon^2 S_{1i}-\omega_{1i}\right)t}\times\cos\left[q_1 x\right.\\ &+\left(\varepsilon^2 S_{1r}-\omega_{1r}\right)t+\delta Log\left(\mathrm{sech}\varepsilon\beta\left(x-V_{g1}t\right)\right)\Big]\\ &+2V_{20}\,\mathrm{sech}\left[\varepsilon\beta\left(x-V_{g1}t\right)\right]e^{-\left(\varepsilon^2 S_{2i}-\omega_{1i}\right)t}\\ &\times\cos\left[\left(\varepsilon D_1-q_1\right)x-\left(\varepsilon^2 S_{2r}+\varepsilon D_1 V_{g1}-\varepsilon^2 D_2\right.\right.\\ &\left.\left.-\omega_{2r}\right)t+\delta Log\left(\mathrm{sech}\varepsilon\beta\left(x-V_{g1}t\right)\right)\right],\end{aligned}\tag{41}$$

where $D_1 = D/2P_2\varepsilon$ and $D_2 = D^2/4P_2$. Obviously, Eq. (41) comprises two wave packets of complex frequencies ω_1 and ω_2. It should be noted that the imaginary parts refer directly to the physiological dissipative character of biological media. Since the energy allowing the cellular cytoskeletal filaments to play each its role efficiently comes from the hydrolysis of GTP, the coupled solution (41) represents the initial energetic excitation received by the dimers on one of the ends of the PF, which is going to be transmitted from near to near all along the MT. In order to numerically appreciate the stable propagation of the coupled energy pulse signal through the entire MT network, Eq. (41) is used as initial input signal.

5.2. Numerical experiments

To assess the stability of the obtained solutions and the accuracy of the proposed parametric predictions, Eq. (14) is numerically integrated as it contains the memory term that is of importance in this work. We examine two scenarios: one where the initial condition is uncoupled, given by Eq. (34), and another where it is coupled, given by Eq. (41), which describes two wave packets with complex frequencies ω_1 and ω_1. In doing so, the fourth-order Runge–Kutta computational scheme is utilized, with spatial and temporal step sizes being $\Delta x = \Delta t = 0.01$, under periodic boundary conditions. The final normalized time is set to $t = 1000$, while 201 dimers are considered spatially. It is clear from Eq. (14) that the parameters γ and η have an impact on the propagation of excitations along the MTs, reflecting the effects of transport memory and the degree of nonlinearity, respectively. The initial signals of Eqs. (34) and (41) are expected to be affected by changes in such parameters, which is confirmed in Figs. 2–6. We aim to identify the conditions under which these soliton solutions can describe communication between two dimers in the cell without disappearing. For an objective analysis, we first consider the case where the initial excitation is decoupled. Considering the same parameter limits used to obtain Figs. 3–4, we numerically generate Figs. 7 and 8 with a focus on the amplitude and width of the single-mode soliton solution.

Fig. 7(a) shows the space–time representation of solution (31), while Fig. 7(b) shows a spatial cross-section of such a solution at time $t = 800$. The full breather solution (34) is shown in Fig. 7(c) at time $t = 800$, under full numerical simulations for a memory constant value $\gamma = 0.2247$. Precision should be made that all the panels of Fig. 7 have been obtained at the order $\epsilon = 0.01$, with the wavenumber $q_1 = 0.36\pi$. They show the type of soliton excitation propagated in the studied MT array, which shows indeed a breather structure. Additionally, the profiles in Fig. 8 highlight the qualitative and quantitative influence of the constants γ and η during the propagation of single-breather solution, since the main goal of these numerical simulations is to verify the capacity of the improved model under study to support the obtained analytical solution. In that direction, panels $(\mathrm{aj})_{j=1,2,3}$ show the influence of changing the memory parameter γ. In general, such an increase of the transport memory constant γ not only spatially expands the breathing structure to more dimers but also reduces the amplitude of the localized solitonic object. In particular, under normalized time and space, the width of the oscillating soliton increases from about $x = 90$ units for $\gamma = 0.21$ to $x = 200$ units for $\gamma = 0.35$, while the amplitude increases from $\varphi = 12.5$ rad ($\gamma = 0.21$) to $\varphi = 1.125$ rad ($\gamma = 0.35$). Along the same line, we also note that the nonlinear character of the wave is proven, as increasing the degree η can change the wave from a breather-structure to a solitary pulse, thus decreasing its amplitude and width as shown in Fig. 8$(\mathrm{bj})_{j=1,2,3}$. These numerical results in the non-coupled mode are, once more, in agreement with the analytical predictions of Fig. 4(a)–(d). As a whole, it is obvious that for ranges of values of the constants $\gamma \in [0.21; 0.35]$ and $\eta \in [0.001; 0.09]$, the effects of transport memory as a function of nonlinearity can potentially lower the height by increasing the solitonic width of the dimer protein filament vibrations in the cell. Therefore, these effects would behave in the chosen constant ranges as constraints that affect conformational changes in MT's vibrational motion. The same spectrum of behaviors has been reported in other studies. In many other biological systems such as the study of cell invasion through soft biological tissues [82], DNA dynamics [17,83,84] and nerve cell networks [85–87], breather waves play important roles in understanding how these processes work. In MTs, some results have reported that breathers may be responsible for triggering the mobility of motor proteins [12,88]. The studies carried out in the last two references considered negligible damping effects. However, we conducted these investigations believing that stronger damping effects of transport memory would yield satisfying results. As shown in Fig. 8(b3), our assumption proved to be correct, with the soliton pulse being a crucial feature of excitable media, such as brain cells, where the MT is in constant motion. These solitary impulses are generally associated with chemical excitations propagating quickly at the subcellular level [89,90].

The coupled-excitation regime is studied next, where one combines two wave packets (ω_1, q_1) and (ω_2, q_2). This is based on the initial condition (41), which results from an extended breathing wave made

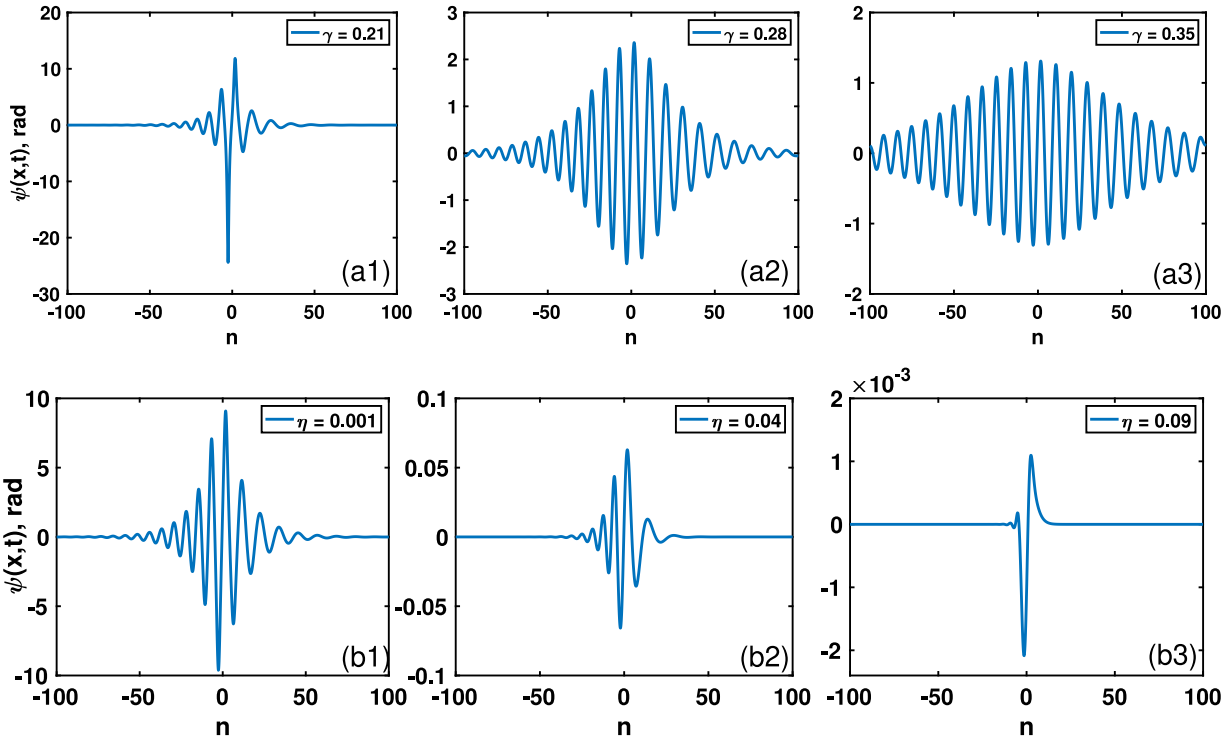

Fig. 8. Direct numerical simulations using solution (34) as initial condition. Panels $(aj)_{j=1,2,3}$ display the single breather excitation under the effect of increasing the transport memory constant γ at time $t = 800$ for $\eta = 0.002$. Panels $(bj)_{j=1,2,3}$ show the effect of increasing the nonlinearity rate η at the same instant $t = 800$, with $\gamma = 0.2247$.

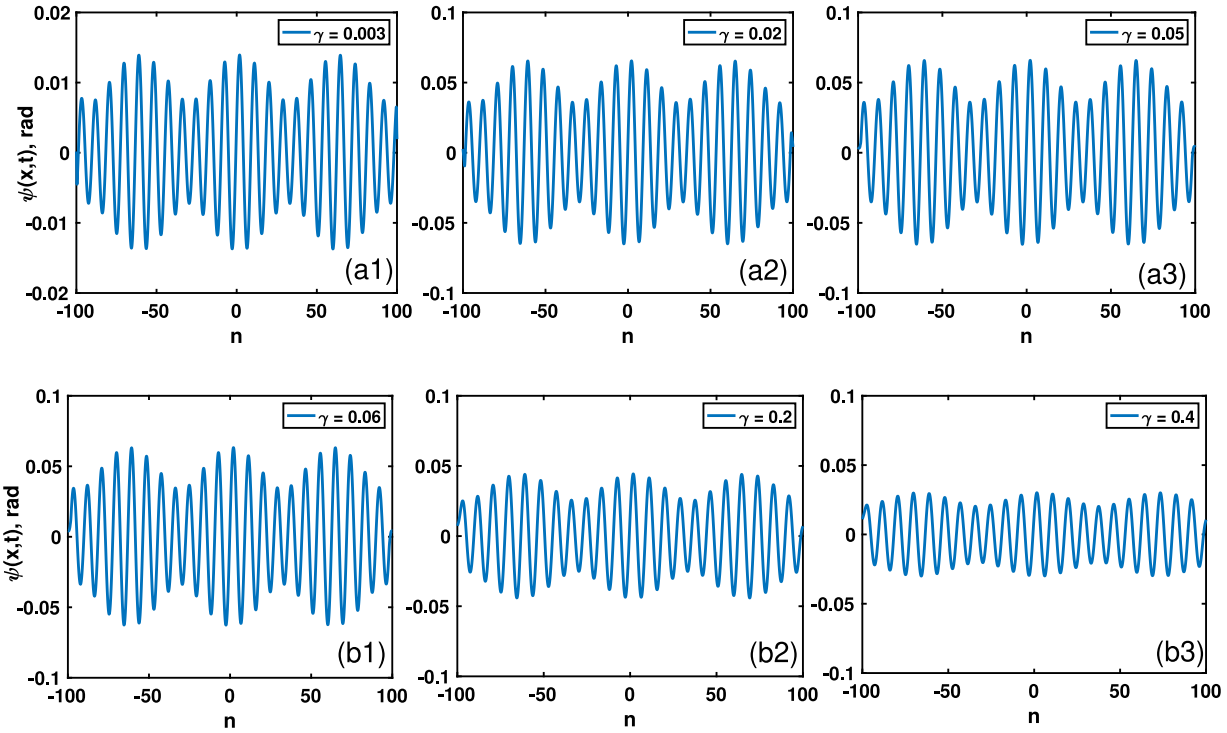

Fig. 9. Direct numerical simulations using solution (41) as initial condition. The panels show the impact of the transport memory constant γ on the coupled breather-soliton solution along the MTs, for $\eta = 0.002$ and $\beta = 0.1$.

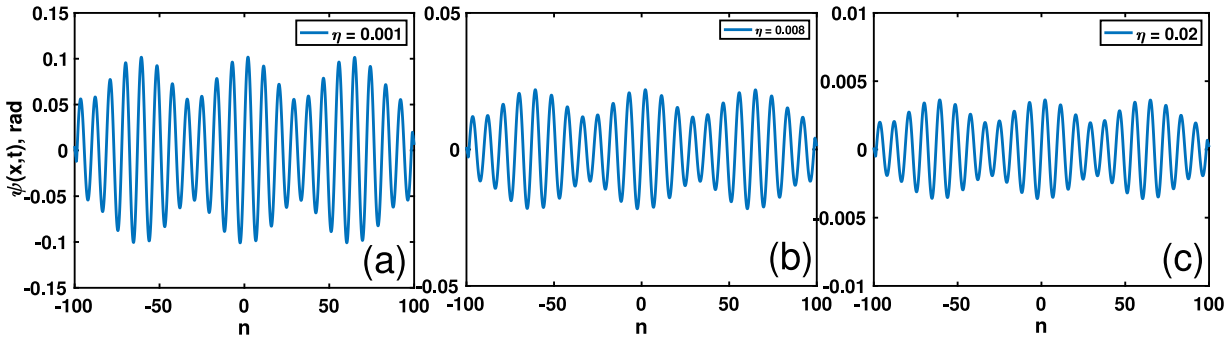

Fig. 10. Direct numerical simulations using solution (41) as initial condition. The panels show the impact of the nonlinearity rate η on the coupled breather-soliton solution along the MTs for $\gamma = 0.02247$ and $\beta = 0.1$, at time $t = 800$.

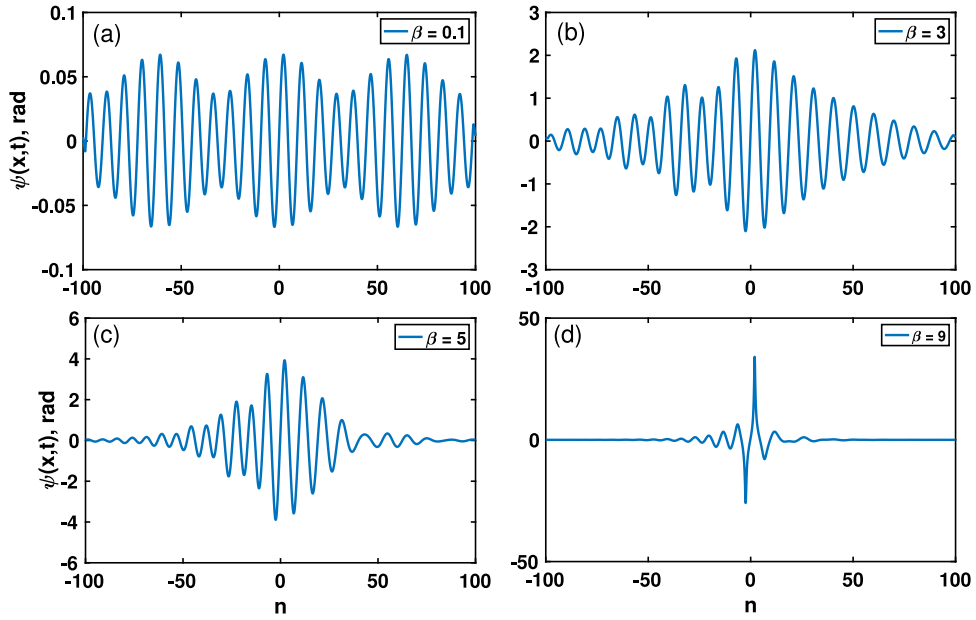

Fig. 11. Direct numerical simulations using solution (41) as initial condition. The panels display the impact of the free parameter β taking into account the inverse of the width of the soliton on the coupled breather-solution envelop along the MTs for $\eta = 0.002$ and $\gamma = 0.02247$, at time $t = 800$.

of a train of three breathers, as shown in Fig. 9 at time $t = 800$, with $\eta = 0.002$ and $\beta = 0.1$. In a biophysical context, the coupling of two breathers would allow the transport of a wider range of information via the MTs. It should be mentioned that the obtained results are not an isolated case, as some works in other biological processes have known more enlightened explanations thanks to the coupled signals of breathers. Among others, we can mention the phenomenon of transcription in DNA physics [18,86,91], the dynamics of negative ions in plasma [92], the process of disassembly and vesicular and organelle transport in MTs [13,64]. The transport memory constant γ, the nonlinearity rate η and the free parameter β are, however, expected to bring about more new features that will help to comprehend the various activities induced by wave propagation in the MT lattices within a living cell. More explicitly, one can control how tubulin dimers move to perform their cellular functions by making a suitable choice of γ, η and β. From the panels of Fig. 9, for example, one notices that the memory effect can act in two ways on the motion of the MTs. To be more precise, Fig. 9(aj)$_{j=1,2,3}$ show that the amplitude of the coupled signal increases for values of γ, while higher values of the memory effects, as shown in Fig. 9(bj)$_{j=1,2,3}$, reduces such an amplitude and preserves the solitonic width. Along the same line, under increasing values of η, the wave amplitude drastically decreases as depicted in Fig. 10, where the nonlinearity rate takes the successive values $\eta = 0.001$, $\eta = 0.08$, and $\eta = 0.02$. The free coefficient β mainly affects its width and amplitude as displayed in Fig. 11 at time $t = 800$, with $\eta = 0.002$ and $\gamma = 0.02247$. Obviously, such a parameter can efficiently be used to transit from multiple-breathing structures to single-breathing patterns, therefore adapting the solitonic width to specific cellular functions.

It should be noted that the studied physical model has undergone significant improvements, particularly in its responsiveness to coupled and uncoupled excitations. The movement of tubulin dimers may vary in speed, depending on the constant γ responsible for the transport memory effects. However, it is important to note that the nonlinearity in both cases remains a deamplification factor. From our observations within the selected value ranges, it behaves solely as an attenuating factor. We believe that our results can be replicated in real-world physical experiments as long as the model parameters of Eq. (14) are set to allow for stable spatiotemporal evolutions of nonlinear wave patterns. Within the cell cytoplasm, MTs undergo continuous conformational changes due to physiological mechanisms such as GTP hydrolysis. It has been suggested that the communication necessary for the movement of molecular motors (dyne and kinesin) is facilitated by soliton-breathers. Given the diverse and complex nature of intracellular transport, similar to information processing in neuronal networks, we believe that the coupled breather is essential for addressing any communication deficiencies within the cell. The MT vibrations shown in Fig. 8 are interesting due to their modulated and localized wave profiles. However, when considering their spatial spread, it becomes clear that the coupled

soliton-breather mode would better facilitate the collection, transport, and redistribution of cellular cargoes through MT dynamics. This could especially be true when certain model parameters are varied, resulting in changes to the speed, number, and distribution of dimers in the cytoplasmic environment as they carry out their biological functions. We discussed earlier how MTs with an overdamped movement may display transport memory effects. This idea is motivated by the contribution of Oahu et al. [93], which reveals that MTs have multilevel memory traits. Their scanning tunneling microscope experiments showed that memory states were linked to the orientations of tilted dipoles (dimers). We argue that these tilts would cause depolymerization followed by polymerization, leading to the attachment of kinesin/dynein via signaling relayed by the coupled breather excitation. This would enable the movement of suitable and useful cargo. Additionally, this would provide valuable insight into the nonlinear dynamics of MTs in the brain. Therefore, by understanding the behavior of a molecular motor along the axonal PF at a certain point in the network, we can predict and control it at the previous point. When two neurons exchange information, the optimal way to observe the memory transfer is through the soliton-breather coupling. This process involves consistent parameters such as η and β. The behavior of the coupled vibration alternates between amplification and deamplification. Amplification is associated with the collection and transfer of a large amount of information, while deamplification results in a loss of energy. This can disrupt the work of motor proteins that supply certain cell sites with energy. The way information is perceived in the brain, which is overseen by MTs at the level of neuronal axons, may lead to reduced neuronal activities. This, in turn, can cause neurodegenerative conditions like Parkinson's and Alzheimer's diseases [94,95]. We can currently understand how tubulin dimers move in a cytoplasmic environment that is over-damped and scrambled (chirp) when coupled or uncoupled breathing excitations take place. This understanding may contribute to our knowledge of important cellular biological phenomena that are regulated by MT dynamics, including mitosis, mitochondrial motility, and cognitive and memory processes in the brain.

6. Conclusion

The main objective of this work was to investigate the slow movements of MTs in their surrounding cytoplasmic environment. Our results suggest that the latter results in transport memory effects, which may have a significant impact on the nonlinear signals supported by an enhanced angular model of MT vibrational dynamics. Thanks to the multiple-scale expansion method, in the continuum limit approximation, we could translate the problem into a set of CCNLS equations to characterize coupling signals with dual frequencies under the competing effects of transport memory constants and the nonlinearity rate. In the process, single- and coupled-mode solitons were discussed. In the first case, the dynamics was found to be excited by a soliton-breather solution, while the second case was found to support extended trains of breathing solitons. The long-time evolution of the two modes was explored via direct numerical simulations, where they were used as initial conditions. Attention has been particularly paid to the input from the parameters γ, η, and β. Specifically, the memory parameter γ was introduced to the model to characterize the memory effects due to the frictional forces of the biological system, which bring out the dependence of these forces not only in the current dynamics but also in the way the system reached it. The γ parameter values that have been selected carefully in both cases signify that transport memory can have two effects. Firstly, it can significantly reduce the soliton excitations, consequently decreasing the energy or information invested by GTP hydrolysis, which is used for the initiation of the primary functions that the MT needs to perform, such as the processes of polymerization/depolymerization and neuronal transduction. Secondly, the same effects of transport memory can enhance energy transport and storage. This implies that memory effects in MT dynamics can be a valuable tool in controlling the amount of energy required for crucial processes such as the formation or destruction of tubulin dimers, cellular cargo transportation, ionic flow and many more. Remarkably, the inclusion of the memory factor in MT dynamics can be crucial in understanding and regulating physiological processes. In other words, for example, when heterodimers are involved, the sequence of events that would precede depolymerization could exploit the effect of transport memory so that GTP releases the amount of energy necessary for the motion of ions to signal the molecular motors of any intracellular transport action of vesicles or organelles. For its part, the nonlinearity parameter naturally appeared in the solutions, where it characterizes the degree of nonlinearity of the wave propagating along the PFs in the biological environment. In the context of single and coupled modes, we have noted a decrease in the amplitude of the signals. The nonlinear nature of the excitations in the system is confirmed and could even, to some extent, disrupt intracellular communication based on the MTs. Finally, the free parameter β was used to characterize the width of the solitonic excitation, particularly its inverse. We have seen its impact on the coupled soliton-breather, where it led to a reverse relationship between the amplitude and the width of the signal in the cytoplasmic space. Practically, it was argued that using a lower memory constant is recommended to ensure efficient migration and energy transfer. In that direction, the coupled mode was found to be more advantageous as it allows for more information to be transported by motor proteins (such as kinesin or dyne) through MTs, provided that the nonlinearity and free parameters β are properly chosen within the predicted intervals. The intervals were chosen to ensure that the system's conditions and parameters were optimal for soliton excitations to propagate and remain stable, resulting in relevant and biophysically acceptable outcomes. Therefore, the numerical values of these parameters should be chosen carefully to help us understand the various possible biophysical scenarios better, leading to eventual experimental implementation. When the memory constant counteracts the effects of nonlinearity and dispersion, the free parameter β and nonlinear parameter η may facilitate the emergence of diverse vibrational modes in the PFs. The memory effect has a pivotal role in regulating both nonlinear and dispersive factors, as well as impacting the viscosity of the system to a significant degree. This results in the amplification or damping of vibrational signals, which depends on the inherent energy transport through the modulated structures that emerge. Based on our findings, memory effects in MTs are crucial for key cellular processes. Therefore, they provide valuable insights into the complex interactions within cellular dynamics. Consequently, the coupled soliton-breathers excitation is a promising contender for ensuring strong energy harvesting within brain MTs. This is particularly true when physiological control is used to adjust the parameters of transport memory, nonlinearity rate, chirp, and inverse width. This can help predict the proper regulation of neuronal activity, as well as intra-neuronal trafficking and axonal transduction of MTs. There exist alternative models for studying the nonlinear dynamics of MTs, including the longitudinal model, which assumes the movement of the tubulin dimer to be rectilinear. As a result, we can account for two types of simultaneous movements (rotation and translation) in one dimer. This opens new directions for future investigations on exploring memory effects on structural dynamics and intracellular transport in a more comprehensive model of MT dynamics.

CRediT authorship contribution statement

Eric Tankou: Conceptualization, Data curation, Formal analysis, Software, Writing – original draft, Writing – review & editing. **Conrad Bertrand Tabi:** Conceptualization, Data curation, Formal analysis, Investigation, Methodology, Project administration, Supervision, Validation, Writing – original draft, Writing – review & editing. **Alidou Mohamadou:** Conceptualization, Data curation, Formal analysis, Software, Supervision, Writing – review & editing. **Timoléon Crépin Kofané:** Conceptualization, Data curation, Formal analysis, Project administration, Resources, Software, Supervision, Validation, Writing – review & editing.

Declaration of competing interest

The authors declare that they have no known competing financial interests or personal relationships that could have appeared to influence the work reported in this paper.

Data availability

Data will be made available on request.

References

[1] Dustin P. Microtubules. Berlin: Springer; 1984.
[2] Satarić MV, Žakula RB, Tuszynski JA. Nanobiology 1992;1:445.
[3] Tuszynski JA, Hameroff S, Satarić MV, Trpisová B, Nip MLA. J Theoret Biol 1995;174:371.
[4] Tuszynski JA, Brown JA, Crawford E, Carpenter EJ, Nip MLA, Dixon JM, Satarić MV. Math Comput Modelling 2005;41:1055.
[5] Cifra M, Pokorný J, Havelka D, Kučera O. BioSystems 2010;100:122.
[6] Havelka D, Cifra M, Kučera O, Pokorný J, Vrba J. J Theoret Biol 2011;286:31.
[7] Kučera O, Havelka D. Biosystems 2012;109:346.
[8] Audenaert R, Engelborghs Y, Heremans L, Heremans K. Biochim Biophys Acta 1989;996:110.
[9] Zdravković S, Kavitha L, Satarić MV, Zeković S, Petrović J. Chaos Solitons Fractals 2012;45:1378.
[10] Zdravković S, Satarić MV, Zeković S. Europhys Lett 2013;102:38002.
[11] Alexander N, Mónica RF, Gennady BP, Mavromatos NE. Phys Rev E 2016;93:062412.
[12] Zdravković S, Bugay AN, Aru GF, Maluckov A. Chaos 2014;24:023139.
[13] Tabi CB, Tankou E, Mohamadou A. Chaos Solitons Fractals 2017;95:187.
[14] Zdravković S, Satarić MV, Maluckov A, Balaž A. Appl Math Comput 2014;237:227.
[15] Rubinstein SM, Cohen G, Fineberg J. Phys Rev Lett 2006;96:256103.
[16] Dillavou S, Rubinstein SM. Phys Rev Lett 2018;120:224101.
[17] Okaly JB, Ndzana F, Woulaché RL, Tabi CB, Kofané TC. Chaos 2019;29:093103.
[18] Tabi CB, Mohamadou A, Kofané TC. Eur Phys J D 2008;50:307.
[19] Hennig D, Archilla JFR, Agrawal J. Physica D 2003;180:256.
[20] Koko AD, Tabi CB, Ekobena HPF, Mohamadou A, Kofané TC. Chaos 2012;22:043110.
[21] Zdravković S, Satarić MV. Europhys Lett 2007;80:38003.
[22] Mefire GRY, Tabi CB, Mohamadou A, Ekobena HPF, Kofané TC. Chaos 2013;23:033128.
[23] Tabi CB, Mimshe JCF, Ekobena HPF, Mohamadou A, Kofané TC. Eur Phys J B 2013;86:374.
[24] Chou KC, Zhang CT, Maggiora GM. Biopolymers 1994;34:143.
[25] Satarić MV, Tuszyński JA, Žakula RB. Phys Rev E 1993;48:589.
[26] Guemkam GP, Tameh JTB, Kakmeni FM. Chaos 2018;28:023106.
[27] Tabi CB, Tagwo H, Tiofack CGL, Kofané TC. Opt Lett 2022;47:5557.
[28] Tabi CB, Tagwo H, Kofane TC. Phys Rev E 2022;106:054201.
[29] Latchio Tiofack CG, Tabi CB, Tagwo H, Kofané TC. J Opt 2023;25:054001.
[30] Tiofack CGL, Tabi CB, Tagwo H, Kofané TC. Phys Lett A 2023;480:128982.
[31] Zanga D, Fewo SI, Tabi CB, Kofané TC. Phys Rev A 2022;105:023502.
[32] Ndebele KK, Tabi CB, Latchio Tiofack CG, Kofané TC. Phys Rev E 2021;104:044208.
[33] Arecchi FT, Boccaletti S, Ramazza P. Phys Rep 1999;318:1.
[34] Aranson IS, Kramer L. Rev Modern Phys 2002;74:99.
[35] Akhmediev N, Ankiewicz A. Three sources and three component parts of the concept of dissipative solitons. In: Dissipative solitons: from optics to biology and medicine. Lecture notes in physics, vol. 751, Berlin, Heidelberg: Springer; 2008.
[36] Fermann ME, Galvanauskas A, Sucha G, Harter D. Appl Phys B 1997;65:259; Ferreira FS, Facao MMV, Latas SCV. Fiber Integr Opt 2000;19:31.
[37] Gong YD, Shum P, Tang DY, Lu C, Guo X, Paulose V, Man WS, Tam HY. Opt Laser Technol 2004;36:299.
[38] Madimabe EB, Tabi CB, Latchio Tiofack CG, Kofané TC. Phys Rev B 2023;107:184502.
[39] Zaoro NR, Tabi CB, Etémé AS, Kofané TC. Phys Lett A 2020;384:126133.
[40] Okaly JB, Mvogo A, Tabi CB, Ekobena Fouda HP, Kofané TC. Phys Rev E 2020;102:062402.
[41] Hocking LM, Stewartson K. Proc R Soc Lond-Ser A 1972;326:289; Pereira NR, Stenflo L. Phys Fluids 1977;20:1733.
[42] Petviashvili VI, Sergeev AM. Sov Phys Dokl 1984;29:493.
[43] Malomed BA, Winful HG. Phys Rev E 1996;53:5365.
[44] Kabadiang Ngon GF, Tabi CB, Kofané TC. Phys Lett A 2024;494:129291.
[45] Dodd RK, Eilbeck JC, Gibbon JD, Morris HC. Solitons and nonlinear wave equations. London: Academic Press Inc.; 1982.
[46] Kawahara T. J Phys Soc Japan 1973;35:1537–44.
[47] Schoutens JE. J Biol Phys 2005;31:35.
[48] Pokorný J, Jelinek F, Trkal V, Lamprecht I, Hölzel R. Astrophys Space Sci 1997;23:171.
[49] Havelka D, Cifra M, Vrba J. J Phys Conf Ser 2011;329:012014.
[50] Sun Y, Salamon MB, Garnier K, Averback RS. Phys Rev Lett 2003;91:167206.
[51] Mvogo A, Kofané TC. Chaos 2016;26:123120.
[52] Mvogo A, Ben-Bolie GH, Kofané TC. Commun Nonlinear Sci Numer Simul 2017;48:258.
[53] Nigmatullin RR, Baleanu D. Internat J Theoret Phys 2010;49:701.
[54] Guimfack BA, Mbakob RY, Tabi CB, Kofané TC. Chaos Solitons Fractals 2022;157:111936.
[55] Abramson G, Bishop AR, Kenkre VM. Phys Rev E 2001;64:066615.
[56] Manne KK, Hurd AJ, Kenkre VM. Phys Rev E 2000;61:4177.
[57] Kenkre VM. AIP Conf Proc 2003;658:63.
[58] Gradshteyn IS, Ryzhik IM. Table of integrals, series, and products. 7th ed.. Elsevier Academic Press; 2007.
[59] Bitang DC, Ziem A, Mvogo A, Kofané TC. Physica A 2019;517:36.
[60] Kar S, Banik SK, Ray DS. J Phys A Math Gen 2003;36:2771.
[61] Murray JD. Mathematical biology I. An introduction. 3rd ed.. Berlin: Springer; 1993.
[62] Remoissenet M. Phys Rev B 1986;33:2386.
[63] Okaly JB, Mvogo A, Woulaché RL, Kofané TC. Chinese J Phys 2018;56:2613.
[64] Tankou E, Tabi CB, Kofané TC. Chaos Solitons Fractals 2022;162:112446.
[65] Otlaadisa P, Tabi CB, Kofané TC. Phys Rev E 2021;103:052206.
[66] Legoya P, Etémé AS, Tabi CB, Mohamadou A, Kofané TC. Chaos Solitons Fractals 2022;146:112599.
[67] Bansi Kamdem CD, Ndjawa Yomi PA, Tabi CB, Mohamadou A. Eur Phys J Plus 2023;138:176.
[68] Edouma Biloa BP, Tabi CB, Ekobena Fouda HP, Kofané TC. Phys Scr 2023;98:115230.
[69] Bansi CD, Tabi CB, Mohamadou A. Chaos Solitons Fractals 2018;109:170.
[70] Tabi CB, Ekobena HP, Mohamadou A, Kofané TC. Phys Scr 2011;83:035802.
[71] Essimbi BZ, Kofané TC. Phys Scr 2007;76:480.
[72] Mani Rajan MS, Hakkim J, Mahalingam A, Uthayakumar A. Eur Phys J D 2013;67:150.
[73] Mani Rajan MS, Mahalingam A, Uthayakumar A. Ann Physics 2014;346:1.
[74] Vijayalekshmia S, Mani Rajan MS, Mahalingama A, Uthayakumar A. J Modern Opt 2015;62:278.
[75] Kengne E, Abdourahman, Lakhssassi A. Chinese J Phys 2020;63:271.
[76] Yemélé D, Kofané TC. J Phys D: Appl Phys 2006;39:4504.
[77] Li X-X, Cheng R-J, Zhang A-X, Xue J-K. Phys Rev E 2019;100:032220.
[78] Kofané TC, Zebaze M, Zibi A. J Phys D: Appl Phys 1990;23:764.
[79] Kourakis I, Shukla PK, Morfill G. New J Phys 2005;7:153.
[80] Englander SW, Kallenbach NR, Heeger AJ, Krumhansl JA, Litwin S. Proc Natl Acad Sci USA 1980;77:7222.
[81] Toko D, Mohamadou A, Tabi CB, Kofané TC. J Comput Theor Nanosci 2012;9:1.
[82] Domgno WK, Mohamadou A. Commun Nonlinear Sci Numer Simul 2022;110:106360.
[83] Dauxois T, Peyrard M, Bishop AR. Phys Rev E 1993;47:684.
[84] Dauxois T. Phys Lett A 1991;159:390.
[85] Tankou AST, Takembo CN, Ben-Bolie HG, Ateba PO. PLoS One 2019;14(6):0214989.
[86] Tabi CB, Etémé AS, Mohamadou A. Physica A 2017;474:186.
[87] Tabi CB, Etémé AS, Mohamadou A, Kofané TC. Chaos Solitons Fractals 2019;123:116.
[88] Zdravković S, Zeković S, Bugay AN, Satarić MV. Appl Math Comput 2016;285:248.
[89] Deneke VE, Di Talia S. J Cell Biol 2018;217(4):1193.
[90] Kuwayama H, Ishida S. Sci Rep 2013;3:2272.
[91] Tabi CB, Ekobena HP, Kofané TC. J Comput Theor Nanosci 2011;8:2220.
[92] Tabi CB, Panguetna CS, Motsumi TG, Kofané TC. Phys Scr 2020;95:075211.
[93] Sahu S, Ghosh S, Hirata K, Fujita D, Bandyopadhyay A. Appl Phys Lett 2013;102:123701.
[94] Gabor D. J Inst Electr Eng 1946;93:429.
[95] Boashash B. Proc IEEE 1992;80:520.